Universität für Bodenkultur Wien

Department für Wasser, Atmosphäre und Umwelt
Institut für Wasserwirtschaft, Hydrologie und konstruktiven Wasserbau
Vorstand: Univ.Prof. Dipl.Geoökol. Dr.rer.nat. Karsten Schulz

Possible Impacts of Climate Change on the Water Balance with Special Emphasis on Runoff and Hydropower Potential

Dissertation
zur Erlangung des Doktorgrades
an der Universität für Bodenkultur Wien

Eingereicht von

Dipl.Hyd. Simon Frey

Betreuer: Ao.Univ.Prof. Dipl.-Ing. Dr.nat.techn. Hubert Holzmann

Wien, April 2015

Kurzfassung

Die Nutzung von Wasserkraft ist die wichtigste Quelle an erneuerbaren Energien. Weltweit werden ca. 20 % der elektrischen Energie durch Wasserkraft erzeugt. Österreich bezieht sogar 65 % seiner elektrischen Energie aus Wasserkraft. Der Klimawandel beeinflusst die zeitliche und räumliche Verfügbarkeit von Wasser und hat damit direkte Auswirkungen auf das Energiegewinnungspotenzial aus Wasserkraft. Während die Klimamodelle, was den Anstieg der Lufttemperatur um 3.5 bis 4 K angeht, weitgehend übereinstimmen, bestehen große Unsicherheiten bezüglich Niederschlag und Globalstrahlung.

In dieser Arbeit werden zwei Ansätze vorstellt, die sich mit den möglichen Auswirkungen des Klimawandels auf den Wasserkreislauf beschäftigen. Zum einen werden mögliche Auswirkungen in Österreich analysiert, zum anderen liegt der Fokus auf großskaligen Europäischen Gebieten. Mittels Monte Carlo Simulationen werden bei letzteren zusätzlich Unsicherheiten der Klimamodelle und des hydrologischen Modells verglichen. Über statistische Verfahren können Abfluss und Energiegewinnung miteinander in Verbindung gesetzt werden und so mögliche Auswirkungen auf das Potenzial auf Wasserkraftwerke abgeschätzt werden. In beiden Teilen werden die Klimamodelle ALADIN, REMO und RegCM3 verwendet, die jeweils unter Verwendung des IPCC Szenarios A1B betrieben wurden.

In Österreich wurden 10 Einzugsgebiete ausgewählt, die mit einem halbverteilten hydrologischen Konzeptmodell modelliert wurden. Da sich diese Gebiete teils bis in große Höhen erstecken, spielt Schnee eine bedeutende Rolle in der Modellierung. In vielen Studien wird Schnee mit einem temperaturgetriebenen Verfahren modelliert. Das kann zur Folge haben, dass sich Schnee im Hochgebirge ansammelt, da die Temperatur nur sehr selten über die Schneeschmelztemperatur steigt. Dieses Problem wurde in dieser Arbeit mit zwei unterschiedlichen Modellen behandelt. Für das verteilte Niederschlag-Abfluss-Modell COSERO wurde eine Routine entwickelt, welche laterale Schneetransportprozesse empirisch berücksichtigt. Dadurch konnten unrealistisch große Schneeanhäufungen in den oberen Höhen im Einzugsgebiet der Ötztaler Ache vermieden werden. Zusätzlich konnte das Verhalten des Modells bezüglich des Abflusses verbessert werden.

Für das hydrologische Modell, welches für die Klimawandelmodellierung verwendet wurde, wurde eine weitere Routine zur Umverteilung von Schnee entwickelt. Verglichen mit der Routine für COSERO führt diese zu ähnlichen Ergebnissen, was sowohl die Akkumulation als auch die für die Akkumulation kritische Seehöhe angeht. Des Weiteren konnte gezeigt werden, dass das Missachten von Schneeverlagerungsprozessen das Abflussverhalten des Modells in der Mitte des Jahrhunderts deutlich beeinflusst. Schnee sammelt sich in den obersten Höhenschichten über 100 Jahre hinweg und beginnt zu schmelzen, wenn die Temperaturen durch den Klimawandel bedingt in diesen Höhen ansteigen. Dieses Verhalten konnte durch die Implementierung der Schneeverteilung vermieden werden.

Diese modifizierte Version des hydrologischen Modells wurde in den zehn Österreichischen Einzugsgebieten angewandt. Dabei hat sich gezeigt, dass infolge des Klimawandels mit einer Verminderung des jährlichen Abflusses in den meisten Gebieten zu rechnen ist. Saisonal betrachtet ist eine Zunahme der Abflussmengen im Winter wahrscheinlich, da Niederschlag vermehrt in flüssiger Form fällt, welcher rasch zum Abfluss führt. Die verringerte Schneeschmelze zusammen mit erhöhten Werten der Verdunstung und Rückgang der Gletscher führen im Sommer zu einer deutlichen Reduktion des Abflusses.

In den Europäischen Gebieten wurden ähnliche Ergebnisse gefunden. Hier wurde ein Rückgang des Energiegewinnungspotenzials in drei von vier Staaten ermittelt. Dieser bewegt sich im Bereich von 2 bis 10 %. Durch die erhöhten Abflüsse im Winter kann allerdings saisonal mit einem erhöhten Potenzial gerechnet werden.

Schlüsselwörter: Klimawandelfolgenmodellierung; Niederschlag-Abfluss-Modellierung; Schneeprozesse; Modellierung von lateralen Schneetransportprozessen

Abstract

Earth's climate is changing. While climate models agree on warming of about 3.5 to 4 K in alpine regions, evolution of precipitation and global radiation is uncertain. This change has impacts on the hydrological behaviour of catchments and regions and therefore on the hydroelectric power potential. Worldwide hydropower is the most important source of renewable energy as 20 % of the world's electricity is provided by hydropower stations. Austria even gains roughly 65 % of its electric energy from hydropower.

This thesis presents two approaches to study possible impacts of a changing climate on the hydrological cycle. One focusses on the evolution of climate and its hydrological impact in Austria, the other concentrates on large regions in the Alps, focussing on uncertainties of the model chain of climate models and hydrological models and links discharge and electric power generation statistically to derive statements about the evolution of the hydroelectric power potential. In both studies the regional climate models ALADIN, REMO and RegCM3 were used with the IPCC emission scenario A1B.

In Austria ten basins have been selected and modelled using a conceptual, semi-distributed rainfall-runoff model. Since many of these catchments cover high mountainous regions snow processes play a key role. In many recent studies, snow has been modelled using a method that uses only temperature to determine whether precipitation occurs in liquid or solid form and whether snow can melt or not. This may lead to unrealistic high accumulations of snow in the peak regions because no lateral snow transportation processes are taken into account. The presented study deals with that problem. A simple snow redistribution model has been developed for the use in the raster based hydrological model COSERO. This model has been tested in the catchment of Ötztaler Ache, Austria. In a seven year period the standard model without considering redistribution of snow would lead to unrealistic snow accumulation in high elevated regions whereas the updated version of the model does not show accumulation and does also predict discharge more precisely leading to a Kling-Gupta-Efficiency of 0.93 instead of 0.9.

Another approach for preventing snow accumulations in high altitudes has been developed for the semi-distributed model used for climate change impact modelling. Similar behaviour regarding snow accumulations and the critical elevation for this to occur has been found in the Salzach River basin, Austria. It could be shown that not considering snow transport leads to higher discharge rates in the mid-century. Snow that accumulated over a hundred years starts to melt due to higher temperature values in high altitudes. This could be prevented by the use of the redistribution model.

The updated version of the model was applied to the selected basins. Mainly due to warming, snow melt becomes more important in winter and early spring while the total amount of snow being stored in the catchment in the cold season gets lower. Consequently, discharge rates in winter in general are higher than now in summer enhanced evapotranspiration combined with less snow and ice melt lead to lower discharge rates. Annual sums of runoff in most of the basin are decreasing.

Similar results were found in modelling large scaled region in the Alps. Selecting the best 500 runs out of 500 000 Monte Carlo runs performed by a new developed model show that uncertainties arising from hydrological models are small in comparison with uncertainties of climate change models. Runoff then was statistically linked to hydropower potential in national states. In most countries the annual energy potential drops by about 2 to 10 percent. However, due to more equalized seasonal runoff behaviour, higher rates of energy production may be possible during the winter.

Keywords: Climate change impact modelling; rainfall runoff modelling; snow cover processes; lateral snow transportation modelling;

I. Table of Contents

II. List of tables

III. List of figures

IV. List of figures in the appendix

V. List of abbreviations

APCC	Austrian Panel on Climate Change
BMLFUW	Federal Ministry of Agriculture, Forestry, Environment and Water Management
COSERO	COntinuous Semi-distributed RunOff model
DEM	Digital Elevation Model
ENTSO-E	European Network of Transmission System Operators for Electricity
ETA	Actual Evapotranspiration
ETP	Potential Evapotranspiration
FDC	Flow Duration Curve
GCM	Global Circulation Model, sometimes Global Climate Model
IPCC	Intergovernmental Panel on Climate Change
KGE	Kling-Gupta model Efficiency
MODIS	MODerate-resolution Imaging Spectroradiometer
NSE	Nash-Sutcliffe model Efficiency
RCM	Regional Circulation Model, sometimes Regional Climate Model
RSME	Rooted Mean Squared Error
SASWET	Snow And Soil Water balance Estimation Tool
SRES	Special Report on Emission Scenarios (published by the IPCC in 2000)
SWE	Snow Water Equivalent
WaBi	WasserBilanz model (German for water balance model)
WMO	World Meteorological Organization
ZAMG	Zentralanstalt für Meteorologie und Geodynamik (Austrian Weather Service)

1 Introduction

Climate change is undeniable (Ansari et al., 2013; Parmesan et al., 2013). The Intergovernmental Panel on Climate Change estimates that global warming by the end of the 21st century will cause a rise of temperature of up to 5.5 K relative to 1985-2005 (IPCC, 2013). The Global Challenges Foundation names climate change as one of twelve risks to humanity (Pamlin and Armstrong, 2015). Besides the possibly pronounced occurrence of natural hazards such as heavy thunderstorms, heatwaves or droughts (Brooks, 2013) it is expected to have a negative effect on water resources and freshwater ecosystems in all regions of the world (Jiménez Cisneros et al., 2014). Nearly one sixth of world's population lives within snowmelt dominated catchments with low reservoir storage (Barnett et al., 2005). These regions are potentially vulnerable for shifts in runoff caused by climate change (Viviroli et al., 2011). Water resources also play a key role in the mix of regenerative energy sources such as hydropower which by now is the most important source of renewable energy, supplying about 20 % of global electricity demands (Panwar et al., 2011). The greater the alpine region in a country the higher the share of hydropower in the mix of electric energy sources. Roughly 65 % of the electric energy of Austria is provided by hydropower (E-Control, 2013).

What impact does climate change have on water resources? Is it possible to account for changing climate conditions using hydrological models? How do hydrologic systems adapt to changes in climate? Answering these questions is challenging since still little is known about how the climate might evolve and what are the consequences for hydrosphere, cryosphere or marine systems (Ford and Pearce, 2010). Nevertheless, many studies around the globe have tried to give answers to questions of this kind. Pohl et al. (2007) applied a distributed model to a small catchment in the Canadian Arctic to study impacts on snowmelt behaviour. They found a considerable shift in the ascent and the occurrence of peak runoff towards earlier seasons in the year. In analysing hydrological responses of large Himalayan rivers to climate change until the mid-century Immerzeel et al. (2010) found changes in seasonal runoff conditions but stated that these changes differ substantially among river basins and could not be generalized. In a case study in the Tyrolean Alps, Austria, Laghari et al. (2012) reported a change from a rainfall- and snowmelt dominated runoff regime to a rainfall dominated regime. This finding was also reported by several other authors (Beniston, 2012; Holzmann et al., 2010; Koboltschnig et al., 2008).

Many of these studies however concentrate on small to medium scale (i.e. 10s to 100s of square kilometres) catchments. Schaefli et al. (2007) analysed climate change impact on hydropower towards quantifying uncertainties in the 170 km² basin of Mauvoisin in the Swiss Alps. An area of the same order of magnitude was investigated by Alaoui et al. (2014) who focussed on changes in climate as well as on land-use changes in the near future until the year 2028. On the other hand, some work was done focussing on catchments or regions covering 10s to 100s of thousands of square kilometres (Kling et al., 2012; Stanzel and Nachtnebel, 2010).

The leading tools available for projecting future conditions of transient atmospheric variables that have an effect of climate relevant gases such as CO_2, CH_4 or N_2O are global circulation models (GCMs). These models are based on physical equations appropriate at spatial ranges of hundreds of kilometres. Future scenarios are used to generate forcing agents that drive those models. These scenarios are defined by the IPCC. Until the previous report in 2007, the scenarios were based on the emission of greenhouse gases given in CO_2-equivalent (IPCC, 2000). An increase of these gases would cause a surplus of earth's energy intake. More energy would be received than could be emitted by the planet. Since the amount of energy a body is able to emit depends on its surface temperature (Stefan-Boltzmann law), the earth needs to warm up to restore its energy balance (Le Treut et al., 2007). Based on different socio-economic development pathways the IPCC (2000) defined four families of emission scenarios (SRES, special report on emission scenarios) that are given in Table 1-1. These families then were the basis for six emission scenarios all of which were considered possible. However, in many climate change studies (e.g. Kling et al., 2012; Koch et al., 2011; Mauser and Bach, 2009; Samuels et al., 2010) including this thesis, the scenario A1B was only considered. A1B assumes a globalized focus on economic growth with a balanced emphasis on all energy sources (fossil and regenerative). According to Kling et al. (2012) it may be considered as medium or moderate scenario.

Table 1-1: The four families of emission scenarios provided by the IPCC (2000).

	Economic focus	**Environmental focus**
Globalization	A1 (warming of 1.4 to 6.4 K)	B1 (warming of 1.1 to 2.9 K)
Regionalization	A2 (warming of 2.0 to 5.4 K)	B2 (warming of (1.4to 3.8 K)

warming rates relative to 1980-1999

In the latest report by the IPCC (2013), new scenarios have been defined. No longer based on emissions of greenhouse gases, a surplus of radiative forcing is considered directly. Four scenarios have been defined: RCP 2.6, 4.6, 6.0 and 8.5. The numbers hereby refer to the extra radiative forcing in Watts per square metre in the year 2100 with respect to the average from 1850 to 1900. Since the work on this thesis was started in 2011 the old scenario A1B was considered.

Obviously a spatial resolution of hundreds of kilometres which is provided by GCMs is not sufficient for the use of hydrological models on the catchment scale, i.e. some hundreds to few thousands of square kilometres (Bárdossy and Pegram, 2011). Consequently information from GCMs need to be transferred to a higher resolution. This process is called downscaling. The most common methods for downscaling include (i) delta change methods which look at the percentage/amount of change from present to future conditions; (ii) statistical downscaling methods; and (iii) dynamical downscaling using regional circulation models (RCMs) driven by GCMs (Samuels et al., 2010). Chen et al. (2011) compared various techniques in a watershed in Québec, Canada, and concluded that the choice of the method has critical influence on hydrological impact studies. In general statistical downscaling methods lead to good results, yet limitations exist in reproducing regional processes affecting subgrid-scale precipitation patterns (Schmidli et al., 2006). This however is crucial for climate change assessment in alpine regions. Thus, in this thesis, dynamical downscaling using RCMs is used to gain regional information regarding meteorological parameters.

RCMs are similar in their structure to GCMs but operate on the regional scale, i.e. use grid cells with 25 to 50 km edge sizes. An RCM is driven by the output of a GCM (Kendon et al., 2010). They certainly provide meteorological information on a better spatial scale than GCMs, however for studies in mountainous terrain this is still not sufficient (Prasch et al., 2011). Consequently, the RCM output needs further refinement. A common resolution used by many hydrological models is 1 x 1 km (see e.g. Frey and Holzmann, 2015; Koboltschnig et al., 2008; Stanzel and Nachtnebel, 2010). Depending on the topic of research however, this resolution might not be sufficient either. Some authors working on snow processes in mountainous terrain suggest grid cells the size of 10 to 50 metre edge sizes (e.g. Bernhardt and Schulz, 2010; Bernhardt et al., 2010; Warscher et al., 2013). A review of scaling issues in hydrology can be found in (Blöschl and Sivapalan, 1995). In Figure 1-1 a comparison of the spatial resolution of both an RCM and the data on a 1 x 1 km grid is shown for mean temperature values in June during the period from 2003 to 2010 for Austria.

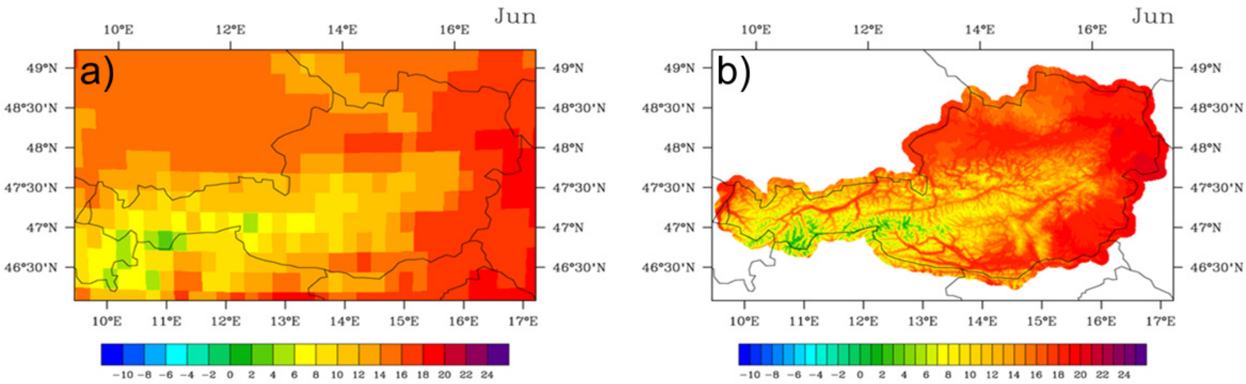

Figure 1-1: Comparison of spatial resolutions of an RCM (a) and localized data (b). The RCM consist of a resolution of 25x25 km while the localized data is scaled down to the resolution of the INCA data of 1 x 1 km. Both show mean temperature values for June during the period 2003-2010. Figures from Frey et al. (2014).

Using high resolution meteorological data it is possible to apply hydrological models to watersheds. These models describe the hydrological cycle in various states of complexity ranging from physically based descriptions of water movement in the soil (e.g. Erdal et al., 2014) to simple water balance equations for large scale (i.e. hundreds of thousands of square kilometres) catchments (see e.g. Gudmundsson et al., 2012; Hannah et al., 2011). Even on the global scale, hydrological models have been applied (Stahl et al., 2012). While conceptual models simplify hydrological processes and therefore need to be calibrated over a certain period of time, physical based models ideally do not have such a need. For instance, Lange et al. (1999) presented a non-calibrated model approach for a semi-arid catchment in Israel. However, physical based models rely on a large number of parameters such as land surface, soil properties or vegetation that are difficult to obtain. Consequently, most of these models need calibration of at least some of their parameters, too (Kunstmann et al., 2006). But simplification of hydrological processes has limits. Seibert (2003) showed that conceptual models may perform well during the time period of calibration but fail when applied to time windows outside that range. According to Bergström (1991), this could mean that a model is over-parameterized, too. Other authors however report good model performances both inside and outside the calibration time window, even when both time series are separated by a copious amount of time (Christensen et al., 2004; Koboltschnig et al., 2008).

One of the most criticized characteristics of (calibrated) hydrological models is equifinality: Many sets of parameters lead to equally well model results (Beven, 1993). This behaviour is unavoidable, yet may be managed by different approaches. Beven and Binley (1992) presented the GLUE (Generalized Likelihood Uncertainty Estimation) procedure to identify a variety of parameter sets leading to similar good results. Using this methodology it is possible to account for uncertainty ranges originating from parameter sets (Beven and Freer, 2001; Schulz et al., 1999). Another approach was presented by Vrugt et al. (2009) who used formal Bayesian statistics to account for uncertainty issues. Also accounting for parameter sensitivity during calibration may help reducing equifinality (Massmann and Holzmann, 2012a; Massmann et al., 2014). In general, a higher degree in model complexity enhances the issue of equifinality. On the other hand a more complex model may lead to better model results during the period of validation compared to a simple model if the model can be calibrated by means of using expert knowledge (Gharari et al., 2014; Hrachowitz et al., 2014).

Many authors have addressed the issue that models should “give the right answers for the right reasons” (e.g. Grayson et al., 1992; Kirchner, 2006; Klemeš, 1988). A well-known example for models giving good results for the wrong reasons was stated by Kirchner (2003) in his “old water paradox” paper. He addressed the fact that storm flow mainly consists of old water yet most hydrological models picture peak discharge as a fast runoff component and therefore assume it would consist of new, young water. Weiler and McDonnell (2004) introduced the concept of virtual experiments to identify first order controls in hillslope hydrology. They conclude getting the answers right for the right reasons also reduces equifinality issues.

Another topic regarding wrong model behaviour is snow accumulation in high elevations. Koboltschnig et al. (2008) noticed a simulated accumulation of more than 10,000 mm SWE (snow water equivalent) during a six year period in the catchment of Salzach. One of the reasons for accumulation of snow is the use of a simple melt model approach using only temperature to trigger melting of snow or ice. A typical example of a temperature index method for snow modelling is the day degree approach (see for example Hock 2003). As long as air temperature does not rise above a certain threshold (often 0 °C), snow does accumulate regardless of any other processes that may lead to snow melt like radiation or turbulent fluxes of latent energy. In high mountainous regions this may be the case for most days during the year leading to an intensive accumulation of snow in these areas. In nature, however, these accumulations are barley existent. Reasons for that are, besides of a more complex melting behaviour of snow than it is assumed in temperature-index approaches, either wind or gravitationally induced lateral snow distribution processes (Elder et al., 1991; Winstral et al., 2002). Resulting snow depths vary greatly on high-resolution scales (e.g. Helfricht et al., 2014) but, when changing the focus from micro (e.g. several square meters) to macro scales (e.g. one to several square kilometres), there are less variations (Melvold and Skaugen, 2013).

During the accumulation period, according to Liston (2004), there are primarily three mechanisms responsible for these variations: (i) snow-canopy interactions in forest covered regions, (ii) wind induced snow redistribution and (iii) orographic influences on snow fall.

Differences in tree species (deciduous vs coniferous trees) as well as the density and height of the canopy layer cause spatial variability of the snow layer (Garvelmann et al., 2013; Liston, 2004; Pomeroy et al., 2002). Besides the impact of vegetation, wind is the most dominant factor influencing snow patterns in alpine terrain. Snow is transported from exposed ridges to the lee side of these ridges, valleys and vegetation covered areas (Essery et al., 1999; Liston and Sturm, 1998; Rutter et al., 2009; Winstral et al., 2002). One has to be aware, that besides of the physical transport of solid snow wind also stimulates sublimation processes (Liston and Sturm, 1998; Strasser et al., 2008). Wind influences snow patterns on scales of some 100s to 1000 square metres (Dadic et al., 2010a). The third mechanism influences snow patterns on a larger scale of one to several kilometres (e.g. Barros and Lettenmaier, 1994). Non-uniform snow distributions are caused by interactions of the atmosphere (air pressure, humidity, atmospheric stability) with topography (Liston, 2004).

In addition to these processes, gravitationally induced processes like avalanches play a role in snow redistribution (Lehning and Fierz, 2008; Lehning et al., 2002; Sovilla et al., 2010). In steep terrain, avalanches mainly depend on the slope angle and are capable of transporting a considerable amount of snow over distances ranging from 10s to several 100s of metres (Dadic et al., 2010b; Sovilla et al., 2010).

During the ablation period, spatial snow distributions are mainly influenced by differences in snow melt behaviours. On the northern hemisphere snowmelt from south-facing slopes is generally higher than snowmelt on north-facing slopes due to the inclination of radiation. Also vegetation influences melting behaviours. Shading reduces snowmelt compared to direct sunlight. Enhanced emitted long wave radiation due to warm bare rocks or trees increases it (Garvelmann et al., 2013; Pohl et al., 2014).

Models trying to deal with accumulations may be classified into two major approaches. One is to model snow distribution patterns process-oriented the other approach is empirical. Examples for process oriented model are SNOWPACK (Bartelt and Lehning, 2002a) used in avalanche research or SnowTran3D (Liston and Sturm, 1998; Liston et al., 2007). A common thread of these models is that they are computationally intensive as they require data in high spatial resolution 100 to 1000s of square metres. Empirical models use the fact that snow patterns form similarly each year (Helfricht et al., 2014, 2012).

Helfricht et al. (2012) used airborne LiDAR measurements to determine snow accumulation gradients for elevation bands in the Ötztaler Alps. These could be used to improve hydrological models regarding snow cover distributions and subsequently to achieve better runoff predictions. LiDAR data, however, are relatively expensive. Often wind speed and -direction are used to model snow drift (e.g. Bernhardt et al., 2009; 2010; Shulski and Seeley, 2004; Winstral et al., 2002; Liston and Sturm, 1998). Also the physical based SNOWPACK model (Bartelt and Lehning, 2002a) used in avalanche research uses wind to determine redistribution of snow. Unfortunately, wind fields are prone to errors, especially if generated by climate models, i.e. GCMs or RCMs, for climate change scenario studies (Nikulin et al., 2011). Furthermore, these models need spatial information on a small scale of grid cells of only 100s to 1000s of square meters (Schöber et al., 2014).

However, the difficulties of snow accumulation also occur when models using coarser cell sizes or even semi-distributed model using elevation levels instead of grid cells are applied to mountainous catchments. These accumulations do not only affect snow patterns but also seasonal melting behaviour and subsequently discharge (Frey and Holzmann, 2015).

The aim of this thesis is to investigate changes on the hydrological cycle caused by possible changes of the climate. To accomplish that, this thesis is split into three parts: (i) modelling of snow cover processes to prevent unrealistic snow accumulations, (ii) comparison of uncertainties arising from climate and hydrological models combined with an impact study on the hydropower potential of national states in Western Europe and (iii) impacts of climate change on the hydropower potential in Austria.

To model possible changes it is important to represent hydrological processes in the alpine zone. These are mainly influenced by snow processes, i.e. accumulation and depletion of the snow cover. To accomplish this a semi-distributed rainfall runoff model presented by (Holzmann et al., 2010) has been adapted and advanced. This model is referred to as SASWET for <u>S</u>now <u>A</u>nd <u>S</u>oil <u>W</u>ater balance <u>E</u>stimation <u>T</u>ool. The same model is used in the third part of this thesis as well. Since the model uses a temperature index approach for modelling snow, accumulation of snow over the period of many years becomes a problem. Therefore one part of this thesis investigates possibilities to avoid this accumulation behaviour. A simple routine has been developed for the use in SASWET. This routine was tested in the catchment of Salzach River, Austria. Since SASWET is designed as a semi-lumped model and uses elevation band to account for elevation dependent processes no spatial distributed information about the snow cover can be used. Hence, another snow redistribution model has been developed for the use in the distributed rainfall runoff model COSERO (Nachtnebel et al., 1993) which already has been applied to climate change studies (e.g. Stanzel and Nachtnebel, 2010). This snow redistribution model operates on a 1 x 1 km grid and was tested in the catchment of the Ötztaler Ache, Austria. The development and results of applying the model in this basin have been published recently by Frey and Holzmann (2015). Hence, the first part of this thesis illuminates snow and snow redistribution processes in mountainous regions.

Besides snow cover processes uncertainties of the model cascade, i.e. GCMs to RCMs to local meteorological data to hydrological model, are of concern for stating the possible impact of climate change to the hydrological cycle. These uncertainties were investigated in a case study in large watersheds and model regions. In this case, large refers to some thousands of square kilometres. For this purpose, a simple water balance tool was developed. This is referred to as WaBi, for Wasser Bilanz (German for water balance) model. This work was part of a project with Verbund AG, an Austrian energy supplier and forms the second part of this thesis.

Taking into account the conclusions from both snow modelling and uncertainty investigations, the third part of this thesis consists of estimating changes in water resources due to climate change signals in Austria and Southern Germany. Ten medium to large scale catchments (i.e. several hundreds to some few thousands of square kilometres) have been chosen for this task.

In chapter 2 the hydrological models developed and used during the course of this work are described. These models are SASWET, used for both snow cover modelling in high altitudes and for hydrological modelling aiming on impacts of climate change on hydropower, WaBi used for uncertainty analysis and assessment of hydropower evolution in alpine European countries and COSERO, used for detailed snow redistribution modelling.

Chapter 3 and 4 describe the characteristics of the sites modelled and the used data to perform the modelling, respectively. The procedures for calibration and validation of the models are described in chapter 5.

Chapter 6 splits into two sections: (i) the results of calibrating and validating the models are given, followed by (ii) the results of each of the three parts including a respective discussion. The results of calibrating COSERO are not included in this part, though. The comparison between an updated version and a standard model approach of COSERO including calibration is described separately. At the end of the thesis the results are summarized and concluded.

2 Hydrological Models

Hydrological models can be subdivided in different ways. Commonly used is the classification in conceptual and physical based models and in lumped, semi-lumped and (fully) distributed models. The border between conceptual and physically based models is not clear, as there often are physically based assumptions used in conceptual models. An example is modelling snow processes using an energy balance approach. On the other hand, some physically based models use equations that were developed for conceptual models. To remain at the modelling of snow, an example is the use of a temperature index approach in the SHE model (Bøggild et al., 1999). It may also be the case that a model fulfils the nature of being physically based on a certain spatial scale, e.g. hillslope, while it does not for other scales like watershed (Liu and Todini, 2002). Spatially classification is more distinct. Lumped models treat the whole watershed as a single unit, with state variables that represent mean values over the catchment area. An example for a lumped model is the GR4J model (Perrin et al., 2003). Distributed models divide the catchment into several distinct units with each of them described by state variables that represent average values over that unit (Beven, 2012). These units are commonly represented by the use of grid cells or hydrological response units (HRUs). Examples of distributed models are the HBV-96 (Lindström et al., 1997), a distributed version of the classical HBV model (Bergström, 1976), the HL-RMS (Koren et al., 2004) and the COSERO model (Nachtnebel et al., 1993) that is used in parts of this work. Often, hydrological models treat some of their components in a distributed way while others are treated as lumped elements. Lumped parts might be aquifers that describe base flow while evapotranspiration or snow-linked processes are coped with spatially distributed components. These models may be called semi-distributed or, sometimes, semi-lumped models. All different kinds of complexities can be found within this group of models. Examples of semi-distributed models are SWAT (Arnold et al., 1998) and the PREVAH model (e.g. Viviroli et al., 2009). Also the models WaBi (Frey and Holzmann, 2014) and SASWET (see e.g. Frey et al., 2013; Holzmann et al., 2010) used in this work can be referred to as semi-distributed models. Since even distributed models average state variables in space one might argue that models should only be classified in lumped and semi-distributed models.

In the following, the hydrological models used in this work will be explained. The models were applied to different countries and catchments that will be described in chapter 3. Both SASWET and WaBi were used to study possible impacts of climate change on the water cycle and therefore on the hydropower potential. Hereby SASWET was applied to ten basins in Austria while the more simple model WaBi was used to model the water balance in five large scale (several thousands of square kilometres) regions in the Western Alps. The third model introduced here, COSERO, was used to study the effects of snow redistribution on a 1 x 1 km grid in the Ötztaler Alps.

2.1 The semi-distributed Model SASWET

Based on the ideas of the widely used HBV model (Bergström, 1976), SASWET (Snow And Soil Water balance Estimation Tool) is a conceptual, semi-distributed rainfall runoff model. A scheme of the model is illustrated in Figure 2-1. The model is able to account for fast surface flow components induced by infiltration excess (in the following referred as HOF) as well as saturation overland flow (SOF), interflow (subsurface flow, SSF) and ground water flow (GWF). It has recently been used for several purposes as climate change analysis on hydrological components (Holzmann et al., 2010), analysis of parameter interaction (Massmann and Holzmann, 2012a, 2012b) or runoff forecasting on mesoscale catchments (Holzmann and Nachtnebel, 2002). The version of SASWET used in this work is a further developed version of the one described in Holzmann et al. (2010). A summary of the parameters used by SASWET is given in Table 2-1. In this study, the model is run using daily time steps, however it is capable of higher temporal resolution (e.g. hours).

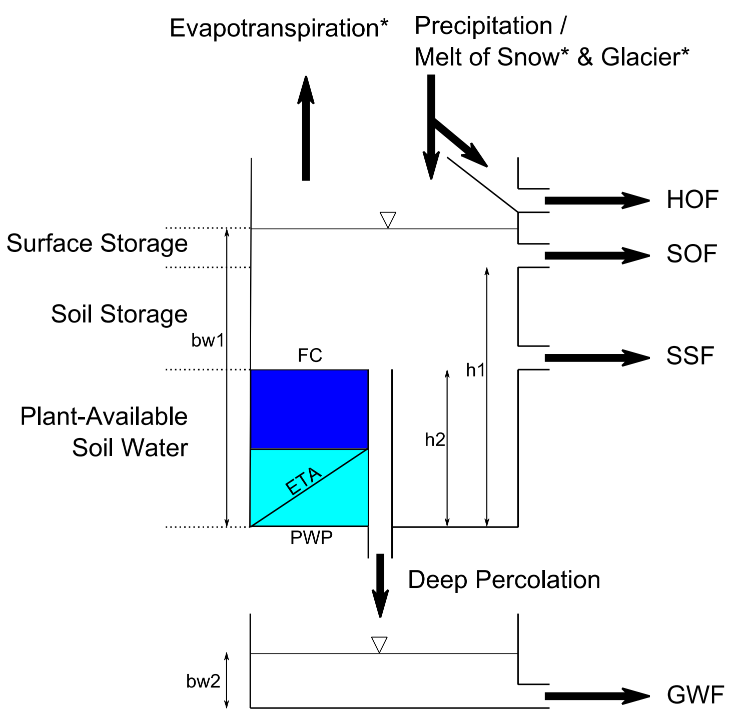

Figure 2-1: Scheme of the hydrological model SASWET (after Frey et al., 2013, edited). Potential evapotranspiration is estimated by a modified method of Turc (Turc, 1961) without considering relative humidity. If the soil water level drops below ½ of the field capacity, ETP is linearly reduced to ETA. The model is capable of modelling fast overland flow (SOF and HOF), interflow (SSF) and baseflow (GWF). State variables marked with an asterisk (*) are calculated on different elevation levels whereas the others are treated in a lumped way.

While precipitation is treated as lumped input, temperature and all temperature-dependent state variables are available on up to seven distinct elevation levels: 250 m, 500 m, 750 m, 1000 m, 1250 m, 1500 m and 2500 m a.s.l. Derived from a high resolution digital elevation model (DEM), the modelled catchment is subdivided into 100 m elevation levels (see Figure 2-2). Information about air temperature is gained by interpolating (extrapolating using a lapse rate of 0.0065 °C m^{-1} if above or below 2500 m or 250 m a.s.l., respectively). This means the model is able to picture inversion weather conditions. Subsequently, ice- and snowmelt are calculated based on these elevation zones.

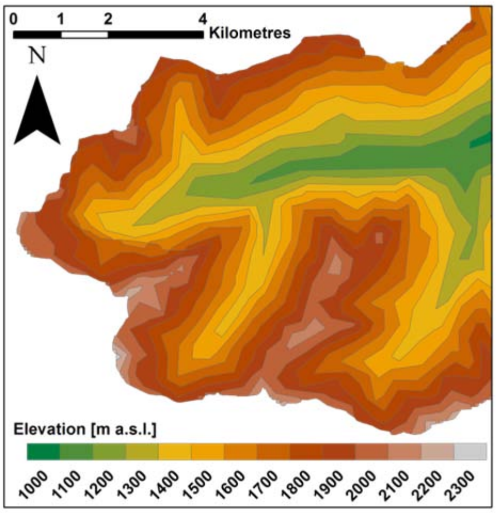

Figure 2-2: Example for elevation bands used by the model SASWET. The model does not consider aspect or angle of the slopes.

2.1.1 Processes in the soil

SASWET treats soil as lumped storage in the watershed (see Figure 2-1). Water enters this bucket-type storage either by liquid precipitation or by snow and ice melt. Processes regarding evapotranspiration are discussed in chapter 2.1.2, ice and snow are described in chapter 2.1.3. In both cases the intensity of which water tries to enter the storage is limited and HOF occurs if that intensity is exceeded. Water may exit the soil either due to evapotranspiration, percolate into a deep groundwater storage or become runoff in form of SOF or SSF. Deep percolation occurs as long as the soil water content exceeds field capacity, surface- and subsurface flow only occur if the water table is high enough to exit the soil through the respective outlet. The outflow (Q) of all storages is parametrized by respective storage constants (k) using Eq. (2-1). All parameters of the model are listed in Table 2-1.

$$Q_t = \frac{1}{k}\exp\left(\frac{-(t-t_0)}{k}\right) \tag{2-1}$$

Table 2-1: Parameters used by SASWET

Parameter	**Description**	**Units**
	Runoff parameters	
k_{HOF}	k-value of hortonian overland flow (HOF).	mm^{-1}
k_{SOF}	k-value of saturation excess overland flow (SOF).	mm^{-1}
k_{SSF}	k-value of subsurface flow (SSF).	mm^{-1}
k_{PERC}	k-value of deep percolation to the groundwater body.	mm^{-1}
k_{GWF}	k-value of groundwater flow (GWF).	mm^{-1}
QC_L	Lower boundary of the runoff coefficient.	[%]
QC_U	Upper boundary of the runoff coefficient.	[%]
k_{API}	k-value of the antecedent precipitation index.	mm^{-1}
	Soil parameters	
h1	Thickness of the soil water reservoir.	mm
h2	Thickness of the plant-available soil water reservoir.	mm
SQ_L	Storage state at QC_L.	mm
SQ_U	Storage state at QC_U.	mm
	Snow parameters	
TSNOW	Threshold temperature to decide whether precipitation is considered fluid or solid and whether snowmelt occurs.	°C
TICE	Threshold temperature to induce ice melt.	°C
CT_{SNOW}	Degree day factor for snowmelt.	mm $°C^{-1}$
CT_{ICE}	Degree day factor for ice melt.	mm $°C^{-1}$
$SPLIT_{MELT}$	Splits melt from snow and ice into direct runoff and water infiltrating the soil.	[%]
PS_{CRIT}	Amount of fresh snow necessary to reset the albedo.	mm d^{-1}
f_{age}	Aging constant to account for lowering the albedo of snow.	d^{-1}
f_{asp}	Factor for correcting melt according to mean aspect	[-]
CT_{AMP}	Amplitude of the mean CT value.	[-]
$TSNOW_{AMP}$	Amplitude of the mean TSNOW and TICE values.	[-]
$DIST_{SHAPE}$	Shape of snow distribution. Shapes can be normal distributed, linearly increasing or linearly decreasing (see Figure 2-6).	[-]
$DIST_{DON}$	Amount of elevation levels acting as donor	[-]
$DIST_{ACC}$	Amount of elevation levels acting as acceptor with respect to a single donor level	[-]
	Meteorological parameters	
radgrad	Elevation dependent gradient for global radiation.	W m^{-2} m^{-1}
tgrad	Elevation dependent gradient for temperature. Only used above/below the highest/lowest elevation surface where temperature information is available.	°C m^{-1}
C_{ETP}	Correction factor for calibrating ETP using Eq. (2-2).	[-]
P_{COR}	Factor to adjust precipitation amounts.	[%]

2.1.2 Evapotranspiration

Evapotranspiration is estimated using a modified version of Turc's method (Turc, 1961) that does not consider relative humidity as this is – in regionalization and climate models – prone to large errors (Fries et al., 2012; Sklenář et al., 2008). This formula is given by Eq. (2-2), where ETP is the potential evapotranspiration in mm, RG is the global radiation in W m^{-2} and TAIR is the air temperature in °C. The method can be calibrated for different sites using the correction coefficient C_{ETP}. To avoid negative values of ETP that would occur at negative air temperature values, the lower bound of ETP is 0.1 mm per day.

$$\mathrm{ETP} = \mathrm{C_{ETP}} \times (\mathrm{RG} + 24) \times \frac{\mathrm{TAIR_t}}{\mathrm{TAIR_t} + 15} \qquad (2\text{-}2)$$

In comparison with the method of Thornthwaite (1948) (see Eq. 2-8), that was originally used, this has two advantages. First, the Thornthwaite method generates monthly mean values for ETP, whereas Turc gives the ETP for each day. Second, Turc's method, in contrast to Thornthwaite's formula, uses global radiation values for the calculation of ETP. For Austria, climate models indicate a significant increase of global radiation in the summer months of the second half of the 21^{st} century and a decrease in the winter season (APCC, 2014). Figure 2-3 compares daily ETP values in the period 1961-1990 using input from the eobs-dataset (Haylock et al., 2008) estimated by both methods. Due to (I) radiation-driven processes and (II) the estimation of ETP on a daily basis, the spread of Turc's approach is wider than Thornthwaite's method. Both lead to a similar yearly sum of 390 mm (Turc) vs 410 mm (Thornthwaite).

Calibration of Eq. (2-2) was done according to the mean annual potential evapotranspiration values (Dobesch, 2007) in the hydrological atlas of Austria (Hydrologischer Atlas Österreichs, HAÖ, BMLFUW, 2007).

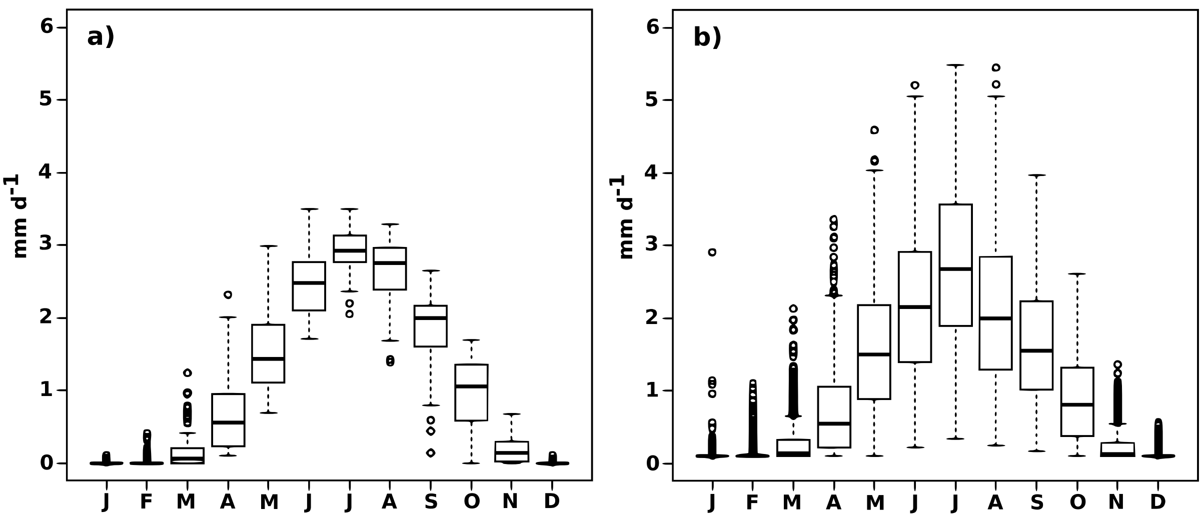

Figure 2-3: Comparison of the estimation methods Thornthwaite (a) and Turc (b). Due to radiation-driven processes, Turc gives higher values for ETP in winter. Also the range of the values is higher because of the generation of daily values while Thornthwaite generates only monthly mean values. Average yearly sums are 390 mm (Turc) and 410 mm (Thornthwaite). Data shown is derived from eobs-data (Haylock et al., 2008) within the period 1961-1990 in the mean catchment elevation of river Salzach.

2.1.3 Snow and ice processes

Ice- and snowmelt are calculated using a simple temperature index model given by Eq. (2-3). Advantages of such an approach are the robustness and the need for knowing only air temperature above the snow pack. A discussion of temperature index melt models is given by Hock, (2003).

$$\Delta SWE_t = \begin{cases} PS_t, & TAIR_t \leq TMELT_t \\ CT_t \times f_{\alpha_t} \times TAIR_t \times CC_t \times f_{asp}, & TAIR_t > TMELT_t \end{cases} \tag{2-3}$$

Where ΔSWE [mm] is the change of snow water equivalent of a snow pack or ice cover at time t, CT is the degree day factor [mm °C^{-1}] that may be lowered by a factor dependent on high albedo values ($f_{\alpha t}$ [-], calculated by Eq. 2-5), $TAIR_t$ [°C] is the air temperature and f_{asp} [-] is a factor for correcting the melt according to the mean aspect of the elevation surface (see Table 2-2). Accounting for inertial processes of the snow pack a cold content (CC_t [-]) is applied to the melt estimation. At air temperature values lower than a certain, time dependent threshold temperature ($TMELT_t$ [°C]) snowfall (PS_t [mm]) occurs.

The relationship between temperature and snowmelt is not constant over the year but is influenced by potential global radiation. Minimum and maximum values therefore occur on the solstices in December and June, respectively (Braun et al., 1994). In between these dates a sine curve is fitted by using Eq. (2-4). Here, Di_i and $Di_{01.01}$ are referring to the number of the day i and first of January, respectively, $iShift$ gives the time shift in days of the sine function and

CT_{AMP} [-] is the amplitude of the sine curve. The same equation is used to adjust the temperature threshold for snowmelt to occur. In this case, variables concerning CT are replaced by those regarding TMELT.

$$CT_t = CT + \left(\frac{\sin(2\pi \times (Di_{01.01} - Di_i) - iShift)}{365}\right) \times CT_{AMP} \tag{2-4}$$

Also the albedo of snow has an influence on the melting behaviour. High values of fresh snow lower the melting rates due to a reduced intake of radiation. The lower the albedo the more radiation can be received and therefore melting rates increase (see e.g. Wiscombe and Warren, 1980). A certain amount of fresh snow (PS_{CRIT} [mm]) is necessary to increase the albedo. Eq. (2-5) estimates this influence of albedo on snowmelt. Here, d_{PS} [d] is the number of days since the last snowfall (PS [mm]) greater than PS_{CRIT} per day occurred and f_{age} [d^{-1}] is an aging constant for lowering the albedo.

$$f_{\alpha_t} = \begin{cases} 1, & PS \geq PS_{CRIT} \\ 1 - exp\left(\frac{-1 \times d_{PS}}{f_{age}}\right), & PS < PS_{CRIT} \end{cases} \tag{2-5}$$

If the air temperature exceeds the threshold temperature snow begins to melt. However, in nature runoff does not occur immediately after a rise of temperature above that threshold. Water may be retained in the snow pack and may even refreeze. More complex models are able to account for that directly. Examples are the COSERO model (Nachtnebel et al., 1993; Stanzel and Nachtnebel, 2010) or explicit snow pack models like SNOWPACK (Bartelt and Lehning, 2002a, 2002b; Lehning et al., 2002). In SASWET the concept of cold content (see e.g. Marks et al., 1999) is used to account for this behaviour. This is done in a relatively easy way, by averaging air temperature values over a period of the last CC_{DUR} days using Eq. (2-6). Only if the average temperature exceeds the threshold temperature for melting snow ($TMELT_t$), snowmelt becomes runoff. CC_{DUR} has values of the magnitude of one to three weeks.

$$CC_t = \sum_{i=t-CC_{DUR}}^{t} \frac{TAIR_i}{CC_{DUR}} \tag{2-6}$$

Even though SASWET is a semi-lumped model and cannot consider differences in small scale topography but uses elevation bands for a spatial disagregation, it considers the mean facing of such an elevation band. Due to a surplus on solar radiation, snow on south facing slopes generarily melts faster than on east and west facing slopes. Shading on north facing surfaces causes these slopes to show the most inertial melting behaviour (Garvelmann et al., 2013; Pohl et al., 2014). Factors for considering faster or slower melting are given by Table 2-2.

Table 2-2: Correction for melt behaviour caused by the aspect of a slope.

Aspect	N	NE	E	SE	S	SW	W	NW	Flat
f_{asp}	0.7	0.8	1	1.3	1.5	1.4	1.1	0.9	1.2

In addition to snowmelt, SASWET considers glaciers. These are treated as surfaces with an infinite depth. A similar approach was used by Schaefli et al. (2005) in the development of the GSM-SOCONT model. Spatial information are received from the Austrian Glacier Inventory (Kuhn et al., 2013; Lambrecht and Kuhn, 2007). The same subdivision for elevations is used for the construction of the glacier DEM as for the DEM of the catchment. All glaciers and parts of glaciers in a watershed are united into one glaciated area. A prerequisite for glacier melt is a full depletion of the snow cover overlying the glaciated surface. If the air temperature rises above TICE, glacier melt is computed using the same approach as snowmelt (Eq. 2-6).

Crucial for the survival of a glacier is an even or positive mass balance. If more snow is accumulated during winter than is melted during the warm summer months a glacier can grow. On the other hand, if accumulation in winter is smaller than melt in summer, the glacier loses mass and shrinks. An even mass balance leads to a glacier being in equilibrium meaning that its mass remains the same. On the lower, warmer parts a glacier loses more ice than it gains whereas in high, cold elevations, more ice can be accumulated than is lost. At least since 1946 the vast majority of European glaciers have a negative mass balance (EEA, 2014, see Figure 2-4) and according to Habersack et al. (2011) they will disappear in the alps by the year 2100 in elevations lower than 3000 m a.s.l. To account for that, glaciated areas are reduced linearly until the end of the century. 70 % of the reduction occurs on the lowest glaciated elevation surface, the other 30 % influence the total glacier area below 3000 m a.s.l. However, neither growth nor movement of glaciers are considered in the model concept.

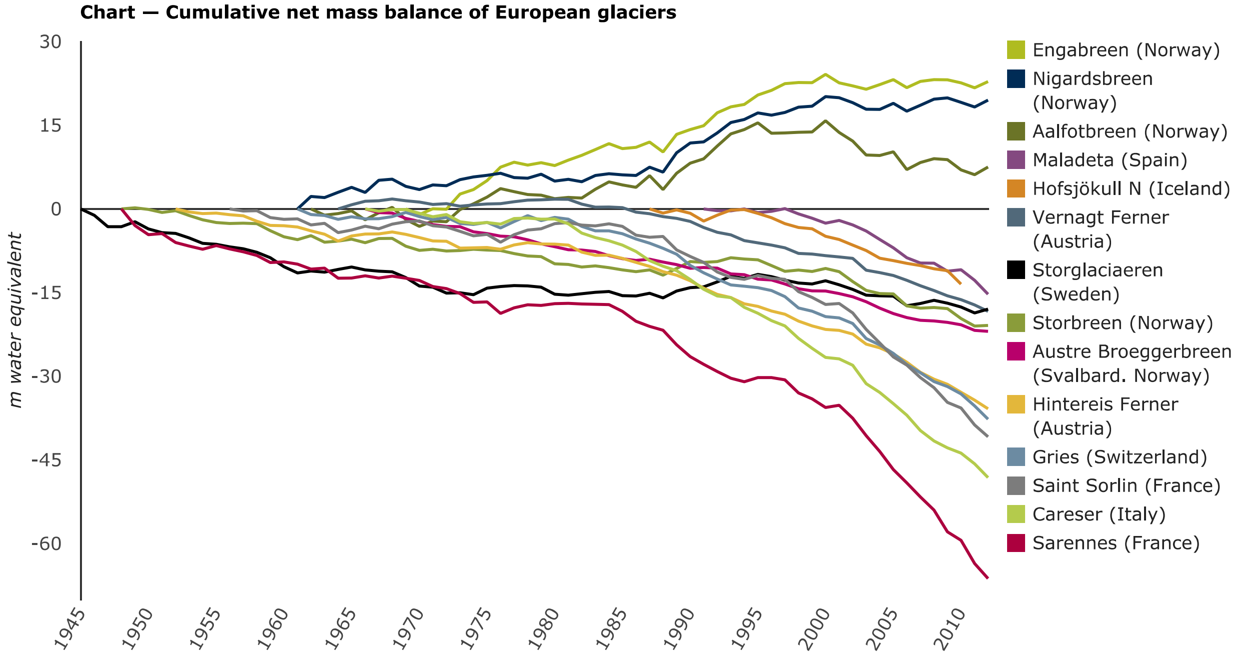

Figure 2-4: Cumulative net mass balance of European glaciers in the period 1946–2012. After (EEA, 2014), edited.

2.1.4 Dealing with snow accumulation in the upper altitudes

The use of a temperature index melt model has the advantage of being quite simple since it uses only the temperature as input to determine whether precipitation occurs in the form of snow or rain and whether snow can be melted or not. A disadvantage of this approach is that snow accumulates as long as the air temperature does not rise above a certain threshold. In high mountainous areas this may be the case for most days during the year leading to an intensive accumulation of snow in these areas.

To avoid such model behaviour, a simple approach has been developed to deal with accumulations of snow in high elevations using only three parameters for redistributing snow (Figure 2-5). Adjusting parameter $DIST_{DON}$ the modeller can set the elevation zones functioning as a donor of snow, $DIST_{ACC}$ gives the number of zones that act as an acceptor of snow and via the third parameter $DIST_{SHAPE}$ the shape of the redistribution function can be set.

Figure 2-5 illustrates the distribution routine which applies to elevation zones i, where lower values of i indicate higher elevation levels. Redistribution of snow takes place during the precipitation event itself. Thus it may be considered as a function of changing the amounts of solid precipitation. On the peak zone of the mountainous region (i = 1) a portion of snow according to the inverse of the parameter $DIST_{ACC}$ accumulates (PSA_i) whereas the rest (PSD_i) is redistributed to lower levels. Lower elevation zones may function as a donor and an acceptor of snow at the same time if $DIST_{DON}$ is set to larger values than one. These zones gain a portion of snow from higher altitudes according to their elevation level and the parameters $DIST_{ACC}$ and

$DIST_{SHAPE}$. In Figure 2-5 n indicates the elevation level right above the actual level i and m describes the elevation zones contributing to snow redistribution for that certain level i, maximum to the peak zone of the catchment. Since those zones act as a donor as well a portion of snow PSD_i takes part in the redistribution process, too. Elevation levels nested underneath the threshold given by parameter $DIST_{DON}$ but still in reach of $DIST_{ACC}$ just benefit from snow from higher levels. Elevation zones underneath the level given by parameter $DIST_{ACC}$ do not take part in the redistribution process.

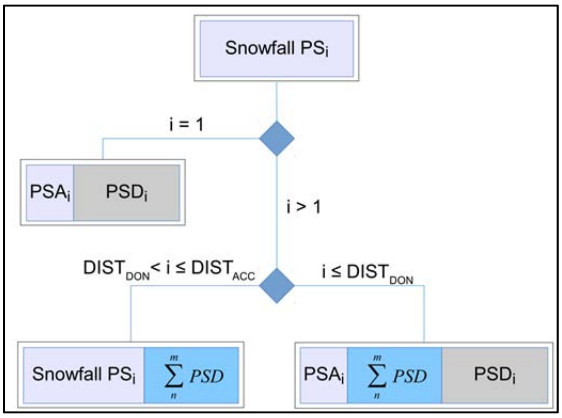

Figure 2-5: Scheme of how the snow distribution routine works. Grey colour indicates snow that is transported to lower levels, blue stands for snow being deposited on that certain area from higher levels and bluish grey indicates snow that is deposited from precipitation without redistribution. $DIST_{ACC}$ and $DIST_{DON}$ are parameters to adjust the number of elevation levels (i) receiving and donating snow, respectively.

In addition to the number of surfaces accepting and receiving snow, the shape of the redistribution function can be set. Here the modeller can chose from three shapes: a) equal distributed, b) linear increasing and c) linear decreasing (see Figure 2-6). Equally distributed snow redistribution means that, with respect to one donor zone, all acceptor zones receive the same amount of snow. Linear decreasing transports more snow to elevation surfaces next to the donor level whereas an increasing distribution transports more snow to elevation levels located further downhill to the donor zone. The concept of all three distribution shapes is indicated in Figure 2-6a while Figure 2-6b shows the result of all redistributions without accounting for melt processes. A useful parametrization of the snow redistribution can be the tree line. In the Alps it normally is situated on elevations between about 1900 and 2200 m a.s.l. (Szerencsits, 2012), but may rise in a warming climate (Gehrig-Fasel et al., 2007; Leonelli et al., 2010). However, since the climatic tree line is already higher than the actual tree line (Leonelli et al., 2010) this possible rise is not considered in the model.

This snow redistribution model is implemented in the snow routine of SASWET and is used in all basins having some regions above the tree line. An explicit study testing the behaviour of the model was carried out in the catchment of Salzach River. The results of this study are given in chapter 6.2.

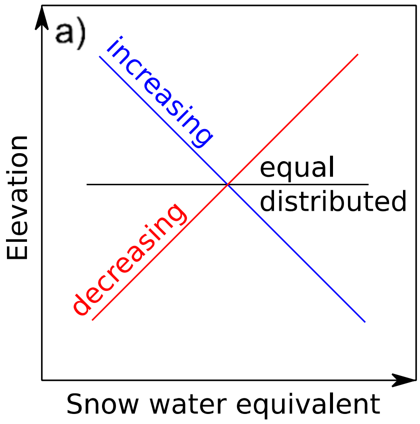

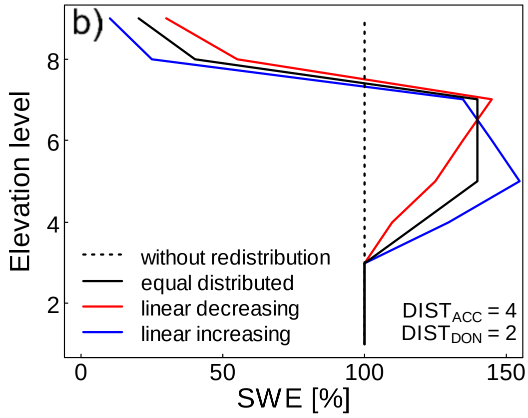

Figure 2-6: a) Different redistribution shapes in respect to one donor level. b) Differences in snow distribution caused by the redistribution routine. $DIST_{ACC}$ and $DIST_{DON}$ give the number of elevation surfaces donating and receiving snow, respectively.

2.1.5 Runoff generation

Total discharge (Q) at the outlet of the modelled basin is the sum of all runoff generation processes of one time step given by Eq. (2-7), where Q_{HOF} and Q_{SOF} represent overland flow (hortonian and saturation excess, respectively), Q_{SSF} is interflow, Q_{GWF} is baseflow and Q_{MELT} represents direct runoff from ice- and snowmelt.

$$Q = Q_{HOF} + Q_{SOF} + Q_{SSF} + Q_{GWF} + Q_{MELT} \tag{2-7}$$

2.2 The semi-distributed Model WaBi

Based on SASWET WaBi (<u>Wa</u>sser<u>Bi</u>lanz Model, German for water balance model) was designed during the work on this thesis. This model is even simpler and consists of only two storages. Like SASWET it is semi lumped in the sense that temperature driven processes are calculated on elevation levels. But unlike SASWET these levels have vertical differences of 500 m. A flow chart of the model is illustrated in Figure 2-7 where interlaced fields signal elevation dependent model components. Input data required for the model are only mean precipitation in the catchment and information about the temperature in up to seven elevation levels, namely 250 m, 750 m, 1250 m, 1750 m, 2250 m, 2750 m and 3250 m a.s.l. These levels match the subdivision of elevation surfaces in the model allowing a direct use of temperature information without the need for interpolation between levels.

The model can be considered as an “as simple as possible” approach to reproduce the long term (i.e. several years) water balance of a catchment or model area. To accomplish this, a temporal resolution of months is sufficient. However, since the model is applied to mountainous regions, snow and ice processes need to be calculated with higher temporal resolution. Although the internal time step is days, the model output nevertheless is months. Altogether only five parameters are necessary to calibrate the model. These are listed in Table 2-3.

Table 2-3: Parameters necessary to calibrate WaBi

Parameter	**Description**	**Units**
k_{one}	k-value of reservoir one	mm^{-1}
k_{two}	k-value of reservoir two	mm^{-1}
CT_{snow}	degree day factor for simulating snowmelt	$mm\ °C^{-1}$
CT_{ice}	degree day factor for simulating ice melt	$mm\ °C^{-1}$
C_{ETP}	Coefficient to correct evapotranspiration	[%]

WaBi is used for the estimation of climate change impacts on the hydrological cycle in European regions in France, Germany, Switzerland and Italy together with an uncertainty analysis of the model parameters and the uncertainty caused due to the use of different climate models.

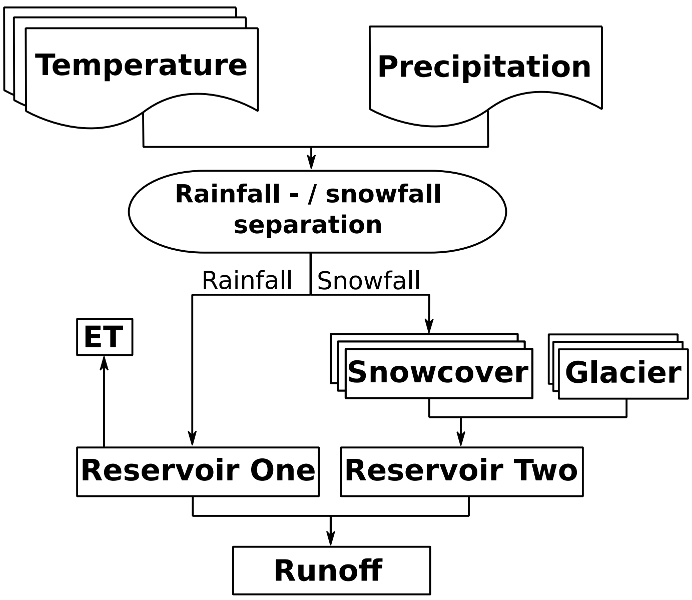

Figure 2-7: Flowchart of the conceptual water balance model WaBi. Snow and ice processes are calculated using a temperature index method. Since air temperature changes inter alia depending on the elevation, processes depending on air temperature values are calculated upon 500 m elevation levels. These model components are interlaced.

2.2.1 Evapotranspiration

Since only temperature data is available for this study, ETP is estimated using the Thornthwaite method given by Eq. (2-8), where L is the day length in hours, N is the number of days in the month being calculated, T_a is the monthly mean temperature (0 if negative) and I is the heat index of the respective month.

$$ETP = 1.6 \times \left(\frac{L}{12}\right) \times \left(\frac{N}{30}\right) \times \left(\frac{10 \times T_a}{I}\right)^{\alpha} \tag{2-8}$$

with

$$\alpha = (6.75 \times 10^{-7}) \times I^3 - (7.71 \times 10^{-5}) \times I^2 + (1.792 \times 10^{-2}) \times I + 0.49239 \tag{2-9}$$

and

$$I = \sum_{i=1}^{12} \left(\frac{T_{ai}}{5}\right)^{1.514} \tag{2-10}$$

Evapotranspiration is draining reservoir one. As long as there is enough water stored in this reservoir, actual evapotranspiration is assumed equal potential evapotranspiration.

2.2.2 Snow and ice

Hydrological processes regarding snow and ice are calculated by a simple degree day method given by Eq. (2-11) where CT is the degree day factor (different for ice and snow), TAIR is the air temperature and TMELT is the threshold temperature above which melt occurs. Ice- and snowmelt is collected by reservoir two which may be interpreted as storage of the ice and snow cover.

Glacier surfaces are derived from version 3.2 of the Randolph Glacier Inventory (Arendt et al., 2012) and glaciers are treated as infinite ice storages. To account for deglaciation glacier surfaces are linearly reduced to zero below 3250 m a.s.l. until the year 2100.

$$\Delta SWE_t = \begin{cases} PS_t, & TAIR_t \leq 0 \\ CT \times TAIR_t, & TAIR_t > 0 \end{cases} \tag{2-11}$$

Accumulation of snow in high elevations is problematic in WaBi as well as it is in other models using temperature driven melt models. To keep the model as simple as possible, snow situated on the highest elevation level (i.e. above 3250 m a.s.l.) is transferred to the subjacent level where temperature values relatively often rise above the threshold temperature allowing snow to melt.

2.2.3 Runoff generation

Discharge is simulated as the sum of the outflows of reservoir one and two, which are represented by linear storage concepts. Both reservoirs are parametrized using Eq. (2-12) with the respective k-values. Here h refers to the storage state of the respective reservoir. Inflow due to precipitation or melt (Q_{in}) and subtraction of ETA are calculated before estimating the outflow.

$$Q = (h + Q_{in} - ETA) \times exp\left(\frac{1}{k}\right) \tag{2-12}$$

2.3 The COSERO Model

Contrary to the models already introduced, COSERO is a raster-based rainfall runoff model. A flow chart of the model components is given in Figure 2-8. Originally developed for modelling discharge of the Austrian rivers Steyer and Enns by Nachtnebel et al. (1993) it has recently been used for different purposed like climate change impact studies (e.g. Kling et al., 2014; Stanzel and Nachtnebel, 2010), investigating evapotranspiration processes in high alpine regions (Herrnegger et al., 2012) or operational flood forecasting (Stanzel et al., 2008). Besides that Herrnegger et al. (2014) used the model to estimate precipitation amounts on the basis of measured discharge rates. A detailed description of the model can be found in (Kling et al., 2014a) who applied the model to several catchments in Africa, Australia and Europe but did not calibrate snow parameters. Therefore the snow processes are not described in detail by Kling et al. (2014a).

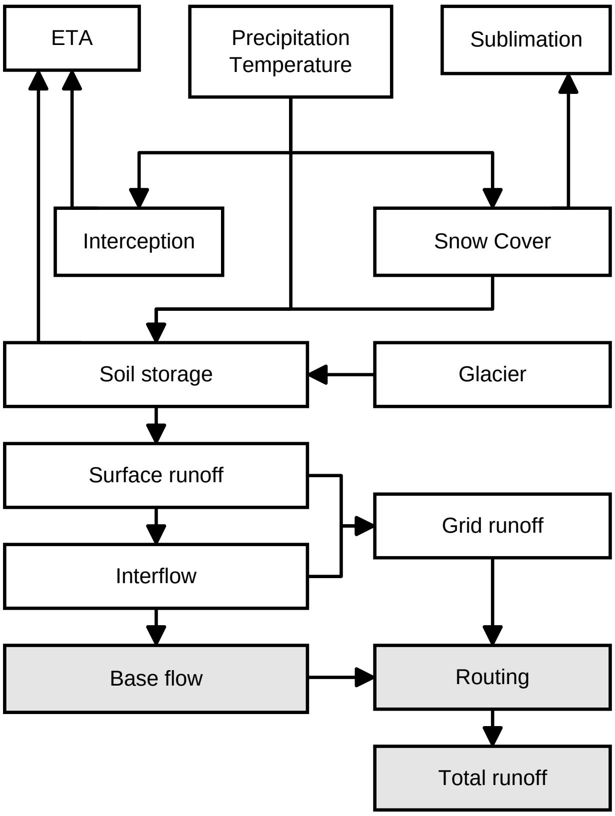

Figure 2-8: Flowchart of the model COSERO (after Frey and Holzmann (2015)). Greyish components are treated on a (sub-)basin scale, white components are distributed based on a 1 x 1 km raster.

For the presented study, the model was improved regarding the snow routine that, besides other small changes, has been extended by a snow redistribution routine (Frey and Holzmann, 2015).

A brief summary (based on the paper by Frey and Holzmann 2015) of the snow routine and the changes made is given in the following.

2.3.1 Snow cover processes

Numerous studies have shown that sub-grid variability of snow depths can be described by a two parameter log-normal distribution (e.g. Donald et al., 1995; Pomeroy et al., 1998). This distribution can be interpreted as a description of snow distribution processes taking place at scales smaller than the 1 x 1 km resolution used by COSERO, i.e. influence of curvature, shelter or vegetation (Hiemstra et al., 2006). According to Liston (2004) these may be caused by differences in the canopy density due to different species like evergreen gymnosperms or clear deciduous trees as well as by wind. The latter causes snow to be transported from the exposed side of ridges to their respective lee sides, depressions and vegetation covered areas (Essery et al., 1999). COSERO uses five snow classes per cell to approximate this lognormal distribution under accumulation conditions, i.e. snowfall is distributed log-normally into these snow classes. Each of these classes acts autonomously in the sense of melting, refreezing and sublimating. The following equations are solved for each snow class separately. Snow redistribution between the classes of one raster cell is not considered in the model. A scheme of the composition of a snow class is illustrated in Figure 2-10. The snow water equivalent (SWE) at a given time t of each class is calculated using Eq. (2-13), where PR and PS are liquid and solid precipitation, respectively, M is snowmelt and ETPS is sublimation of snow estimated by Eq. (2-14) where ETR is a factor that lowers the value of potential evapotranspiration (ETP).

$$SWE_t = SWE_{t-1} + PR_t + PS_t - M_t - ETPS_t \qquad (2\text{-}13)$$

$$ETPS_t = ETP_t \times ETR \qquad (2\text{-}14)$$

Sublimation is calculated for snow covered snow classes only. Hence, fully depleted snow classes enhance the evapotranspiration of a partly snow covered cell. Snow free snow classes may exist due to snow melt or predestination because of steep slopes. Slope angles greater than 45° are considered unable to hold any snow (see e.g. Sovilla et al., 2010) and therefore are snow free regardless of the SWE in the total cell. In Figure 2-9 an example of partitioning a cell into five snow classes is illustrated for a mountainous region (Figure 2-9 a).

The hatched parts in Figure 2-9 b) are assumed to be part of another raster cell and therefore do not take part in this description. The parts being snow free are steeper than 45° (reddish coloured area in Figure 2-9 b). These parts are recognized by the model by a pre-processing step (using a high resolution DEM in any GIS software). The model will round the fraction of steep areas to the next 20 % given by one of the five snow classes. Assuming these parts cover about 11 to 30 percent of the area covered by the grid cell (assuming the viewer does not stand at the edge of the cell but somewhere inside and therefore does not have an overview about the entire cell) the model identifies one snow class to be not capable of holding any snow. Precipitation in the form of snow then is subdivided into the remaining four snow classes. In Figure 2-9 b) and c) the reddish coloured class is not capable of holding snow. Snow therefore is subdivided into four classes in a log-normal distributed way. Figure 2-9 c) shows the log-normal distribution of snow depths (in mm SWE) between the four remaining snow classes.

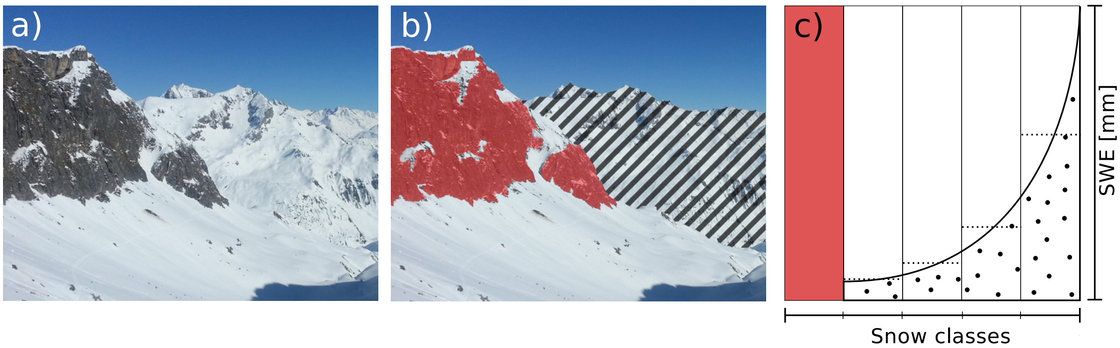

Figure 2-9: Determination of predestined snow free snow classes in COSERO. A mountainous area (a) is divided into raster cells. The hatched parts in b) are assumed to be part of another raster cell, the reddish parts are as steep or steeper as 45° and therefore are unable to be covered by snow. c) is a view of the raster cell covering the terrain of a) and b) where one of five snow classes is snow free. But c) also shows the log-normal distribution of snow depth between the four remaining snow classes. Dashed lines indicate the snow depths used by the model. Every class is composed in the way illustrated in Figure 2-10. Note that the log-normal distribution may be disrupted by melt processes or by redistributing snow to other raster cells. Dispersal between the snow classes of one grid cell does not occur. Photograph is own work.

Snowmelt is calculated using a temperature index melt method. This method is more complex than both melting models implemented in the other hydrological models SASWET and WaBi. Snowmelt, computed by Eq. (2-15), not only depends on the degree day factor (CTA) and the air temperature ($TAIR_t$) but also on an energy input by rain (ε). The temperature of rainwater is assumed to be equal the air temperature. Similar to SASWET, values of CTA describe a sine curve (Eq. 2-16) with the maximum and minimum on the respective solstices. In Eq. (2-16), JD is the Julian day of a year CT_U and CT_L are the upper and lower boundaries of CTA, respectively, and MRED is a reduction factor to account for the higher albedo caused by freshly fallen snow calculated by Eq. (2-17).

$$M_t = min(SWE_t; PR_t \times \varepsilon \times TAIR_t + CTA_t \times TAIR_t) \tag{2-15}$$

$$CTA_t = \left(-cos\left(JD \times \frac{2\pi}{365}\right) \times \frac{CT_U - CT_L}{2} + \frac{CT_U - CT_L}{2}\right) \times MRED_t \tag{2-16}$$

With

$$MRED_t = \begin{cases} CTRED, & SD \geq CSD \\ MRED_{t-1} + \frac{(1 - MRED_{t-1})}{5}, & SD < CSD \end{cases} \tag{2-17}$$

Where CSD is the critical snow depth of fresh snow in mm necessary to increase the albedo and SD is the actual snow depth of fresh snow in mm. For fresh snow depth larger than CSD, CTA is lowered to a reduced melting factor CTRED.

Additionally, the model treats snow pack as a porous medium capable of holding a certain amount of water. This water holding capacity is dependent on the depth of the snow pack as well as its density ρ (see Eq. 2-18). Furthermore, liquid water stored in the snow pack may refreeze in the snow layer if the air temperature after a melting period again drops below the threshold necessary for inducing snowmelt. For the estimation of refreezing Eq. (2-19) is used, where SRP is the amount of refrozen water and CTN is a refreezing factor similar to the snowmelt factor CTA. Needless to say that the amount of refreezing water is limited by the amount of liquid water stored in the snow pack.

$$WH_t = (SWE_t - WH_{t-1}) \times \left(WHC_{MAX} - (\rho_t - \rho_{MAX}) \times WHC_\rho\right) \quad (2\text{-}18)$$

$$SRP = CTN \times \left(TAIR_t \times (-1)\right) \quad (2\text{-}19)$$

Fresh snow has a density that depends on the air temperature the day snowfall occurs. Its density is computed by a sigmoid function given by Eq. (2-20), where the minimum density (ρ_{MIN}) has the value 0.1 g cm^{-3}. This value can often be found in literature (see e.g. Elder et al., 1991; Judson and Doesken, 2000) although some report lower values. The maximum density (ρ_{MAX_NEW}) of fresh snow is assumed to be 0.3 g cm^{-3}, a value that is also used by SnowTran (Prasad et al., 2001).

$$\rho = (\rho_{MAX\_NEW} - \rho_{MIN}) \times \left(\frac{T_{tr}}{\sqrt{1 + (T_{tr})^2}} + 1\right) \times 0.5 + \rho_{MIN} \quad (2\text{-}20)$$

With

$$T_{tr} = \frac{TAIR_t}{\rho_{scale}} + T_{scale} \quad (2\text{-}21)$$

In Eq. (2-21) $TAIR_t$ is the air temperature at the given time step t, ρ_{scale} scales the x-axis and T_{scale} scales the y-axis. Both ρ_{scale} and T_{scale} have fixed values.

Once fallen, snow can reach higher densities. The settling of the snowpack is calculated by Eq. (2-22) (derived from Riley et al., 1973), where ρ_{SET} is the settlement constant, SWE is the snow water equivalent ρ_{MAX} is the maximum density of the snow pack and SH is the snow depth.

$$\rho_{MAX} = \frac{\rho_{SET} \times \left(\frac{SWE_t}{\rho_{MAX}} - \frac{SH_t}{2} + SH_t\right)}{1 + \frac{\rho_{SET}}{2}} \quad (2\text{-}22)$$

The maximum density of the snow pack is estimated a priori. A value of 0.45 g cm^{-3} is assumed which matches the density reported by other authors (Jonas et al., 2009; Schöber et al., 2014).

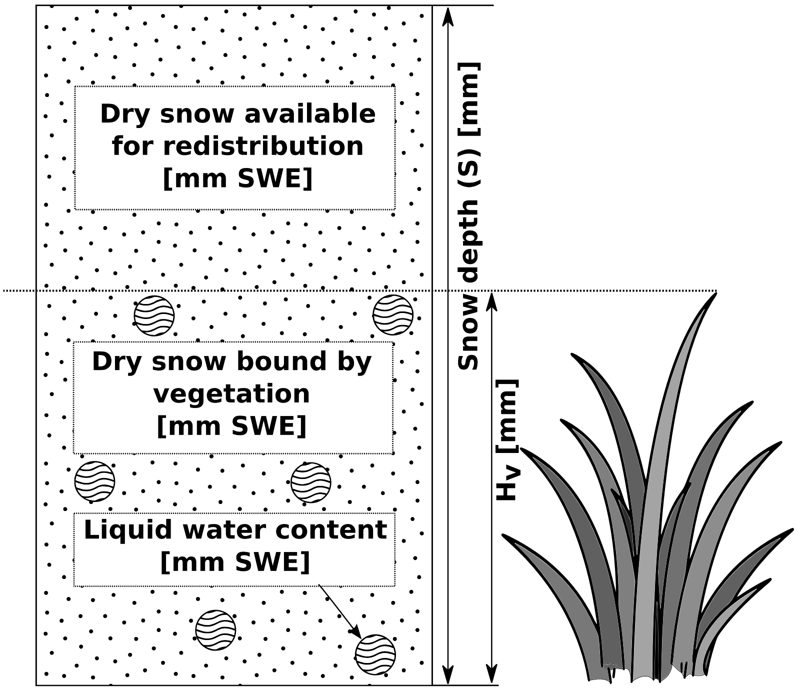

Figure 2-10: Concept of the snow cover in COSERO (after Frey and Holzmann (2015), edited). Each raster cell consists of five snow classes (see Figure 2-9) each of which is composed in the shown way but acts autonomously regarding refreezing, melting and sublimating. Snow classes within one cell may differ in all properties but vegetation cover (H_v).

2.3.2 Dealing with snow accumulation in high elevations

Since COSERO uses a temperature index method for modelling snow melt, snow accumulates in high elevations, where air temperature values seldom rise above the melting temperature of snow. A redistribution routine was developed to prevent this behaviour. The development and testing of this redistribution has been published by Frey and Holzmann (2015). In the following, a brief summary is given of how the model works. Results can be found in chapter 6.3.

Numerous authors reported the slope angle has an important influence on snow depths (Bernhardt and Schulz, 2010; Kirchner et al., 2014; Schöber et al., 2014). Since other geomorphological properties than slope angle influencing snow patterns are most important on scales smaller than the grid size of COSERO (1 x 1 km), slope was selected as driving force for the model. One has to be aware that this is a simplification and under realistic conditions snow might not necessarily be transported only on the steepest route (Bernhardt and Schulz, 2010; Winstral et al., 2002). The model redistributes snow from a given cell to its adjacent cell with the steepest (downward) slope. Uphill transport is not considered in the model. A scheme of the transport model is shown in Figure 2-11. Redistribution within the snow classes of one single cell is impossible. In the following, the cell distributing snow is referred to as donor cell the one receiving snow will be addressed as acceptor cell. If the snow depth of the donor cell (SH_D) exceeds the threshold for vegetation (H_V) snow redistribution is activated using Eq. (2-23). The actual amount of snow being redistributed (SWE_A) depends on the slope angle (α), the density of snow (ρ_t), the type of land cover of the donor cell and the snow depth on the donor cell. The model can be adjusted by the correction factor C. This is necessary to prevent unrealistic accumulation on (flat) grid cells that receive snow from more than one higher elevated grid cell. Less dense snow can be transported easier than wet, dense snow. If more than one neighbour cell features the same (steepest) slope, redistributed snow will be partitioned equally between the numbers of acceptor cells (A). The relationship between slope, snow density and redistribution given by Eq. (2-24) and is visualized in Figure 2-11.

$$SWE_A = max(SH_D - H_V; 0) \times f_\rho \times \frac{1}{\sum A} \times C \qquad (2\text{-}23)$$

With

$$f_\rho = \left(\frac{(\rho_{MAX} - \rho_t)}{\rho_{MAX}} \times e^{\left(-\frac{\rho_t}{\rho_{MAX}}\right)}\right) \times \frac{\alpha}{90} \qquad (2\text{-}24)$$

The routine is organized in the form of a loop starting at the highest cell in the catchment and ending at the lowest point. Consequently, snow cannot be transported uphill and transport of snow into already processed grid cells can be avoided.

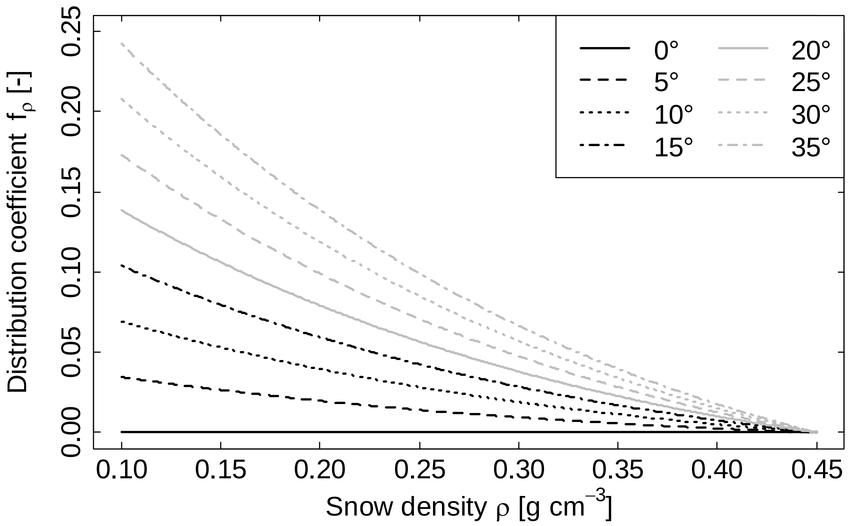

Figure 2-11: Relationship between slope angle, snow density and redistribution of snow.

Transported snow is treated in the same way as fresh snow in the sense that it is distributed to the snow classes of the acceptor cell according to the log-normal distribution. Its density is estimated in dependency of the air temperature of the acceptor cell using Eq. (2-20). If the temperature of the air mass above the acceptor cell is higher than the melting temperature, redistributed snow is treated as liquid precipitation.

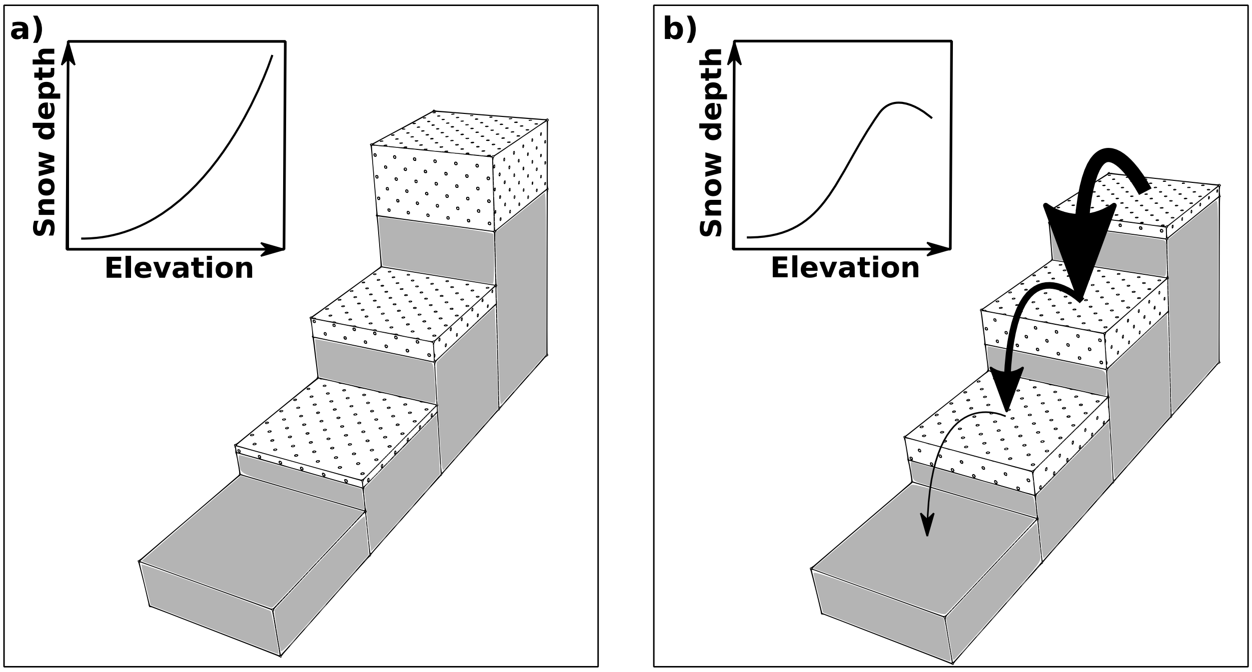

Figure 2-12: Conceptual snow accumulations in mountainous regions without (a) and with (b) considering lateral snow transport processes. Dotted blocks represent exaggerated snow accumulations. Applying the redistribution model snow is transported from the highest grid cell to its neighbour where it is treated like solid precipitation. From this grid cell a portion of snow gets transported to the downward neighbour again and so forth until either the terrain is too flat or snow depth do not exceed the threshold for vegetation (see Figure 2-10). Consequently less snow remains in the summit region whereas lower grid cells show enhanced accumulation. Underneath the melting level snow does not accumulate due to melting. This behaviour is sketched in the plots in both a) and b). Although snow depths in the summits are reduced due to redistribution, the amount of snow covered cells remains similar.

COSERO and especially its snow module is indeed rich of parameters. This obviously enhances the problem of equifinality. To counteract such behaviour, some of the parameters are estimated a priori. Due to the study's focus on snow processes only the snow relevant parameters are listed in Table 2-4. Note that the snow redistribution routine only adds two parameters (H_v and C) of which one is estimated a priori (H_v). All other parameters used in this module have already been established previously.

Table 2-4: Parameters used by the snow module of COSERO. While the model consists of many parameters, the majority of those used in the snow module are estimated a priori. Note that the snow redistribution model only adds two parameters of which one is also estimated a priori.

Parameter	**Description**	**Value**	**Units**	**a priori**
ETR	Factor reducing ETP to sublimation	0.3	-	X
CT_U	Upper bound of snow melt factor	4 - 7	mm °C^{-1} d^{-1}	
CT_L	Lower bound of snow melt factor	0.5 - 3	mm °C^{-1} d^{-1}	
CTRED	Factor accounting for higher albedo caused by fresh snow	0.7	-	X
WHC_{MAX}	Maximum water holding capacity of snow	0.1	g cm^{-3}	X
WHC_{ρ}	decrease of WHC with increasing snow density	0.0015	1 g^{-1} cm^{3}	X
CTN	Refreezing factor of liquid water in the snow pack		mm °C^{-1} d^{-1}	X
ρ_{MIN}	Minimum density of snow	0.1	g cm^{-3}	X
ρ_{MAX_NEW}	Maximum density of (freshly fallen) snow	0.3	g cm^{-3}	X
ρ_{MAX}	Maximum density of (already laying) snow	0.45	g cm^{-3}	X
ρ_{SCALE}	Scaling coefficient for estimating the snow density (Y-axis)	1.2	-	X
T_{SCALE}	Scaling coefficient for estimating the snow density (X-axis)	1	-	X
H_V	Threshold of vegetation or land cover holding snow	See Table 5-5	mm*	X
C	Factor for adjusting snow redistribution	0.2 - 3	-	
RAINTRT	Threshold above which precipitation is considered as pure rain	1 - 4	°C	X
SNOWTRT	Threshold below which precipitation is considered as pure snow	-1 - 0	°C	X
NVAR	Variance for distributing new snowfall with a log-normal distribution	0.5 - 1.5	-	X

* unlike the CT values H_V has the dimension mm meaning snow depth not SWE

3 Site descriptions

In Austria ten basins have been modelled using SASWET. The aim of modelling was to study possible impacts of climate change on the water balance and subsequently on the hydropower potential in these basins. The basins have been selected according to their relevance for the hydropower stations operated by VERBUND AG. Also the modelling of the five regions located in the Western Alps using the model WaBi was done in cooperation with VERDBUND AG. Since a simple snow redistribution model has been developed for the use in SASWET, this model has been tested in the catchment of Upper Salzach. Therefore this catchment is described in more detail than the other Austrian catchments. The work using WaBi had the aim of studying climate change impacts on the hydropower potential but in addition an uncertainty analysis of both the hydrological model and the uncertainties arising from the use of different climate model was done. In addition to the two climate change impact studies, a snow redistribution model has been developed for the use in COSERO. This model has been applied to the catchment of Ötztaler Ache in Tyrol, Austria.

In the following the catchments modelled using the three hydrological models SASWET, WaBi and COSERO are described. Their hydrological characteristics can be found in chapter 4.1.

3.1 Basins modelled with SASWET

Ten catchments located mainly in Austria and Southern Germany are modelled with SASWET. Aim of the modelling was an estimation of influences of climate change scenarios on the water balance with respect to hydropower potential in these basins. An overview of these watersheds is provided by Figure 3-1 and a summary of their hydrological characteristics is given in Table 4-1. In Figure 3-1 the coloured borders refer to a clustering of the basins. The clusters attend to a classification to regionalize parameters found to non-explicitly modelled basins (see Table 3-1). This was part of a study done by the Institute for Meteorology of the BOKU but is not part of this thesis. The classification into five clusters is given by Table 3-1. Annual discharge values of these watersheds are illustrated in Figure 4-1 in the order of the clusters. Cluster one refers to row one, cluster two to row two and so forth.

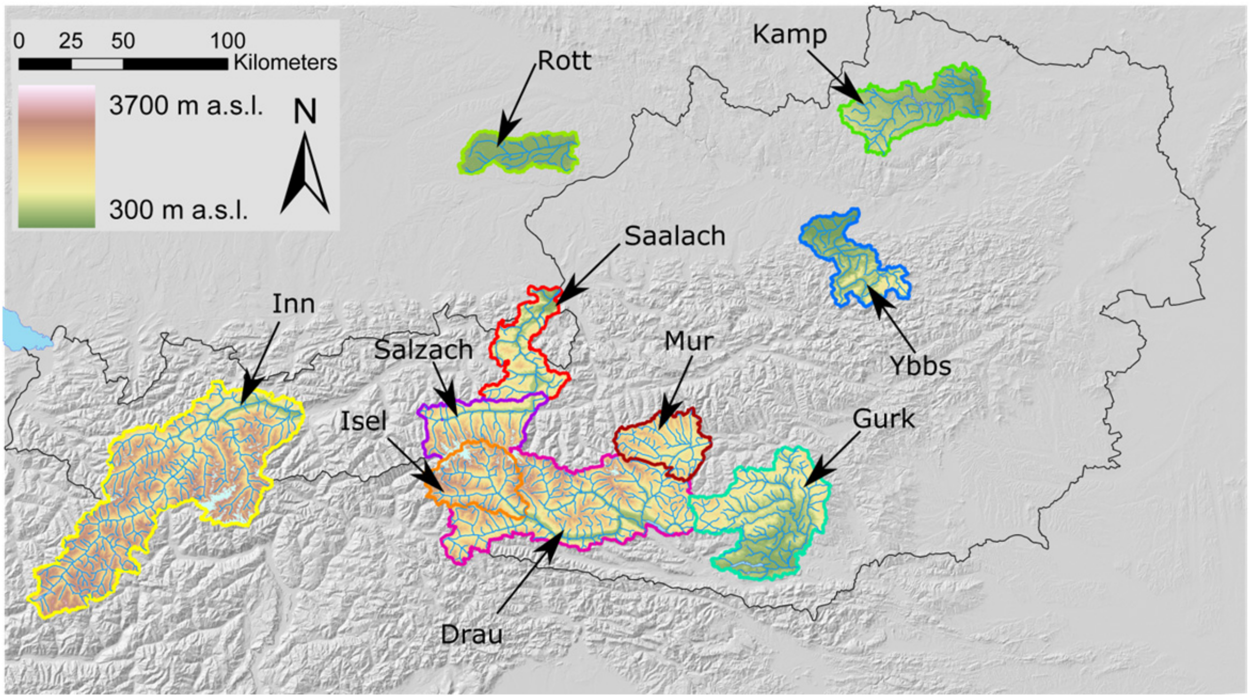

Figure 3-1: Overview map of the ten catchments modelled using SASWET. Greenish colours refer to cluster 1, bluish colours to cluster 2, reddish are cluster 3, 4 and 5 are represented by violet and orange colours, respectively.

Table 3-1: Classification of the basins into five clusters. (Modelled basins are marked with an asterisk)

Cluster	**Basins**
Hill country (1)	Kamp*, Rott*
Alpine upland (2)	Gurk*, Isar, Mangfall, Mürz, Sulm, Traun, Vellach, Ybbs*
Limestone Alps (3)	Enns, Gail, Lech, Mur*, Saalach*
Tauern (4)	Drau*, Lower Salzach, Upper Salzach*, Sill
Nival (5)	Inn*, Isel*, Ziller

River Isel is a tributary to river Drau. Both are modelled in this study. To avoid redundancy, the catchment of river Drau is modelled without considering the Isel watershed. Instead, model results from Isel are added to the results of Drau.

3.1.1 Case study of snow transport in the Upper Salzach basin

In chapter 2.1.4 treatment of snow accumulation in high elevations is described. This procedure is applied to all Austrian catchments that are high enough for the problem to occur. However, a case study about the impact of this model routine is carried out in the basin of Salzach shown in Figure 3-2.

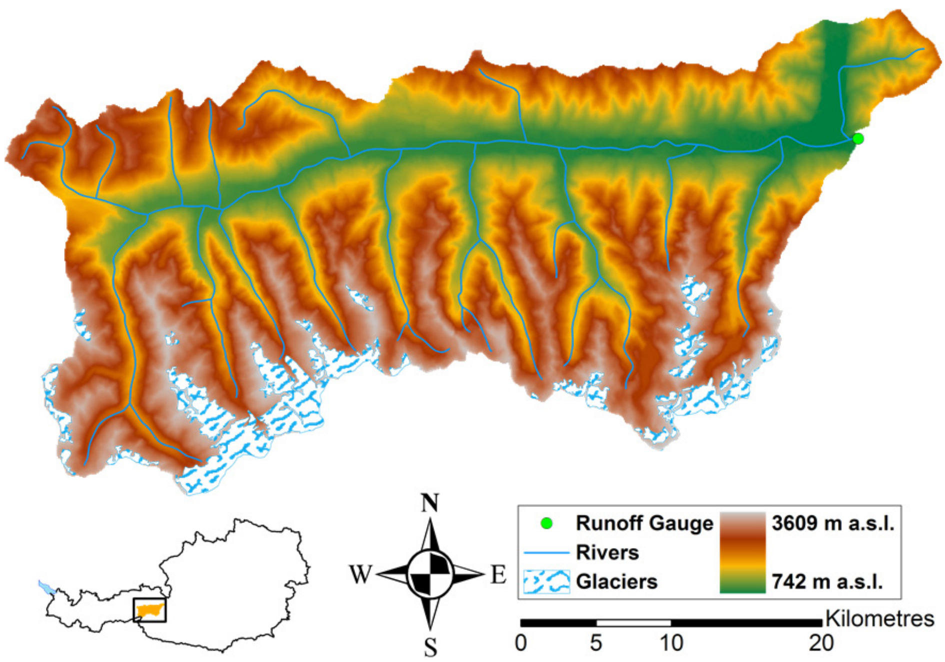

Figure 3-2: Detailed look at the Upper Salzach basin until gauge Bruck (Frey and Holzmann, 2013, edited). This basin is location for the case study of snow redistribution in SASWET.

3.2 Areas modelled with WaBi

WaBi is used to model areas in Western Europe. These areas were chosen to cover the most important sites of hydro power plants with respect to the national states Germany, Switzerland, France and Italy. Hydro power sites need some gradient in elevation. Therefore they are located mainly in mountainous regions. The Alps provide such conditions. Modelled areas regarding Italy and Germany are located in the Alps. Additionally to the French basin of river Rhône, a modelled area located in the Massif Central was selected. Figure 3-3 presents a map and summarizes the geographic characteristics of the modelled regions.

Discharge gauges where selected on the basis of available discharge data from the Global Runoff Data Centre (GRDC, 2013). While the modelled areas of river Rhine and Rhône match with the respective watersheds, the regions of northern Italy and Massif Central do not match a particular basin. Lake Como and Lake Maggiore with their respective outflowing rivers Adda and Ticino are used as proxy for the region of northern Italy. Gauges located downstream of lakes are greatly influenced by the lakes acting as buffers. In the Massif Central, runoff gauges are located at the rivers Maronne and Tarn. To fit the model for the total region, the respective gauges have to be comparable. This is tested by the relative discharge in the respective regions.

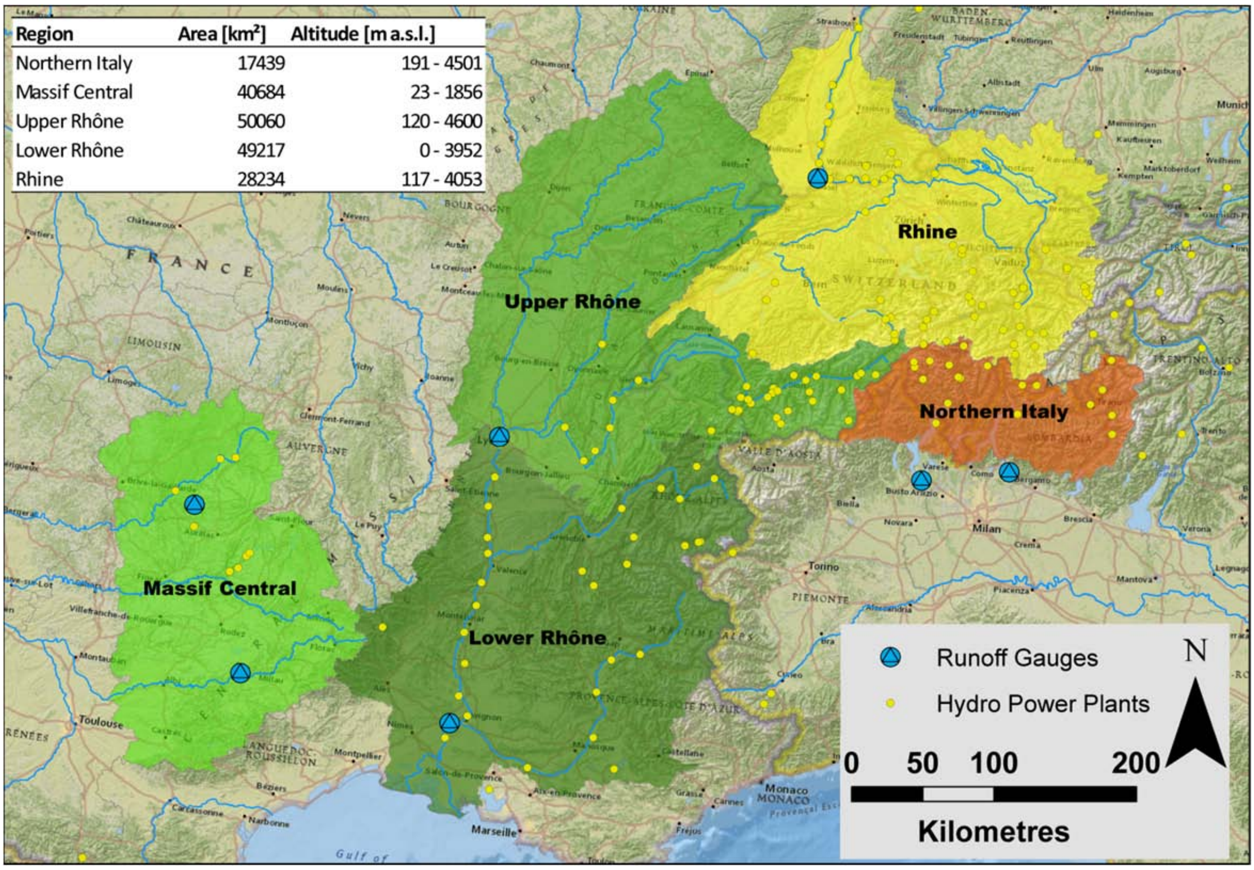

Figure 3-3: Model regions for estimation of hydro power potential of national states Germany, Switzerland, France and Italy. Runoff gauges are part of the Global Runoff Data Centre (GRDC, 2013).

Similar to the Drau/Isel system in Austria, the catchment of lower Rhône depends on the basin of upper Rhône. Hence, lower Rhône is modelled by taking into account the model results from upper Rhône basin. Due to the temporal resolution of months and the travel time of water between both gauges being much shorter, no time shift between the two basins is necessary (Wagner et al., 1994).

3.3 Ötztaler Ache modelled with COSERO

The developed snow redistribution model implemented in the hydrological model COSERO is applied to the catchment of Ötztaler Ache, Tyrol, Austria. The outlet of the watershed at gauge Huben is situated in a forested region at 1185 m a.s.l., the highest peaks reach up to 3770 m a.s.l. Total area of the catchment is 511 km². Mean precipitation in the catchment is about 1300 mm per year. About 1160 mm are transformed to runoff, evapotranspiration is about 140 mm a year.

Based on the time series from 1979 to 2012 (BMLFUW, 2014), mean runoff (MQ) is about 22 $m^3 s^{-1}$ while floods easily reach up to 70 $m^3 s^{-1}$ (HQ_1).

Glaciers cover about 19 % leading to an annual ice melt contribution of about 25 % of the total runoff at Huben, while 41 % of the discharge has its origin in snowmelt (Weber et al., 2010). Land-use characteristics are given in Table 3-2 and Figure 3-4 gives an impression of the basin.

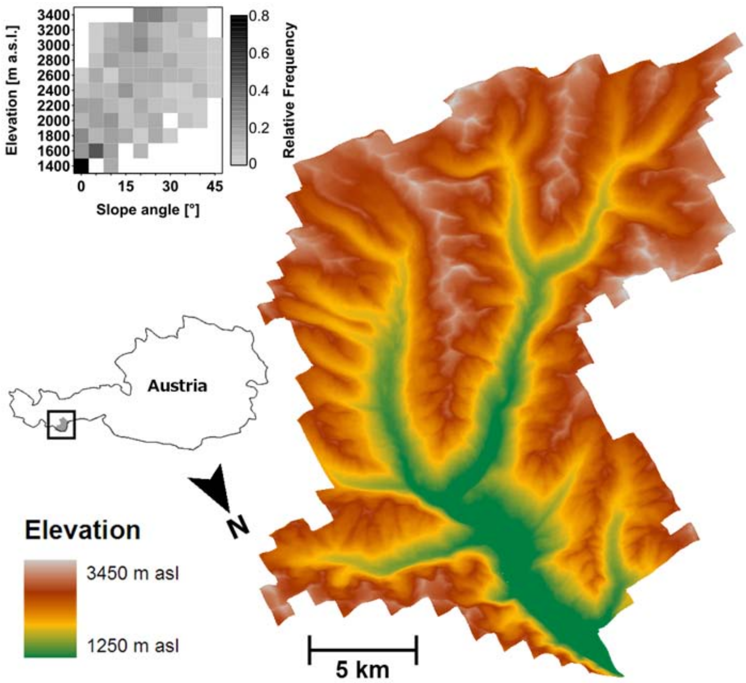

Figure 3-4: Catchment of Ötztaler Ache, Austria, after Frey and Holzmann (2015), edited. Due to the use of a 1 x 1 km grid, elevations differ from the one given in the text. Frequency distribution of slope angles derived from 1 x 1 km grid are shown (upper left). Slopes in general are steeper in the summit regions than in the valleys. However, glacier covered areas at the summits are rather flat. Note that instead of the average slope of a grid cell only steepest vertical gradients are plotted. For visualization of the catchment the freely available oe3d DEM (Rechenraum, 2014) was used.

Table 3-2: Land-use in the watershed of Ötztaler Ache, Austria

Land-use	**proportion [%]**
Build-up areas	1.2
Pastures and meadows	20.9
Coniferous forests	8.1
Sparsely vegetated areas	20.9
Bare rocks	29.5
Glaciers	19.4

4 Available Data

All studies in this thesis rely on the availability of meteorological input data and measured runoff at gauging stations. In addition, both the models COSERO and SASWET use spatial information on snow cover, provided by MODIS. Data regarding future climate scenarios are used by SASWET and WaBi. In the following the available data are described, beginning with the hydrological data provided by the Federal Ministry of Agriculture, Forestry, Environment and Water Management (BMLFUW) and the Global Runoff Data Centre (GRDC). Meteorological data are provided by the ZAMG (Austrian weather service) as well as by the EOBS network for the past and by combinations of Global and Regional Climate Models for the future. The study using WaBi additionally relies on data regarding generation of electric energy. These data are provided by ENTSO-E. The last topic in this chapter describes data regarding spatial extend of glaciers and snow cover.

4.1 Hydrological Data

In Austria, hydrological gauging stations are operated by the Federal Ministry of Agriculture, Forestry, Environment and Water Management (BMLFUW). These data are freely accessible via the internet in a temporal resolution of at least days and are referred to as eHYD data (BMLFUW, 2014). Outside of Austria, hydrological data are provided by the Global Runoff Data Centre in Koblenz, Germany (GRDC, 2013). In the following, both data sources are briefly described.

4.1.1 eHYD

The Federal Ministry of Agriculture, Forestry, Environment and Water Management provides hydrological data on river discharge, groundwater and surface water tables, water temperature and sediment transport in river systems. Besides that, several rain gauges are operated by the ministry. These data are accessible via the internet (ehyd.gv.at, accessed January 26th, 2015). For this work, data with temporal resolution of days were used. eHYD data were the basis of the modelling the Austrian basins with SASWET as well as for the case study in the catchment of Ötztaler Ache.

4.1.2 Global Runoff Data Centre

The GRDC provides data on discharge of about 9000 gauging stations around the world. While many stations solely provide discharge as monthly values, some provide daily discharge rates, as well. These data are free of charge but need to be ordered from the GRDC and are not available for commercial use. All European regions modelled with WaBi use data from the GRDC.

4.1.3 Hydrological characteristics of the Austrian catchments

Table 4-1 gives an overview of the hydrological and meteorological characteristics of the ten catchments modelled with SASWET while the mean monthly runoff in these catchments is shown in Figure 4-1. Some statistics regarding runoff of the Austrian watersheds during the years 1996 to 2010 are given in Table 4-2. Here, Q5 and Q95 refer to discharge values being exceeded on 5 and 95 % of the days, respectively.

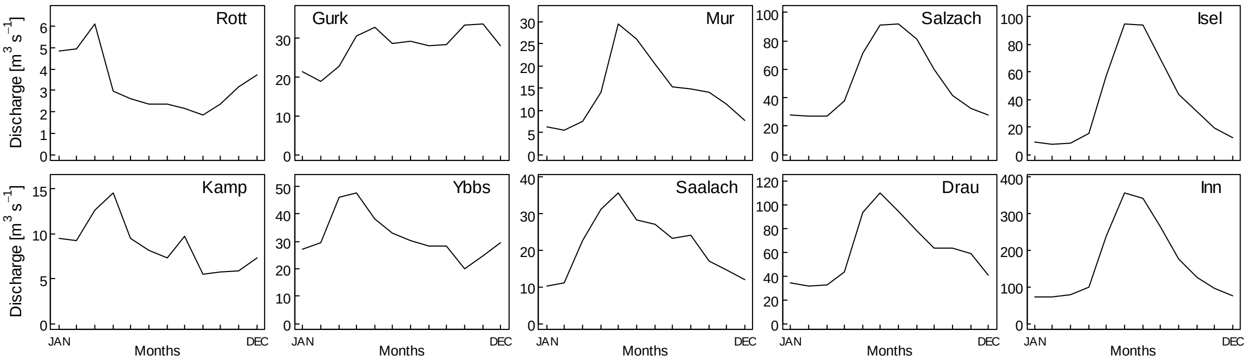

Figure 4-1: Mean monthly discharge of the Austrian catchments (1996-2010). Note that the range of the y-axis differs between the figures. Column one refers to cluster one, column two to cluster two and so forth. For the clusters see Table 3-1.

Table 4-1: Hydrological characteristics of the watersheds modelled using SASWET. Data regarding precipitation and evapotranspiration taken from (BMLFUW, 2007), discharge data from eHYD (BMLFUW, 2014).

Basin	**Area [km²]**	**Glaciated area [%]**	**Altitude [m a.s.l.]**	**Annual precipitation [mm]**	**Annual ETA [mm]**	**Mean Annual Discharge [m^3 s^{-1}]**
Rott	860	0	346 – 548	760	440	250
Kamp	1535	0	219 – 1046	740	560	200
Gurk	2554	0	396 – 2372	950	570	360
Ybbs	1116	0	263 – 1841	1440	600	860
Mur	956	0	938 – 3020	1200	400	780
Saalach	1152	0	416 – 2818	1740	510	1200
Salzach	1166	6.0	742 – 3609	1640	350	1360
Drau*	4479	2.5	526 – 3649	1230	560	1100
Isel	1197	6.9	674 – 3649	1330	260	1430
Inn	5773	3.8	571 - 3900	930	230	880

* includes the catchment of river Isel since this is a tributary to river Drau

The catchments in cluster one (for the clusters see Table 3-1) are dominated by pluvial types of runoff regimes. The higher the (mean) catchment elevation the more important are nival runoff generation processes. While the regime of river Gurk still shows characteristics of pluvial behaviour there are already signs of important snow processes. This is more emphasized in river Ybbs, which is of the same cluster as Gurk but is located on the northern side of the Alps. River Mur and Saalach are dominated by snow processes, yet there are no glaciers located in these catchments as are in the catchments of cluster four (Salzach and Drau) and five (Isel and Inn).

Table 4-2: Statistical characteristics on runoff of the Austrian watersheds regarding the time series 1996 to 2010. Q5 and Q95 refer to discharge values being exceeded on 5 and 95 % of the days, respectively.

Basin	**Q5** **[m^3 s^{-1}]**	**HQ_{MAX}** **[m^3 s^{-1}]**	**MQ** **[m^3 s^{-1}]**	**NQ_{MIN}** **[m^3 s^{-1}]**	**Q95** **[m^3 s^{-1}]**	**NQ to HQ ratio* [-]**
Rott	19	179.1	6.7	0.8	1.6	0.31
Kamp	21.2	554.0	8.8	0.4	2.2	0.37
Gurk	56.1	172.8	28.1	6.3	13.5	0.56
Ybbs	81.6	682.5	31.5	4.9	9.9	0.42
Mur	53.1	195.5	22.2	5.2	7.2	0.19
Saalach	102.0	639.0	45.3	10.9	14.4	0.28
Salzach	110.0	356.0	52.7	9.7	18.1	0.29
Drau	275.6	693.8	127.9	29.8	47.5	0.29
Isel	112.2	247.8	39.0	2.5	7.5	0.08
Inn	404.6	1122.4	168.1	15.9	52.0	0.20

* ratio is based on mean monthly discharge rates

4.1.4 Hydrological characteristics of the European catchments

As previously stated, discharge information of European regions are provided by the Global Runoff Data Centre in Koblenz, Germany. To fit the hydrological model to the regions equipped with two gauging stations (Northern Italy and Massif Central in France) the discharge values of the respective gauges have to be comparable. Their relative runoff behaviours are shown in Figure 4-3. Mean monthly discharge values of the gauges located at Rhine, upper and lower Rhône are visualized in Figure 4-2.

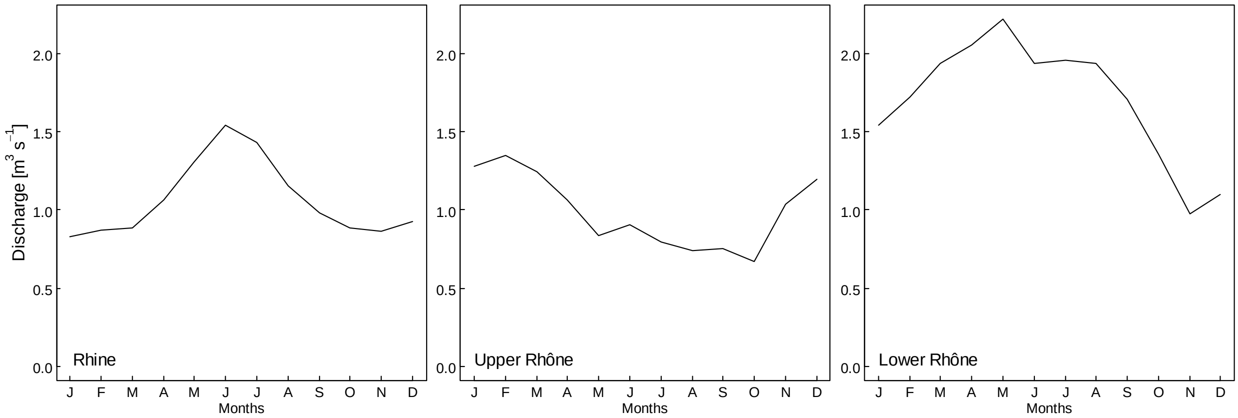

Figure 4-2: Observed monthly mean discharge of the gauges at Rhine, upper and lower Rhône. Data from GRDC (2013).

Although there are big differences in the absolute discharge of the French rivers Maronne and Tarn in the Massif Central, the dynamic of these two rivers is very similar. Both are influenced greatly by the oceanic climate with annual low flows in August. The two rivers in northern Italy are more complex, but, nevertheless, their dynamic is comparable. The peak discharge occurs in early summer (May to June) but a second maximum discharge exists in October. Both gauges are heavily influenced by their respective upstream lake.

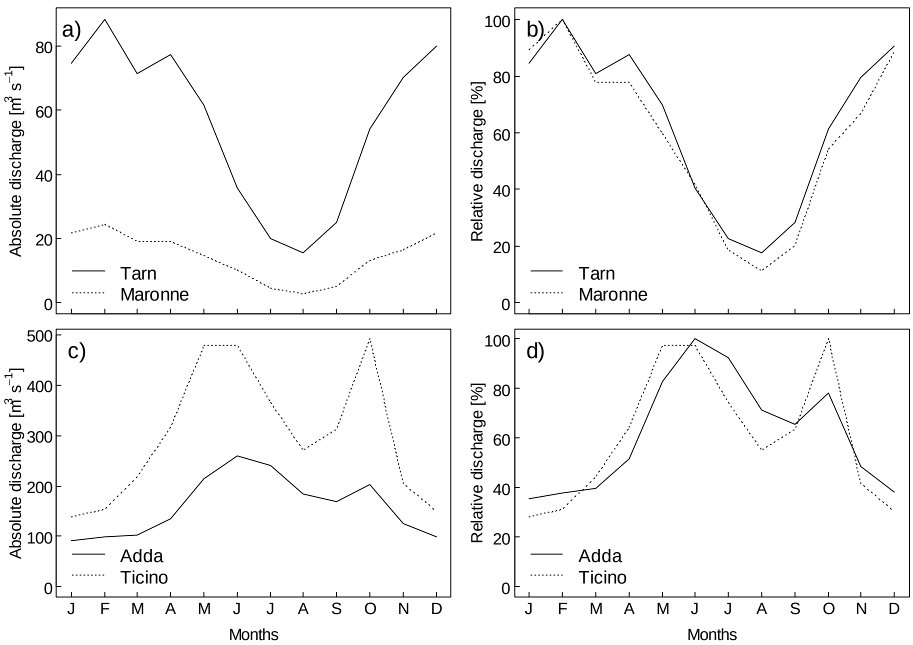

Figure 4-3: Comparison of the runoff behaviour of the rivers in the Massif Central (a, b) and northern Italy (c, d). a) and c) show specific discharge, b) and d) show relative discharge in the respective regions. Relative discharges signal that the runoff behaviour is comparable. Data from GRDC (2013).

4.2 Climatological Data

Hydrological models need some meteorological input to calculate runoff at a given point in time and space. Most models need at least information about air temperature and precipitation at a certain temporal resolution. While liquid precipitation becomes runoff relatively fast depending on the runoff process, solid precipitation is stored in the catchment's snow storage where it forms runoff with a significant delay. Temperature determines whether precipitation is treated liquid (i.e. rain or dew) or solid (i.e. snow or rime) and regulates – to some certain extent, depending on the model – snow melt behaviour. Furthermore, temperature influences evapotranspiration and sublimation. Both evapotranspiration and snow melt are influenced by global radiation.

4.2.1 Meteorological data of the past and present

In Austria, the Austrian weather service ZAMG (Zentralanstalt für Meteorologie und Geodynamik) provides meteorological data on a 1 x 1 km grid scale with a temporal resolution of up to 15 minutes. These data are referred to as INCA data (Haiden et al., 2011). Besides the data regarding precipitation, air temperature and global radiation, also information regarding wind (i.e. speed and direction) are available. However, in none of the models used in this thesis, wind is considered. The extent of the INCA data set shown in Figure 4-4 covers all Austrian and German catchments modelled in this thesis.

Additionally, also outside that extent, meteorological data are provided by the e-obs data set (Haylock et al., 2008; Van Den Besselaar et al., 2011). These data have a spatial resolution of 25 x 25 km and a temporal resolution of days.

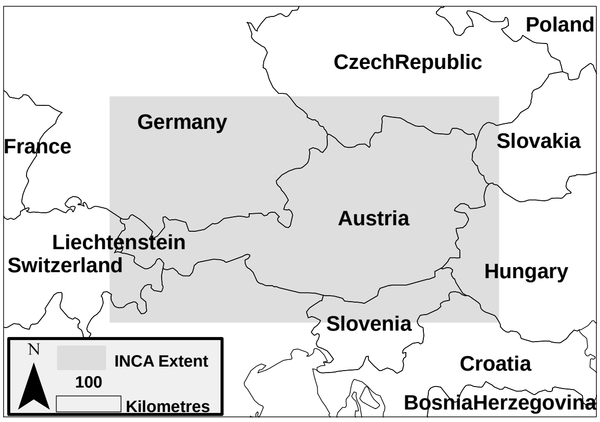

Figure 4-4: Extent of the INCA data set. All Austrian and German basins are covered by the extent.

Meteorological data for the period of calibration and validation of the respective watersheds using the respective model was provided by the Institute of Meteorology of the BOKU (BOKU-Met) together with the data regarding future climatic scenarios described in the subsequent chapter. The processed and corrected data for the period of calibration and validation for the Austrian basins where verified by data provided by VERBUND AG. The latter data were available for four distinct altitudes per basin and are based on the INCA data set as well.

4.2.2 Meteorological data of the future

Future climatic conditions are considered by the use of three regional climate models (RCMs): ALADIN (see e.g. Farda et al., 2010), driven by the global circulation model (GCM) ARPEGE (Déqué et al., 1994), REMO (e.g. Jacob et al., 2001) and RegCM3 (e.g. Pal et al., 2007), both driven by the GCM ECHAM5 (Roeckner et al., 2003). All three RCMs use the emission scenario A1B (IPCC, 2000) which can be treated as medium scenario (Kling et al., 2012) and provide data on a 25 x 25 km scale. By now, the IPCC has changed its future scenarios. No longer based on emissions, now a surplus of energy (W m^{-2}) is used. According to Snover et al. (2013), A1B is similar to the new scenario RCP 6.0 by the end of the 21st century but predicts lower temperature values in the mid-century. As shown in Figure 4-5 A1B still is located within the range of climate change scenarios and therefore is still valid.

Before RCM data can be used for hydrological modelling, they have to be corrected to remove an existing bias. In addition, the spatial resolution has to be refined. Both were done by the Institute of Meteorology of the BOKU and therefore will be described only briefly in this thesis. Bias correction was done using the e-obs data set and the output was scaled down to a resolution of 1 x 1 km using the INCA data set provided by the ZAMG. The first was carried out by using quantile mapping (Déqué, 2007). A detailed description can be found in Formayer (2011).

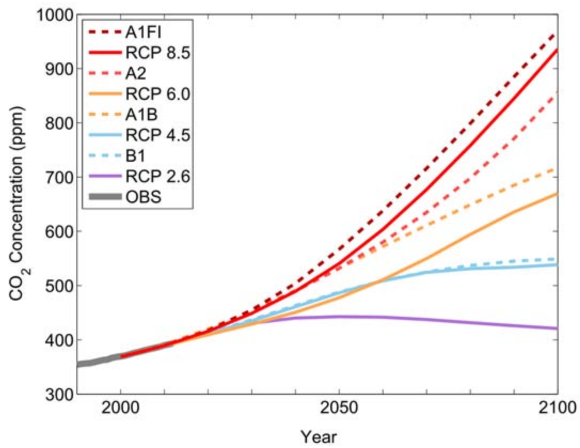

Figure 4-5: Comparison of the "old" and "new" climate scenarios provided by the IPCC. Figure from Snover et al. (2013).

A spatial comparison of the possible evolution of climate parameters is shown in Figure 4-6 for temperature and in Figure 4-7 for precipitation and a temporal course of all three drivers including shortwave radiation is illustrated Figure 4-8. REMO and RegCM3 are both driven by the same GCM. Thus, their change signals resemble each other in comparison to ALADIN. As expected, all three climate models indicate similar behaviour regarding evolution of temperature whereas precipitation and shortwave radiation are highly uncertain. All three models are treated equally. A brief summary of the general trends is given in the following.

4.2.3 Temperature

Warming until the year 2030 can be expected to be about 1 °C, until 2050 mean annual temperatures will rise about 1.5 to 2 °C and will reach about 3.5 to 4 °C at the end of the 21st century. All three climate models indicate similar annual temperature trends. However, on the seasonal scale, ALADIN portends considerably higher warming rates in summer than REMO and RegCM3, while the increase of temperature in winter is indicated higher by these two ECHAM5 driven models (see Figure 6-29 and Figure A 10 to Figure A 18 in the appendix).

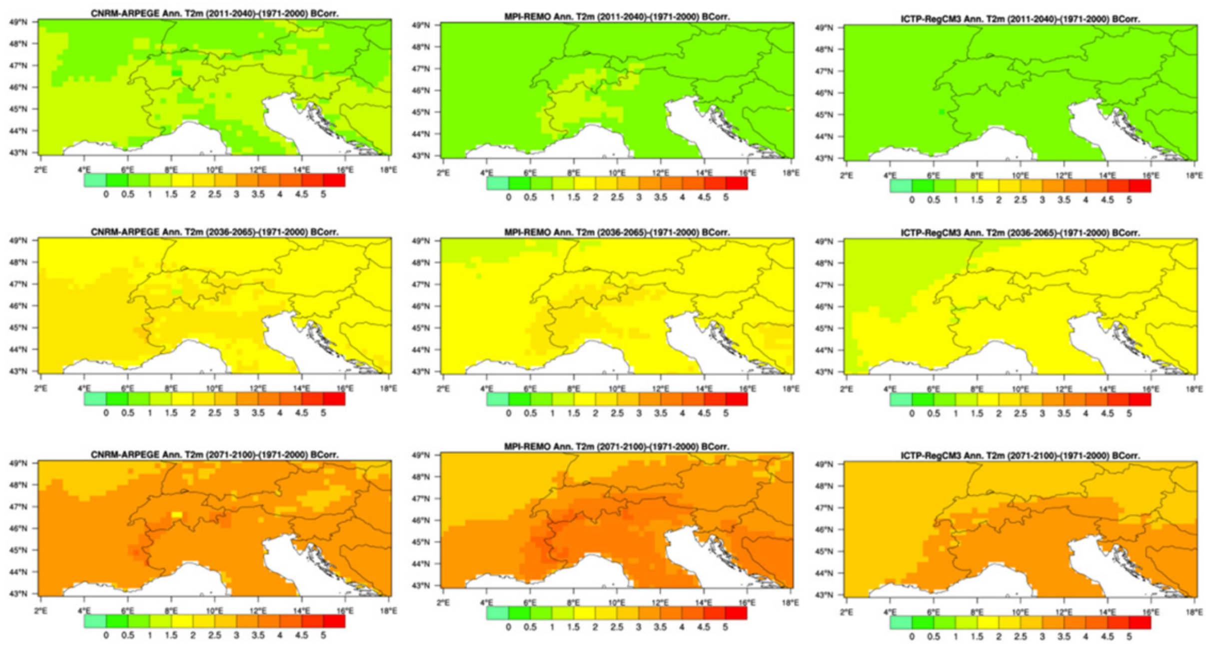

Figure 4-6: Change in mean annual temperature by the climate models ALADIN (left), REMO (centre) and RegCM3 (right) for the periods 2011-2040 (top), 2036-2065 (centre) and 2071-2100 (bottom). Figure from Frey et al. (2014).

4.2.4 Precipitation

By the end of the century both ECHAM5 driven models indicate a surplus of precipitation in the order of about 5 %, whereas ALADIN shows a decrease in annual precipitation in the same order. Thus, ALADIN can be referred to as dry, the other two models as wet model realizations. In addition, ALADIN portends a further decrease in summer precipitations than REMO and RegCM3 while differences in winter precipitation between the three models are less pronounced.

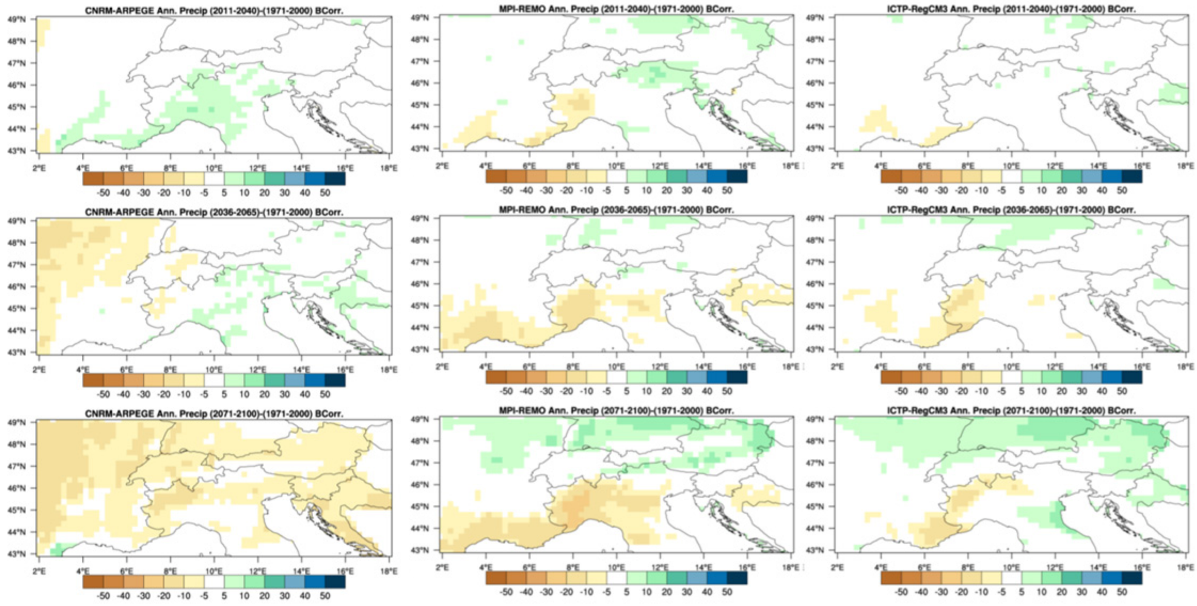

Figure 4-7: Change in annual precipitation sums by the climate models ALADIN (left), REMO (centre) and RegCM3 (right) for the periods 2011-2040 (top), 2036-2065 (centre) and 2071-2100 (bottom). Figure from Frey et al. (2014).

4.2.5 Shortwave radiation

In general time periods of low shortwave radiation are attended by wet periods due to high cloudiness. Thus shortwave radiation signal follows the precipitation signal oppositional. At the end of the century RegCM3 shows an increase of global radiation during the summer months. However, in the annual mean no clear trend can be observed in any of the models. The mean annual values fluctuate in the order of about 5 %.

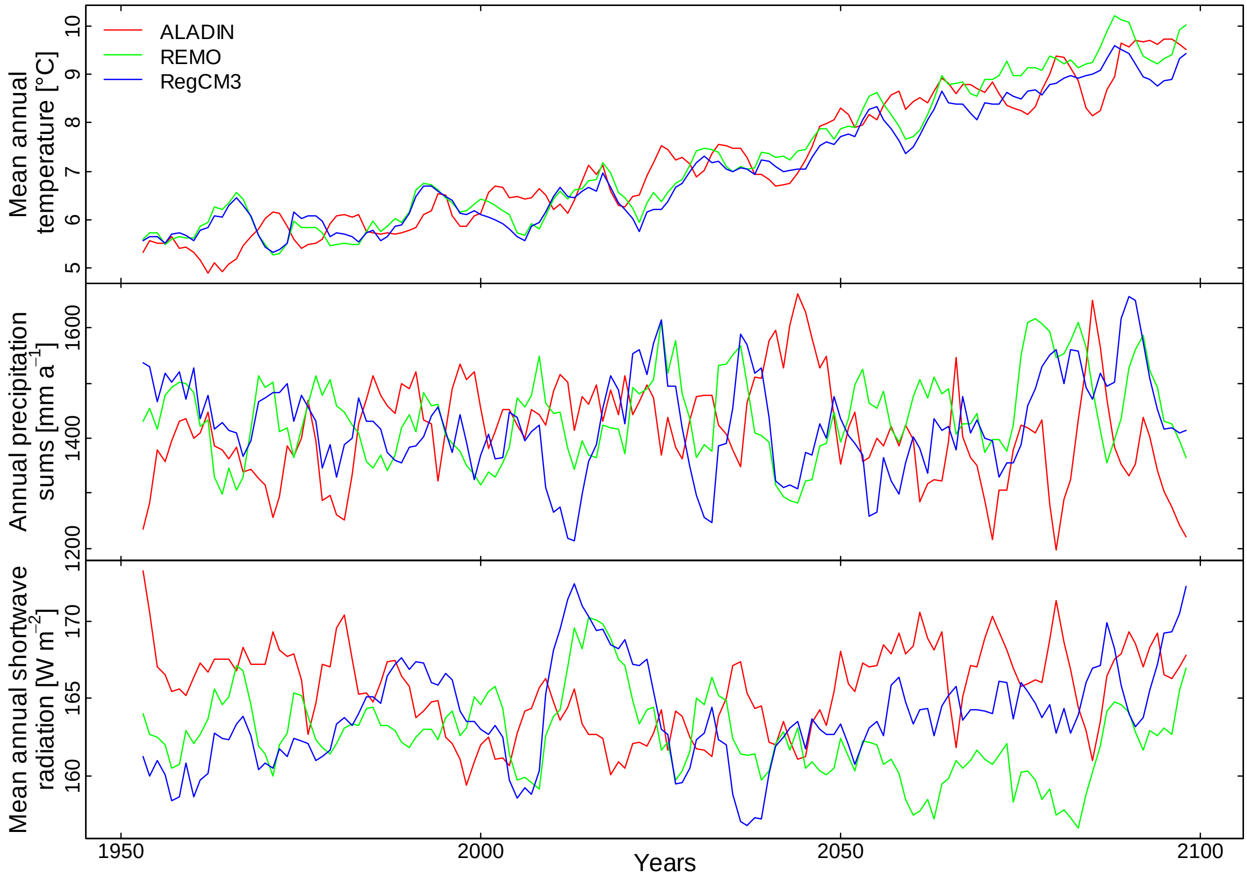

Figure 4-8: Evolution of temperature (top) on the 1000 m a.s.l level, precipitation (centre) and shortwave radiation (bottom) in the catchment of Salzach. These drivers are shown as five year moving averages. Similar behaviour can be found in all modelled basins.

4.3 Defining reference period and future periods

Results of climate change impact studies may vary according to the reference time period chosen to compare future scenarios to (e.g. Scherrer et al., 2006). The WMO (1959) stated, that for climate statistics time periods of at least 30 years should be considered. These time periods were defined by the WMO as standard normals (or climate normals) ranging from 1 January 1901 to 31 December 1930, 1931 to 1960, 1961 to 1990 and 1991 to 2020 and so forth. In general, the last completed normal is considered as reference period. This means that the future scenarios would be compared to the standard normal 1961 to 1990.

Some authors, including the WMO itself, suggested, that the WMO member states should update their climate normals every ten years (Arguez and Vose, 2011; Scherrer et al., 2006; WMO, 1959). However, not all of the member states take that effort. Nevertheless, since this study was carried out rather at the end of the climate normal 1991 to 2020, the reference period is chosen to be the 30 year period from 1981 to 2010. All hydrological statements regarding future scenarios are based on that period. Consequently, future climate normals then are defined as the periods ranging from 2011 to 2040, 2041 to 2070 and from 2071 to 2100. The period from 1951 to 1980 is referred to as standard normal of the past.

To compare future conditions, the reference period refers to the data of each RCM separately. Thus model results regarding ALADIN during the climate normal 2071-2100, for instance, are compared to the period 1981-2010 using ALADIN, too.

4.4 MODIS snow cover information

NASA operates two satellites equipped with optical sensors that are used for MODIS images. One is called TERRA, launched on December 18th, 1999, the other AQUA, launched on May 2nd, 2002. Both operate in an orbit of roughly 700 km circling earth in 98 minutes with swath dimensions between 10 km and 2330 km at their nadir and cross track, respectively. Thus, the total surface of the planet is covered every one to two days. MODIS acquires data in 36 spectral bands of which the short-wave infrared bands are used for snow cover products on a 500 x 500 m grid cell size. A detailed technical description can be found in Hall et al. (2002, 2001a, 2001b).

Its biggest source of errors is cloud cover. Other sources of errors are vegetation, especially forests. One has to be aware of these errors. However, while the error due to clouds is easy to numeralize, the vegetation based error is relatively hard to estimate. It is reported by several authors to be between 3 up to 20 % (e.g. Hall and Riggs, 2007; Simic et al., 2004) whereas higher error values occur in evergreen forests.

A major limitation of the MODIS snow cover product is its binary nature. Only the occurrence or absence of snow can be detected but not the actual snow depth.

Snow cover information is used by SASWET and COSERO. However different snow cover products are used in the respective study. The following passages describe these different products.

4.4.1 Snow cover data used by SASWET

In general, MODIS data are available since 2000. However in this part of this thesis, a snow cover product that was pre-processed by ENVEO IT GmbH on behalf of Verbund AG was used. Pre-processing included clipping MODIS images to the borders of the catchments and minimizing errors due to cloud cover. These data are available since 2003 and only in the respective period of ablation, i.e. from the end of December until the beginning of June. Once every week information of snow cover extent, cloud cover and snow free area per elevation level and catchment exist.

4.4.2 Snow cover data used by COSERO

The watershed modelled using COSERO differs in its borders from any of the basins modelled by SASWET and therefore no pre-processed MODIS data are available. Thus, for this study, the 8-Day L3 Global 500m Grid, Version 5 snow cover product (Hall et al., 2006) was used. By the spatial resolution of COSERO, MODIS information are not aggregated to elevation levels but remain in their native resolution.

4.5 Data on glacier extent

There are several data bases available holding information about glaciers in the Alps. In the case study in the Ötztal, glacier information from the Randolph Glacier Inventory Version 3.2 (Arendt et al., 2012) were used. This data base holds information about glacier surfaces around the world and is updated in regular time steps. Also in the study about the electric energy generation potential in European countries, glaciers were characterized using this source of data.

For the Austrian basins, version 2 of the Austrian Glacier Inventory (Kuhn et al., 2013; Lambrecht and Kuhn, 2007) was used. This inventory holds information on the extent of glaciers between 1997 and 2002.

4.6 Data on electric energy of national states

The European Network of Transmission System Operators for Electricity (ENTSO-E) provides information on generation of electric energy in European countries since 1991 with a temporal resolution of months. In this data set the total amount of electric energy generated in a country is subdivided into the respective sources of energy, e.g. nuclear, hydro, coal et cetera. Hydropower itself again is subdivided into pump- and run-of-river power plants. However, it is not classified into dedicated power plants. These data are used to link runoff of overlapping regions to electric energy potential in national states using multiple linear regression analysis.

5 Calibration and Validation

Conceptual hydrological models use at least some variables that cannot be directly linked to physical processes. These variables need some calibration in order for the model to be able to represent a certain objective, such as runoff. It should be noted that even physically based models and variables might need calibration (see e.g. Sahoo et al., 2006). In the following, calibration and validation of the different models in this thesis will be described and discussed.

5.1 SASWET

Meteorological data are available in the basins modelled with SASWET in the period from 1996 to 2010. During that time discharge data are available, too. Calibration was done in the period from 1996 to 2005 followed by the validation in 2006 to 2010. Target of calibrating the model was runoff. However besides discharge, a good compliance with snow cover data provided by MODIS satellite images was part of the calibration procedure. A scheme of the calibration and validation process is given by Figure 5-1.

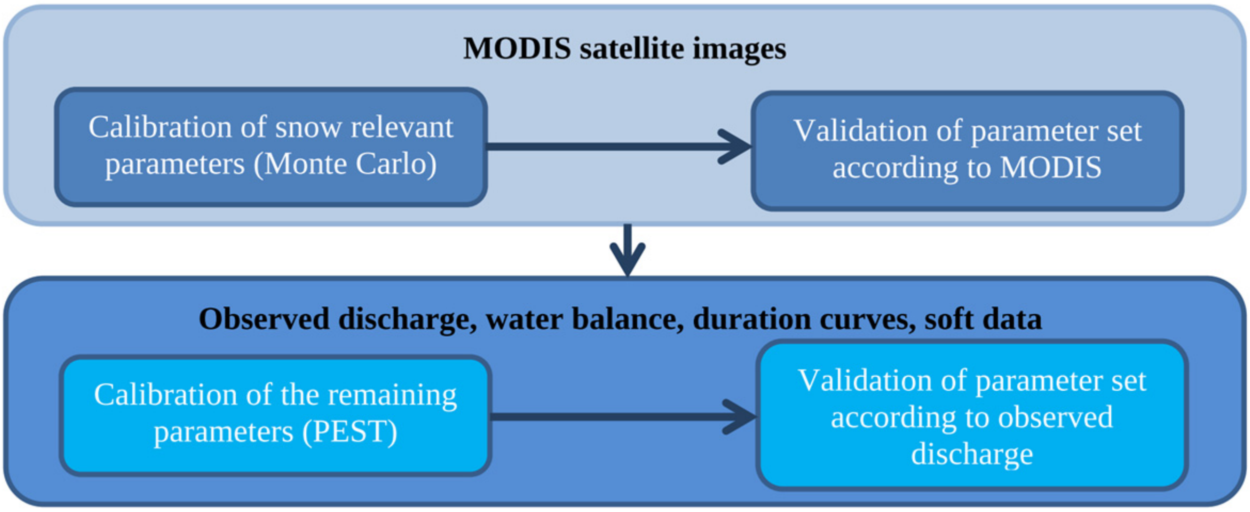

Figure 5-1: Scheme of the process of calibration and validation used for the model SASWET. In a first step, snow relevant parameters are calibrated against MODIS data. This is done using Monte Carlo runs. After a validation the parameters found are fixed and the remaining parameters are calibrated using the software tool PEST. A constraint for the parameter set is the match of the water balance. If necessary, precipitation input may be adjusted by hand. Target of calibration is daily discharge (NSE, Nash-Sutcliffe model efficiency, Nash and Sutcliffe, 1970) as well as flow duration curves (RMSE, root mean squared error). For validating besides both NSE and RMSE, soft data are used: If the parameter set leads to obviously implausible runoff components, it is dismissed and calibration is done again using other starting points or/and parameter boundaries.

While the model provides 28 parameters (see Table 2-1) some of these were excluded from the calibration process due to different reasons. These parameters not calibrated and the respective reasons for that are listed in Table 5-1. Four of the 18 remaining parameters where used to calibrate the snow module. These were CT_{SNOW} and CT_{AMP} as well as the ones responsible for snow distribution, namely $DIST_{DON}$ and $DIST_{ACC}$.

Table 5-1: Parameters in SASWET not being calibrated.

Parameter	**Reason for not being calibrated**
radgrad	physically predetermined
tgrad	data predetermined
f_{age}	insensitive
PS_{CRIT}	physically predetermined
TSNOW	physically predetermined
TICE	physically predetermined
$TSNOW_{AMP}$	physically predetermined
$DIST_{SHAPE}$	conceptually predefined
P_{COR}	used in pre-processing to match water balance data by BMLFUW (2007)
C_{ETP}	used in pre-processing to match water balance data by BMLFUW (2007)

5.1.1 Calibration of snow relevant parameters

Since the time period of calibration covers only two years of available MODIS data, snow cover was calibrated in the years 2003 to 2007 and validated in 2008 to 2010. Calibration was done using 100 000 Monte Carlo runs per basin (see Figure 5-1). Upper and lower boundaries of each parameter are given by Table 5-2. Objective function of the calibration was minimizing the root mean squared error (RMSE) of the snow cover predicted by the model with respect to MODIS data. Only the data set leading to the best model results during both the calibration and validation period was used for further modelling.

Table 5-2: Boundaries of snow relevant parameters in the calibration using Monte Carlo runs.

Parameter	**Lower bound**	**Upper bound**	**Additional restraints**
CT_{SNOW}	1	9	$0.5 < CT_{SNOW} + CT_{AMP} < 9.5$
CT_{AMP}	0.1	3	
$DIST_{DON}$	1	Highest level in basin minus forest line	$DIST_{DON} + DIST_{ACC}$ = Forest line
$DIST_{ACC}$	1		

5.1.2 Calibration of the remaining parameters

The remaining parameters were calibrated using PEST (Doherty, 2010), a software package for estimating parameters using different optimization algorithms. In this study, SCE-UA (Shuffled Complex Evolution – University of Arizona, see Duan et al., 1992) was used. SCE-UA is a global optimization algorithm designed for conceptual hydrological models.

Multi-objective functions allow the modeller to concentrate to more than one calibration target. PEST lets the modeller weight calibration objectives. This weighted multi-objective function is normalized to assure that all targets are of the same magnitude. Different objective functions were chosen depending on the parameters intended to be optimized. Massmann and Holzmann (2012a) pointed out, that dependent on different factors such as time scale, time period or flow conditions, different parameters are dominant. For instance, ground water recession is dominant under low flow conditions but rather unimportant during peak discharge. An overview of flow conditions to which each parameter was calibrated to and the respective objectives is given by Table 5-3. Quality criterion for the flow duration curve (FDC) was its respective rooted mean squared error. Thereby, only the values in between the 2.5 and 97.5 percentiles were taken into account.

Table 5-3: Objectives for parameter estimation and flow conditions where parameters are important.

Parameter	**Objectives**	**Flow conditions**		
		Low flow	**Rising limb**	**Descending limb**
k_{HOF}	NSE; FDC		x	
k_{SOF}	NSE; FDC		x	
k_{SSF}	NSE; FDC		x	x
k_{PERC}	NSE; FDC		x	x
k_{GWF}	RMSE; FDC	x		
$h1$	NSE; FDC		x	x
$h2$	NSE; FDC		x	x
$SPLIT_{MELT}$	NSE; FDC		x	x
CT_{ice}	NSE; FDC		x	x
QC_L	NSE; FDC	x		x
QC_U	NSE; FDC		x	x
k_{API}	NSE; FDC	x	x	x
SQ_L	NSE; FDC	x		x
SQ_U	NSE; FDC		x	x

NSE = Nash-Sutcliffe Efficiency; FDC = Flow Duration Curve; RMSE = Root Mean Squared Error

A prerequisite for calibration was that the model is able to close the water balance with its given input data. By use of the parameters P_{COR} and C_{ETP} for adjusting precipitation and potential evapotranspiration, respectively, this prerequisite could be achieved in all basins.

Validation was done using the same quality criteria as for calibration. In addition, soft data based on personal expertise (see e.g. Seibert and McDonnell, 2002, 2015) were used to check whether calibration results in reasonable composition of discharge components. Soft data refer to reasonable runoff composition. A data set, for instance, leading to well model efficiency but at the same time leading to only surface flow would be rejected.

All Austrian basins were calibrated in the way described above. Only for the catchment of Upper Salzach, the procedure was different, since it was calibrated with and without considering snow redistribution.

5.2 WaBi

Since WaBi is not designed to reproduce discharge on a daily basis, it has been calibrated using long-time monthly mean discharge (see Figure 4-3 and Figure 4-2). Quality criteria were coefficient of determination (R^2) for monthly runoff values and rooted mean squared error of the flow duration curve. All five parameters have been calibrated at once. Since available time series of discharge data are of different lengths, individual time windows for calibration and validation were selected for the European regions. These are given by Table 5-4. Monte Carlo simulations were done to study uncertainties of the model and compare them with uncertainties of climate models. Per basin, 500 000 runs were performed and the best 500, in terms of mean error were picked.

Table 5-4: Available runoff time series and time windows used for calibration and validation of WaBi.

Region/Basin	Time series	Calibration window	Validation window
Upper Rhône	1900 – 1976	1950 – 1961	1962 – 1972
Lower Rhône	1920 – 1999	1950 – 1970	1971 – 1999
Rhine	1891 – 2011	1950 – 1980	1981 – 2000
Massif Central	1961 – 1996	1950 – 1970	1971 – 1996
Northern Italy	1946 – 1994	1950 – 1970	1971 – 1996

For linking runoff to the potential of generating electricity linear multiple regression on a monthly (mean) basis is performed, meaning that for every month a relationship between electric energy and runoff is estimated using Eq. (5-1), where the response EE_s is the electric energy potential of a national state S, provided by ENTSO-E data, a is the regression coefficient and Q is simulated runoff of the respective overlapping region i out of the total amount of overlapping regions j.

$$EE_S = \sum_{i=1}^{j} a_i \times Q_i \qquad (5\text{-}1)$$

For further analysis only data on run-of-river stations are considered, since pumped storage power stations are more independent from hydrological conditions compared to riverine power stations.

5.3 COSERO

COSERO was calibrated during the period from 2005 to 2008 using a Rosenbrock's automated optimization routine (Rosenbrock, 1963). Target of the calibration was a good fit of runoff using the Kling-Gupta-Model-Efficiency (Gupta et al., 2009; Kling et al., 2012). Both calibration and validation have been done with and without using the snow drift module. In the following model A refers to the model using snow transport, whereas model B stands for the standard model. Like SASWET, parameters of COSERO were calibrated depending on the flow conditions where the respective parameter is important.

Validation period was the years 2009 and 2010. Vegetation threshold values for snow detention were taken from previous studies (Liston and Sturm, 1998; Prasad et al., 2001). These are given by Table 5-5. For evaluation, besides runoff in the validation period, snow cover data from MODIS (8 day maximum snow cover, version 5) satellite images (Hall et al., 2002) were used to compare the performance of both the model with and without using snow redistribution.

Table 5-5: Snow holding capacities of different land-use types taken from (Liston and Sturm, 1998; Prasad et al., 2001). Note that snow holding capacity has the dimension mm, meaning the actual snow depth, not SWE.

	Build-up areas	**Pastures and meadows**	**Coniferous forests**	**Sparsely vegetated areas**	**Bare rocks**	**Glaciers**
Snow holding capacity [mm]	100	500	2500	300	200	200

6 Results and discussion

6.1 Calibration and validation

6.1.1 SASWET

Objectives of the calibration of SASWET were Nash-Sutcliffe model efficiency (hydrograph) and performance (RMSE) of the model regarding flow duration curves. Condoning possible equifinality of parameter sets, only one parameter set was selected per basin with which the further analyses were carried out. Figure A 1 in the appendix illustrates these parameter sets. All basins, with exception of Kamp and Rott, were calibrated using snow redistribution. The maximum altitude of Kamp and Rott is elevated as low as snow accumulation does not play any role. Influences and the importance of considering snow transport is discussed in the case study of the river Salzach basin in chapter 6.2.

An overview of the model efficiency of SASWET in the Austrian catchments in terms of Nash-Sutcliffe model efficiency (NSE) is shown in Figure 6-1 a), while the ability to reproduce the snow cover in the basins compared to MODIS data is shown in Figure 6-1 b). SASWET is able to reproduce the hydrological behaviour of all modelled watersheds. However, while giving good results in alpine catchments with steep slopes it has difficulties representing the rather flat catchments Rott and Kamp.

The same accounts for the representation of the snow cover. It should be stated, that the basin of Rott is partitioned to only three elevation levels. Since the model does not account for processes on scales smaller than elevation bands, differences in the snow cover per elevation band in flat basins are weighted stronger than in steep ones. This leads to higher relative errors in the basin of Rott than it does in the catchment of Ybbs, for instance.

Besides Nash-Sutcliffe efficiency, the ability of the model to match the flow duration curve was a criterion. As the model was not calibrated to reproduce the extreme runoff events – both low and high flows, duration curves were calculated on the basis of data in between the 2.5 and 97.5 percentile. Figure 6-2 represents flow duration curves during both calibration and validation time periods. In general, model results regarding flow durations curves during both time periods are satisfying as well. Again, the model has difficulties to reproduce the characteristics of Rott and Kamp, though.

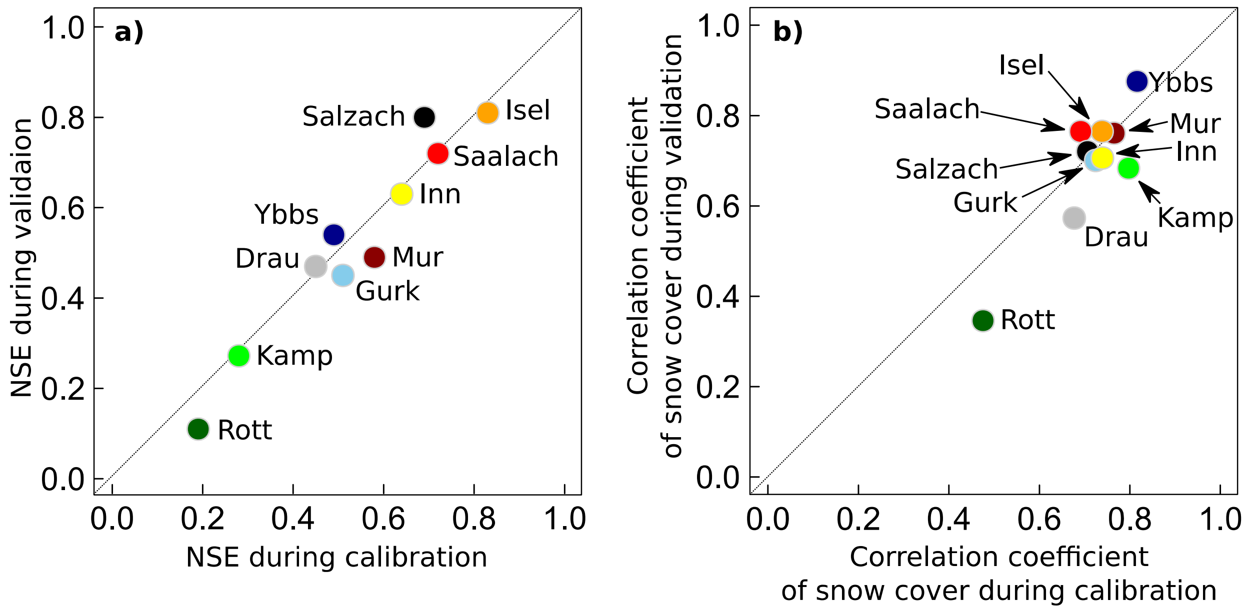

Figure 6-1: a) Nash-Sutcliffe model efficiency (Nash and Sutcliffe, 1970) in the period of calibration and validation regarding the hydrograph. b) Correlation coefficients as indicator for model efficiency regarding snow cover observed by MODIS. Due to the few measured data available regarding snow cover, correlation coefficients have been used instead of NSE.

A jump in observed discharge of river Rott to lower values occurred in the summer of 2003 for unknown reasons. The gross of the calibration takes place before that date so the model is not able to reproduce the adjusted runoff behaviour in the validation period. Since this affects runoff in all ranges (high flows as well as low and medium flows) in the same way, the model anyhow is appropriate for climate change impact studies in this catchment.

River Kamp is heavily influenced by barrages for hydropower plants (Reszler et al., 2008). Since the model only represents a hydrological view on a non-influenced watershed, this impedes the model to be calibrated to the influenced gauging station. However, biggest differences occur in the range of high flows.

Similar model efficiencies regarding both NSE and compliance with flow duration curves as well as representing the snow ablation behaviour compared to MODIS could be achieved during calibration and validation in all basins. Hence, according to several authors (e.g. Bergström, 1991) the model is not over-parametrized and it should be able to state hydrological condition of future scenarios.

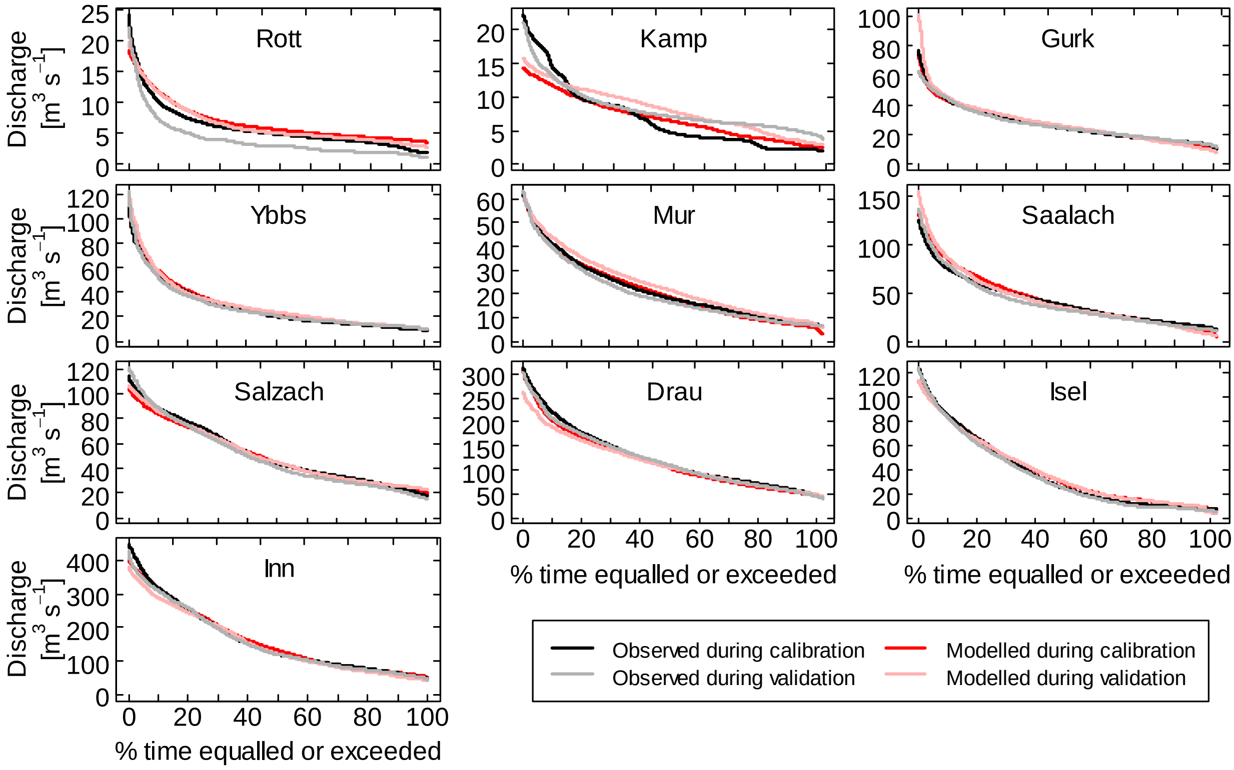

Figure 6-2: Flow duration curves during the time period of calibration and validation for all ten basins.

6.1.2 WaBi

The coefficient of determination of mean monthly discharge rates was used as objective function on the one hand and RMSE of flow duration curves on the other hand. For the regions equipped with two gauges at different water bodies (i.e. Northern Italy and the Massif Central, France), the sum of both discharge time series (see Figure 4-3) was considered instead of only one of two gauging stations. The results of the calibration are part of the case study and therefore are presented and discussed in chapter 6.4.

6.1.3 Calibration and validation of COSERO

Since calibration of COSERO was part of the case study in the watershed of Ötztaler Ache only, the results are shown and discussed in the part of this particular case study. Here, only the efficiency of the model in terms of snow cover and discharge are listed in Table 6-1.

Table 6-1: Comparison of performances of model A (considering snow redistribution) and B (not considering snow redistribution) with respect to snow cover and runoff. For snow cover coefficient of determination (R^2) was used, whereas Kling-Gupta-Efficiency (Gupta et al., 2009; Kling et al., 2012) was used for runoff. Note, that snow cover was not used as calibration criterion.

	Calibration		**Validation**	
	Snow cover (R²)	**Runoff (KGE)**	**Snow cover (R²)**	**Runoff (KGE)**
MODEL A	0.78	0.93	0.74	0.92
MODEL B	0.70	0.88	0.66	0.90

6.2 Case study of snow transport using SASWET in the Salzach watershed

Snow distribution has an influence on the behaviour of a hydrological model. The results of snow redistribution in order to prevent snow accumulation in high elevations implemented in the semi lumped model SASWET are presented and discussed in the following. Here the model realization using snow redistribution will be referred to as model A whereas model B will stand for not considering snow drift.

6.2.1 Discharge

Using snow redistribution implemented into SASWET enables the model to lead to better results in terms of runoff than disregarding that process. Results regarding discharge of both models are given in Figure 6-3. Model A does not only predict runoff more precisely in terms of its efficiency (Nash-Sutcliffe) but is also able to match the water balance of the catchment more accurate (Figure 6-3b). A surplus snow in lower areas due to snow redistribution leads to higher runoff in the early melting season in spring. However, the additional discharge has its origin not only in snowmelt but also in enhanced glacier melt. Glacier melt is enabled solely if the overlaying snow layer is completely depleted. Figure 6-4 compares glacier melt by both models on daily basis and cumulated over year 2008. Note that since glaciers cover only 6 % of the catchment, 74 mm melt from glacier areas equals 4.3 mm glacier runoff with respect to the total catchment area. Less snow in the beginning of the melt season therefore leads to earlier glacier melt. Moreover, model B accumulates snow over years in higher altitudes and consequently glacier melt in these elevation levels is prevented completely. In total, model A predicts a surplus of discharge of 43 mm of which 10 % originate from enhanced glacier melt as illustrated in Figure 6-5.

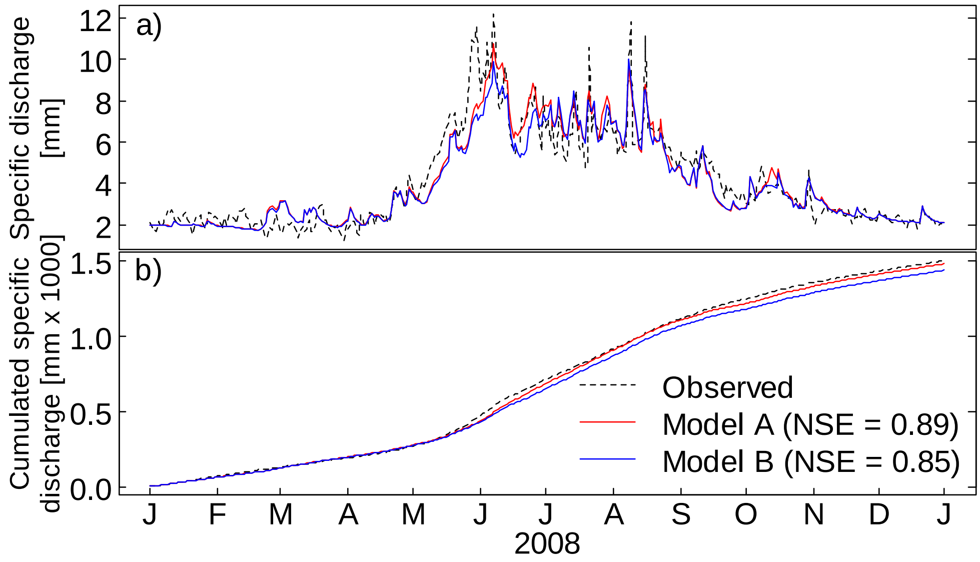

Figure 6-3: Comparison of model A and B with observed specific discharge. a) Model B tends to underestimate runoff especially in spring while model A covers that period better. b) Model A is able to reproduce the water balance with higher precision.

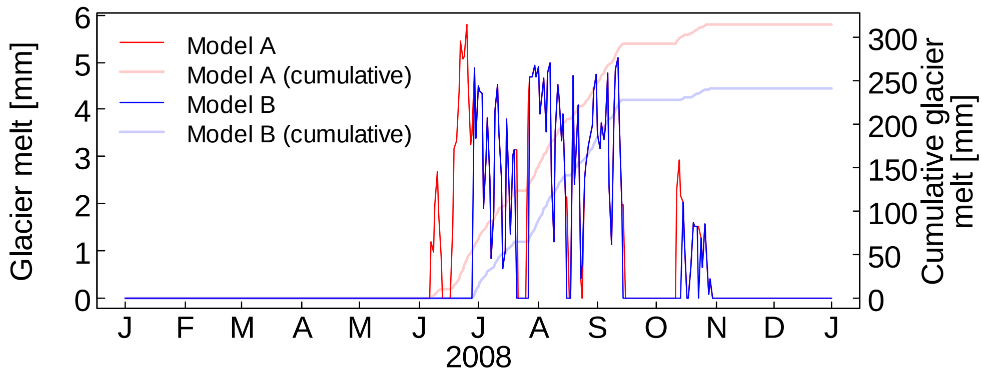

Figure 6-4: Comparison of model A and B with respect to glacier melt. Enhanced glacier melt due to earlier snow free areas leads to an additional loss of 74 mm in 2008. Note that glaciers cover only 6 % of the catchment area.

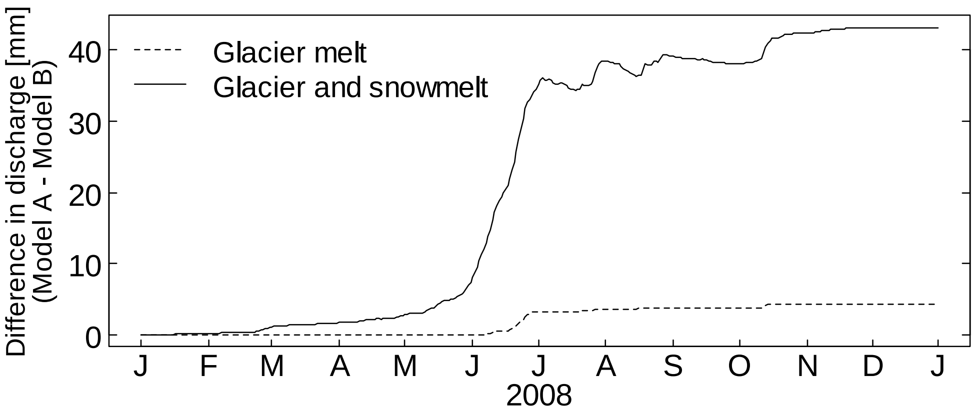

Figure 6-5: Cumulated differences in runoff and origin of these between model A and B. Model B leads to a snow accumulation of about 43 mm SWE compared to model A with respect to the whole catchment area. About 4.3 of these 43 mm in 2008 originate from enhanced glacier melt.

6.2.2 Snow cover

Since snow cover is one criterion in calibrating SASWET it is interesting how model A competes with model B with respect to MODIS data on snow cover and on accumulating snow in higher altitudes. The first is illustrated in Figure 6-6 for the same period as the comparisons with runoff in the previous chapter.

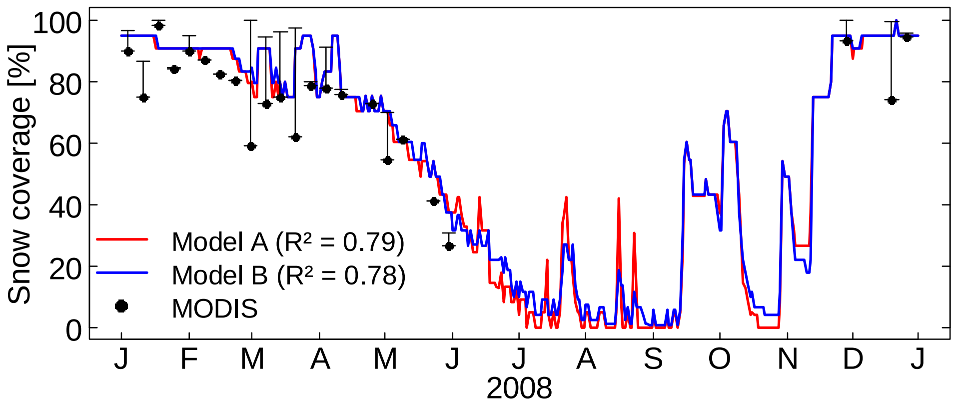

Figure 6-6: Comparison of both models with MODIS satellite based snow cover data. Errors arise from cloud cover. According to the coefficient of correlation (R^2) both models behave similar. Unfortunately, in summer where the main differences occur, no MODIS data are available for this work. Note that MODIS only can tell if there is snow but not how much.

As mentioned before, MODIS data used for this study were pre-processed by ENVEO-IT GmbH and because of that are available during the ablation period only. Therefore model efficiencies can be calculated only during that period, too. Since clouds obscure the information about cloud cover, for comparison only dates have been selected where clouds cover less than 50 % of the catchment. In Figure 6-6 cloud obscuration is indicated by the error bars assuming that all cloud covered area might be either snow free or snow covered (or something in between). The first case would mean, only the observed percentage of the catchment is snow covered, the latter, that snow covered area plus the clouds add up a maximum of 100 %. Of course, the error bars cannot reach below the observed snow cover extent of the catchment (if errors due to measurement uncertainties are neglected).

Both models predict snow with similar accuracy with respect to MODIS data. The coefficient of correlation (R^2) was calculated on the basis of the MODIS dates given in Figure 6-6 but with neglecting errors due to cloud cover. If accounting the possibility of cloud covered areas being covered by a snow layer, R^2 of both models would reach up to 0.95. However, more important than the coefficient of correlation with some few data points is the general shape of the ablation curve. Again, both models match that shape indicated by MODIS quite well.

Due to the structure of the model using elevation bands and snow information of MODIS being binary, sudden drops and jumps occur in the modelled snow cover. If one or more of these elevation bands are close to the 0 °C line and either get little snow or lose the last bit of snow, the surface is accounted completely for being snow covered or snow free. This could be prevented using a smooth function for deciding whether a surface is fully snow covered, fully snow free, or covered by snow to some extent. This however would pretend a model accuracy that is not necessarily given.

6.2.3 Snow accumulation

Although there are no big differences in comparing both models to the binary MODIS data set, there are differences in the behaviour of accumulating snow in the high elevations. These differences are shown in Figure 6-7, where a) refers to model A and b) to model B. While model B leads to snow accumulations of up to roughly 16300 mm SWE in 15 years of modelling, model B does not show any accumulation behaviour throughout several years. If the amount of snow accumulated would be distributed over the whole catchment area, the area would be covered by roughly 41 mm SWE at the end of the modelled time series.

However, in the realization of model A, snow does not melt completely every year. For instance, in the winter of 2005/2006, some 100 mm SWE remain in the peak region since that winter was colder than average (Förster et al., 2014; Ottaviani et al., 2010).

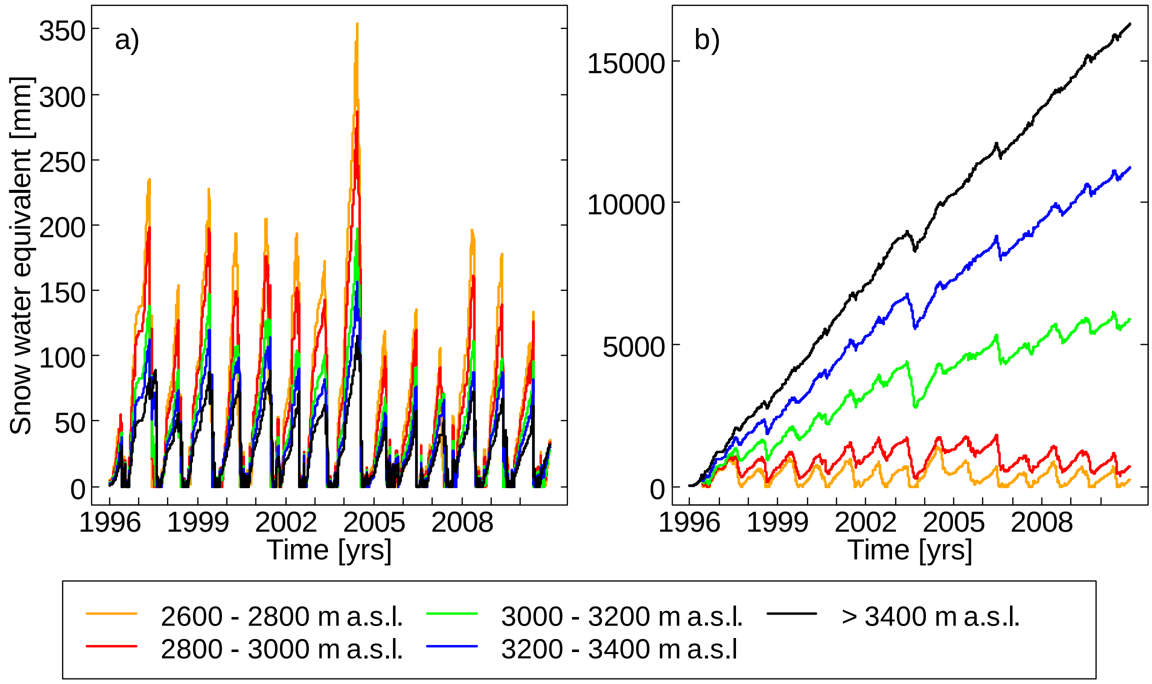

Figure 6-7: Snow accumulation in the upper 1000 m of the Salzach basin modelled with model A and model B. While using model A no accumulation throughout several years occurs (a), model B leads to snow accumulations of about 16300 mm SWE in 15 years of modelling (b).

Furthermore, using model B, the higher the elevation the more snow accumulates, while model A does show contrary behaviour in the upper altitudes. That can be explained by the redistribution routine and the shape of the peak regions. Since the area of each of the elevation levels grows moving downslope, a certain snow depth (mm SWE) transported from a smaller surface and distributed to a larger one becomes lesser in depth.

6.2.4 Conclusions and consequences for climate change impact modelling

Using a classical snow melt approach only considering temperature, snow accumulates on elevation levels where temperature values scarcely rise above the threshold for inducing snowmelt. This accumulation amounts up to about 1100 mm SWE per year. Hence it does not only picture snow behaviour in an inaccurate way but also influences discharge. It could be demonstrated that this behaviour of the model can be prevented using a simple redistribution routine that leads to model efficiencies (NSE) that could be improved by 0.04 to 0.89. Differences between both model A and B on the water balance in 2008 are about 2.8 % in which model A leads to more discharge and being closer to the observed runoff. Roughly 90 % of that difference originates from snow being transported to lower and hence warmer regions. Furthermore, due to glaciated surfaces being cleared earlier from their overlaying snow masses, glaciers also react differently enhancing their amount of melt. Some of the glacier area does not even get snow free in the classical model approach and therefore does not take part in the ablation process.

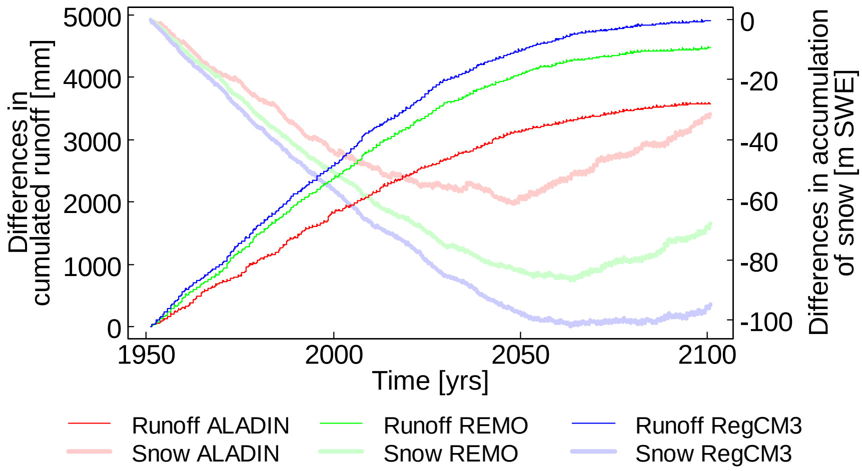

Figure 6-8: Influences of snow redistribution on the accumulated runoff and snow accumulation behaviour. Discharge is shown as cumulated differences between model A and B, meaning that the higher the values, the more discharge is predicted by model A in comparison with model B. Snow accumulation is shown as the accumulated differences of the mean snow depth at the top 600 metres of Salzach catchment and is given in metres SWE.

Given that knowledge it appears to be vital to account for snow redistribution when studying impacts of climate change on hydrological systems. This is fortified by Figure 6-8, where the influences of redistributing snow on the snow layer (mean of upmost 600 metres) and discharge over a time period of 150 years are shown for the realizations of the three used climate models. Differences in snow accumulation are large if climate conditions are similar to the conditions nowadays but decrease if the atmosphere is getting warmer. This may lead to an enhanced snowmelt in the second half of the 21st century that is caused from snow that is up to 100 years old and starts to melt because the temperature starts to rise above 0 °C on these altitudes more often. Consequently this leads to different runoff conditions. Relative deviations in runoff (25th, 50th and 75th percentile) are given by Table 6-2. While deviations regarding low flows are rather negligible, the median and third quartile differs considerably. Until the second half of the 21st century, more runoff is generated by model A, in the last 30-year period, REMO and RegCM3 lead to less runoff using model A due to the reasons discussed before. Differences are up to 4 % and therefore do considerably affect the results of the climate change impact study, where differences in runoff of about 6 to 18 % are reported. See chapter 6.5.4, especially Figure 6-37.

Table 6-2: Relative runoff deviations of the 25th, 50th and 75th percentile of model B in respect to model A.

	ALADIN			**REMO**			**RegCM3**		
Percentile	**25th**	**50th**	**75th**	**25th**	**50th**	**75th**	**25th**	**50th**	**75th**
1951-1980	0.0%	1.2%	2.8%	1.2%	1.1%	3.3%	1.2%	1.6%	4.3%
1981-2010	0.0%	0.8%	3.3%	0.0%	0.9%	2.7%	0.4%	2.3%	3.8%
2011-2040	0.0%	0.3%	2.4%	0.4%	1.6%	2.5%	0.0%	0.3%	4.1%
2041-2070	0.0%	1.1%	1.6%	0.0%	0.6%	1.3%	0.4%	0.9%	1.4%
2071-2100	0.4%	0.3%	0.2%	-0.4%	-0.3%	0.4%	0.0%	-0.3%	-0.4%

6.3 Snow redistributing in COSERO – A case study in the Ötztaler Ache

Snow accumulation in high elevated areas might be a problem when using temperature-only methods for estimating snowmelt as already shown in the previous chapter. However, since SASWET is not capable of taking processes into account that are important on a scale smaller than the elevation levels used in the model, it is of interest, how a raster based hydrological model can deal with this challenge. The results shown here are published in Frey and Holzmann (2015). This chapter therefore is based on said publication.

6.3.1 Discharge

Figure 6-9 shows a comparison of total discharge using model A and B at the gauge Huben for the year 2006. Both models result in similar quality criteria in the calibration as well as in the validation period (see Table 6-1).

In spring, at the beginning of the melting season, more runoff is generated by model A due to a larger amount of snow in lower altitudes. Later in the year enhanced glacier melt is mainly responsible for higher discharge rates. Maximum differences in the mean daily discharges between the two models reach up to 2 mm d^{-1} (12.1 m^3 s^{-1}). This leads to a relative difference of minus 9 up to 44 % of model A in respect to model B. In total, model A generates about 300 mm more discharge in five years than model B (Figure 6-10). About 200 mm have their origin in enhanced snowmelt, while the remaining 100 mm originate in amplified melt of glaciers. Assigned to the glaciated area in the basin, this leads to an additional loss of 500 mm of glaciers. The reason for this is transport of snow in warmer altitudes and therefore no or less snow will remain on the glacier surfaces. This leads to earlier and more snow free glacier areas producing more runoff due to glacier melt (see Figure 6-10).

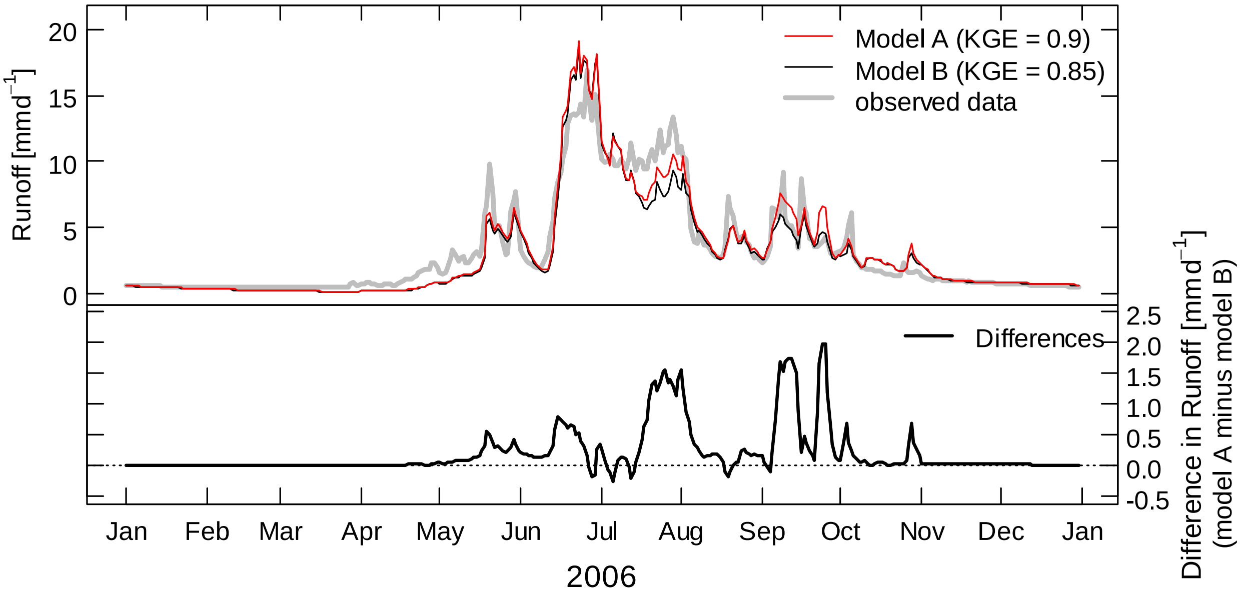

Figure 6-9: Runoff at the outlet at Huben is modelled with (model A) and without (model B) using the snow redistribution routine. In the early snow melt period, more runoff is generated by model A because snow accumulates rather in lower than in higher levels. In summer, enhanced glacier melt leads to more runoff by model A.

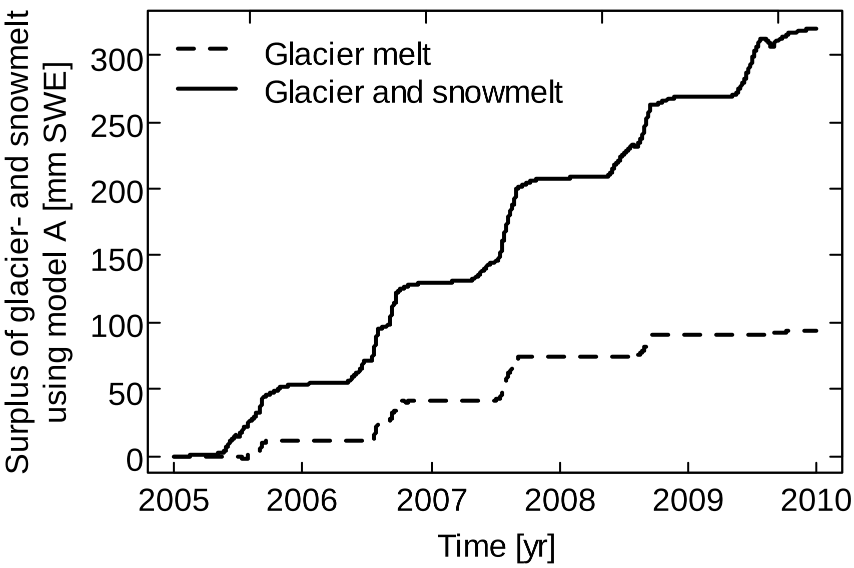

Figure 6-10: Accumulated differences (model A minus model B) in discharge at gauge Huben. Using model B, about 300 mm SWE in five years are remaining in the catchment due to snow accumulation processes and less glacier melt.

6.3.2 Spatially distributed snow cover data

Figure 6-11 compares model A and B with MODIS data. As well the accumulation period in winter as the ablation period in spring and summer are represented well by both models. This means that only little effect of the transport model can be noticed comparing model A and B with MODIS data and both models show similar model efficiencies (Figure 6-11).

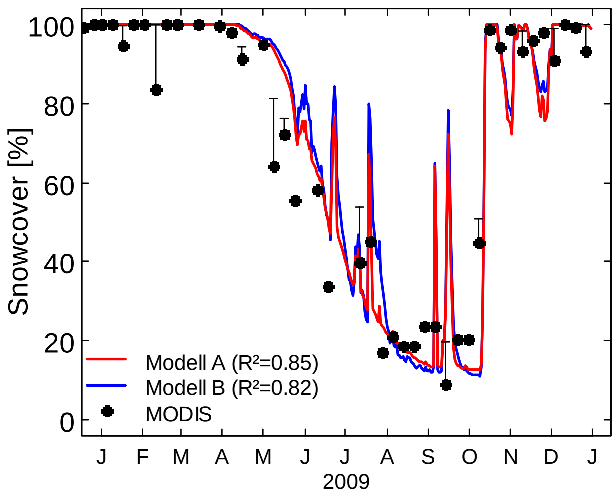

Figure 6-11: Snow cover in 2009 modelled by both model A and B compared with MODIS data. Error bars refer to uncertainties due to cloud cover.

The reasons therefore lay in the threshold due to vegetation and roughness of the surface. Satellite based snow cover information by MODIS are binary and so is the model output for comparing these results. Even if snow is transported to other cells, a residual of snow remains on the donor cell. In a binary system, no difference can be distinguished between cells holding copious or little amounts of snow.

6.3.3 Snow accumulation

The main reason for developing a snow transport model was the prevention of “snow towers” – accumulation of snow over several years in high mountainous regions. Figure 6-12 presents model behaviour of model A and B with respect to the accumulation of snow in elevations above 2800 m a.s.l. This elevation was chosen because here none of the models indicates snow accumulation for more than one year and therefore snow accumulation in lower altitudes is no problem. Similar behaviour could be observed in the watershed of Salzach River, even though this basin was modelled by a different model. After seven years of modelling, model B shows snow of approx. 2900 mm SWE in elevations above 3400 m a.s.l. whereas model A does only show little accumulation behaviour in these altitudes. The remaining accumulation is explainable by the neglect of processes regarding snow metamorphosis to ice. To include this however, the model would need a sophisticated glacier module including snow metamorphosis and movement of glaciers. Note that in Figure 6-12 only model results from 2005 to 2010 are shown while the warm-up period is missing due to a better perceptibility. Therefore snow depth does not start at zero in the figure while it does at the beginning of the modelling.

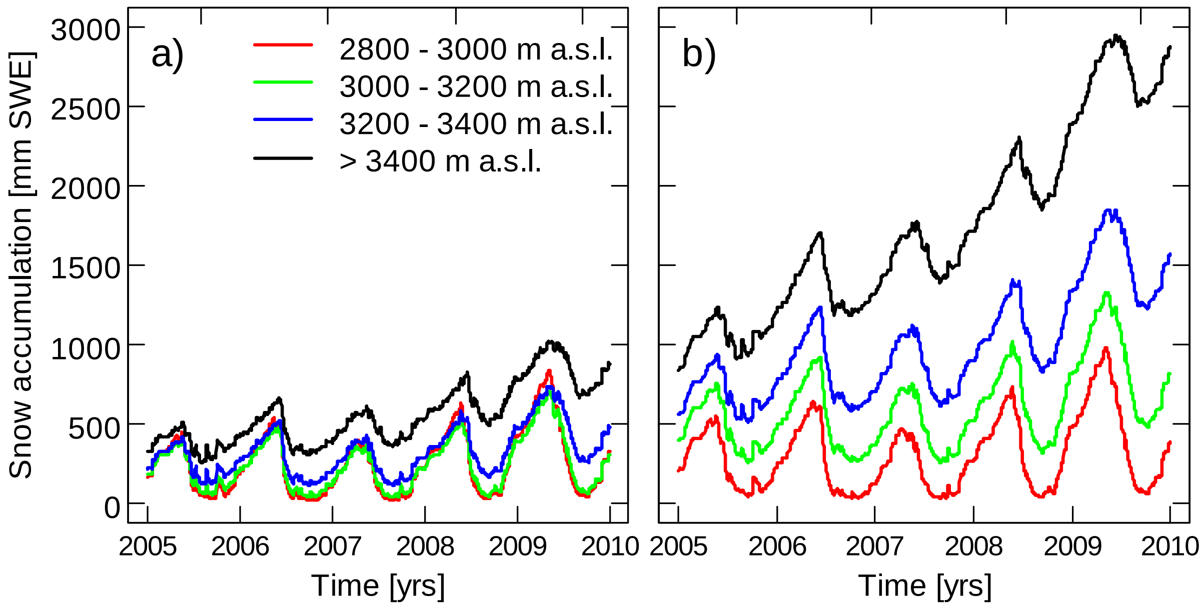

Figure 6-12: Behaviour of snow accumulation and melt of model A (a) and B (b) in the upper elevations. Model B leads to “snow towers” of approx. 2900 mm SWE in regions above 3400 m a.s.l. in seven years of modelling, whereas model A does not show such behaviour. On elevations lower 2800 - 3000 m a.s.l. neither model A nor B show accumulation behaviour. Note that model results are shown from 2005 to 2010 without the warm-up period.

While using model B, the higher the elevation the more snow is situated on. However, model A shows less pronounced and in some time periods even contrary behaviour in the upper altitudes. This is a result of the slope dependency of the distribution model that transports more snow towards greater slopes. Since mountains, in general, are steeper at their peaks and more flat in the lower parts, snow will preferably be transported from the peak cell over a steep slope to the adjacent cell which normally has a moderate slope to its downward neighbour. Subsequently, less snow is transported from this cell. This does reflect snow accumulations that can be observed in nature where peaks might be nearly snow free in spring while flatter parts are still covered by a snow layer. Figure 6-13 illustrates the spatially distributed net loss and gain of snow per cell during the time period of one year. While the raster cells covering peak regions act as donators only those cells located on slopes may receive and distribute snow at the same time. Valley regions only receive snow. However, due to the binary nature of MODIS data, the spatial snow depth distribution cannot be validated with observed satellite based data.

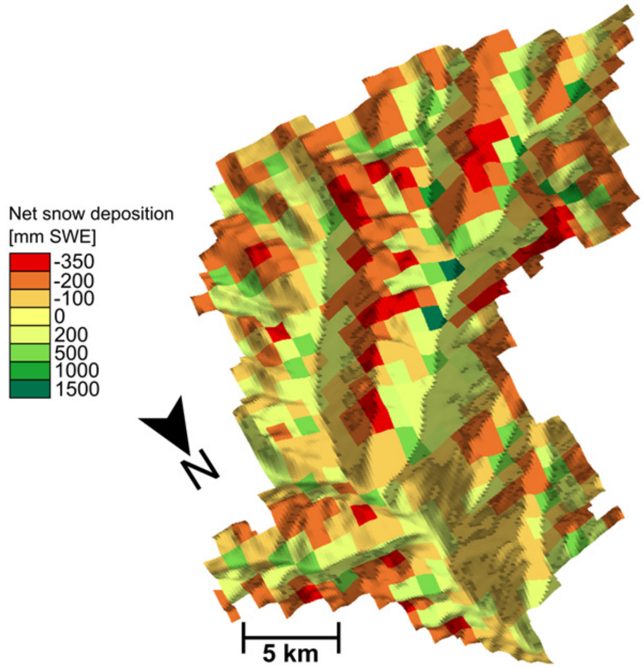

Figure 6-13: Net snow deposition in the catchment during the time period of one year. Negative values refer to a net loss, positive to a net gain of snow. Raster cells in the peak regions act as donor cells and do not receive any snow whereas lower cells may act as donor and acceptor in the same time. Note that, since only the net deposition of snow is shown, values cannot be linked to snow depths at the end of the time period.

6.3.4 Parameter Uncertainty

Although the model uses many parameters snow redistribution only adds two more: (i) the height of vegetation and surface roughness to determine the threshold for snow redistribution (H_v) and (ii) the correction coefficient (C). H_v is estimated a priori based on studies by other authors (Liston and Sturm, 1998; Prasad et al., 2001). Anyway, a model using many parameters necessarily suffers from equifinality issues. This issue cannot be overcome. Adding parameters on the one hand enhances this issue, but on the other hand by allowing the model to account for more processes may also make the model more robust (Gharari et al., 2014; Hrachowitz et al., 2014).

A Monte Carlo simulation was performed to study robustness and behaviour of model A compared to model B (Figure 6-14). Snow relevant parameters (CT_U, CT_L, NVAR, RAINTRT, SNOWTRT and the correction factor for snow redistribution C) were varied according to normal distribution. The parameters did vary in every grid cell separately. Both model A and model B were run with the identical parameter set. Model A not only leads to better model efficiencies regarding runoff but also seems to be more robust (Figure 6-14 a) and b)). In addition model A leads to less snow accumulation in the summit region.

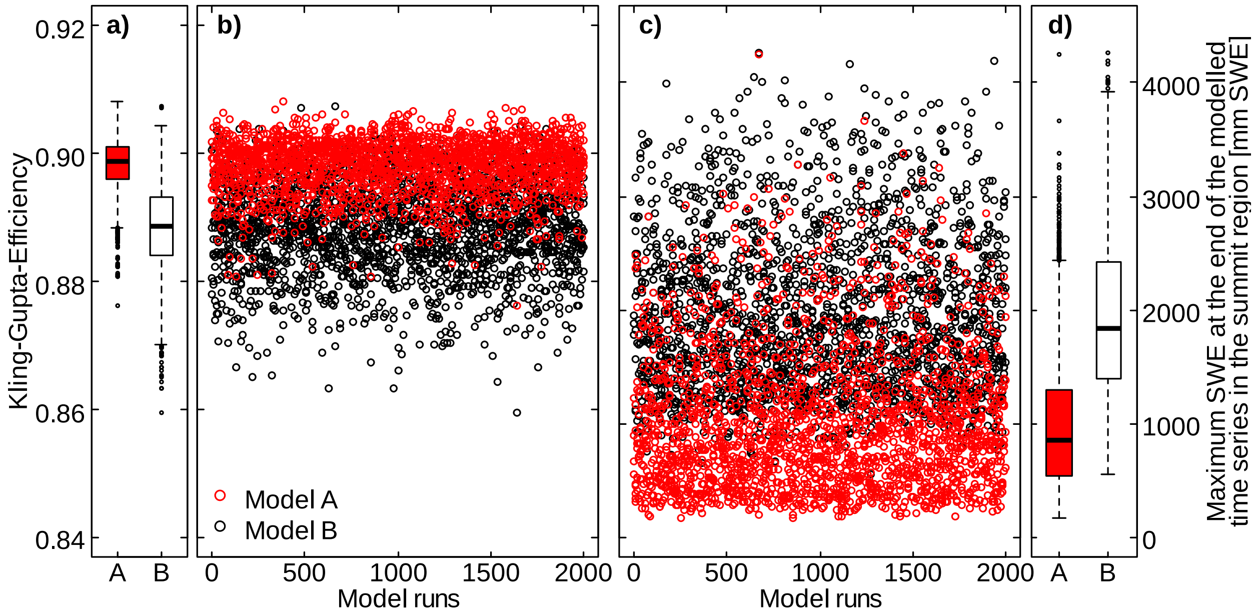

Figure 6-14: Model efficiency regarding runoff (a, b) and snow depth in the summit region (c, d). A Monte Carlo simulation of 2000 runs was performed varying the parameters CT_U, CT_L, NVAR, RAINTRT, SNOWTRT and the correction coefficient for snow redistribution C. The input was generated according to normal distributed parameter distributions. The parameters did vary in every cell separately. Both model A and model B used the same parameter set per run. Model A clearly leads to better model results according both runoff and snow accumulation behaviour. It also seems to be more robust. Note that only the maximum snow accumulation in the summits (> 3400 m a.s.l.) is plotted in c) and d).

The robustness of model A compared to model B needs more research. A possible explanation is that lower values for CT_U and CT_L are causing model B to perform worse due to snow accumulation issues whereas model A is capable of melting snow even when using low CT values. When applying high CT values both models lead to good efficiencies because also model B is able to melt snow in most of the cells. That makes model A less sensitive for the parameters CT_U and CT_L and allows to modeller to use more realistic values of these. The term realistic in this case refers to lower values. Based on the topography and the resulting radiation index, Kling et al., (2006) reported ranges for CT_L and CT_U of 1.2 to 2.2 and 2.0 to 3.0 mm °C^{-1} d^{-1}, respectively, for Austria. Most modellers would use way higher values especially for CT_U.

6.3.5 Snow redistribution in larger catchments

The smaller the portion of high altitude regions in a catchment compared to the entire area of the basin, the less important is snow redistribution for modelling runoff. The ratio of summit regions to total catchment size is usually smaller for larger catchments. The catchment of river Inn (gauge Oberaudorf at the Austrian-German border), for instance, covers an area of about 10000 km² yet only 733 km² are located at elevations where intensive snow accumulations and mobilizations occur (above 2800 m a.s.l.). In the basin of the Ötztal 204 of 511 km² are located above 2800 m a.s.l. If model A is applied to the catchment of river Inn in five years of modelling about 15 mm SWE (with respect to the entire river basin) remain in the catchment due to snow accumulation processes instead of 300 mm in the Ötztal. This may be the major reason why snow redistribution is often not considered in hydrological models on larger scales.

6.4 Uncertainties in hydrological modelling – A case study using WaBi

In this case study influences of model uncertainties of hydrological models are compared to differences between climate models. Since different climate models necessarily lead to different climatological data this may be interpreted as uncertainty originating from the side of climate modelling. The combination of both uncertainty sources lead to a combined uncertainty in climate change impact studies regarding hydrological response. Additionally, since this study was part of a project aiming towards an estimate of the hydroelectric power potential of the national states Switzerland, Germany, France and Ital, model results from the hydrological model WaBi are statistically linked to the generation of electric power in the those countries provided by ENTSO-E data (see chapter 4.6). Based on this statistical relationship the hydroelectric power potential under changing climate conditions can be estimated using the same ensemble of regional climate models as for estimating the impact climate change has on Austrian basins.

Even though energy cannot be generated or produced but only transferred from one form to another, the terms of energy production or energy generation are commonly used in literature (e.g. Frey and Linke, 2002; IEA, 2014; Katsigiannis and Stavrakakis, 2014) and therefore will be used in this work as well.

6.4.1 Calibrating the model to discharge

Since the water balance model WaBi is a very simple model and therefore runs very fast (one model run over 150 years needs about 5 seconds), allowing to perform many runs within maintainable time, it is suitable for testing uncertainties of hydrological modelling versus climate model uncertainties. Each of the five regions upper and lower Rhône, Central Massif, northern Italy and the catchment of river Rhine was modelled using Monte Carlo simulations. The range of parameters was defined using the functions *rnorm* and *rlnrom* in the software *R*. Those functions generate random deviates from a mean value with given standard deviations. While *rnorm* uses a normal distribution, *lrnorm* uses a log-normal distribution. Normal distribution were used for the parameters CT_{snow} and CT_{ice} while k_{one}, k_{two} and C_{ETP} were generated using log-normal distribution. Standard deviations were set to one in the case of normal and to 0.25 in the case of log-normal distributions. Log-normal distributions were used to postpone the expected value towards the left side within the normal distributed parameter space. Mean values were predefined by manual model fitting and hence differ among the different catchments. Using only the mean and standard deviation has the advantage that no strict upper or lower boundaries are necessary.

The quantity of runs was chosen on the basis of density functions (see Figure 6-15) to be certain, that the density distribution of each parameter does not differ anymore when performing more runs. This was achieved at the stage of 500 000 runs. The best 1 ‰, i.e. 500 simulations, in terms of mean error were picked for further analysis. These are visualized in Figure 6-16. In general, the model is able to reproduce the annual hydrological dynamic of all regions leading to rather narrow uncertainty bands. Problems exist in winter and early spring of the basin of lower Rhône. One has to be aware that the lower Rhône strongly depends on discharge of the upper Rhône and that both (sub)basins are influenced by hydropower plants. The second basin, on which the modelled discharge differs from the observed, is northern Italy. As mentioned before, both gauging stations in northern Italy are located downstream of lakes. These lakes influence the hydrograph of the rivers by natural and anthropological reasons. The model however is not capable of considering lakes. This explains why the modelled discharge rises and falls earlier in the year than the observed discharge. Runoff in winter in the region of Massif Central is underestimated by all parameter sets.

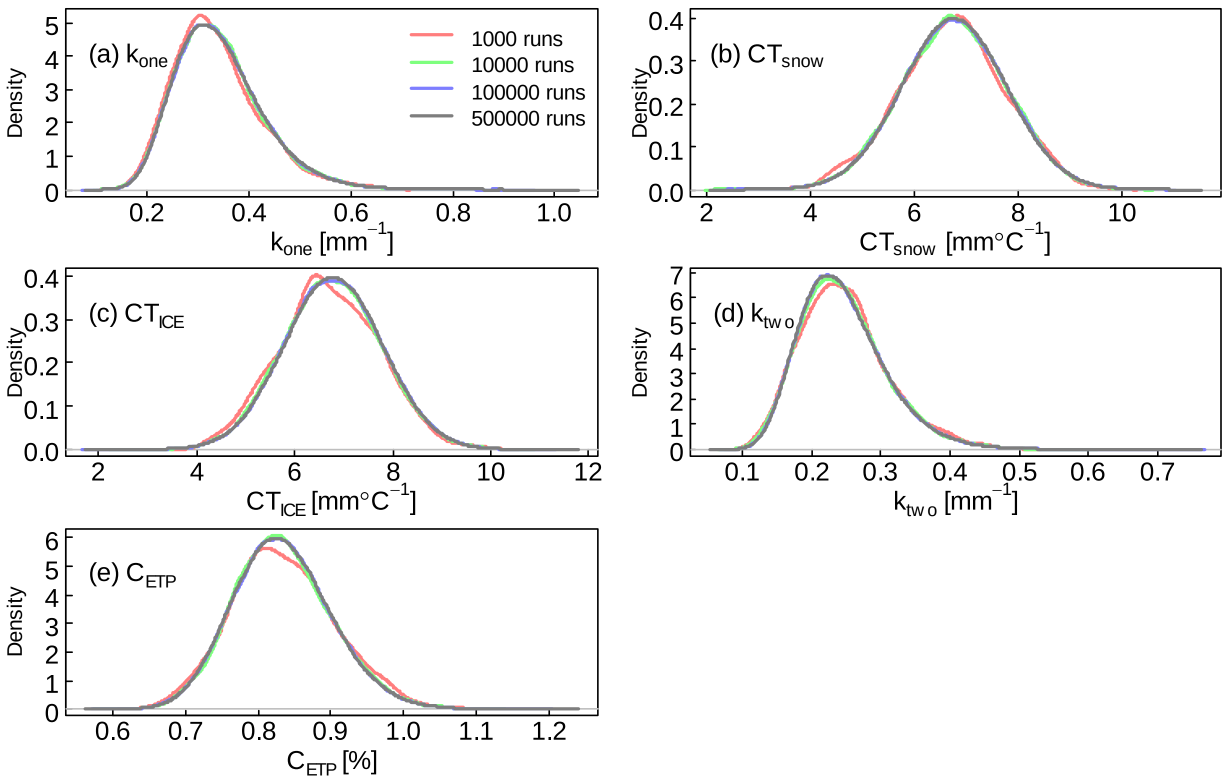

Figure 6-15: Densities of parameters for different sample sizes of Monte Carlo simulations for the catchment of river Rhine. No differences between 100 000 and 500 000 simulations can be observed.

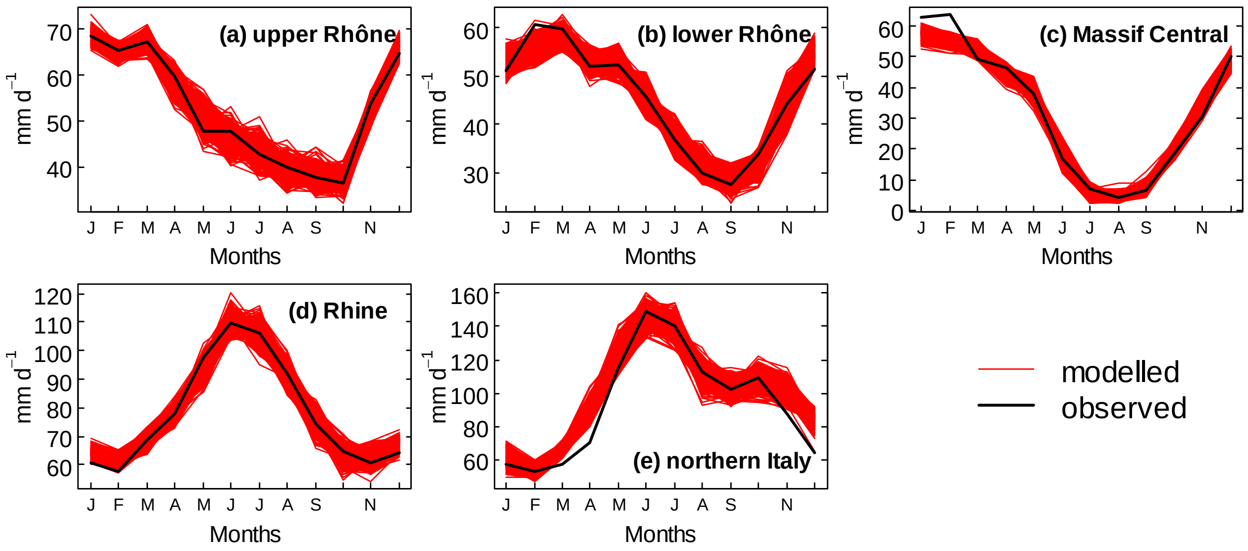

Figure 6-16: Calibration results of WaBi performing 500 000 Monte Carlo simulations and visualizing the best 500 runs in terms of mean error (after Frey and Holzmann, 2014, edited).

6.4.2 Climate change impact modelling

The parameter sets (best 500 of 500 000) found in the calibration procedure were used to perform climate change impact analysis on annual discharge behaviour at the end of the 21st century. Every one of these calibrated model realizations was run using climate input from three RCMs ALADIN, REMO and RegCM3, the same RCMs used for the impact studies in Austria. This results in a total of 1 500 model realizations per region. Figure 6-17 shows the predicted runoff conditions in the time period 2071 to 2100 including uncertainties provoked by both the hydrological model and differences between the used RCMs.

High uncertainties in predicting runoff for lower Rhône (Figure 6-17b) are caused by the hydrological input (discharge) from upper Rhône being insecure and the uncertainties of the basin of lower Rhône itself. As stated before, lower Rhône depends on the discharge of its upstream watershed. If two uncertain models are added up, the uncertainty of the total output will be higher.

It should be noted that only one realization per RCM is used in this study. Similar to hydrological models, climate models are prone to parameter uncertainty as well. One parameter set of the RCM REMO for instance does not necessarily lead to the same climate signal as another parameter set. However, this was not considered in this study.

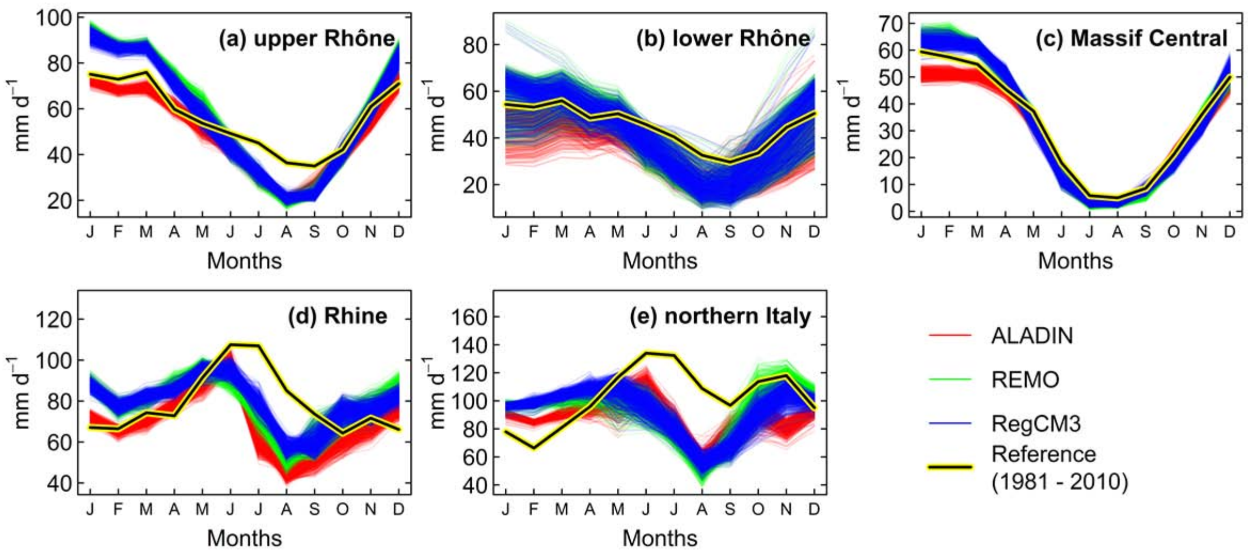

Figure 6-17: Runoff conditions at the end of the 21st century in the five regions (after Frey and Holzmann, 2014, edited). Uncertainties within the climate models are caused by the parameter sets found by the calibration procedure. High uncertainties in the basin of lower Rhône can be explained by the uncertainties of the input to the basin by the runoff from upper Rhône added to uncertainties from lower Rhône itself.

6.4.3 Linking runoff to electric energy potential

Based on the selection of model regions, electric energy potential for France is estimated using upper and lower Rhône as well as Massif Central, Germany is represented by the river Rhine only. The same accounts for Italy which is represented by the region of northern Italy. Switzerland is overlapped by the upper Rhône, river Rhine and northern Italy. The application of a multiple regression in the form of Eq. (5-1) implies a linear relationship between runoff and electric power generation. Turbines used in run-of-river power plants show an approximately linear relationship between river runoff and the energy they provide for a vast range of discharge (see e.g. Madani and Lund, 2009). Only close to the edges of the flow duration curve (e.g. high and low flows) this relationship is not valid anymore. Since runoff is modelled on the basis of monthly data, these extreme events are not included in time series of discharge which allows for applying linear regression. Nevertheless, other types of regression analysis have been tested including logarithmic and cubic functions as well as fourth degree polynomial functions. The best fit could be achieved using linear regression, though. Other fits are not shown in this thesis.

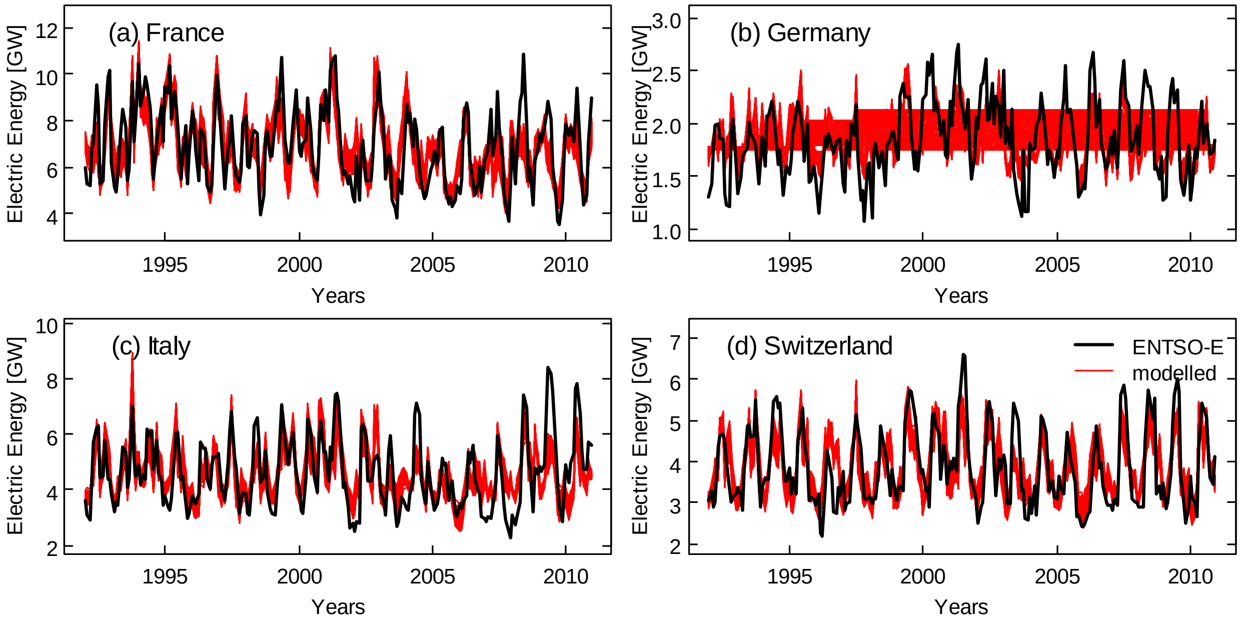

Figure 6-18: Linking modelled runoff in different regions to generation of electric energy in four European countries using multiple regression analysis. Correlations (R^2) vary between 0.72 and 0.85 for France, 0.58 and 0.71 for Germany, 0.63 and 0.82 for Italy and 0.63 and 0.78 for Switzerland.

In Figure 6-18 time series of modelled and observed data on electric energy generation are plotted. In general, a good estimation of electric energy generation could be achieved, whereupon results are more confident in France and Switzerland than in Germany and Italy. This can be explained by the number of overlapping model regions leading to a more accurate regression. In addition to that, electric energy generation of Germany is represented by the Alps only which is a vague simplification as a significant amount of power plants are located downstream of river Rhine and in the low mountain ranges in Germany.

Given the good results in both calibrating WaBi and in transferring modelled runoff to electric energy generation it is possible not only to estimate runoff conditions under a changing climate but also to link these new conditions to electric power generation. This assumes however that no power plants are built or shut down since this would change the relationship between runoff and power generation.

6.4.4 Estimating electric power generation in the future

Using the relationships found by transferring runoff to observed power generation, future trends in generating electric energy are estimated. Again, these estimations are carried out for the 500 model realizations of WaBi found to be the best during calibration. This allows for giving more detailed information about uncertainties in future electric energy generation than the use of only one parameter set for WaBi would allow. In Figure 6-19 uncertainties derive from (i) parameter uncertainties of WaBi and (ii) variability within the respective climate normal. Data basis of

Figure 6-19 is mean annual electric energy generation. Additionally the multiple regression method causes uncertainties as well. However, this was not considered in this study.

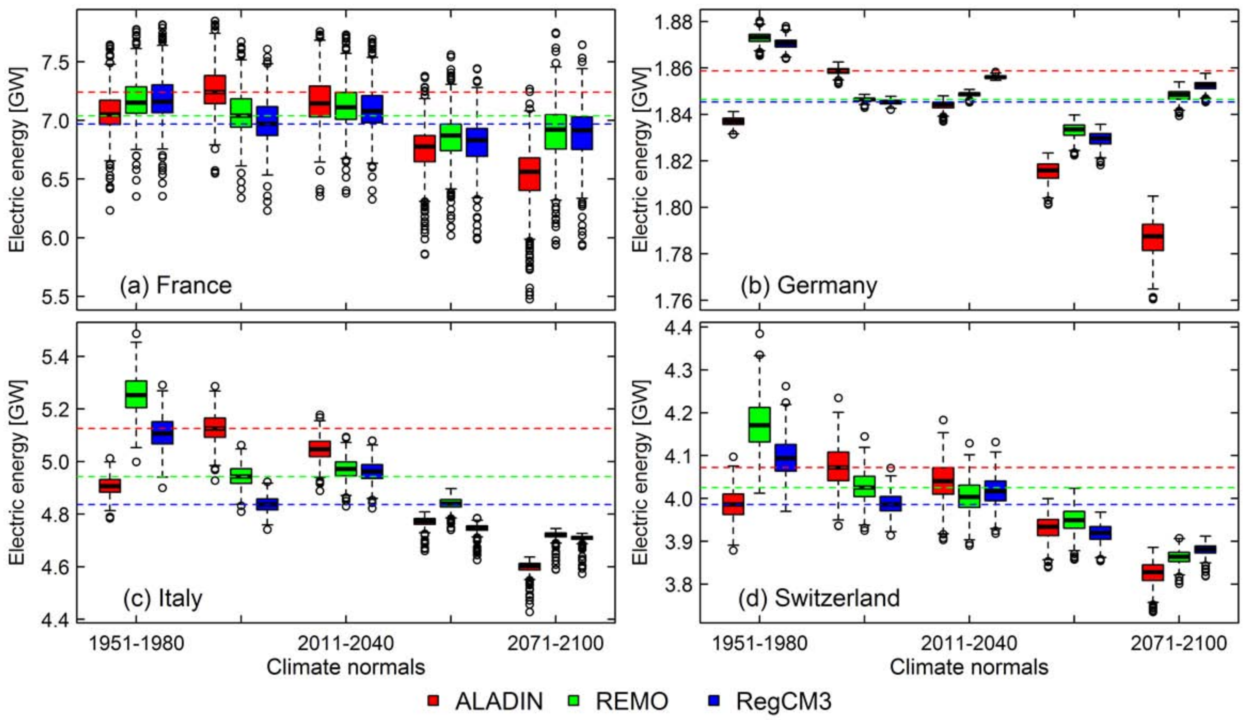

Figure 6-19: Generation of electric power partitioned five climate normals. Boxes mark the first and third quartiles, whiskers represent 1.5 times these quartiles. Uncertainties originate from (i) the hydrological uncertainty due to the parameter set and (ii) the variability within the respective climate normal. Dashed lines mark the median levels of the realizations using the respective RCM during the reference period 1981 to 2010.

Uncertainties in France are greater than in the other countries. The reason for this is the catchment of lower Rhône. As discussed before, estimation of discharge in this basin is more uncertain due to the blurry hydrological input from its upstream basin (see Figure 6-17 and its discussion).

In general, the potential of generating electric energy out of run-of-river stations will most likely decrease until the end of the 21st century. The realizations using both ECHAM5 driven RCMs in Germany however signal a slight increase of electric energy generation possibilities.

Net generation of electric energy over the year does only picture influences of climate change on hydropower potential to a certain extent. Figure 6-20 pictures the situation of electric energy generation at the end of the 21st century for the respective countries on a monthly resolution (for other climate normals see Figures A 2 to A 5 in the appendix). In three of the four countries it may be the case that the average energy generation potential drops while in some seasons, particularly in winter, it may be possible to benefit from climate change. This is especially interesting, since the need for energy in general is higher in winter than it is in summer.

However, this might not be true for a warmer climate, when cooling plays a more important role than it does now (Hamlet et al., 2010).

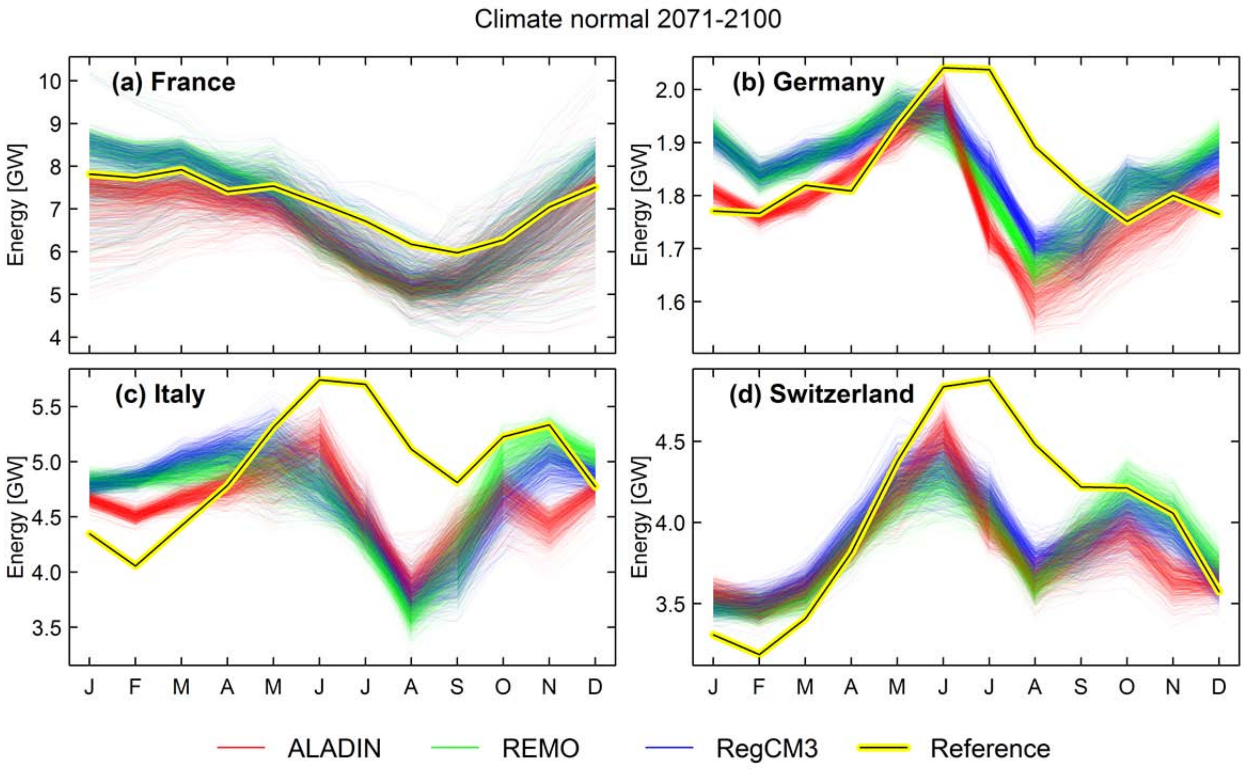

Figure 6-20: Average energy generation potential per month in the climate normal 2071 to 2100. Reference period represents the power generation averaged over both climate and hydrological model in the climate normal 1981 to 2010.

6.4.5 Conclusions and outcomes

In this study hydrological uncertainties have been compared to differences in miscellaneous climate models. Many parameter sets of a hydrological model may lead to similar model efficiencies. This finding of equifinality is not new, in fact is has been stated very often by several authors (e.g. Beven, 1993, 2001; McDonnell et al., 2007 amongst many more). The use of more than one parameter set allows statements about the uncertainties of the hydrological model. In this study, an ensemble of 500 model parameter sets per model region out of 500 000 have been used for further analysis. Density distribution analysis of the parameter distribution shows that the count of 500 000 parameter sets is appropriate. The selection of the 500 best runs representing the best 1 ‰ of model realizations is somewhat subjective. However similar choices have to be made when using other uncertainty analysis methods like GLUE (Beven and Binley, 1992). Using this set of parameter combinations leads to ranges of uncertainties in each model region in terms of (i) runoff and – in combination with multiple regression analysis – (ii) electric power generation in national states. Hereby a linear relationship between runoff in overlapping regions and generation of electric power of the respective countries is assumed. Good correlations (R^2) between discharge and electric power potential have been found ranging from 0.58 to 0.85.

Performing model runs using meteorological input data from different climate models shows that the hydrological uncertainties often are superimposed by differences between climate models. Similar results were found by Teng et al. (2012) for different structures of hydrological models applied to Australian basins. In general, two major outcomes may be stated on the basis of this (see Figure 6-17):

(i) Uncertainties caused by the use of different climate models are higher than the uncertainty caused by the hydrological model. Using WaBi for climate change analysis on the monthly to annual scale therefore is limited by fuzzy climate data caused by the use of different RCMs. However, exactly that behaviour is wanted to cover a more realistic range, than the use of just one model would allow.
WaBi indeed is a very simple model with only few parameters, however, for the use of representing annual discharge series it fulfils its needs. It should be stated that when using a more complex model, hydrological uncertainties may be greater, though.

(ii) Although the use of three climate models covers a wide range in climate change impacts, some general behaviour can clearly be stated. Runoff in the cold season of the year is likely to be increased, while during the summer months a decrease in discharge has to be expected. Most distinct, this can be observed in the runoff of river Rhine and in northern Italy. Same accounts for the basin of upper Rhône, albeit differences are less pronounced. Due to the high uncertainties of lower Rhône for said reasons, clear statements are difficult. However, most model realizations signal a decrease in summer discharge. Different situation is in the region of Massif Central. In the reference period, runoff in summer is already close to zero (see also Figure 6-16c), hence hardly any further decrease is expected or even possible. Only in winter to early spring there is a difference compared to the reference. But even here, models do not agree upon the direction of change.
The main reason for changes in runoff is increasing air temperature. Snow melts earlier in the year leading to enhanced runoff in winter and thus to lower discharge rates in the summer months. The latter is amplified by shrinking glacier masses producing less melt water. Additionally, higher values of ETP occur in summer.

Linked to the generation potential of electric energy production the results are affected by the uncertainties of the hydrological model as well as by both differences in RCMs and uncertainties caused by multiple linear regressions. The signal of climate change in most cases however is as strong as valid conclusions may be carried out. Mean annual power production potential drops in the majority of the study countries. Only in France are the uncertainties as big, as no clear statements are appropriate. However, even in this case a trend towards lower energy potential is

recognisable. Germany may, according to the realizations of both ECHAM5 driven RCMs, benefit from a changing climate. It needs to be stated, that the statistical correlation between runoff and energy production in Germany is the lowest.
On the seasonal scale, the energy production potential of most countries will increase in winter. This is caused by less water being stored in the snowpack in the respective regions and subsequently higher discharge rates in winter. Even if total net annual energy production in a country decreases this country may benefit from higher energy production potentials in winter. The demand for energy is generally higher in winter. However, due to an increased demand for electric energy for cooling in summer as a result of higher temperatures, this may not be true for the future.

6.5 Future discharge conditions in Austrian basins

6.5.1 Can the hydrological model predict discharge in a changing climate?

Often climate change impact studies using conceptual hydrological models are criticized for conceptual models would not be able to reproduce the hydrological behaviour of a watershed under changing conditions (Efstratiadis and Koutsoyiannis, 2010). The lack of feedback mechanisms is often named as main reason for that. However, if one assumes there already has been a change in climate since the 1950s and the model is able to reproduce runoff up to at least a certain extent, one can rely on the model for future scenarios. Due to the use of RCM data to reproduce the runoff behaviour in the past, it cannot be expected that the model is able to reproduce discharge on a daily basis with the same accuracy as it is during calibration and validation, though. For river Salzach, shown in Figure 6-21, the model produces monthly average discharge values close to the observed discharge. The use of ALADIN leads to generally lower discharge rates than the other two RCMs. While summer discharge values in general are rather underestimated by the model, runoff in autumn and early winter is slightly overestimated. Flow duration curves produced by the model realizations match the observed runoff in the greatest parts well. Only the high flows are underestimated by all models.

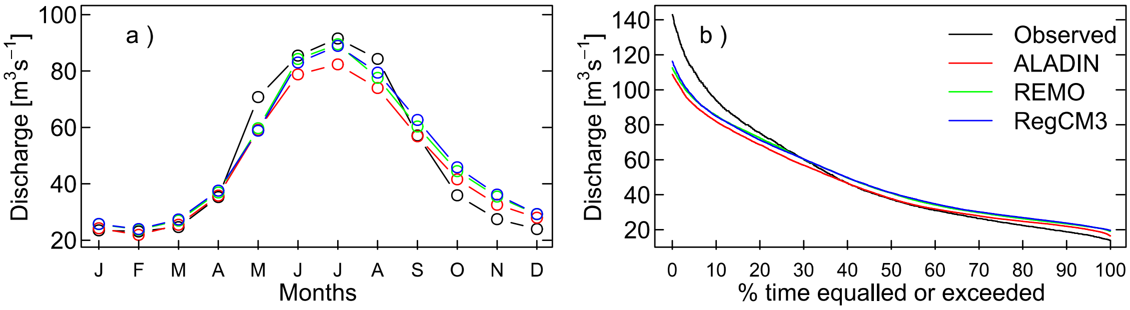

Figure 6-21: Comparison of observed and modelled discharge of river Salzach during the climate normal 1951 to 1980 using meteorological input data of the RCMs ALADIN, REMO and RegCM3. Part a) of the figure represents monthly average discharge rates while the flow duration curve in b) is computed on the basis of daily discharge data.

The results shown in Figure 6-21 for Salzach River are valid for other basins, too. The results not being as good as the results during the calibration and validation periods was expected for two major reasons: (i) data quality and (ii) anthropogenic caused structural differences (e.g. river dams) since the 1950s.

(i) The model was run using meteorological input generated by RCMs. While these are able to reproduce long term characteristics of a catchment, they fail reproducing meteorological data on a daily basis even though they were bias corrected.

(ii) The model was calibrated to the characteristics of the catchment in the time period 1996 to 2006. Thus it represents the hydrological response according to these catchment characteristics. In the Salzach River basin, several hydropower plants were built in between the 50s and the 90s (e.g. Uttendorf I/II, Schneiderau, (ÖBB, 2015; Seefeldner, 1961)). In addition to that several other changes on the infra-structure like roads, railways etc. have been made since the 1950. Changes in the structure of a watershed influence its behaviour. However, the hydrological model is not able to react on these changes.

Climate change does not only affect future climate but already has had impacts on climate conditions in the past. The WMO 1999 reported an increased temperature of 0.7 °C in the Swiss Alps in comparison to 1900 (WMO, 1999). The fact that the hydrological model is able to reproduce runoff under climatic conditions different to those when it was calibrated with good efficiency supports the theory that it is convenient for stating runoff conditions under further changing climatic conditions. However, the model cannot react to changes in the watershed that may arise due to land-use or structural buildings. A further constraint may be given by non-linear processes that may occur in a warming environment such as evapotranspiration processes. The lack of feedback mechanisms still exists, of course. Hence, the results presented in chapter 6.5 and discussed in the following have to be seen under these restrictions.

6.5.2 Evolution of the annual amount of available discharge

Looking at the evolution of annual runoff in the ten basins gives an estimate about the general trends in hydropower potential since runoff and the potential to produce electricity using hydropower are correlated. Figure 6-22 gives an overview of the evolutions in runoff in the ten study basins. Note that in Figure 6-22 the moving average over five years is shown which smoothes the curves eliminating extreme values. In most watersheds a decreasing trend in runoff can be observed during the last 50 years of the 21st century. ALADIN shows the most distinct trend whereas the other two RCMs show less pronounced trends and in some watersheds even a slight increase within the last decade of the century.

Besides a possible decrease in runoff caused by decreasing precipitation, less water reaches the outlet of a basin due to increased evapotranspiration rates. Figure 6-24 shows both actual and potential annual evaporation rates during the modelled time of 150 years.

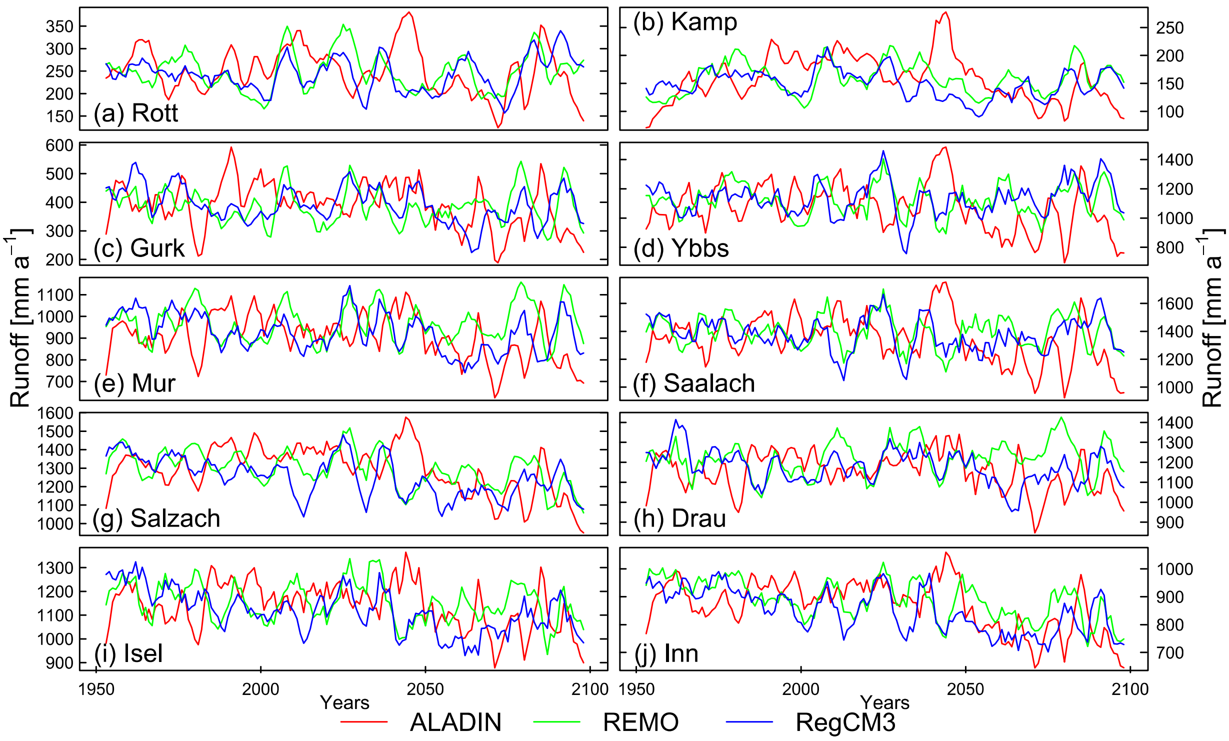

Figure 6-22: Five year moving average of annual mean discharge in the ten basins.

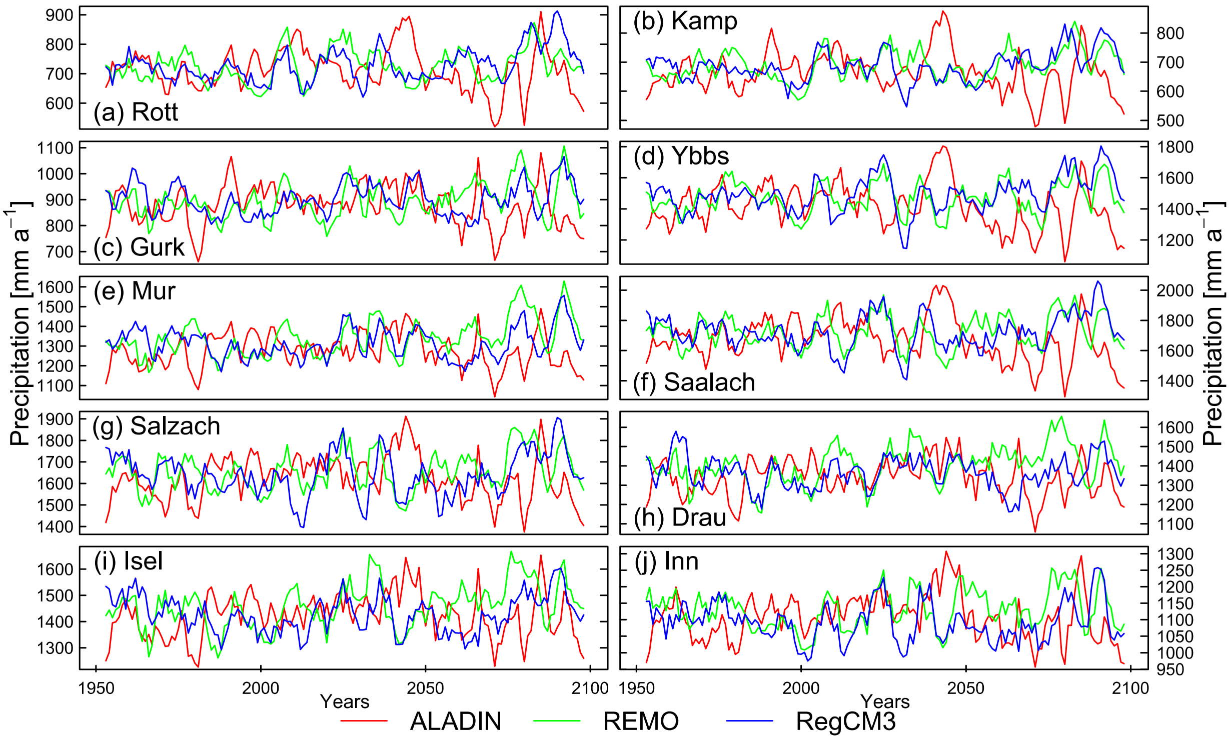

Figure 6-23: Five year moving average of annual mean precipitation in the ten basins.

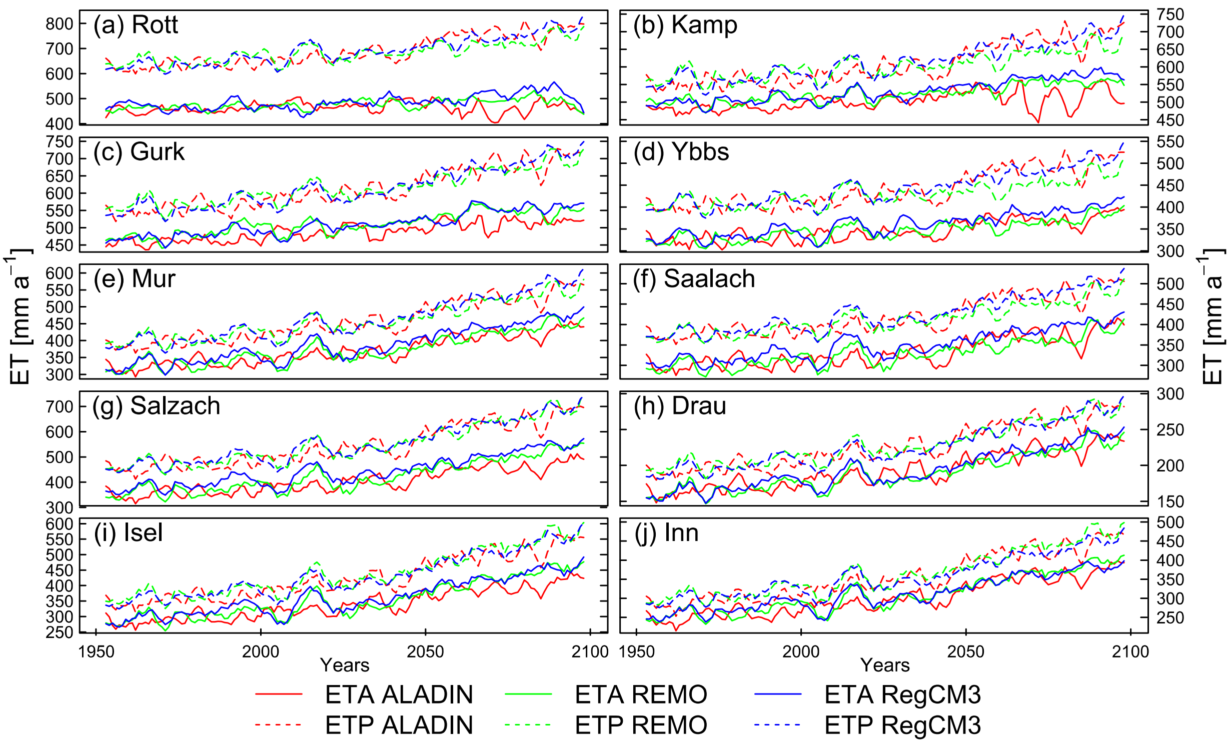

Figure 6-24: Five year moving average of annual mean actual and potential evapotranspiration in the ten basins. Since the actual evapotranspiration in the model is a lumped state variable both ETA and ETP rates are areal weighted averages of the watersheds.

It is noticeable, especially in mountainous catchments, that rates of evapotranspiration in general did not start to rise before the year 2000 although values of air temperature increased since the start of the model period. The mean annual air temperature (area weighted) per watershed is given in Figure 6-25.

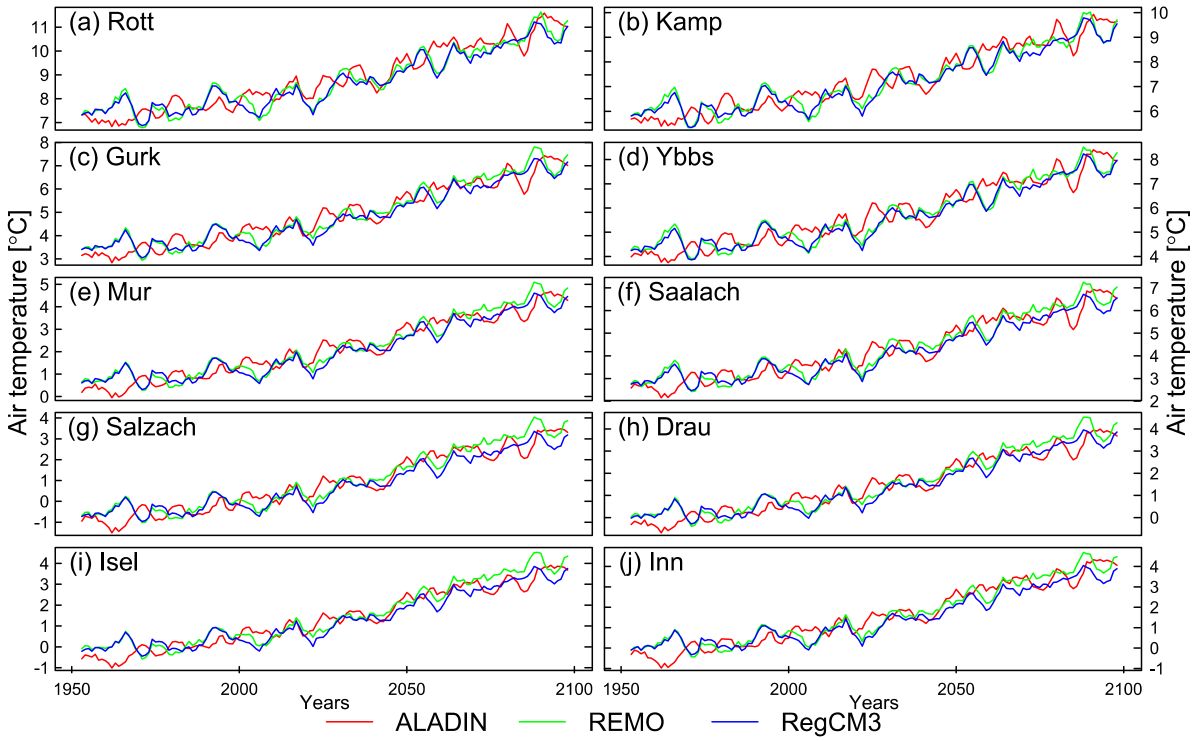

Figure 6-25: Five year moving average of annual mean temperature in the ten basins.

Regarding the rise of air temperature values, all three RCMs match each other predicting an increase of temperature of about 3.5 to 4 °C. Due to the noise of the precipitation signal, runoff on a yearly basis becomes noisy as well even when displaying the five year average. This enables statements about uncertainties but makes it hard to conclude long term trends. Figure 6-26 illustrates the relative changes in runoff in the respective climate normal compared to the reference period. Differences are calculated for each RCM separately. Using ALADIN the hydrological model estimates runoff in all basins and in every climate normal to be lower than during the reference period. The only exception is river Rott in the standard normal 2011-2040, but this positive signal is very weak. At the end of the century a decrease in annual runoff between roughly 12 and 35 % is indicated by ALADIN. In the same climate normal REMO shows differences between plus 10 and minus 9 % while RegCM3 covers a range from plus to minus 10 %. Clear trends can be observed in the catchments that nowadays hold glaciers that will shrink significantly until the year 2100. These catchments are Salzach, Isel and Inn. Glaciated areas of the river Drau catchment, compared to the total area, are very small. The influence of glaciers in the water balance therefore is nearly negligible. In Table 6-3 relative shares of snowmelt and, for glaciated basins also ice melt, are listed.

Table 6-4 shows absolute shares. In most basins, snowmelt and ice melt, if present, decreases until the year 2100. Exceptions are the nival basins Inn and Isel. In both catchments the low of glacier melt occurs in the period 2041 to 2070. During the last climate normal, ice melt is enhanced again but stays below the level of the reference period. Relative shares of ice melt are higher at the end of the century compared to the reference, though. For detailed results and discussion regarding glaciers see chapter 6.5.3.

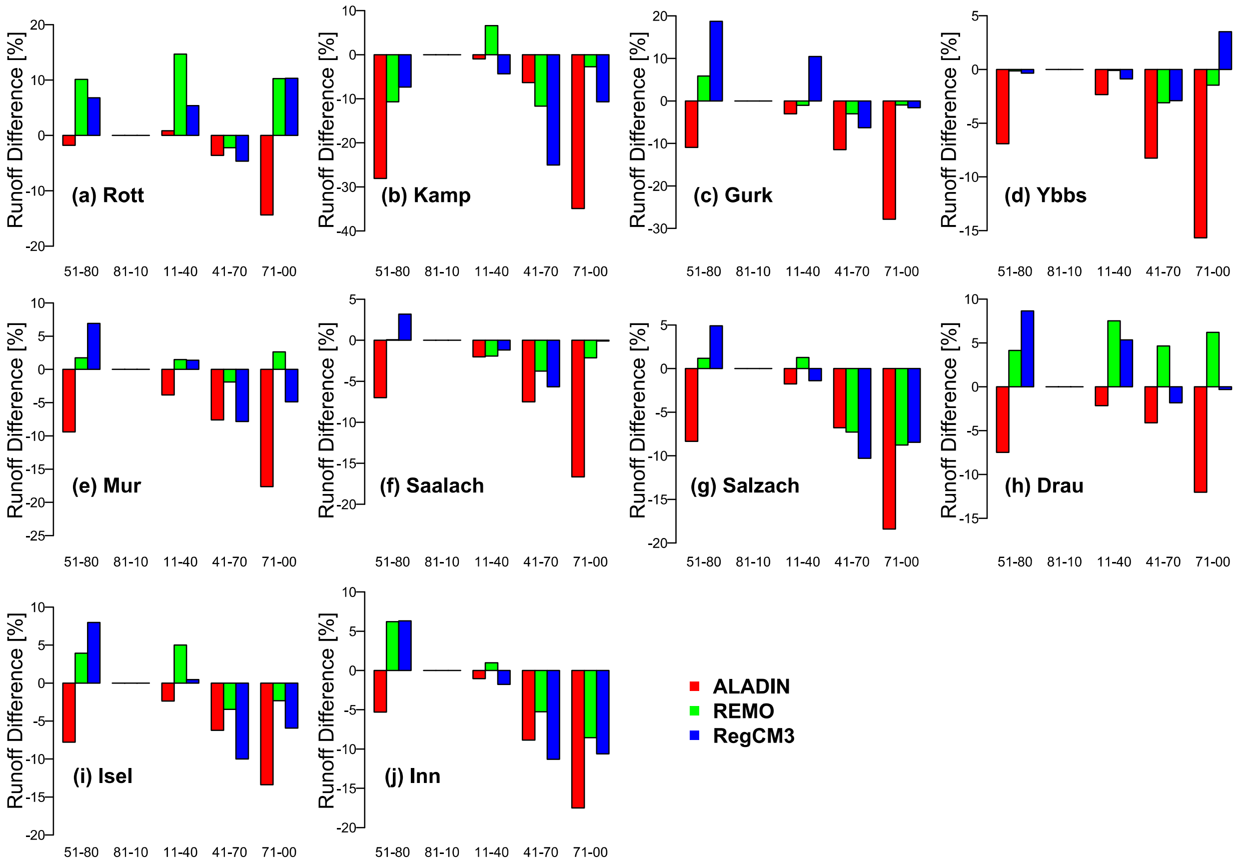

Figure 6-26: Evolution of annual discharge in the ten study basins. Reference period is 1981 to 2010 of the model realization using the respective RCM data. In most of the basins a clear trend towards lower discharge rates at the end of the century can be observed.

Table 6-3: Evolution of relative share of snow and ice melt (in brackets) in the studied basins.

	Relative share of runoff components snow and ice melt [%]				
Catchment	**1951-1980**	**1981-2010**	**2011-2040**	**2041-2070**	**2071-2100**
Rott	16.6	15.7	14.3	13.4	8.7
Kamp	27.7	22.5	21.1	19.1	15.7
Gurk	12.9	12.1	11.2	10.0	8.1
Ybbs	23.2	22.6	21.7	20.3	17.0
Mur	29.1	30.2	28.3	28.7	27.5
Saalach	25.7	25.3	24.7	22.9	19.9
Salzach	29.5 (7.7)	29.0 (8.3)	27.5 (8.2)	25.9 (7.2)	24.4 (3.4)
Drau	26 (0.7)	25.3 (0.9)	23.3 (0.7)	20.9 (0.6)	19.4 (0.3)
Isel	31.2 (5.5)	31.5 (6.2)	30.0 (5.8)	28.2 (5.4)	26.8 (6.9)
Inn	38.0 (9.9)	38.1 (11.1)	36.9 (11.0)	35.0 (10.4)	33.8 (12.4)

Table 6-4: Evolution of absolute share of snow and ice melt (in brackets) in the studied basins. Note that only the share of melt that leads to direct runoff according to the parameter $SPLIT_{MELT}$ is shown.

	Absolute share of runoff components snow and ice melt [mm a^{-1}]				
Catchment	**1951-1980**	**1981-2010**	**2011-2040**	**2041-2070**	**2071-2100**
Rott	45.1	40.2	38.6	31.1	21.5
Kamp	49.7	45.2	43.2	32.7	27.7
Gurk	57.8	51.5	46.3	37.5	29.6
Ybbs	328.4	313.8	291.3	242.4	208.8
Mur	344.8	341.7	303.2	269.2	247.5
Saalach	430.6	404.8	378.1	312.0	271.8
Salzach	446.2 (148.1)	429.5 (159.0)	393.2 (151.3)	328.0 (116.4)	301.4 (48.5)
Drau	359.8 (11.5)	340.3 (11.9)	312.1 (10.3)	258.3 (7.4)	231.7 (4.2)
Isel	405.5 (111.5)	388.7 (118.6)	359.7 (106.4)	305.9 (84.9)	283.3 (103.7)
Inn	425.9 (140.0)	402.9 (149.9)	375.3 (138.0)	316.5 (108.4)	289.5 (114.9)

6.5.3 Decrease of glacier areas

As described above, glaciers are not modelled fully dynamically in the sense that accumulation and ablation as well as ice flow is considered. In a semi-lumped model as SASWET this is hardly possible, since the model has no information about the three dimensional shape of each and every glacier. It only considers glaciers as elevation bands (according to the Austrian Glacier Inventory). To account for glacier retreat in a warming climate, the glacier surfaces are reduced. Figure 6-27 shows the extent of glaciers in the four glaciated watersheds in the year 2000, 2050 and 2100 per elevation level. The same colour coding for the three points in time is used in Figure 6-28, where the spatial extent of Austrian glaciers is shown. While large areas are becoming free from ice cover until 2050 the further reduction of glaciers until the year 2100 is less. In the model, glaciers are starting to retreat in the year 1990. Hence, until 2050 glaciers have been retreating for 60 years, 10 years longer than the remaining time to 2100. Since the reduction is linear, a larger share has been depleted in the first time period than in the second.

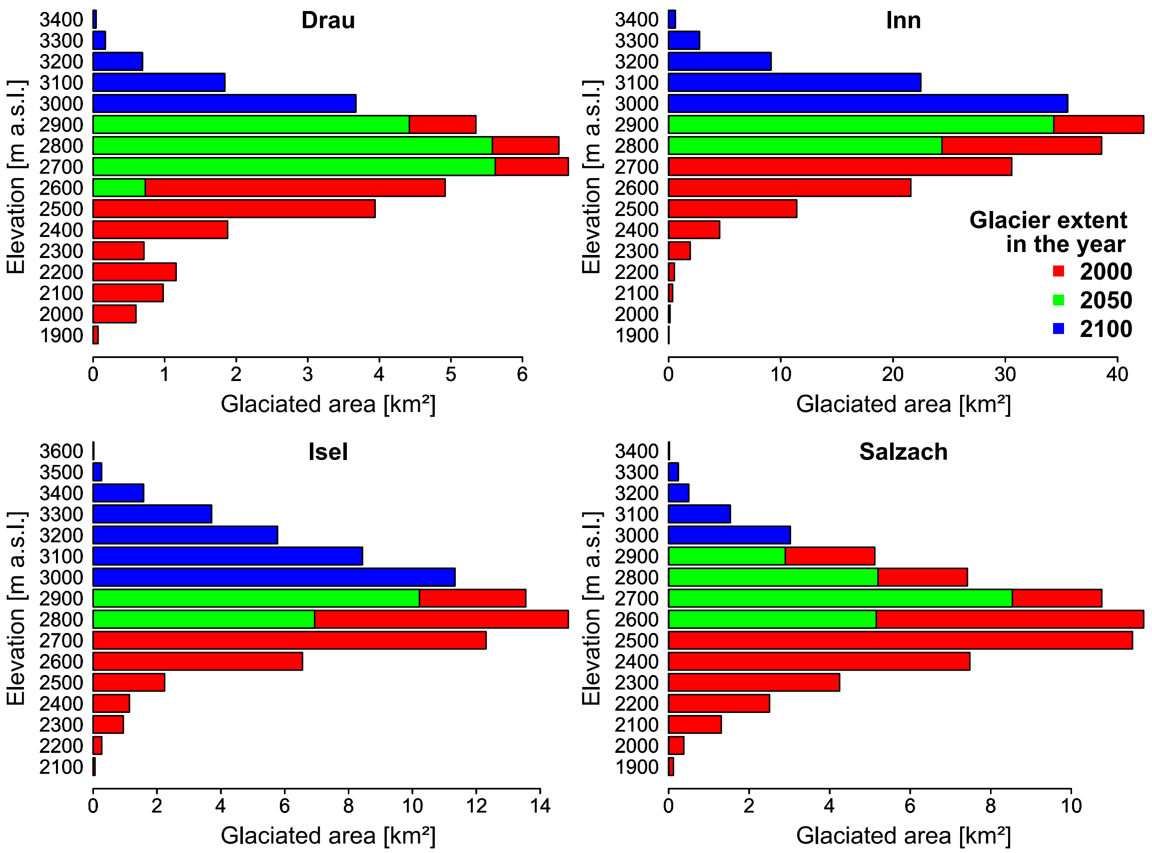

Figure 6-27: Glacier extent with respect to the elevation in the year 2000, 2050 and 2100. Deglaciation is not modelled explicitly but is predetermined by the model. Until the end of the 21st century, glaciers below 3000 m a.s.l. will be fully depleted (see chapter 2.1.3).

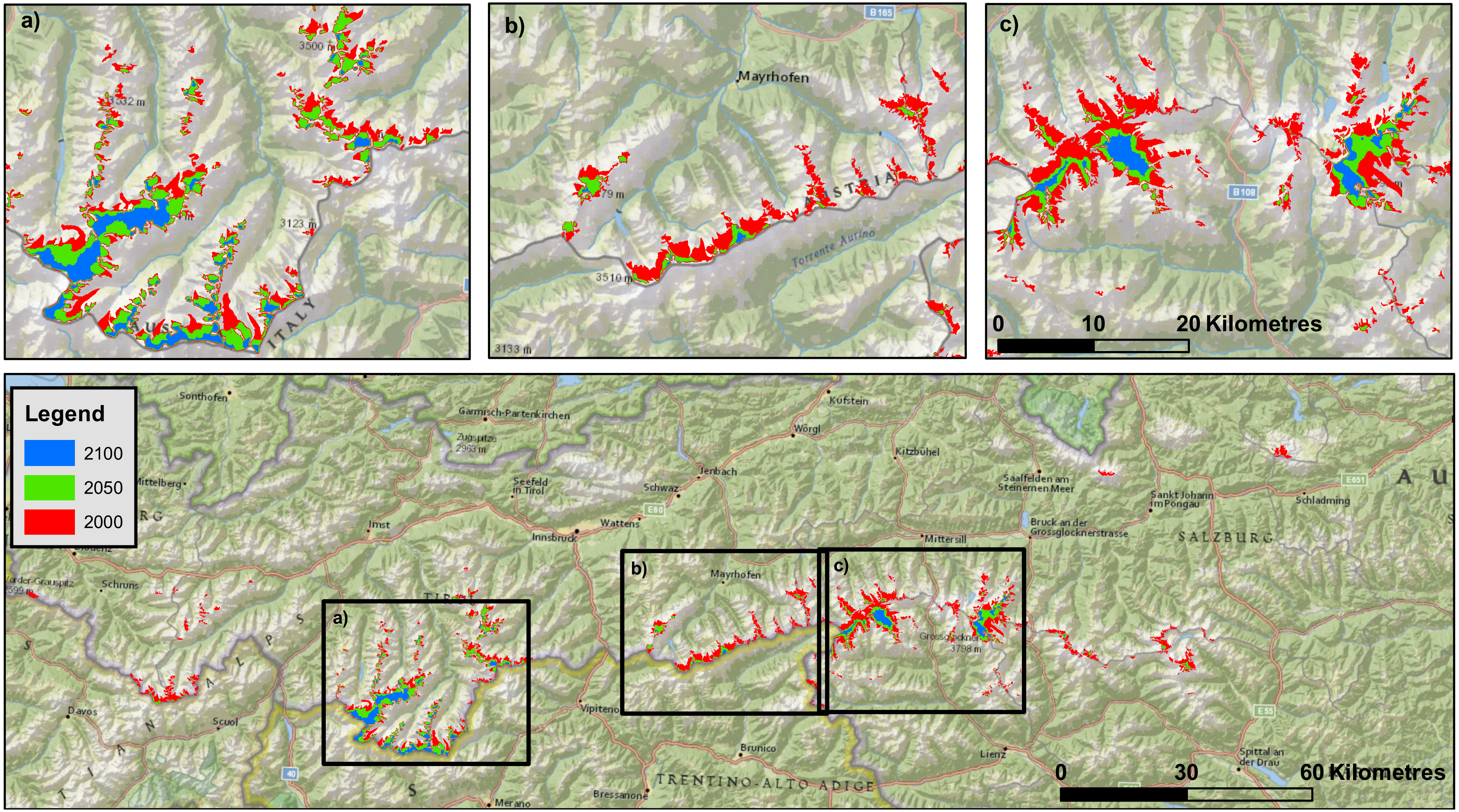

Figure 6-28: Spatial extent of glaciers in the Austrian Alps at the year 2000, 2050 and 2100. Only in elevation above 3000 m a.s.l. glaciers are existent at the end of the century. Since the model only accounts for elevation bands, deglaciation also happens on those bands. Hence, in this figure the elevation levels still holding glaciers in the respective year are plotted.

6.5.4 Seasonal variations and impact to hydroelectric energy resources

Besides the general trends in annual discharge, changes in seasonal runoff behaviour are of great importance for estimating influences on the energy generation potential. Even if the total amount of annual discharge decreases until the end of the 21st century, the energy production potential does not necessarily do the same. At both extreme ends of the flow duration curve, i.e. droughts and floods, the relationship between runoff and electricity generation is not linear. At high flows, the drop height of run-of-river station diminishes due to a higher water table on the downstream side of the station. In addition, if the water table reaches a certain level, the dams of run-of-river stations are overflown reducing the efficiency of the plants. In times of low flows, turbines suffer the loss of efficiency rapidly (Vinogg and Elstad, 2003). The discharge rate of 1.5 times the MQ (MQ1.5) and the discharge that is exceeded on 330 days per year (Q330) are considered critical for the energy production to drop.

If the periods with extreme runoff conditions are getting less, the electric power potential might rise. On the other hand, if extreme events occur more often, the potential for generating electric energy from hydropower will decrease even if the total annual discharge may be higher in future.

In Figure 6-30 to Figure 6-39 seasonal variations in discharge are illustrated along with the relative annual differences and the share of snow and ice melt for all ten basins and for the climate normal 1981-2010 (a), 2011-2040 (b), 2041-2070 (c) and 2071-2100 (d). The period 1951-1980 is missing for clarity reasons. It is important to note that only direct runoff from snow and ice is plotted in these figures. Only the minor part of melt becomes direct runoff, the major share infiltrates into the soil and is treated equal to rainfall. Direct-runoff-to-infiltration (DRI) ratios are given in Table 6-6 for all basins. This ratio accounts for both ice and snowmelt.

Figure 6-40 compares the actual evaporation in the reference normal with the one at the end of the 21st century. Flow duration curves including mentioned characteristic discharge measures MQ, MQ1.5 and Q330 are shown in Figure 6-41 for all basins for the standard normal 2071 to 2100. These characteristics are listed in Table 6-5 as well. For flow duration curves regarding other standard normal (excluding the reference period) see Figure A 6 to Figure A 8 in the appendix.

Since the discharge at the outlet of a watershed is the hydrological response of meteorological input in the respective basin it is important to survey climatological data as well. For river Saalach, these data are shown in Figure 6-29.

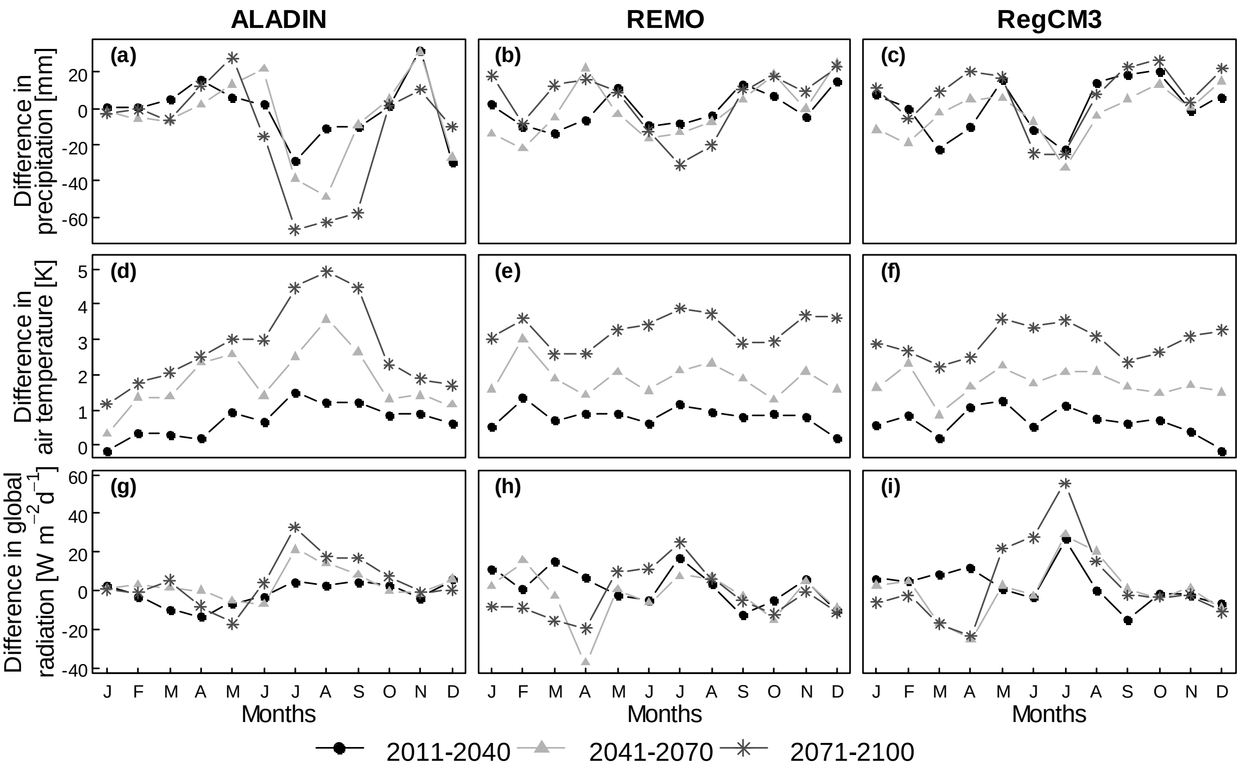

Figure 6-29: Monthly changes in climatological data compared to the reference period (1981-2010) for the catchment of river Saalach. Both ECHAM5 driven RCMs show similar behaviour in precipitation and temperature while precipitation drops drastically during the summer months and air temperature rises more extreme in the summer using ALADIN. Only little similarity regarding global radiation between the RCMs is observable (e.g. the peak in July).

While RegCM3 and REMO (Figure 6-29) show similar behaviour as well in precipitation as in air temperature, ALADIN differs. Both ECHAM5 driven RCMs signal an even rise of air temperature over the year, ALADIN indicates a massive decrease of precipitation along (minus 60 to 70 mm) with a high increase of air temperature (roughly 5 K) during the summer months. In winter, however, temperature levels in ALADIN rise less than in both other RCMs. Hence, ALADIN can be considered as being the driest RCM and being warm summer, cold in winter. Changes in mean daily global radiation vary between +60 and -40 W m^{-2} d^{-1}. Greatest changes in both directions occur during the summer months. Only little similarity to the different RCMs can be observed.

The evolution of climate in the other catchments is comparable, with some differences, to the catchment of Saalach River. Thus the data of the other basins are shown in Figure A 10 to Figure A 18 in the appendix. In general, RegCM3 signals the largest differences in global radiation. No clear trend towards higher or lower changes regarding altitude or geographical position (i.e. northern or southern side of the Alps) occurs. The same accounts for precipitation and for air temperature.

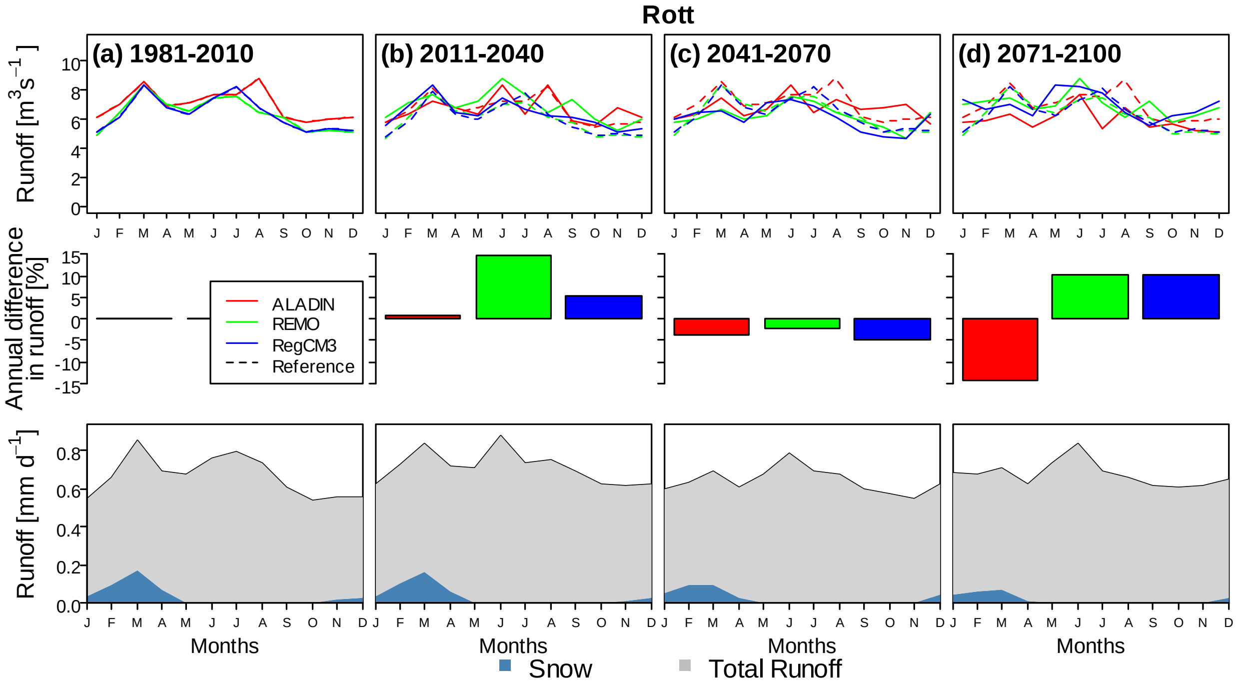

Figure 6-30: Seasonal and annual variation and share of snow on the runoff in the catchment of river Rott in the hill country. Components are given as mean over all three RCMs.

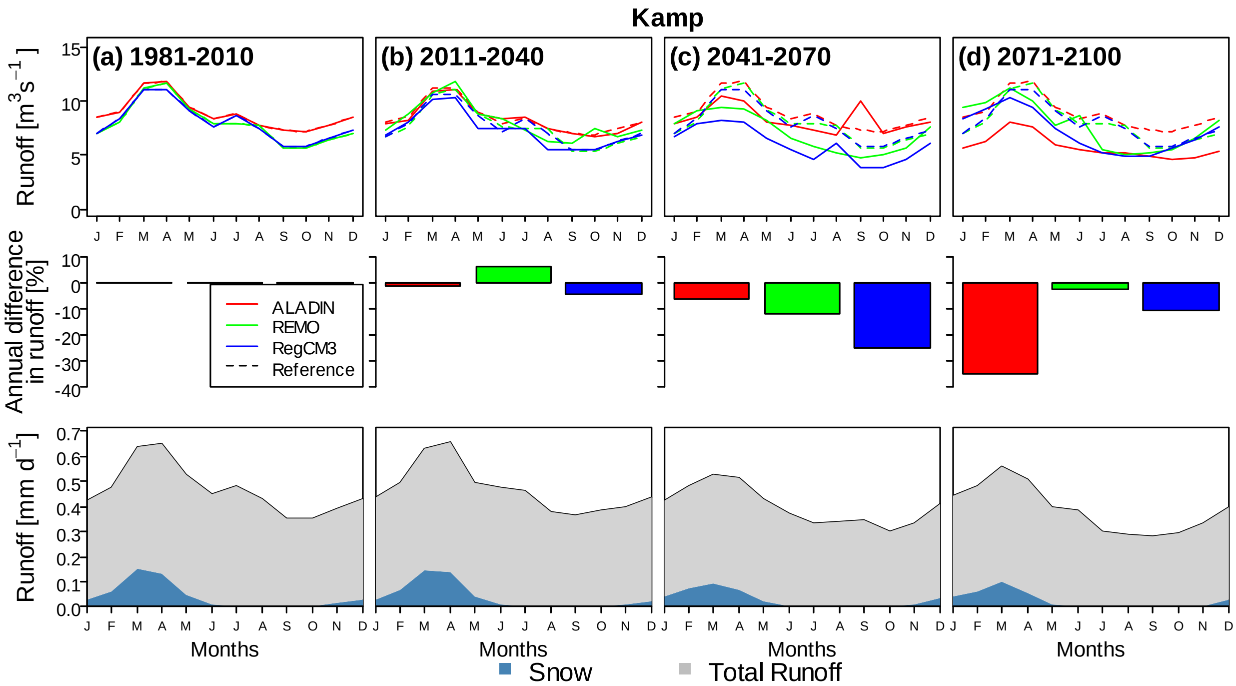

Figure 6-31: Seasonal and annual variation and share of snow on the runoff in the catchment of river Kamp in the hill country. Components are given as mean over all three RCMs.

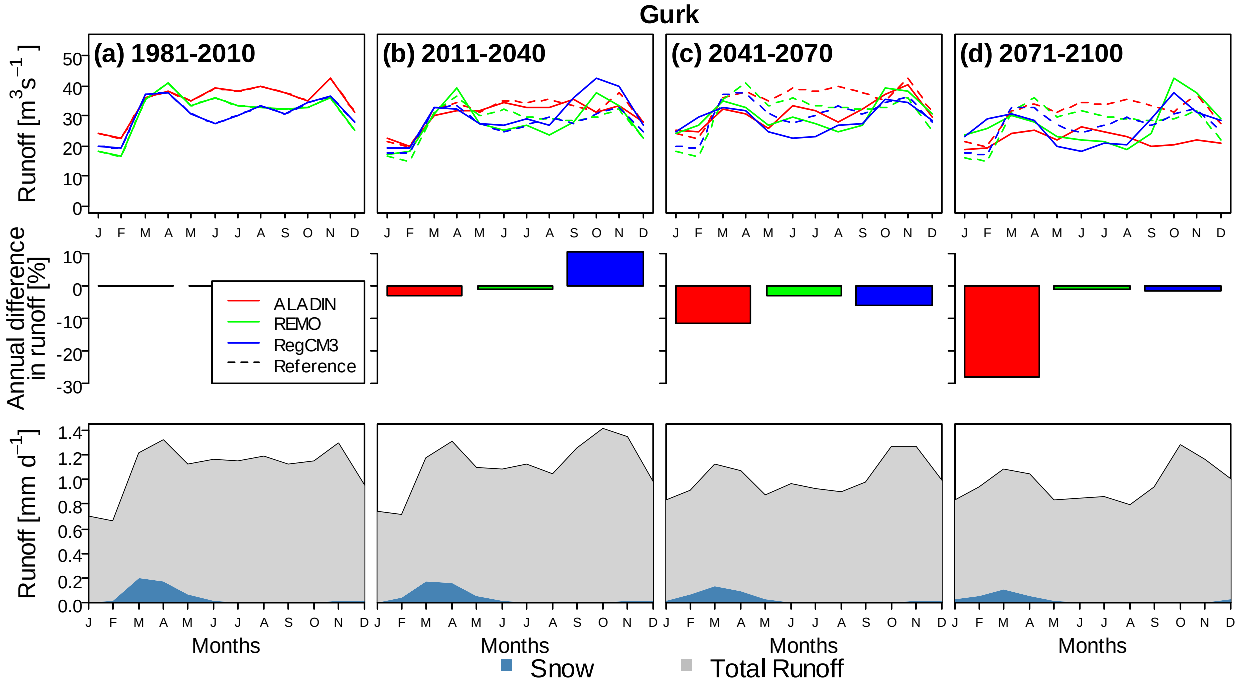

Figure 6-32: Seasonal and annual variation and share of snow on the runoff in the catchment of river Gurk in the alpine upland on the south side of the Alps. Components are given as mean over all three RCMs.

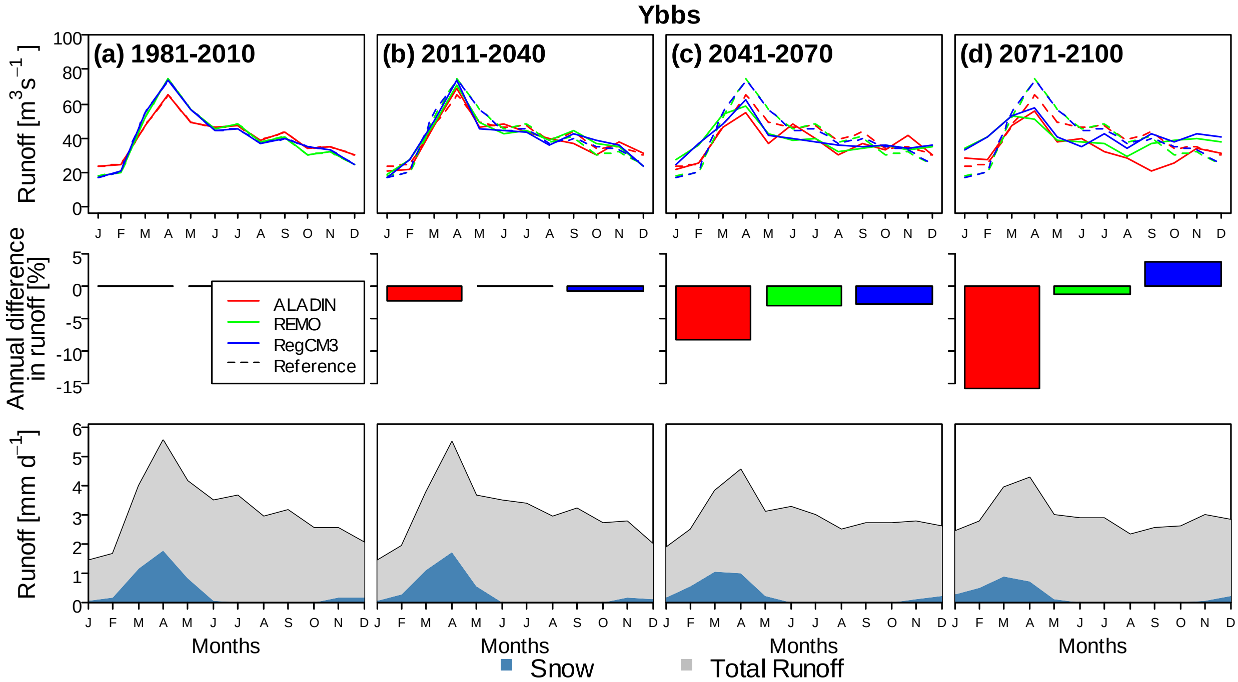

Figure 6-33: Seasonal and annual variation and share of snow on the runoff in the catchment of river Ybbs in the alpine upland on the north side of the Alps. Components are given as mean over all three RCMs.

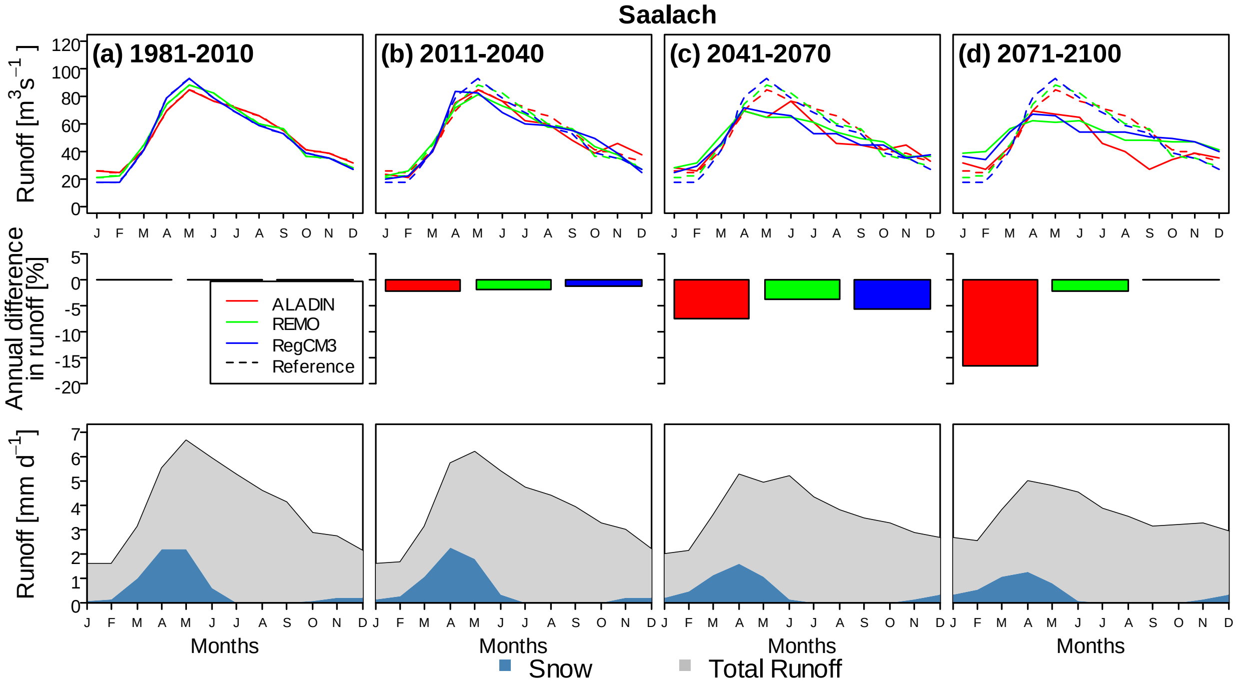

Figure 6-34: Seasonal and annual variation and share of snow on the runoff in the catchment of river Saalach in the limestone Alps. Components are given as mean over all three RCMs.

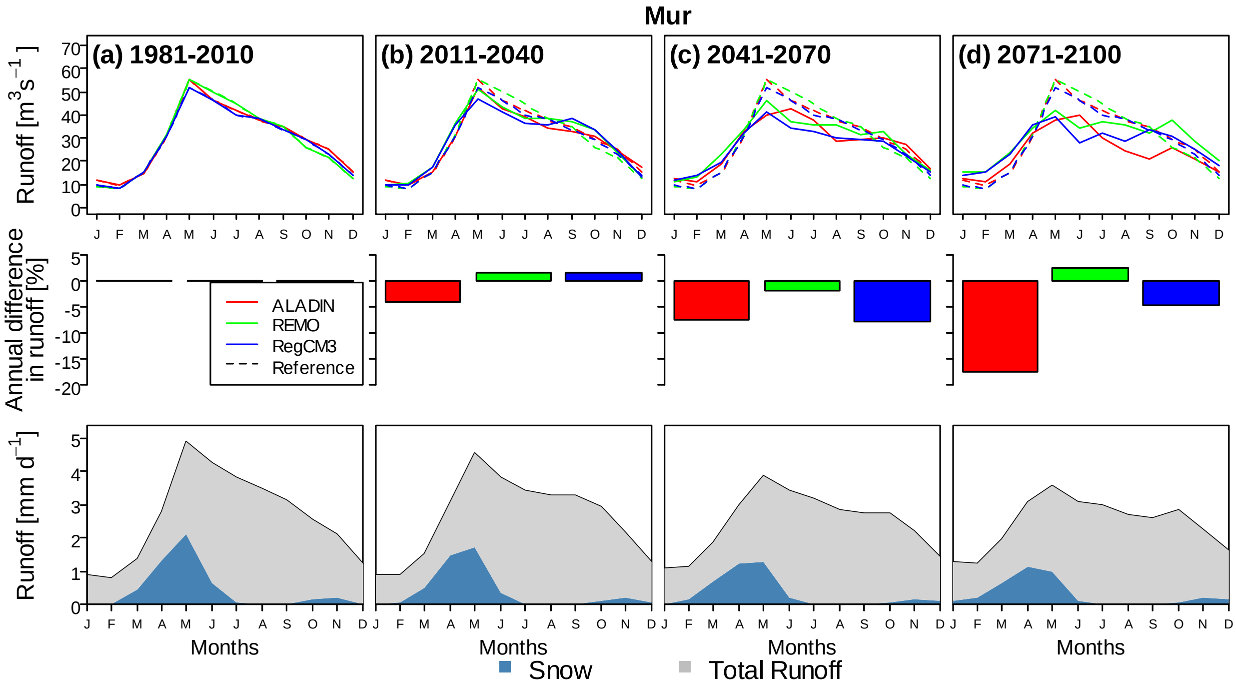

Figure 6-35: Seasonal and annual variation and share of snow on the runoff in the catchment of river Mur in the limestone Alps. Components are given as mean over all three RCMs.

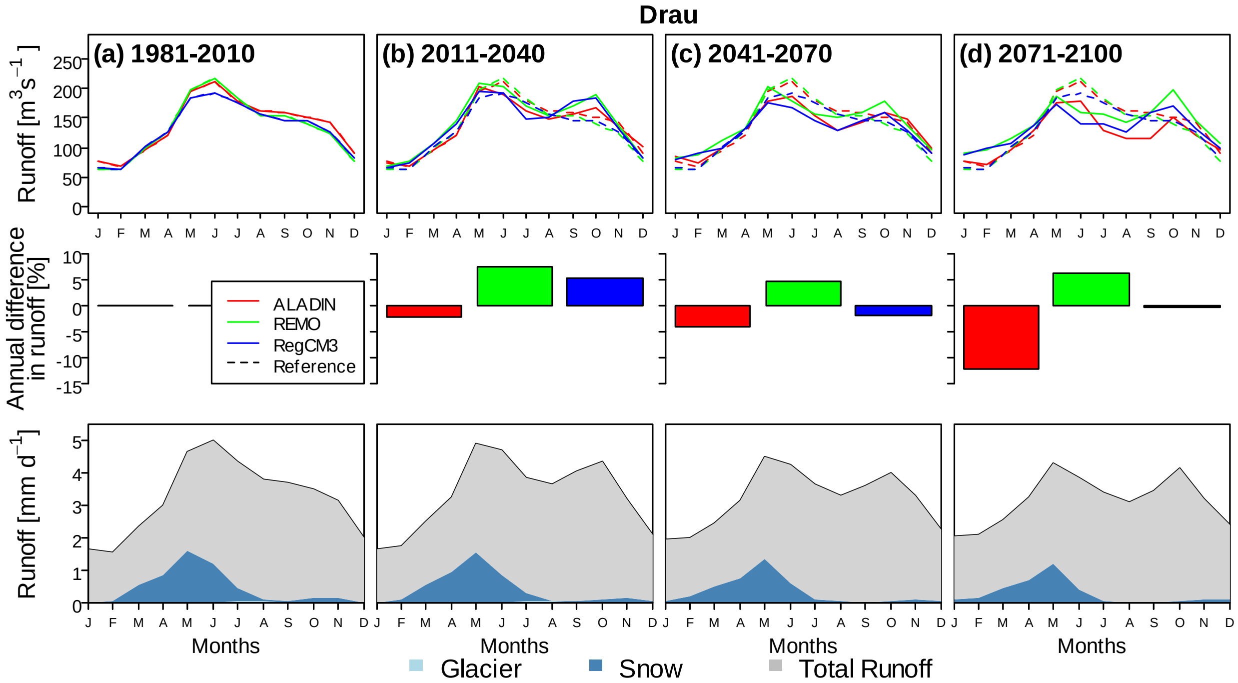

Figure 6-36: Seasonal and annual variation and share of snow on the runoff in the catchment of river Drau in the Tauern region. Snowmelt adds up to ice melt. Components are given as mean over all three RCMs.

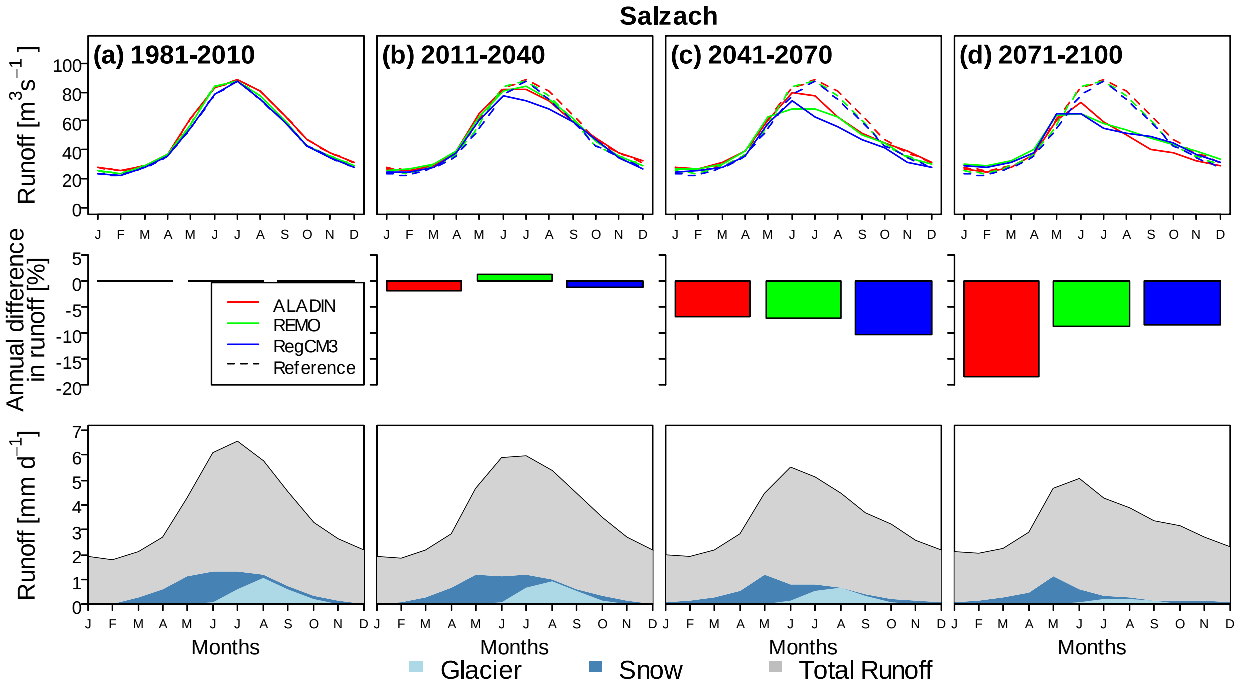

Figure 6-37: Seasonal and annual variation and share of snow on the runoff in the catchment of river Salzach in the Tauern region. Snowmelt adds up to ice melt. Components are given as mean over all three RCMs.

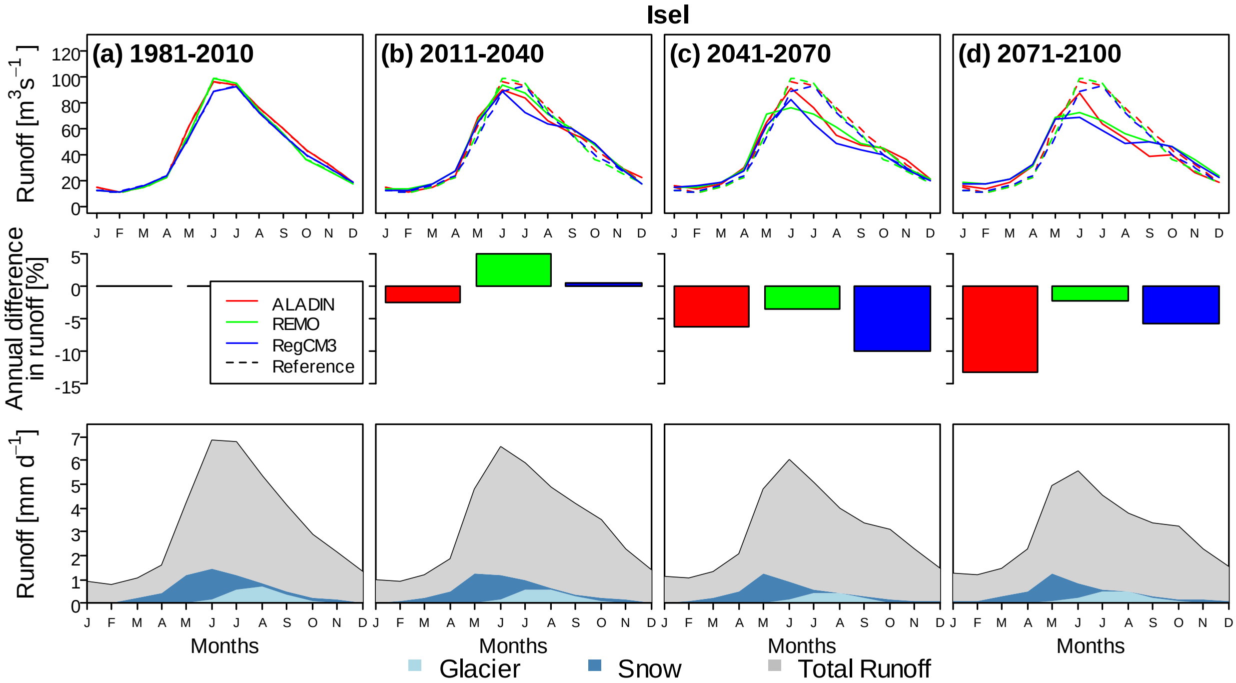

Figure 6-38: Seasonal and annual variation and share of snow on the runoff in the catchment of river Isel in the nival region of the Alps. Snowmelt adds up to ice melt. Components are given as mean over all three RCMs.

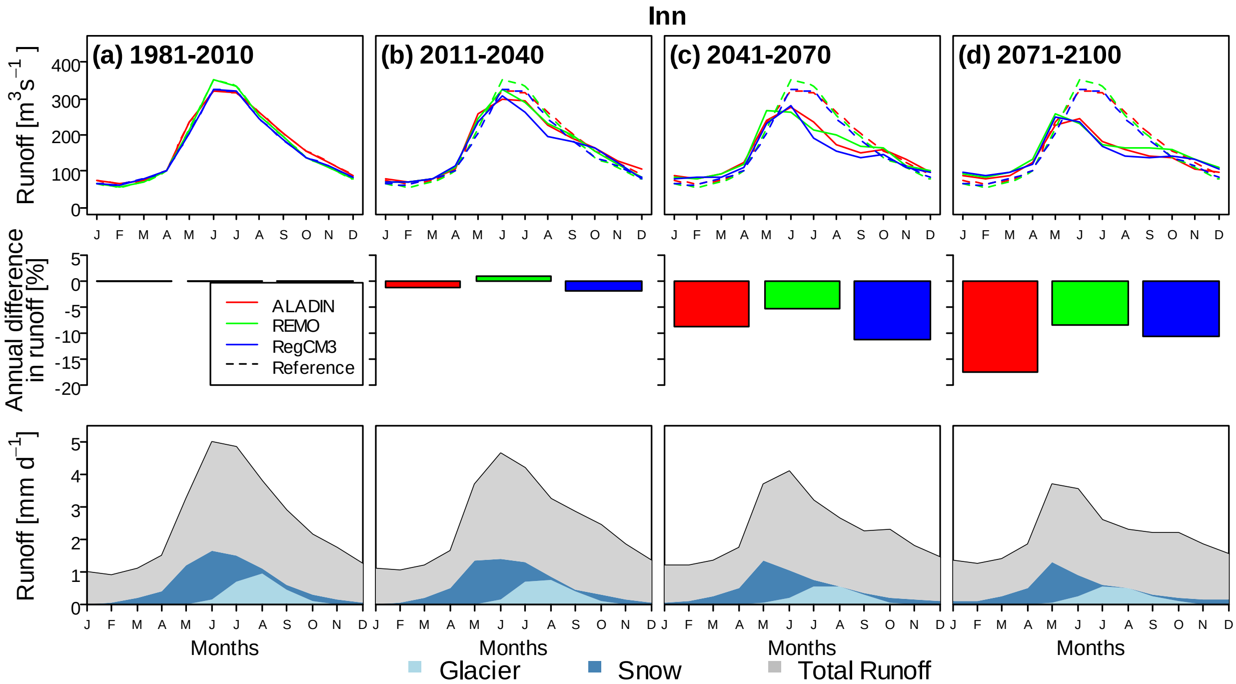

Figure 6-39: Seasonal and annual variation and share of snow on the runoff in the catchment of river Inn in the nival region of the Alps. Snowmelt adds up to ice melt. Components are given as mean over all three RCMs.

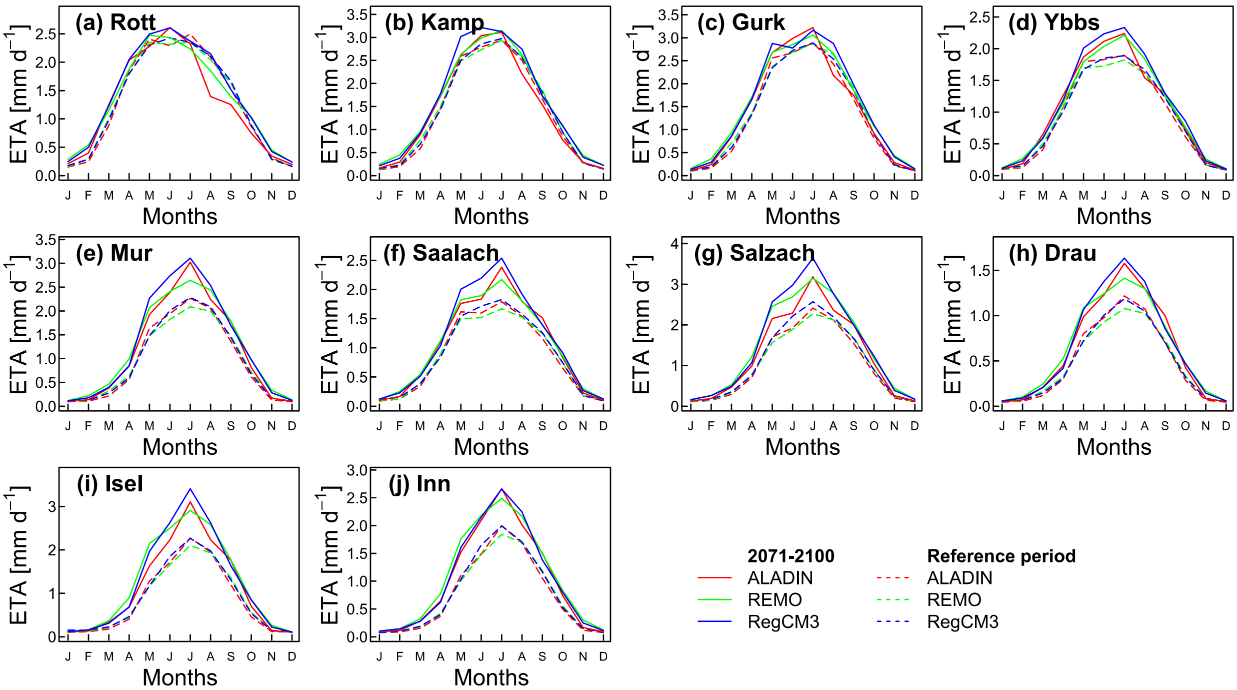

Figure 6-40: Comparison of monthly actual evapotranspiration within the reference period and the climate normal at the end of the 21st century. Changes occur mainly during the summer months and are greater the higher the maximum elevation of the catchment.

Table 6-5: Essential hydrological characteristics of the study basins at the end of the modelled time series. MQ1.5 refers to 1.5 times the MQ and is given in days the runoff exceeds that value. In brackets are MQ1.5 values during the reference period ($MQ1.5_{REF}$). Q330 refers to days the runoff exceeds the value, that was Q330 during the reference period. MQ is given in relative difference to the respective value during the reference period which is given in the brackets (MQ_{REF}).

Basin	MQ1.5 [Days]			Q330 [Days]			MQ [% ($m^3 s^{-1}$)]		
	RCM1	RCM2	RMC3	RCM1	RCM2	RCM3	RCM1	RCM2	RCM3
Rott	48 (47)	58 (47)	60 (47)	231	306	297	-17 (6)	+3 (6)	+3 (6)
Kamp	12 (27)	34 (27)	29 (27)	136	226	203	-38 (8)	-13 (8)	-13 (8)
Gurk	24 (44)	36 (44)	33 (44)	227	288	284	-26 (31)	-26 (31)	-10 (31)
Ybbs	52 (64)	65 (64)	70 (64)	249	288	302	-18 (39)	-5 (39)	0 (39)
Mur	44 (75)	68 (75)	54 (75)	304	351	335	-18 (28)	0 (28)	-7 (28)
Saalach	45 (68)	58 (68)	57 (68)	285	329	326	-18 (50)	-4 (50)	-4 (50)
Salzach	31 (69)	31 (69)	32 (69)	281	334	330	-16 (49)	-10 (49)	-12 (49)
Drau	36 (46)	51 (46)	39 (46)	295	348	334	-11 (131)	+2 (131)	-5 (131)
Isel	66 (94)	67 (94)	58 (94)	319	354	353	-12 (43)	-7 (43)	-9 (43)
Inn	28 (82)	45 (82)	36 (82)	327	353	347	-14 (160)	-10 (160)	-13 (160)

RCM1 = ALADIN; RCM2 = REMO; RCM3 = RegCM3

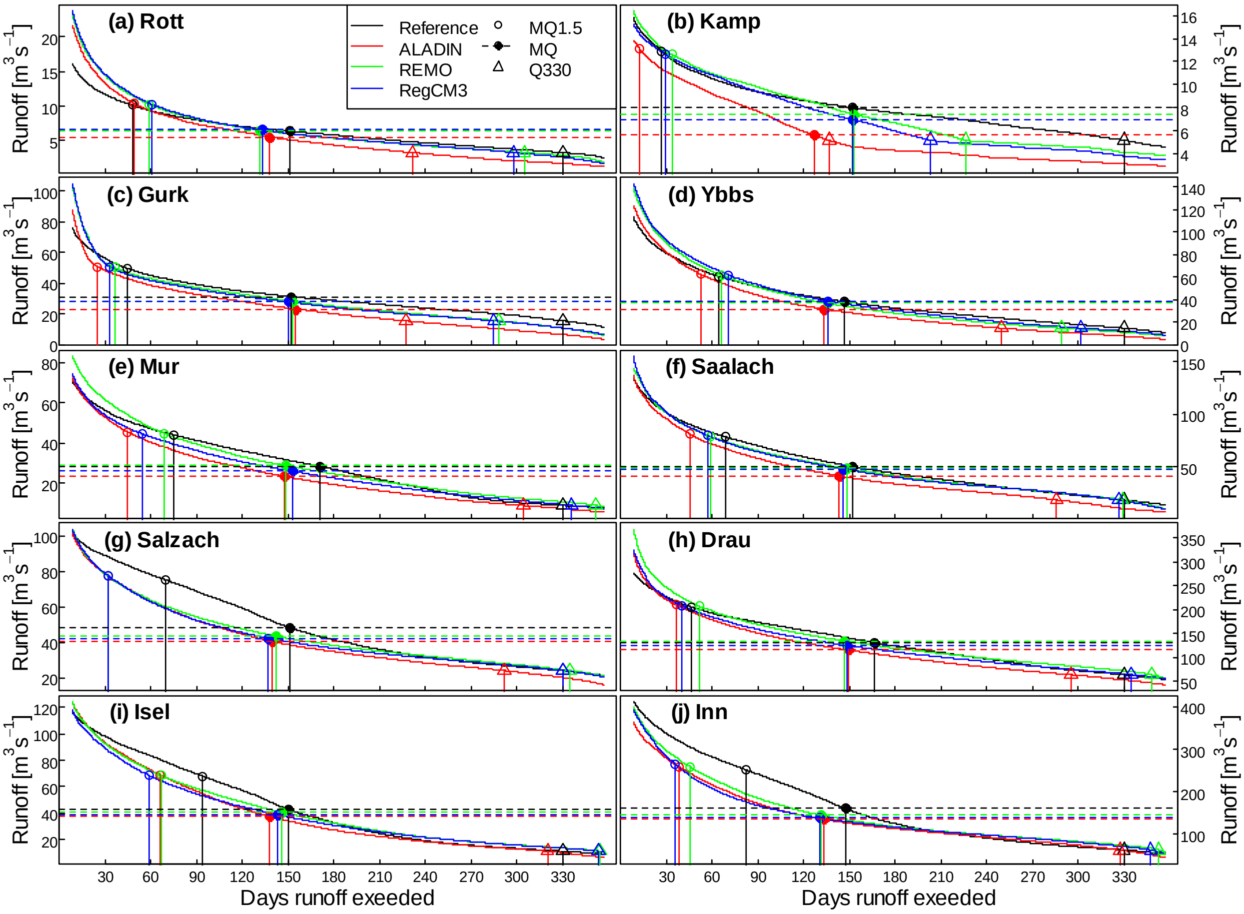

Figure 6-41: Essential hydrological characteristics of the study basins at the end of the modelled time series plotted along the flow duration curves. MQ1.5 refers to 1.5 times the MQ_{REF}. Q330 refers to days the runoff exceeds the value, that was Q330 during the reference period ($Q330_{REF}$). Dashed lines highlight the discharge rates of MQ during the reference period (black) and at the end of the century. Vertical bars indicate the shift in the frequenties of exceedance.

Table 6-6: Direct-Runoff-to-Infiltration (DRI) ratios accounting for ice and snowmelt for all ten basins. These are equal to the parameter $SLPI_{MELT}$.

Basin	DRI Ratio	Basin	DRI-Ratio
Rott	1:5	Mur	1:2.2
Kamp	1:6.5	Salzach	1:3.7
Gurk	1:6.3	Drau	1:2.2
Ybbs	1:2.2	Isel	1:3.9
Saalach	1:2.0	Inn	1:2.7

According to similarities in runoff behaviour (e.g. runoff regime, glacier extent, etc.) the Austrian basins have been arranged in five clusters. The aim was to regionalize the results found in the hydrological modelling to other basins of the same cluster (see chapter 3.1). This regionalization however is not part of this thesis. The results according to these clusters are described in the following.

Cluster One – Rivers Kamp and Rott

Both river Rott and Kamp (see Figures 6-30 and 6-31, respectively) do not change their general runoff characteristics. Even though their maximum altitude is only 1046 and 548 m a.s.l., respectively, snowmelt behaviour changes. While the time period of snowmelt does hardly change, the amount of snowmelt decreases. Changes in runoff therefore are caused by changing snowmelt, precipitation and by increased evapotranspiration. The latter, however, does not change as greatly as it does in other catchments due to enhanced water scarcity opening the gap between actual and potential evapotranspiration in a warmer climate (see Figures 6-24 and 6-40).

By the end of the 21st century, the MQ of Kamp drops about 13 – 38 % and river Rott carries up to 17 % less water. However, realizations of REMO and RegCM3 signal a rise in the MQ of 3 %. Subsequently the $MQ1.5_{REF}$ of river Kamp is exceeded at 12 to 34 instead of at 27 days. At 138 to 229 days runoff dips below the $Q330_{REF}$. The discharge of river Rott exceeds $MQ1.5_{REF}$ at 48 to 60 instead of at 47 days and dips below the $Q330_{REF}$ at 59 to 134 days.

One has to keep in mind that the hydrological model efficiency in both catchments is relatively low causing a high degree of uncertainty in comparison with the other watersheds. Especially in river Rott great floodings occur whereas the baseflow is very low. These floodings cause an unsteady runoff regime.

Cluster Two – Rivers Gurk and Ybbs

A slight change in runoff behaviour of the rivers Ybbs and Gurk (Figures 6-32 and 6-33, respectively) can be noticed in the form of increasing winter runoff and at the same time decreasing runoff in summer. This change is primarily caused by enhanced evapotranspiration and earlier and less snowmelt. In addition the period of snowmelt is getting shorter. Evapotranspiration however is more important in river Ybbs than it is in river Gurk, where the actual evapotranspiration only barely rises. In the case of river Ybbs, a change in the runoff regime from nival to nivo-pluvial can be observed.

Mean discharge (MQ) changes in river Ybbs of about plus 0.4 to minus 18 %, river Gurk on the south side of the Alps carries around 10 up to 26 % less water. High flows above $MQ1.5_{REF}$ occur less often at river Gurk (34 to 36 instead of 44 days) but fluctuate around the reference value of 64 days at river Ybbs (52 to 70 days). In both catchments, days with low flow conditions occur more often with 63 to 116 and 77 to 138 days in river Ybbs and Gurk, respectively.

Cluster Three – Saalach and Mur

A similar change can be reported for the third cluster, which is composed of the rivers Saalach and Mur, shown in Figures 6-34 and 6-35, respectively. Due to their altitude, snow processes are more important in these catchments than in the hill country and alpine upland. Warmer climate however causes snowmelt to be less important in the late 21st century and the snowmelt season starts earlier which leads to enhanced runoff during the winter months. Together with a significant rise of actual evapotranspiration (see Figure 6-40) discharge rates during the summer are decreasing.

The processes lead to a reduction of the mean discharge rate of 4 to 18 % of Saalach and up to 18 % as well at Mur. The model realization using REMO however signals hardly any change in mean runoff for river Mur (plus 0.4 %), where high flows occur less frequent than in the reference (44 to 68 days instead of 75). Even low flows may occur only at 14 (REMO) days but the realization using ALADIN signals with 61 days a rise of these days. At river Saalach, low flow conditions occur at 36 to 80 days whereas discharge rates exceed $MQ1.5_{REF}$ at 45 to 58 instead of at 68 days.

Cluster Four – Salzach and Drau

The catchments located in the Tauern region are glaciated. The results for rivers Drau and Salzach are shown in Figures 6-36 and 6-37, respectively. Note that in these figures, ice melt sums up to snowmelt. Shrinking glaciers amplify the trend observably in the other, lower catchments. Discharge originating from melting glaciers in the basin of river Drau is almost negligible even nowadays. The glacier-total catchment ratio is very small. Increased evapotranspiration rates in summer cause an additional decrease in runoff. Other than in the lower catchments, only a slight increase in winter runoff is indicated by the model. This increase is greater in river Drau than it is in Salzach. However, model results seem more homogenous in river Salzach. In high elevations even at the end of the century, snowmelt in winter does not start to rise drastically earlier than it does in lower altitudes. Nevertheless it becomes less in total and reaches its apex earlier in the year. Subsequently, melt from glaciers starts earlier in the year, too.

The mean discharge of these rivers is likely to dip about 10 to 16 % at Salzach and up to 11 % at Drau. However, caused by higher runoff values in winter, mean discharge of river Drau may be increased slightly of 2 %. Lower runoff values at Salzach lead to less days with high flow conditions. Only at 31 to 32 days a year discharge exceeds the value of $MQ1.5_{REF}$ but draughts may become more important since runoff dips below $Q330_{REF}$ at 31 to 84 days a year.

Cluster Five – Rivers Isel and Inn

Like the catchments in cluster four, these basins hold glaciers that will lose great amounts of their surfaces and masses in the course of the 21st century. However the relative share of glacier melt in both catchments does not get less (see Table 6-3). The apex of glacier melt is lower in future, though. Less accumulation and subsequently less melt of snow (and ice) lead to reduced discharge rates in summer. At the end of the century evapotranspiration will have been greatly increased amplifying the lack of discharge in summer in these watersheds. Discharge in winter will be slightly greater than during the reference period. Therefore a change of the runoff regime from glacial to nival is likely to be observed. Results for rivers Isel and Inn are given by Figures 6-38 and 6-39, respectively.

Both rivers carry less water during the year leading to a reduced MQ of 7 to 12 at Isel and 10 to 14 % at river Inn. Less water in summer and more in winter means that low flow conditions occur at 11 to 46 and 12 to 38 days for Isel and Inn, respectively, while the $MQ1.5_{REF}$ is exceeded at 58 to 67 instead of 94 days and at 28 to 45 instead of 82 days in these respective rivers.

6.6 Discussion to future discharge conditions in Austrian basins

6.6.1 Long term annual changes in the amount of runoff

Often contrary behaviour between the ECHAM5 and the ARPEGE driven RCMs is observable (see Figure 6-22). Looking at annual precipitation trends shown in Figure 6-23 the reason for the opposing runoff behaviour is obvious. Similar precipitation patterns result in similar discharge patterns in the respective watersheds. One has to keep in mind that the meteorological and hydrological data in Figure 6-22 to Figure 6-25 are given as five year moving averages. Any runoff delaying processes as snowmelt for instance are not accounted for at this temporal resolution. Runoff becomes a function of (mean annual) precipitation and evapotranspiration only. Thus, the correlation between rainfall and runoff is very good (see Figure 6-42b).

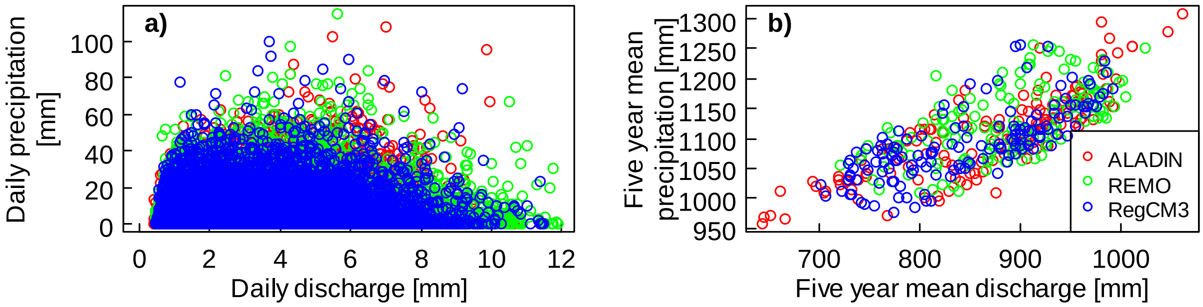

Figure 6-42: Correlation between discharge and precipitation on daily (a) and on five year moving average (b) basis in the catchment of river Saalach. On a daily basis correlations vary between 0.18 and 0.24 whereas correlations between 0.6 and 0.82 are reached on the basis of a five year moving average.

The jump in potential evapotranspiration observable in several catchments like Mur or Salzach around the year 2000 can be explained by the use of Turc's formula for estimating ETP (Eq. 2-2). At negative air temperatures ETP is set to be 0.1 mm per day. As long as temperature values stay below this mark, no change in ETP will occur no matter how far air temperature values have been increased.

In some catchments, especially ones with low elevation (Rott, Kamp and Gurk), an opening gap can be observed. Potential evapotranspiration rises more than actual ET does. Potential evaporation is increased by (i) radiation and (ii) air temperature. However, actual evapotranspiration is limited by the amount of water available in the soil. This may lead to rising levels of potential evapotranspiration although actual transpiration stagnates on a certain level as can be observed most clearly in the catchment of river Rott. Since the plant available water capacity of soil is a parameter in the model, this is a direct consequence of the parameter set found in the calibration.

In a warmer climate less snow is able to accumulate and subsequently snowmelt is lowered leading to lower discharge values originating from snow. In principle, the same accounts for the melt of glaciers as well. However, both nival catchments indicate a u-shaped melting evolution with the respective minimum of melt in the period 2041 to 2070. Increasing melting rates of glaciers at the end of the century will be caused by increasing temperature levels in regions above 3000 m a.s.l. Increasing temperatures mean these areas are fully depleted earlier in the year and thus enabling ice melt. Consequently the annual time span where glacier melt occurs gets longer, leading to more melt. This compensates for shrinking glaciers.

Composition of discharge during the reference period in the watersheds of river Inn and river Salzach are comparable to values reported by Weber et al. (2010) who used the RCM REMO in combination with a hydrological model based on the Promet model (Mauser and Bach, 2009) to estimate the contribution of rain, snow- and ice melt in the Danube catchment. However, they report almost entirely diminishing glacier contributions until 2060. The Promet model is a detailed physical based hydrological model that accounts for glacier mass balance including movement, and geometry evolution. Thus it is much more complex than the model used in the present study.

Melting rates in the (far) future might not necessarily be ‘correct’ due to the fact that glacier surface areas above 3000 m a.s.l. do not change. However, the resulting error is considerably smaller than the uncertainty originating from other factors such as climate models (see chapter 6.4).

6.6.2 Seasonal changes

On the annual scale discharge rates decrease in the vast majority of the basins and for the use of most RCMs. Using ALADIN a positive trend cannot be observed in a single catchment. The other RCMs tend – at least in some basins – to slightly increase discharge rates. To understand that difference in between the realizations using different RCMs one has to look at seasonal changes in climatology and the resulting hydrologic reaction of the respective catchment. Seasonal evolution of climatology is given in Figure 6-29 for the river Saalach. Climatological evolution in the other basins is similar as shown in the appendix (Figure A 10 to Figure A 18).

Increasing air temperatures result in increasing evapotranspiration rates. Thus the use of ALADIN should lead to the highest evapotranspiration rates during summer. However, as indicated in Figure 6-40 the highest rates of ETA are produced by the use of RegCM3. This can be caused by two reasons: (i) less precipitation during the hot months in summer (ALADIN) lower high rates of ETA or (ii) the large surplus of global radiation predicted by RegCM3 has as great an effect that compensates for the lower temperature. According to Figure A 9 RegCM3 signals the highest surplus in ETP as well but with less difference to ALADIN.

The higher the air temperature the less sensitive is the estimation of ETP using Eq. (2-2) on temperature changes. At low temperatures, a change in temperature is more sensitive than changing global radiation. The relationship between global radiation and ETP is linear. This relationship is shown in Figure 6-43 for the range in air temperature values between 0 and 25 °C and global radiation values between of 20 and 300 W m^{-2} d^{-1}. These values often occur in mountainous regions during the summer months. Note that ETP is set zero at negative air temperature values. The use of this method for estimating ETP therefore amplifies values of ETP when temperature levels are medium, yet radiation levels are high. High values on global radiation are caused primarily by clean sky conditions. Hence, the choice of the approach for estimating ETP has an influence on the model results even if the evapotranspiration rates during calibration are similar. It should be noted, however, that values of global radiation in climate models (RCMs as well as GCMs) are prone to larger errors than precipitation or air temperature (Randall et al., 2007).

Higher rates of ETA using RegCM3 than using ALADIN, therefore, are the result of a combination of less precipitation generated by ALADIN and higher values for global radiation predicted by RegCM3.

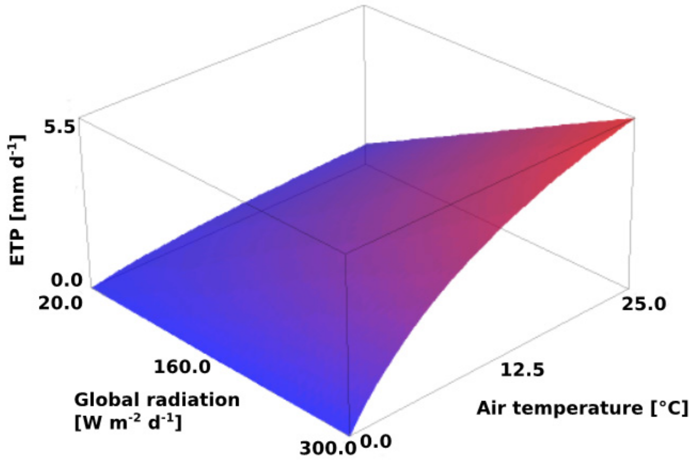

Figure 6-43: Values of ETP in dependency on air temperature and global radiation values. While values of ETP depend linear on global radiation, influence of air temperature converges against a threshold value.

In general, discharge in winter is likely to become higher in the future. This statement is true especially for mid elevation catchments, i.e. Mur, Saalach and Ybbs, and to some extent for Drau, which indeed is located in the high alpine cluster; however large parts of the catchment are situated in mid elevation ranges. Exceptions from that statement can be found for river Kamp, especially using the RCM ALADIN and for river Gurk using the same RCM. Subsequently the catchments snow storage is getting smaller causing a decrease in discharge during the melting season in spring and early summer.

This rise of winter runoff is caused primarily by higher air temperature rates leading to a greater fraction of liquid precipitation. The total amount of precipitation (i.e. solid and liquid) during the winter months do hardly change in any of the catchments and for none of the RCMs. Also rates of evapotranspiration – both actual and potential – hardly rise in the winter months. In winter, global radiation levels are usually rather low due to short length of days. As shown in Figure 6-43 rates of ETP are only little increased if temperature levels rise, but global radiation stays low. Beginning around March, rates of ETP start to rise and remain higher until around November. In catchments located in higher elevations a rise in temperature occurs as well. However, as long as air temperature levels stay below the freezing point of water, neither snowmelt processes nor evapotranspiration is affected by that. Consequently discharge rates in those high elevation basins during winter months do not rise as strong as in lower catchments. Figure 6-44 summarizes the evolution of the hydrograph and the reasons for that evolution in alpine catchments in the course of changing climate conditions.

The lower the (mean) elevation of a catchment, the greater the influence of liquid precipitation on the hydrograph. Since the evolution of precipitation is more uncertain than air temperature, differences between the realizations using different RCMs concerning discharge in low catchments are, in general, greater than in higher catchments. Furthermore, runoff conditions during climate normals differ more in low catchments. This accounts particularly for the basin of river Rott (Figure 6-30) but also, in alleviated form, for the basins of Kamp and Gurk (see Figures 6-31 and 6-32, respectively). It should be noted however, that the model in these low catchments performs not as well as it does in mountainous basins. This clearly has an influence on the significance of the evolution of the discharge behaviour. Nevertheless some principle statements are valid for those submontane basins, too (see next chapter).

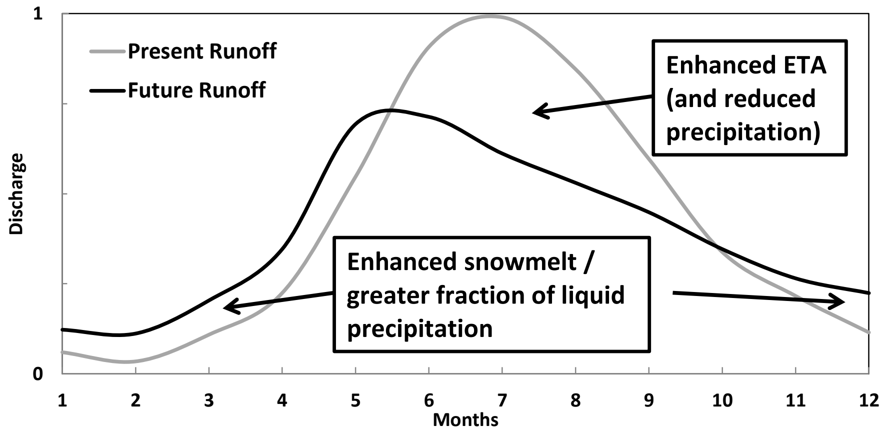

Figure 6-44: Conceptual hydrographs for actual and changing runoff conditions in alpine catchments.

6.6.3 Key characteristics relevant for hydropower

Hydropower relies on the supply of water. In general, the more discharge can be provided by unit of time (e.g. hours, days, months, etc.) the more electric energy can be generated by the turbines. This relationship is almost linear for a wide range of discharge rates. It depends on the characteristics of a power plant such as the kind of turbines, storage depth, etc. However, at the edges of the flow duration curve of a river, this relationship becomes non-linear (see chapter 6.5.4). The discussion regarding key characteristics is based on Figure 6-41. High flows refer to the MQ1.5, low flows to Q330.

The vast majority of studied rivers show reduced exceedance probabilities for high flows at the end of the century using all three climate models. Exceptions are the low elevation basins of river Rott and Kamp as well as river Ybbs for at least some of the RCMs. Fewer days featuring high flow conditions mean fewer days with reduced plant efficiency and therefore a greater energy production potential. The yield regarding high flows is greater the higher the elevation of a catchment. At river Inn for instance, the exceedance time drops from roughly 90 to about 30-45 days per year.

At the far right side of the flow duration curve statements regarding low flow conditions can be made. Other than for high flows, the exceedance probability for low flow conditions drops in the majority of the basins meaning that power generation losses due to droughts are more likely to occur. For catchments situated in high elevation ranges this might not be true, though. Staying with the example of River Inn, low flow conditions at the end of the century will occur at 17 to 23 days less than present. However, the RCM ALADIN signals roughly no change in low flows (327 instead of 330 days).

The centre of the FDC represents mean flow conditions (MQ). Generally speaking, a rise in MQ means better, a decreasing MQ worse conditions for generating electric energy from hydro power. Besides the pure discharge rate at the MQ, one may interpret a shift in the days when MQ is exceeded to the right (i.e. more days a year) as a benefit and a shift to the left as loss. In nearly every catchment a left-shift is indicated by all RCMs. However, in most of the basins this shift is quite narrow affecting only some days. Here, no clear statements can be concluded whether this shift is greater or lesser in mountainous than in flat regions.

Assuming there is good efficiency in the range between low and high flows one can derive the time span for optimal generation conditions and state whether these evolve better or worse. This is done for the three future climate normals and shown in Table 6-7. While the time span featuring good conditions shortens in low, flat catchments, mountainous catchments with high altitudes provide a larger good time range.

Table 6-7: Days with good conditions for generating electric energy from hydro power. Good conditions are assumed between low and high flow conditions. Given is the mean of the range of different RCMs.

Basin	**Days with optimal production conditions**		
	2011-2040	**2041-2070**	**2071-2100**
Rott	-34 ± 8	-72.5 ± 10.5	-68.5 ± 31.5
Kamp	-71 ± 23	-103 ± 40	-145 ± 34
Gurk	-28.5 ± 8.5	-36.5 ± 4.5	-58.5 ± 24.5
Ybbs	-57.5 ± 2.5	-48 ± 13	-51.5 ± 17.5
Mur	-12.5 ± 0.5	7.5 ± 4.5	16.5 ± 11.5
Saalach	-29 ± 4	-5.5 ± 12.5	-6.5 ± 15.5
Salzach	-1 ± 7	13.5 ± 1.5	15 ± 26
Drau	-19.5 ± 0.5	5.5 ± 15.5	-6 ± 19
Isel	3.5 ± 0.5	35 ± 1	38 ± 13
Inn	8.5 ± 3.5	41 ± 5	55.5 ± 4.5

Obviously, this only vaguely estimates the evolution of the electric power potential in these catchments. At higher discharge rates within these ranges better efficiency conditions exist than at low discharge rates. Nevertheless, it gives an overview of trends. In a catchment where the range providing good conditions gets shorter the power potential is likely to drop, whereas when the range gets wider, for said reasons, it may be increased.

An exact measure of the power potential however would necessitate explicit knowledge of the existing run-of-river stations. Furthermore, the approach in Table 6-7 does not consider edificial changes such as the construction of new stations or technical advances as the refinement of turbines.

7 Summary and conclusions

Runoff conditions are influenced by climate conditions. Thus under changing climate conditions runoff behaviours are likely to change, as well. Predictions of climate change are highly uncertain. How does the economy develop in next century? An economy relying on fossil energy produces climate relevant gases such as CO_2 or CH_4. But how do these gases influence the climate?

To overcome these questions and study the effects of climate change on different aspects like water cycle, climate change scenarios are used. These are defined by the Intergovernmental Panel on Climate Change and include socioeconomic pathways. Commonly used is the scenario A1B, that may be seen as medium scenario. Since the previous climate change report in 2007, the IPCC has changed the nomenclature and meaning of its scenarios (IPCC, 2013). Instead of emitted climate relevant gases and their consequences on earth’s climate, new scenarios now directly consider a surplus of energy. Most similar to A1B is the new scenario RCP6.0 referring to an additional intake of the earth’s surface of 6.0 $W\ m^{-2}$. The old and new scenarios cover a similar range in additional climate relevant gases (CO_2 equivalent) and subsequently the use of A1B still is valid.

To represent the complex nature of earth’s climate including feedback processes of land and oceans as well as uncertainties in a highly dynamic system a set of three different climate models are used to study effects of climate change on the water cycle. ALADIN is driven by the global circulation model ARPEGE, REMO and RegCM3 are driven by ECHAM5. All of these models are of equal value meaning that none of the model results is more likely than any other. While all three models picture the evolution of air temperature (annual mean) similarly, differences regarding precipitation and global radiation do exist. No coinciding trend is observable regarding the latter two meteorological variables. On a seasonal scale however, even the consensus on temperature evolution is missing. While ALADIN indicates hot summers with temperature rises of more than 5 K with respect to the climate normal 1981-2010 air temperature during the winter months is increased by only about 1 K. REMO and RegCM3 indicate an even rise in temperature values throughout the year by approximately 3.5 to 4 K.

Feeding a hydrological model with data provided by these climate models possible impacts on the hydrological cycle with focus on energy generation from hydro power stations within ten model basins in Austria is studied. This model is based on the ideas of the widely used conceptual rainfall runoff model HBV (Bergström, 1976). Although the model was calibrated at the turn of the 20th century it is able to reproduce runoff characteristics during the standard normal 1951-1980. Therefore it is able to model discharge under changing climate conditions and hence it is appropriate for the use of climate change impact studies. Recently Vaze et al. (2010) have shown that hydrological models generally may be applied in climate change studies, if mean annual precipitation does not vary more than roughly 20 %.

Since many of the modelled catchments are located in mountainous regions, snow processes play a key role in the runoff generation processes in these catchments. These processes are modelled using a simple approach only considering air temperature. Simplicity on the one hand competes against a detailed description of snow processes influenced by other factors such as radiation or latent heat fluxes. However, more information about meteorological state variables increases the source of errors of the model. The idea is to keep the model as simple as possible (Thorsen et al., 2010). Yet a simple temperature index approach leads to intensive accumulation of snow in altitudes where the air temperature scarcely rises above the melting point of snow (i.e. 0 °C). To overcome this behaviour a simple approach has been developed transferring snow to lower altitudes enabling snowmelt. This approach has been tested in the catchment of river Salzach, Austria. It could be shown that not accounting for lateral snow redistribution processes not only leads to a significant portion of water being stored in the catchment but also inhibits glacier melt. If no redistribution processes are taken into account in long term hydrological modelling, large piles of snow will have been developed in high elevations after some 10s of years of modelling. In a warming environment, snowmelt is getting enhanced. This applies for high altitudes, as well. Consequently, snow that has accumulated for years begins to melt, altering the model results in a considerable range of up to 4.3 %. Since the response of the hydrological model to climate change for Salzach River basin is in similar range (10 to 15 %) snow redistribution should be considered in climate change impact studies regarding alpine regions.

Implementation of a snow redistribution routine in the spatial distributed rainfall-runoff model COSERO (Nachtnebel et al., 1993) endorses these findings (Frey and Holzmann, 2015). In the catchment of the Ötztaler Ache, Austria, it could be shown that snow redistribution to lower regions amplifies glacier melt of 100 mm per year and prevents the appearance of “snow towers” in high altitudes. Furthermore, it could be demonstrated that including lateral snow processes improves discharge at the gauge Huben in the Ötztal by 0.05 units of Kling-Gupta-Efficiency in the calibration and 0.02 units in the validation period. However, the influence of snow transport processes on discharge at the outlet of a catchment decreases with an increasing catchment size, since large parts are situated in low elevations where snow accumulation is not problematic. Although there are additional parameters needed the integration of a snow transport module promotes the demand, that models work “right for the right reasons” and is an attempt to integrate more real process understanding into the model approach. A better mapping of realistic runoff processes may help to reduce model uncertainties due to narrower parameter boundaries. However more research would be needed to ensure this statement. An additional open question arises from the rather minor enhancements regarding areal snow cover. Since MODIS provides only binary information no statements about the SWE can be derived from this information. In addition the resolution of MODIS is relatively coarse featuring a 500 m cell edge size. This resolution, although higher than the model grid cell size of 1 x 1, might not be high enough to picture peak regions in an accurate way. Landsat provides images with spatial resolution of 30 x 30 m (available online at http://glovis.usgs.gov) that could be useful in validating snow covered or snow free regions.

To quantify parameter uncertainties regarding the model cascade climatological model to hydrological model, a very simple hydrological water balance model was developed and applied to five model regions across the Alps and Massif Central. This model can be described as “as simple as possible” since it uses only five parameters. It has been proven to be suitable for representing discharge conditions within these regions using a monthly temporal resolution. The simplicity of the model and use of an efficient programming language (FORTRAN) in terms of computing time made the model suitable for uncertainty analysis using large amounts of model runs. While model uncertainties obviously exist, these are superimposed by differences between climate change models. Those differences may be addressed as uncertainties ranging from climate change. It is evident that more complex hydrological models using more parameters lead to higher uncertainties due to equifinality reasons, though.

Good correlations (R^2) between runoff conditions on a monthly basis and generation rates of electric energy in national states covering the model regions were found using multiple regression analysis. These were up to 0.85 for France, 0.71 for Germany, 0.82 for Italy and 0.78 for Switzerland. By assuming no changes within these relationships due to whatever reason (e.g. edificial, socio-economic, etc.) possible future energy generation potential can be derived from evolving discharge rates in the modelled regions. By the end of the 21st century, the biggest deficits regarding power potential occur during the summer months, when runoff is reduced due to enhanced ETA and reduced snowmelt. In winter, the energy generation potential most likely will rise as less precipitation is stored in the catchments in the form of snow. However, the rise in winter does not compensate for losses during the summer months in all countries except Germany for the use of REMO and RegCM3. Despite the use of an ensemble of parameter sets for the hydrological model, uncertainty bands within the same RCM, except in France, are rather narrow.

For the Austrian basins, using a semi-lumped water balance model, the modelled hydrological results are similar to the European catchments. Discharge rates during the summer months will most likely drop due to enhanced evapotranspiration and less snow- and icemelt. In addition, especially ALADIN signals dry summer months amplifying this behaviour. Less precipitation in summer limits ETA especially in low elevation catchments. However, one has to be aware that the used model performs not as well in these catchments as it does in steeper regions. During winter months, discharge rates will most likely be increased due to rising air temperature that causes precipitation to fall augmented in liquid form. This effect is most distinct in mid-elevation catchments that are influenced by snow but are located low enough for a rise of temperature above 0 °C in winter by the end of the century. These are the catchments of the rivers Saalach, Mur, Ybbs, Drau and, to some extent, Gurk. Temperature rises in nival catchments as well, however as long as temperature values seldom exceed the melting point of snow it has little influence on the discharge behaviour.

Evolution of the electric power potential depends on (i) the total amount of (annual) discharge in a basin and (ii) the time range in which run-of-river stations can operate with good efficiency.

While the first can easily be estimated using the hydrological model the latter may be defined as range of the flow duration curve between the discharge rate at 1.5 times the MQ and the discharge that is exceeded on 330 days a year (Q330). This range is likely to get wider in alpine and nival catchments and shortens in low- to mid-elevation catchments. In general, a wider range means more days providing good runoff conditions. This may compensate for decreasing discharge rates throughout the year. However, exact measures of the power potential would necessitate explicit knowledge of the existing power stations. In addition, this approach does not account for edificial changes in the catchments or technical advances such as refinement of turbines, for instance. The availability of river runoff is the key component for the potential of generating electric energy from hydro power.

Since updated climate change scenarios are available, climate change impact studies in the future should be carried out using these new scenarios. The use of more than one scenario will lead to a wider span of possible impact on the hydrological cycle and consequently on the electric power potential. In addition the use of different hydrological models could solidify statements made in this thesis. General findings in this thesis regarding climate change impact on the hydrological cycle however are reported by other studies as well (e.g. Laghari et al., 2012; Schaefli et al., 2007; Schöner et al., 2011).

However, socioeconomic and political factors influencing the actual value of electricity on the market play an important role in the decision making process of power suppliers and may superimpose hydrologic conditions.

8 References

Alaoui, A., Willimann, E., Jasper, K., Felder, G., Herger, F., Magnusson, J., Weingartner, R., 2014. Modelling the effects of land use and climate changes on hydrology in the Ursern Valley, Switzerland. Hydrol. Process. 28, 3602–3614. doi:10.1002/hyp.9895

Ansari, S.S., Wijen, F., Gray, B., 2013. Constructing a Climate Change Logic: An Institutional Perspective on the “Tragedy of the Commons.” Organ. Sci. 7039, 1–27. doi:10.1287/orsc.1120.0799

APCC, 2014. Österreichischer Sachstandsbericht Klimawandel 2014. Verlag der Österreichischen Akademie der Wissenschaften, Wien, Österreich.

Arendt, A., Bolch, T., Cogley, J.G., Gardner, A., Hagen, J.-O., Hock, R., Kaser, G., Pfeffer, W.T., Moholdt, G., Paul, F., Radić, V., Andreassen, L., Bajracharya, S., Barrand, N., Beedle, M., Berthier, E., Bhambri, R., Bliss, A., Brown, I., Burgess, D., Burgess, E., Cawkwell, F., Chinn, T., Copland, L., Davies, B., De Angelis, H., Dolgova, E., Filbert, K., Forester, R.R., Fountain, A., Frey, H., Giffen, B., Glasser, N., Gurney, S., Hagg, W., D., H., Haritashya, U.K., Hartmann, G., Helm, C., Herreid, S., Howat, I., Kapusti, G.G., Khromova, T., Kienholz, C., Köonig, M., Kohler, J., Kriegel, D., Kutuzov, S., Lavrentiev, I., Le Bris, R., Lund, J., Manley, W., Mayer, C., Miles, E., Li, X., Menounos, B., Mercer, A., Mölg, N., Mool, P., Nosenko, G., Negrete, A., Nuth, C., Pettersson, R., Racoviteanu, A., Ranzi, R., Rastner, P., Rau, F., Raup, B., Rich, J., Rott, H., Schneider, C., Seliverstov, Y., Sharp, M., Siguosson, O., Stokes, C., Wheate, R., Winsvold, S., Wolken, G., Wyatt, F., Zheltyhina, N., 2012. Randolph Glacier Inventory - A Dataset of Global Outliners: Version 3.2. Boulder Colorado, USA.

Arguez, A., Vose, R.S., 2011. The definition of the standard WMO climate normal: The key to deriving alternative climate normals. Bull. Am. Meteorol. Soc. 92, 699–704. doi:10.1175/2010BAMS2955.1

Arnold, J.G., Srinivasan, R., Muttiah, R.S., Williams, J.R., 1998. Large Area Hydrologic Modeling and Assessment Part I: Model Development. J. Am. Water Resour. Assoc. 34, 73–89. doi:10.1111/j.1752-1688.1998.tb05961.x

Bárdossy, A., Pegram, G., 2011. Downscaling precipitation using regional climate models and circulation patterns toward hydrology. Water Resour. Res. 47, 1–18. doi:10.1029/2010WR009689

Barnett, T.P., Adam, J.C., Lettenmaier, D.P., 2005. Potential impacts of a warming climate on water availability in snow-dominated regions. Nature 438, 303–309. doi:10.1038/nature04141

Barros, A.P., Lettenmaier, D.P., 1994. Dynamic modeling of orographically induced precipitation. Rev. Geophys. 32, 265. doi:10.1029/94RG00625

Bartelt, P., Lehning, M., 2002a. A physical SNOATACK model for the Swiss avalanche warning Part I: numerical model. Cold Reg. Sci. Technol. 35, 123–145. doi:10.1016/S0165-232X(02)00074-5

Bartelt, P., Lehning, M., 2002b. A physical SNOWPACK model for the Swiss avalanche warning Part III: meteorological forcing, thin layer formation and evaluation. Cold Reg. Sci. Technol. 35, 123–145. doi:10.1016/S0165-232X(02)00074-5

Beniston, M., 2012. Impacts of climatic change on water and associated economic activities in the Swiss Alps. J. Hydrol. 412-413, 291–296. doi:10.1016/j.jhydrol.2010.06.046

Bergström, S., 1991. Principles and confidence in hydrological modelling. Nord. Hydrol. 22, 123–136. doi:10.2166/nh.1991.009

Bergström, S., 1976. Development and application of a conceptual runoff model for Scandinavian catchments. SMHI Reports RHO No. 7, Norrköping.

Bernhardt, M., Liston, G.E., Strasser, U., Zängl, G., Schulz, K., 2010. High resolution modelling of snow transport in complex terrain using downscaled MM5 wind fields. Cryosph. 4, 99–113. doi:10.5194/tc-4-99-2010

Bernhardt, M., Schulz, K., 2010. SnowSlide: A simple routine for calculating gravitational snow transport. Geophys. Res. Lett. 37, L11502. doi:10.1029/2010GL043086

Bernhardt, M., Zängl, G., Liston, G.E., Strasser, U., Mauser, W., 2009. Using wind fields from a high-resolution atmospheric model for simulating snow dynamics in mountainous terrain. Hydrol. Process. 23, 1064–1075. doi:10.1002/hyp.7208

Beven, K., 2012. Rainfall-Runoff Modelling: The Primer: Second Edition, 2. Edition. ed, Rainfall-Runoff Modelling: The Primer: Second Edition. John Wiley & Sons, New York. doi:10.1002/9781119951001

Beven, K., 2001. How far can we go in distributed hydrological modelling? Hydrol. Earth Syst. Sci. doi:10.5194/hess-5-1-2001

Beven, K., 1993. Prophecy, reality and uncertainty in distributed hydrological modelling. doi:10.1016/0309-1708(93)90028-E

Beven, K., Binley, A., 1992. The future of distributed models: model calibration and uncertainty prediction. Hydrol. Process. 6, 279–298. doi:10.1002/hyp.3360060305

Beven, K., Freer, J., 2001. Equifinality, data assimilation, and uncertainty estimation in mechanistic modelling of complex environmental systems using the GLUE methodology. J. Hydrol. 249, 11–29. doi:10.1016/S0022-1694(01)00421-8

Blöschl, G., Sivapalan, M., 1995. Scale issues in hydrological modelling: A review. Hydrol. Process. 9, 251–290. doi:10.1002/hyp.3360090305

BMLFUW, 2014. eHYD [WWW Document]. URL http://ehyd.gv.at/ (accessed 1.19.15).

BMLFUW, 2007. Hydrologischer Atlas Österreichs, 3. ed. Bundesministerium für Land- und Forstwirtschaft, Umwelt und Wasserwirtschaft, Wien.

Bøggild, C.E., Knudby, C.J., Knudsen, M.B., Starzer, W., 1999. Snowmelt and runoff modelling of an Arctic hydrological basin in west Greenland. Hydrol. Process. 13, 1989–2002. doi:10.1002/(SICI)1099-1085(199909)13:12/13<1989::AID-HYP848>3.0.CO;2-Y

Braun, L.N., Aellen, M., Funk, M., Hock, R., Rohrer, M.B., Steinegger, U., Kappenberger, G., Müller-Lemans, H., 1994. Measurements and simulation of high alpine water balance components in the Linth-Limmern head watershed (north-eastern Switzerland). Zeitschrift für Gletscherkd. und Glazialgeol. 30, 161–185.

Brooks, H.E., 2013. Severe thunderstorms and climate change. Atmos. Res. doi:10.1016/j.atmosres.2012.04.002

Chen, J., Brissette, F.P., Leconte, R., 2011. Uncertainty of downscaling method in quantifying the impact of climate change on hydrology. J. Hydrol. 401, 190–202. doi:10.1016/j.jhydrol.2011.02.020

Christensen, N.S., Wood, A.W., Voisin, N., Lettenmaier, D.P., Palmer, R.N., 2004. The effects of climate change on the hydrology and water resources of the Colorado River basin. Clim. Change 62, 337–363. doi:10.1023/B:CLIM.0000013684.13621.1f

Dadic, R., Mott, R., Lehning, M., Burlando, P., 2010a. Parameterization for wind-induced preferential deposition of snow. Hydrol. Process. 24, 1994–2006. doi:10.1002/hyp.7776

Dadic, R., Mott, R., Lehning, M., Burlando, P., 2010b. Wind influence on snow depth distribution and accumulation over glaciers. J. Geophys. Res. Earth Surf. 115, F01012. doi:10.1029/2009JF001261

Déqué, M., 2007. Frequency of precipitation and temperature extremes over France in an anthropogenic scenario: Model results and statistical correction according to observed values. Glob. Planet. Change 57, 16–26. doi:10.1016/j.gloplacha.2006.11.030

Déqué, M., Dreveton, C., Braun, A., Cariolle, D., 1994. The ARPEGE/IFS atmosphere model: a contribution to the French community climate modelling. Clim. Dyn. 10, 249–266. doi:10.1007/BF00208992

Dobesch, H., 2007. Mean annual potential evapotranspiration, in: BMLFUW (Ed.), Hydrologischer Atlas Österreichs. Bundesministerium für Land- und Forstwirtschaft, Umwelt und Wasserwirtschaft, Vienna, p. 3.2.

Doherty, J., 2010. PEST - Model-Independent Parameter Estimation. User Manual, 5th ed. Watermark Numerical Computing, Brisbane, Australia.

Donald, J.R., Soulis, E.D., Kouwen, N., Pietroniro, A., 1995. A Land Cover-Based Snow Cover Representation for Distributed Hydrologic Models. Water Resour. Res. 31, 995–1009. doi:10.1029/94WR02973

Duan, Q., Sorooshian, S., Gupta, V., 1992. Effective and efficient global optimization for conceptual rainfall-runoff models. Water Resour. Res. 28, 1015–1031. doi:10.1029/91WR02985

E-Control, 2013. Stromkennzeichnunsbericht 2013. Vienna.

EEA, 2014. Cumulative net mass balance of European glaciers [WWW Document]. URL http://www.eea.europa.eu/data-and-maps/daviz/cumulative-specific-net-mass-balance-1#tab-chart_3 (accessed 2.15.15).

Efstratiadis, A., Koutsoyiannis, D., 2010. One decade of multi-objective calibration approaches in hydrological modelling: a review. Hydrol. Sci. J. doi:10.1080/02626660903526292

Elder, K., Dozier, J., Michaelsen, J., 1991. Snow accumulation and distribution in an Alpine Watershed. Water Resour. Res. 27, 1541–1552. doi:10.1029/91WR00506

Erdal, D., Neuweiler, I., Wollschläger, U., 2014. Using a bias aware EnKF to account for unresolved structure in an unsaturated zone model. Water Resour. Res. 50, 132–147. doi:10.1002/2012WR013443

Essery, R., Li, L., Pomeroy, J., 1999. A distributed model of blowing snow over complex terrain. Hydrol. Process. 13, 2423–2438. doi:10.1002/(SICI)1099-1085(199910)13:14/15<2423::AID-HYP853>3.0.CO;2-U

Farda, A., Déué, M., Somot, S., Horányi, A., Spiridonov, V., Tóth, H., 2010. Model ALADIN as regional climate model for Central and Eastern Europe. Stud. Geophys. Geod. 54, 313–332. doi:10.1007/s11200-010-0017-7

Ford, J.D., Pearce, T., 2010. What we know, do not know, and need to know about climate change vulnerability in the western Canadian Arctic: a systematic literature review. Environ. Res. Lett. doi:10.1088/1748-9326/5/1/014008

Formayer, H., 2011. Correction of RegCM3 model output data using a rank matching approach applied on various meteorological parameters. BOKU contribution Report. Vienna.

Förster, K., Meon, G., Marke, T., Strasser, U., 2014. Effect of meteorological forcing and snow model complexity on hydrological simulations in the Sieber catchment (Harz Mountains, Germany). Hydrol. Earth Syst. Sci. 18, 4703–4720. doi:10.5194/hess-18-4703-2014

Frey, G.W., Linke, D.M., 2002. Hydropower as a renewable and sustainable energy resource meeting global energy challenges in a reasonable way. Energy Policy 30, 1261–1265. doi:10.1016/S0301-4215(02)00086-1

Frey, S., Goler, R., Formayer, H., Holzmann, H., 2013. Die Auswirkungen möglicher Klimawandelszenarien auf das Erzeugungspotenzial von Wasserkraftwerken. Forum für Hydrol. und Wasserbewirtschaftung 32.13, 145 – 152.

Frey, S., Goler, R., Leidinger, D., Formayer, H., Holzmann, H., 2014. POWERCLIM - Endbericht. Vienna.

Frey, S., Holzmann, H., 2015. A conceptual, distributed snow redistribution model. Hydrol. Earth Syst. Sci. Discuss. 12, 609–637. doi:10.5194/hessd-12-609-2015

Frey, S., Holzmann, H., 2014. Hydrological model uncertainies in climate change impact studies (poster). EGU Gen. Assem.

Frey, S., Holzmann, H., 2013. Dealing with snow accumulation in high mountains - A simple conceptual snow drift model (poster). EGU Gen. Assem.

Fries, A., Rollenbeck, R., Nauß, T., Peters, T., Bendix, J., 2012. Near surface air humidity in a megadiverse Andean mountain ecosystem of southern Ecuador and its regionalization. Agric. For. Meteorol. 152, 17–30. doi:10.1016/j.agrformet.2011.08.004

Garvelmann, J., Pohl, S., Weiler, M., 2013. From observation to the quantification of snow processes with a time-lapse camera network. Hydrol. Earth Syst. Sci. 17, 1415–1429. doi:10.5194/hess-17-1415-2013

Gehrig-Fasel, J., Guisan, A., Zimmermann, N.E., 2007. Tree line shifts in the Swiss Alps: Climate change or land abandonment? J. Veg. Sci. 18, 571–582. doi:10.1111/j.1654-1103.2007.tb02571.x

Gharari, S., Hrachowitz, M., Fenicia, F., Gao, H., Savenije, H.H.G., 2014. Using expert knowledge to increase realism in environmental system models can dramatically reduce the need for calibration. Hydrol. Earth Syst. Sci. 18, 4839–4859. doi:10.5194/hess-18-4839-2014

Grayson, R.B., Moore, I.D., McMahon, T.A., 1992. Physically based hydrologic modeling 2. Is the concept realistic? Water Resour. Res. doi:10.1029/92WR01259

GRDC, 2013. The Global Runoff Data Centre. 56068 Koblenz, Germany.

Gudmundsson, L., Tallaksen, L.M., Stahl, K., Clark, D.B., Dumont, E., Hagemann, S., Bertrand, N., Gerten, D., Heinke, J., Hanasaki, N., Voss, F., Koirala, S., 2012. Comparing large-scale hydrological model simulations to observed runoff percentiles in Europe. doi:10.1175/JHM-D-11-083.1

Gupta, H. V., Kling, H., Yilmaz, K.K., Martinez, G.F., 2009. Decomposition of the mean squared error and NSE performance criteria: Implications for improving hydrological modelling. J. Hydrol. 377, 80–91. doi:10.1016/j.jhydrol.2009.08.003

Habersack, H., Wagner, B., Hauer, C., Jäger, E., Krapesch, G., Strahlhofer, L., Volleritsch, M., Holzapfel, P., Schmutz, S., Schinegger, R., Pletterbauer, F., Formayer, H., Gerersdorfer, T., Pospichal, B., Prettenthaler, F., Steiner, D., Köberl, J., Rogler, N., 2011. DSS_KLIM:EN: Entwicklung eines Decision Support Systems zur Beurteilung des Wechselwirkungen zwischen Klimawandel, Energie aus Wasserkraft und Ökologie. Endbericht. Kommunalkredit AG, Vienna.

Haiden, T., Kann, A., Wittmann, C., Pistotnik, G., Bica, B., Gruber, C., 2011. The Integrated Nowcasting through Comprehensive Analysis (INCA) System and Its Validation over the Eastern Alpine Region. Weather Forecast. 26, 166–183. doi:10.1175/2010WAF2222451.1

Hall, D.K., Foster, J.L., Salomonson, V. V., Klein, A.G., Chien, J.Y.L., 2001a. Development of a Technique to Assess Snow-Cover Mapping Errors from Space. IEEE Trans. Geosci. Remote Sens. 39, 232–238.

Hall, D.K., Riggs, G. a., 2007. Accuracy assessment of the MODIS snow products. Hydrol. Process. 21, 1534–1547. doi:10.1002/hyp.6715

Hall, D.K., Riggs, G.A., Salomonson, V. V, DiGirolamo, N.E., Bayr, K.J., 2002. MODIS snow-cover products. Remote Sens. Environ. 83, 181–194. doi:10.1016/S0034-4257(02)00095-0

Hall, D.K., Riggs, G.A., Salomonson, V. V., 2006. MODIS/Terra Snow Cover 8-day L3 Global 500m Grid V005, January 2005 to December 2010. National Snow and Ice Data Center, Boulder, Colorado, USA.

Hall, D.K., Riggs, G.A., Salomonson, V. V., 2001b. Algorithm Theoretical Basis Document (ATBD) for the MODIS Snow and Sea Ice-Mapping Algorithms.

Hamlet, A.F., Lee, S.-Y., Mickelson, K.E.B., Elsner, M.M., 2010. Effects of projected climate change on energy supply and demand in the Pacific Northwest and Washington State. Clim. Change. doi:10.1007/s10584-010-9857-y

Hannah, D.M., Demuth, S., van Lanen, H.A.J., Looser, U., Prudhomme, C., Rees, G., Stahl, K., Tallaksen, L.M., 2011. Large-scale river flow archives: Importance, current status and future needs. Hydrol. Process. 25, 1191–1200. doi:10.1002/hyp.7794

Haylock, M.R., Hofstra, N., Klein Tank, a. M.G., Klok, E.J., Jones, P.D., New, M., 2008. A European daily high-resolution gridded data set of surface temperature and precipitation for 1950-2006. J. Geophys. Res. Atmos. 113, D20119. doi:10.1029/2008JD010201

Helfricht, K., Schöber, J., Schneider, K., Sailer, R., Kuhn, M., 2014. Interannual persistence of the seasonal snow cover in a glacierized catchment. J. Glaciol. 60, 889–904. doi:10.3189/2014JoG13J197

Helfricht, K., Schöber, J., Seiser, B., Fischer, A., Stötter, J., Kuhn, M., 2012. Snow accumulation of a high alpine catchment derived from LiDAR measurements. Adv. Geosci. 32, 31–39. doi:10.5194/adgeo-32-31-2012

Herrnegger, M., Nachtnebel, H.-P., Haiden, T., 2012. Evapotranspiration in high alpine catchments – an important part of the water balance! Hydrol. Res. 43, 460. doi:10.2166/nh.2012.132

Herrnegger, M., Nachtnebel, H.P., Schulz, K., 2014. From runoff to rainfall: inverse rainfall–runoff modelling in a high temporal resolution. Hydrol. Earth Syst. Sci. Discuss. 11, 13259–13309. doi:10.5194/hessd-11-13259-2014

Hiemstra, C.A., Liston, G.E., Reiners, W.A., 2006. Observing, modelling, and validating snow redistribution by wind in a Wyoming upper treeline landscape. Ecol. Modell. 197, 35–51. doi:10.1016/j.ecolmodel.2006.03.005

Hock, R., 2003. Temperature index melt modelling in mountain areas. J. Hydrol. 282, 104–115. doi:10.1016/S0022-1694(03)00257-9

Holzmann, H., Lehmann, T., Formayer, H., Haas, P., 2010. Auswirkungen möglicher Klimaänderungen auf Hochwasser und Wasserhaushaltskomponenten ausgewählter Einzugsgebiete in Österreich (in german). Österreichische Wasser- und Abfallwirtschaft 62, 7–14. doi:10.1007/s00506-009-0154-9

Holzmann, H., Nachtnebel, H.P., 2002. Abflussprognose für mittelgroße Einzugsgebiete - Methodik und Anwendungen (in german). Österreichische Wasser- und Abfallwirtschaft 54, 141–153.

Hrachowitz, M., Fovet, O., Ruiz, L., Euser, T., Gharari, S., Nijzink, R., Freer, J., Savenije, H.H.G., Gascuel-Odoux, C., 2014. Process consistency in models: The importance of system signatures, expert knowledge, and process complexity. Water Resour. Res. 50, 7445–7469. doi:10.1002/2014WR015484

IEA, 2014. Tracking Clean Energy Progress 2014. IEA Publications, Paris.

Immerzeel, W.W., van Beek, L.P.H., Bierkens, M.F.P., 2010. Climate change will affect the Asian water towers. Science (80-.). 328, 1382–1385. doi:10.1126/science.1183188

IPCC, 2013. Climate Change 2013: The Physical Science Basis. Contribution of Working Group I to the Fifth Assessment Report of the Intergovernmental Panel on Climate Change. Cambridge University Press, Cambridge, UK and New York, NY, USA. doi:10.1017/CBO9781107415324

IPCC, 2000. Special report on emission scenarios (SRES): A Special Report of Working Group III of the Intergovernmental Panel on Climate Change. Cambridge University Press, Cambridge, UK.

Jacob, D., Van den Hurk, B.J.J.M., Andrea, U., Elgered, G., Fortelius, C., Graham, L.P., Jackson, S.D., Karstens, U., Köpken, C., Lindau, R., Podzun, R., Rockel, B., Rubel, F., Sass, B.H., Smith, R.N.B., Yang, X., 2001. A comprehensive model inter-comparison study investigating the water budget during the BALTEX-PIDCAP period. Meteorol. Atmos. Phys. 77, 19–43. doi:10.1007/s007030170015

Jiménez Cisneros, B.E., Oki, T., Arnell, N.W., Benito, G., Cogley, J.G., Döll, P., Jiang, T., Mwakalila, S.S., 2014. Freshwater resources, in: Field, C.B., Barros, V.R., Dokken, D.J., Mach, K.J., Mastrandrea, M.D., Bilir, T.E., Chatterjee, M., Ebi, K.L., Estrada, Y.O., Genova, R.C., Girma, B., Kissel, E.S., Levy, A.N., MacCracken, S., Mastrandrea, P.R., White, L.L. (Eds.), Climate Change 2014: Impacts, Adaptation, and Vulnerability. Part A: Global and Sectoral Aspects. Contribution of Working Group II to the Fifth Assessment Report of the Intergovernmental Panel of Climate Change. Cambridge University Press, Cambridge, UK and New York, NY, USA, pp. 229–269.

Jonas, T., Marty, C., Magnusson, J., 2009. Estimating the snow water equivalent from snow depth measurements in the Swiss Alps. J. Hydrol. 378, 161–167. doi:10.1016/j.jhydrol.2009.09.021

Judson, A., Doesken, N., 2000. Density of Freshly Fallen Snow in the Central Rocky Mountains. Bull. Am. Meteorol. Soc. 81, 1577–1587. doi:10.1175/1520-0477(2000)081<1577:DOFFSI>2.3.CO;2

Katsigiannis, Y.A., Stavrakakis, G.S., 2014. Estimation of wind energy production in various sites in Australia for different wind turbine classes: A comparative technical and economic assessment. Renew. Energy 67, 230–236. doi:10.1016/j.renene.2013.11.051

Kendon, E.J., Jones, R.G., Kjellström, E., Murphy, J.M., 2010. Using and designing GCM-RCM ensemble regional climate projections. J. Clim. 23, 6485–6503. doi:10.1175/2010JCLI3502.1

Kirchner, J.W., 2006. Getting the right answers for the right reasons: Linking measurements, analyses, and models to advance the science of hydrology. Water Resour. Res. 42. doi:10.1029/2005WR004362

Kirchner, J.W., 2003. A double paradox in catchment hydrology and geochemistry. Hydrol. Process. 17, 871–874. doi:10.1002/hyp.5108

Kirchner, P.B., Bales, R.C., Molotch, N.P., Flanagan, J., Guo, Q., 2014. LiDAR measurement of seasonal snow accumulation along an elevation gradient in the southern Sierra Nevada, California. Hydrol. Earth Syst. Sci. Discuss. 11, 5327–5365. doi:10.5194/hessd-11-5327-2014

Klemeš, V., 1988. A hydrological perspective. J. Hydrol. doi:10.1016/0022-1694(88)90179-5

Kling, H., Fuchs, M., Paulin, M., 2012. Runoff conditions in the upper Danube basin under an ensemble of climate change scenarios. J. Hydrol. 424-425, 264–277. doi:10.1016/j.jhydrol.2012.01.011

Kling, H., Fürst, J., Nachtnebel, H.P., 2006. Seasonal, spatially distributed modelling of accumulation and melting of snow for computing runoff in a long-term, large-basin water balance model. Hydrol. Process. 20, 2141–2156. doi:10.1002/hyp.6203

Kling, H., Stanzel, P., Fuchs, M., Nachtnebel, H.-P., 2014a. Performance of the COSERO precipitation-runoff model under non-stationary conditions in basins with different climates. Hydrol. Sci. J. 141217125340005. doi:10.1080/02626667.2014.959956

Kling, H., Stanzel, P., Preishuber, M., 2014b. Impact modelling of water resources development and climate scenarios on Zambezi River discharge. J. Hydrol. Reg. Stud. 1, 17–43. doi:10.1016/j.ejrh.2014.05.002

Koboltschnig, G.R., Schöner, W., Zappa, M., Kroisleitner, C., Holzmann, H., 2008. Runoff modelling of the glacierized Alpine Upper Salzach basin (Austria): Multi-criteria result validation, in: Hydrological Processes. John Wiley & Sons, Ltd., pp. 3950–3964. doi:10.1002/hyp.7112

Koch, F., Prasch, M., Bach, H., Mauser, W., Appel, F., Weber, M., 2011. How will hydroelectric power generation develop under climate change scenarios? A case study in the upper danube basin. Energies 4, 1508–1541. doi:10.3390/en4101508

Koren, V., Reed, S., Smith, M., Zhang, Z., Seo, D., 2004. Hydrology laboratory research modeling system (HL-RMS) of the US national weather service. J. Hydrol. 291, 297–318. doi:10.1016/j.jhydrol.2003.12.039

Kuhn, M., Lambrecht, A., Abermann, J., 2013. Austrian Glacier Inventory 1998. doi:10.1594/PANGAEA.809196

Kunstmann, H., Heckl, A., Rimmer, A., 2006. Physically based distributed hydrological modelling of the Upper Jordan catchment and investigation of effective model equations. Adv. Geosci. doi:10.5194/adgeo-9-123-2006

Laghari, A.N., Vanham, D., Rauch, W., 2012. To what extent does climate change result in a shift in Alpine hydrology? A case study in the Austrian Alps. Hydrol. Sci. J. doi:10.1080/02626667.2011.637040

Lambrecht, A., Kuhn, M., 2007. Glacier changes in the Austrian Alps during the last three decades, derived from the new Austrian glacier inventory, in: Annals of Glaciology. pp. 177–184. doi:10.3189/172756407782871341

Lange, J., Leibundgut, C., Greenbaum, N., Schick, A.P., 1999. A noncalibrated rainfall-runoff model for large, arid catchments. Water Resour. Res. 35, 2161–2172. doi:10.1029/1999WR900038

Le Treut, H., Somerville, R., Cubasch, U., Ding, Y., Mauritzen, C., Mokssit, A., Peterson, T., Prather, M., 2007. Historical Overview of Climate Change, in: Solomon, S., Qin, D., Manning, M., Chen, Z., Marquis, M., Averyt, K.B., Tignor, M., Miller, H.L. (Eds.), Climate Change 2007: The Physical Science Basis. Contribution of Working Group I to the Fourth Assessment Report of the Intergovernmental Panel on Climate Change. Cambridge University Press, Cambridge, UK and New York, NY, USA, pp. 93–128.

Lehning, M., Bartelt, P., Brown, B., Fierz, C., Satyawali, P., 2002. A physical SNOWPACK model for the Swiss avalanche warning: part II. Snow microscrutcure. Cold Reg. Sci. Technol. 35, 147–167. doi:10.1016/S0165-232X(02)00073-3

Lehning, M., Fierz, C., 2008. Assessment of snow transport in avalanche terrain. Cold Reg. Sci. Technol. 51, 240–252. doi:10.1016/j.coldregions.2007.05.012

Leonelli, G., Pelfini, M., Morra, U., Garavaglia, V., Morra di Cella, U., Garavaglia, V., 2010. Climate Warming and the Recent Treeline Shift in the European Alps: The Role of Geomorphological Factors in High-Altitude Sites. Ambio 40, 264–273. doi:10.1007/s13280-010-0096-2

Lindström, G., Johansson, B., Persson, M., Gardelin, M., Bergström, S., 1997. Development and test of the distributed HBV-96 hydrological model. J. Hydrol. 201, 272–288. doi:10.1016/S0022-1694(97)00041-3

Liston, G., Sturm, M., 1998. A snow-transport model for complex terrain. J. Glaciol. 44.

Liston, G.E., 2004. Representing Subgrid Snow Cover Heterogeneities in Regional and Global Models. J. Clim. 17, 1381–1397. doi:10.1175/1520-0442(2004)017<1381:RSSCHI>2.0.CO;2

Liston, G.E., Haehnel, R.B., Sturm, M., Hiemstra, C. a., Berezovskaya, S., Tabler, R.D., 2007. Simulating complex snow distributions in windy environments using SnowTran-3D. J. Glaciol. 53, 241–256. doi:10.3189/172756507782202865

Liu, Z., Todini, E., 2002. Towards a comprehensive physically-based rainfall-runoff model. Hydrol. Earth Syst. Sci. 6, 859–881. doi:10.5194/hess-6-859-2002

Madani, K., Lund, J.R., 2009. Modeling California’s high-elevation hydropower systems in energy units. Water Resour. Res. 45, n/a–n/a. doi:10.1029/2008WR007206

Marks, D., Domingo, J., Susong, D., Link, T., Garen, D., 1999. A spatially distributed energy balance snowmelt model for application in mountain basins. Hydrol. Process. 13, 1935–1959. doi:10.1002/(SICI)1099-1085(199909)13:12/13<1935::AID-HYP868>3.0.CO;2-C

Massmann, C., Holzmann, H., 2012a. Analysis of the behavior of a rainfall-runoff model using three global sensitivity analysis methods evaluated at different temporal scales. J. Hydrol. 475, 97–110. doi:10.1016/j.jhydrol.2012.09.026

Massmann, C., Holzmann, H., 2012b. Global sensitivity analysis for the flow components of a conceptual rainfall-runoff model, in: Seppelt, R., Voinov, A.A., Lange, S., Bankamp, D. (Eds.), Proceedings of the 2012 International Congress on Environmental Modelling and Software. Managing Resources of a Limited Planet: Pathways and Visions under Uncertainty, Sixth Biennial Meeting. Leipzig, Germany.

Massmann, C., Wagener, T., Holzmann, H., 2014. A new approach to visualizing time-varying sensitivity indices for environmental model diagnostics across evaluation time-scales. Environ. Model. Softw. 51, 190–194. doi:10.1016/j.envsoft.2013.09.033

Mauser, W., Bach, H., 2009. PROMET - Large scale distributed hydrological modelling to study the impact of climate change on the water flows of mountain watersheds. J. Hydrol. 376, 362–377. doi:10.1016/j.jhydrol.2009.07.046

McDonnell, J.J., Sivapalan, M., Vaché, K., Dunn, S., Grant, G., Haggerty, R., Hinz, C., Hooper, R., Kirchner, J., Roderick, M.L., Selker, J., Weiler, M., 2007. Moving beyond heterogeneity and process complexity: A new vision for watershed hydrology. Water Resour. Res. doi:10.1029/2006WR005467

Melvold, K., Skaugen, T., 2013. Multiscale spatial variability of lidar-derived and modeled snow depth on Hardangervidda, Norway. Ann. Glaciol. 54, 273–281. doi:10.3189/2013AoG62A161

Nachtnebel, H.P., Baumung, S., Lettl, W., 1993. Abflussprognosemodell für das Einzugsgebiet der Enns und Steyer (in German). Vienna.

Nash, J.E., Sutcliffe, J.V., 1970. River flow forecasting through conceptual models part I — A discussion of principles. J. Hydrol. 10, 282–290. doi:10.1016/0022-1694(70)90255-6

Nikulin, G., Kjellström, E., Hansson, U., Strandberg, G., Ullerstig, A., 2011. Evaluation and future projections of temperature, precipitation and wind extremes over Europe in an ensemble of regional climate simulations. Tellus A 63, 41–55. doi:10.1111/j.1600-0870.2010.00466.x

ÖBB, 2015. ÖBB INFRA Werksgruppe Mitte [WWW Document]. URL http://www.oebb.at/infrastruktur/de/_p_3_0_fuer_Kunden_Partner/3_6_Bahnstromversorgung/3_6_1_Energieversorgungsanlagen/Kraft-_und_Umformerwerke/Werksgruppe_Mitte.jsp (accessed 2.12.15).

Ottaviani, D., De La Rocque, S., Khomenko, S., Gilbert, M., Newman, S.H., Roche, B., Schwabenbauer, K., Pinto, J., Robinson, T.P., Slingenbergh, J., 2010. The cold European winter of 2005-2006 assisted the spread and persistence of H5N1 influenza virus in wild birds. Ecohealth 7, 226–236. doi:10.1007/s10393-010-0316-z

Pal, J.S., Giorgi, F., Bi, X., Elguindi, N., Solmon, F., Rauscher, S.A., Gao, X., Francisco, R., Zakey, A., Winter, J., Ashfaq, M., Syed, F.S., Sloan, L.C., Bell, J.L., Diffenbaugh, N.S., Karmacharya, J., Konaré, A., Martinez, D., da Rocha, R.P., Steiner, A.L., 2007. Regional Climate Modeling for the Developing World: The ICTP RegCM3 and RegCNET. Bull. Am. Meteorol. Soc. 88, 1395–1409. doi:10.1175/BAMS-88-9-1395

Pamlin, D., Armstrong, S., 2015. Global Challenges – Twelve risks that threaten human civilisation – The case for a new category of risks. Global Challenges Foundation, Stockholm.

Panwar, N.L., Kaushik, S.C., Kothari, S., 2011. Role of renewable energy sources in environmental protection: A review. Renew. Sustain. Energy Rev. 15, 1513–1524. doi:10.1016/j.rser.2010.11.037

Parmesan, C., Burrows, M.T., Duarte, C.M., Poloczanska, E.S., Richardson, A.J., Schoeman, D.S., Singer, M.C., 2013. Beyond climate change attribution in conservation and ecological research. Ecol. Lett. 16, 58–71. doi:10.1111/ele.12098

Perrin, C., Michel, C., Andréassian, V., 2003. Improvement of a parsimonious model for streamflow simulation. J. Hydrol. 279, 275–289. doi:10.1016/S0022-1694(03)00225-7

Pohl, S., Garvelmann, J., Wawerla, J., Weiler, M., 2014. Potential of a low-cost sensor network to understand the spatial and temporal dynamics of a mountain snow cover. Water Resour. Res. 50, 2533–2550. doi:10.1002/2013WR014594

Pohl, S., Marsh, P., Bonsal, B.R., 2007. Modeling the impact of climate change on runoff and annual water balance of an arctic headwater basin. Arctic 60, 173–186. doi:10.14430/arctic242

Pomeroy, J.W., Gray, D.M., Hedstrom, N.R., Janowicz, J.R., 2002. Prediction of seasonal snow accumulation in cold climate forests. Hydrol. Process. 16, 3543–3558. doi:10.1002/hyp.1228

Pomeroy, J.W., Gray, D.M., Shook, K.R., Toth, B., Essery, R.L.H., Pietroniro, A., Hedstrom, N., 1998. An evaluation of snow accumulation and ablation processes for land surface modelling. Hydrol. Process. 12, 2339–2367. doi:10.1002/(SICI)1099-1085(199812)12:15<2339::AID-HYP800>3.0.CO;2-L

Prasad, R., Tarboton, D.G., Liston, G.E., Luce, C.H., Seyfried, M.S., 2001. Testing a blowing snow model against distributed snow measurements at Upper Sheep Creek, Idaho, United States of America. Water Resour. Res. 37, 1341–1356. doi:10.1029/2000WR900317

Prasch, M., Marke, T., Strasser, U., Mauser, W., 2011. Large scale integrated hydrological modelling of the impact of climate change on the water balance with DANUBIA. Adv. Sci. Res. 7, 61–70. doi:10.5194/asr-7-61-2011

Randall, D.A., Wood, R.A., Bony, S., Colman, R., Fichefet, T., Fyfe, J., Kattsov, V., Pitman, A., Shukla, J., Srinivasan, J., Stouffer, R.J., Sumi, A., Taylor, K.E., 2007. Climate Models and Their Evaluation, in: Solomon, S., Qin, D., Manning, M., Chen, Z., Marquis, M., Averyt, K.B., M.Tignor, Miller, H.L. (Eds.), Climate Change 2007: The Physical Science Basis. Contribution of Working Group I to the Fourth Assessment Report of the Intergovernmental Panel on Climate Change. Cambridge University Press, Cambridge, UK and New York, NY, USA, pp. 579–662.

Rechenraum, 2014. Der oe3d Datensatz [WWW Document]. URL www.oe3d.at (accessed 12.13.14).

Reszler, C., Bloschl, G., Komma, J., 2008. Identifying runoff routing parameters for operational flood forecasting in small to medium sized catchments. Hydrol. Sci. J. doi:10.1623/hysj.53.1.112

Riley, J., Israelsen, E., Eggleston, K., 1973. Some approaches to snowmelt prediction. Role Snowmelt Ice Hydrol. IAHS Publ. 107 956–971.

Roeckner, E., Bäuml, G., Bonaventura, L., Brokopf, R., Esch, M., Giorgetta, M., Hagemann, S., Kirchner, I., Kornblueh, L., Manzini, E., Rhodin, A., Schlese, U., Schulzweida, U., Tompkins, A., Kichner, I., Kornblueh, L., Manzini, E., Rhodin, A., Schlese, U., Schulzweida, U., Tompkins, A., 2003. Report No . 349 The atmospheric general circulation model ECHAM5 Part I: Model description. Hamburg, Germany.

Rosenbrock, H.H., 1963. Some general implicit processes for the numerical solution of differential equations. Comput. J. 5, 329–330. doi:10.1093/comjnl/5.4.329

Rutter, N., Essery, R., Pomeroy, J., Altimir, N., Andreadis, K., Baker, I., Barr, A., Bartlett, P., Boone, A., Deng, H., Douville, H., Dutra, E., Elder, K., Ellis, C., Feng, X., Gelfan, A., Goodbody, A., Gusev, Y., Gustafsson, D., Hellström, R., Hirabayashi, Y., Hirota, T., Jonas, T., Koren, V., Kuragina, A., Lettenmaier, D., Li, W.P., Luce, C., Martin, E., Nasonova, O., Pumpanen, J., Pyles, R.D., Samuelsson, P., Sandells, M., Schädler, G., Shmakin, A., Smirnova, T.G., Stähli, M., Stöckli, R., Strasser, U., Su, H., Suzuki, K., Takata, K., Tanaka, K., Thompson, E., Vesala, T., Viterbo, P., Wiltshire, A., Xia, K., Xue, Y., Yamazaki, T., 2009. Evaluation of forest snow processes models (SnowMIP2). J. Geophys. Res. Atmos. 114. doi:10.1029/2008JD011063

Sahoo, G.B.B., Ray, C., De Carlo, E.H., 2006. Calibration and validation of a physically distributed hydrological model, MIKE SHE, to predict streamflow at high frequency in a flashy mountainous Hawaii stream. J. Hydrol. 327, 94–109. doi:10.1016/j.jhydrol.2005.11.012

Samuels, R., Rimmer, A., Hartmann, A., Krichak, S., Alpert, P., 2010. Climate Change Impacts on Jordan River Flow: Downscaling Application from a Regional Climate Model. J. Hydrometeorol. 11, 860–879. doi:10.1175/2010JHM1177.1

Schaefli, B., Hingray, B., Musy, A., 2007. Climate change and hydropower production in the Swiss Alps: quantification of potential impacts and related modelling uncertainties. Hydrol. Earth Syst. Sci. doi:10.5194/hess-11-1191-2007

Schaefli, B., Hingray, B., Niggli, M., Musy, A., 2005. A conceptual glacio-hydrological model for high mountainous catchments. Hydrol. Earth Syst. Sci. 9, 95–109. doi:10.5194/hess-9-95-2005

Scherrer, S.C., Appenzeller, C., Liniger, M.A., 2006. Temperature trends in Switzerland and Europe: Implications for climate normals. Int. J. Climatol. 26, 565–580. doi:10.1002/joc.1270

Schmidli, J., Frei, C., Vidale, P.L., 2006. Downscaling from GCM precipitation: A benchmark for dynamical and statistical downscaling methods. Int. J. Climatol. 26, 679–689. doi:10.1002/joc.1287

Schöber, J., Schneider, K., Helfricht, K., Schattan, P., Achleitner, S., Schöberl, F., Kirnbauer, R., 2014. Snow cover characteristics in a glacierized catchment in the Tyrolean Alps - Improved spatially distributed modelling by usage of Lidar data. J. Hydrol. 519, 3492–3510. doi:10.1016/j.jhydrol.2013.12.054

Schöner, W., Böhm, R., Haslinger, K., Blöschl, G., Kroiß, H., Merz, R., Blaschke, A.P., Viglione, A., Parajka, J., Salinas, J.L., Drabek, U., Laaha, G., Kreuzinger, N., Kreuzlinger, K., 2011. Anpassungsstrategien an den Klimawandel für Österreichs Wasserwirtschaft. Lebensministerium, Wien.

Schulz, K., Beven, K.J., Huwe, B., 1999. Equifinality and the problem of robust calibration in nitrogen budget simulations. doi:10.2136/sssaj1999.6361934x

Seefeldner, E., 1961. Salzburg und seine Landschaften, 1st ed. Das Bergland-Buch, Salzburg.

Seibert, J., 2003. Reliability of Model Predictions Outside Calibration Conditions. Nord. Hydrol. 34, 477–492. doi:10.2166/nh.2003.028

Seibert, J., McDonnell, J.J., 2013. Gauging the Ungauged Basin: The Relative Value of Soft and Hard Data. J. Hydrol. Eng. 20, 130607193631000. doi:10.1061/(ASCE)HE.1943-5584.0000861

Seibert, J., McDonnell, J.J., 2002. On the dialog between experimentalist and modeler in catchment hydrology: Use of soft data for multicriteria model calibration. Water Resour. Res. 38, 23–1–23–14. doi:10.1029/2001WR000978

Shulski, M.D., Seeley, M.W., 2004. Application of Snowfall and Wind Statistics to Snow Transport Modeling for Snowdrift Control in Minnesota. J. Appl. Meteorol. doi:10.1175/JAM2140.1

Simic, A., Fernandes, R., Brown, R., Romanov, P., Park, W., 2004. Validation of VEGETATION, MODIS, and GOES + SSM/I snow-cover products over Canada based on surface snow depth observations. Hydrol. Process. 18, 1089–1104. doi:10.1002/hyp.5509

Sklenář, P., Bendix, J., Balslev, H., 2008. Cloud frequency correlates to plant species composition in the high Andes of Ecuador. Basic Appl. Ecol. 9, 504–513. doi:10.1016/j.baae.2007.09.007

Snover, A.K., Mauger, G.S., Whitely Binder, L.C., Krosby, M., Tohver, I., 2013. Climate Change Impacts and Adaptation in Washington State: Technical Summaries for Decision Makers. Universiy of Washington, Seattle.

Sovilla, B., Mcelwaine, J.N., Schaer, M., Vallet, J., 2010. Variation of deposition depth with slope angle in snow avalanches: Measurements from Vallée de la Sionne, Journal of Geophysical Research. doi:10.1029/2009JF001390

Stahl, K., Tallaksen, L.M., Hannaford, J., Van Lanen, H.A.J., 2012. Filling the white space on maps of European runoff trends: Estimates from a multi-model ensemble. Hydrol. Earth Syst. Sci. 16, 2035–2047. doi:10.5194/hess-16-2035-2012

Stanzel, P., Kahl, B., Haberl, U., Herrnegger, M., Nachtnebel, H.P., 2008. Continuous hydrological modelling in the context of real time flood forecasting in alpine Danube tributary catchments. IOP Conf. Ser. Earth Environ. Sci. 4, 012005. doi:10.1088/1755-1307/4/1/012005

Stanzel, P., Nachtnebel, H.P., 2010. Mögliche Auswirkungen des Klimawandels auf den Wasserhaushalt und die Wasserkraftnutzung in Österreich (in German). Österreichische Wasser- und Abfallwirtschaft 62, 180–187. doi:10.1007/s00506-010-0234-x

Strasser, U., Bernhardt, M., Weber, M., Liston, G.E., Mauser, W., 2008. Is snow sublimation important in the alpine water balance? Cryosph. 2, 53–66. doi:10.5194/tc-2-53-2008

Szerencsits, E., 2012. Swiss Tree Lines - a GIS-Based Approximation. Landsc. Online 28, 1–18. doi:10.3097/LO.201228

Teng, J., Vaze, J., Chiew, F.H.S., Wang, B., Perraud, J.-M., 2012. Estimating the Relative Uncertainties Sourced from GCMs and Hydrological Models in Modeling Climate Change Impact on Runoff. J. Hydrometeorol. 13, 122–139. doi:10.1175/JHM-D-11-058.1

Thornthwaite, C.W., 1948. An Approach toward a Rational Classification of Climate. Geogr. Rev. 38, 55–94.

Thorsen, S.M., Roer, A.G., van Oijen, M., 2010. Modelling the dynamics of snow cover, soil frost and surface ice in Norwegian grasslands. Polar Res. 29, 110–126. doi:10.1111/j.1751-8369.2010.00157.x

Turc, L., 1961. Evaluation des besoins en eau d'irrigation, evapotranspiration potentielle, formule climatique simplifee et mise a jour. (in French). Ann. Agron. 12, 13–49.

Van Den Besselaar, E.J.M., Haylock, M.R., Van Der Schrier, G., Klein Tank, A.M.G., 2011. A European daily high-resolution observational gridded data set of sea level pressure. J. Geophys. Res. Atmos. 116, D11110. doi:10.1029/2010JD015468

Vaze, J., Post, D.A., Chiew, F.H.S., Perraud, J.-M., Viney, N.R., Teng, J., 2010. Climate non-stationarity - Validity of calibrated rainfall-runoff models for use in climate change studies. J. Hydrol. 394, 447–457. doi:10.1016/j.jhydrol.2010.09.018

Vinogg, L., Elstad, I., 2003. Mechanical equipment. Norwegian University of Science and Technology, Trondheim.

Viviroli, D., Archer, D.R., Buytaert, W., Fowler, H.J., Greenwood, G.B., Hamlet, A.F., Huang, Y., Koboltschnig, G., Litaor, M.I., López-Moreno, J.I., Lorentz, S., Schädler, B., Schreier, H., Schwaiger, K., Vuille, M., Woods, R., 2011. Climate change and mountain water resources: Overview and recommendations for research, management and policy. Hydrol. Earth Syst. Sci. 15, 471–504. doi:10.5194/hess-15-471-2011

Viviroli, D., Zappa, M., Gurtz, J., Weingartner, R., 2009. An introduction to the hydrological modelling system PREVAH and its pre- and post-processing-tools. Environ. Model. Softw. 24, 1209–1222. doi:10.1016/j.envsoft.2009.04.001

Vrugt, J.A., ter Braak, C.J.F., Gupta, H. V., Robinson, B.A., 2009. Equifinality of formal (DREAM) and informal (GLUE) Bayesian approaches in hydrologic modeling? Stoch. Environ. Res. Risk Assess. 23, 1011–1026. doi:10.1007/s00477-008-0274-y

Wagner, G., Mahmoudian, B., Schröder, H.G., 1994. Water-budget of Upper Lake Constance: An estimation of total supply based on runoff and water level variations. Aquat. Sci. 56, 179–189. doi:10.1007/BF00877207

Warscher, M., Strasser, U., Kraller, G., Marke, T., Franz, H., Kunstmann, H., 2013. Performance of complex snow cover descriptions in a distributed hydrological model system: A case study for the high Alpine terrain of the Berchtesgaden Alps. Water Resour. Res. 49, 2619–2637. doi:10.1002/wrcr.20219

Weber, M., Braun, L., Mauser, W., Prasch, W., 2010. Contribution of rain, snow- and icemelt in the upper Danube discharge today and in the future. Geogr. Fis. e Din. Quat. 33, 221–230.

Weiler, M., McDonnell, J., 2004. Virtual experiments: A new approach for improving process conceptualization in hillslope hydrology. J. Hydrol. 285, 3–18. doi:10.1016/S0022-1694(03)00271-3

Winstral, A., Elder, K., Davis, R.E., 2002. Spatial Snow Modeling of Wind-Redistributed Snow Using Terrain-Based Parameters. J. Hydrometeorol. 3, 524–538. doi:10.1175/1525-7541(2002)003<0524:SSMOWR>2.0.CO;2

Wiscombe, W.J., Warren, S.G., 1980. A Model for the Spectral Albedo of Snow. I: Pure Snow. J. Atmos. Sci. 37, 2712–2733. doi:10.1175/1520-0469(1980)037<2712:AMFTSA>2.0.CO;2

WMO, 1999. WMO Statement on the status of the global climate in 1998. Geneva.

WMO, 1959. Technical Regulations No. 49. Volume 1., 2nd ed. World Meteorological Organization, Geneva, Switzerland.

9 Appendix

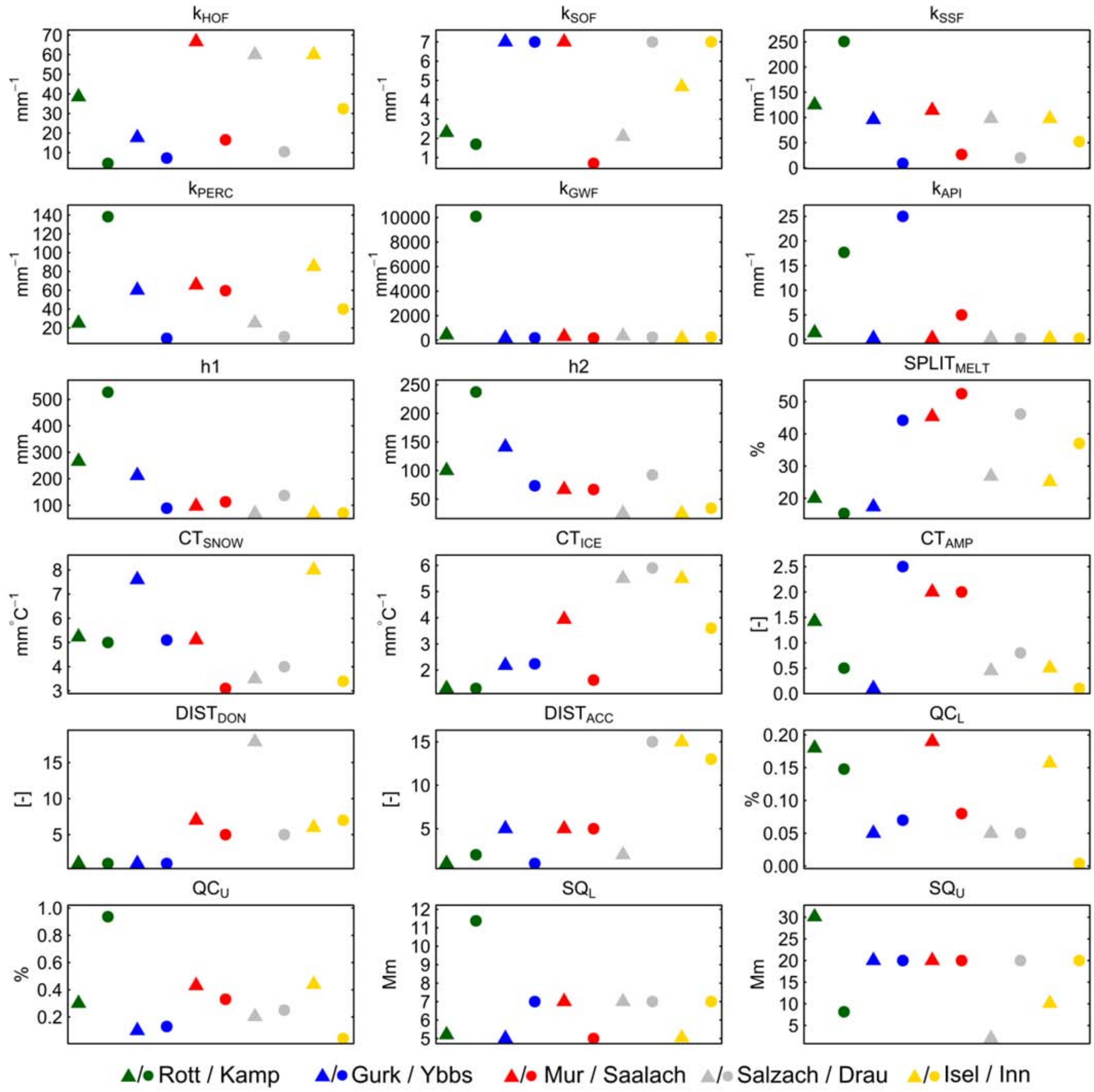

Figure A 1: Overview of the parameter sets used by SASWET for calibrating the Austrian watersheds.

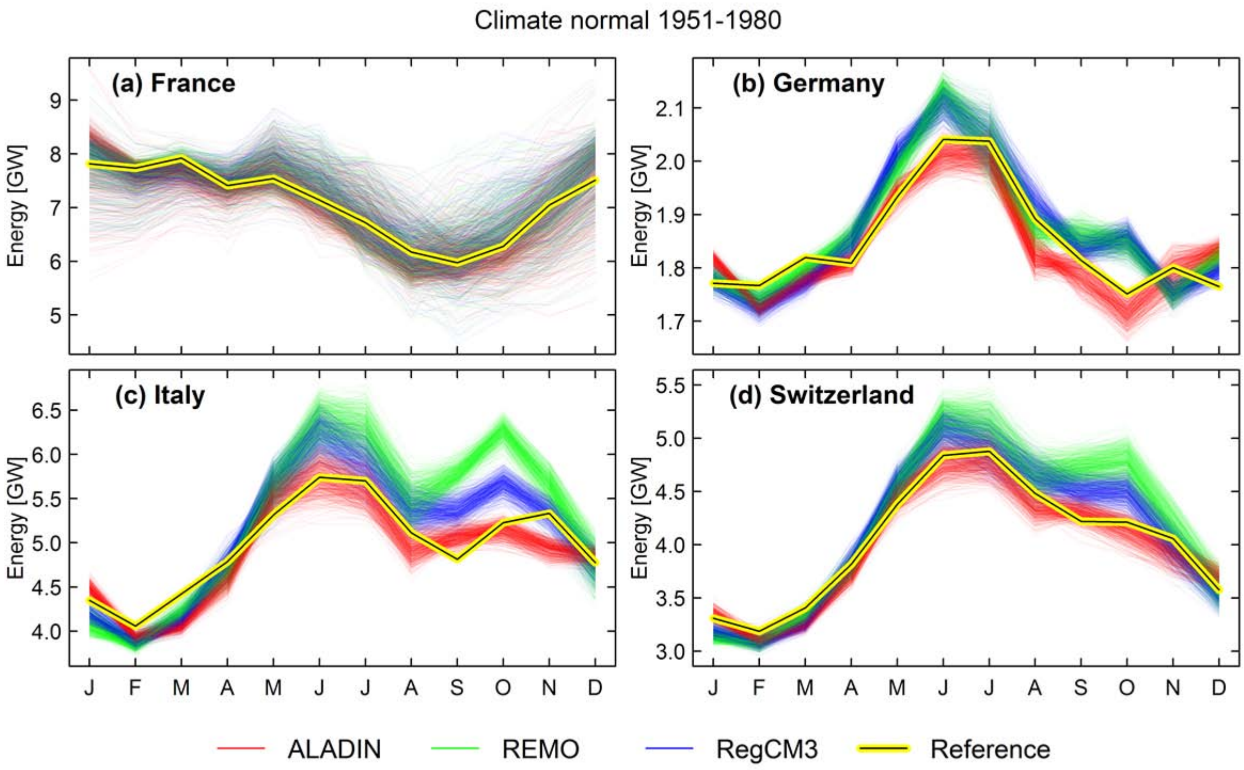

Figure A 2: Average energy generation potential per month in the climate normal 1951 to 1980.

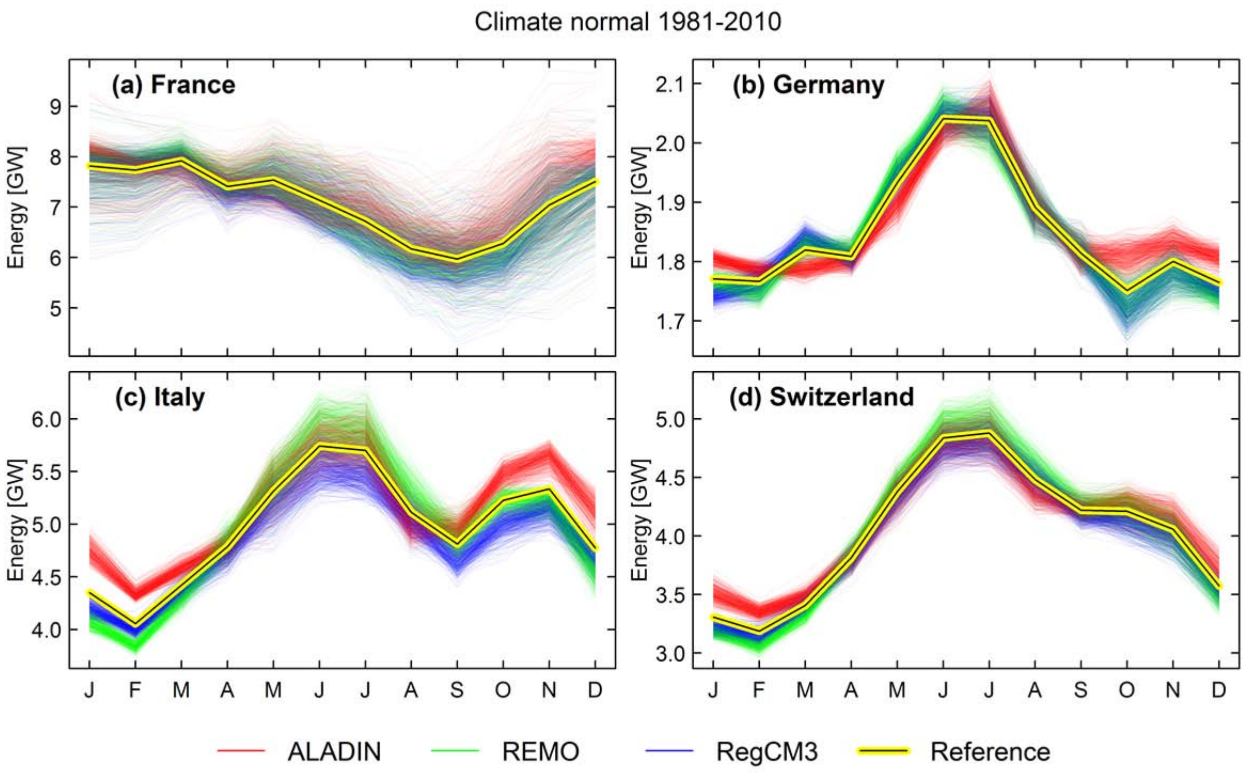

Figure A 3: Average energy generation potential per month in the climate normal 1981 to 2010. Since this is the reference period, only little difference between the models and the reference line exists.

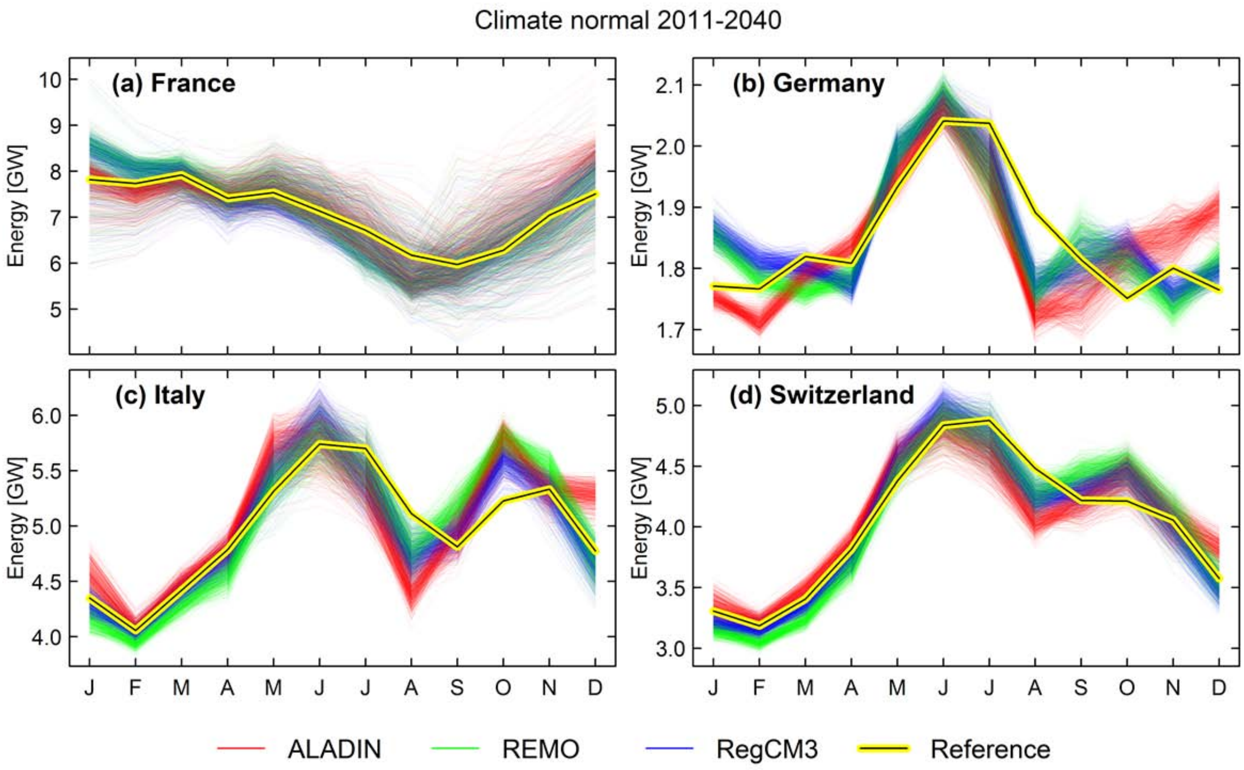

Figure A 4: Average energy generation potential per month in the climate normal 2011 to 2040.

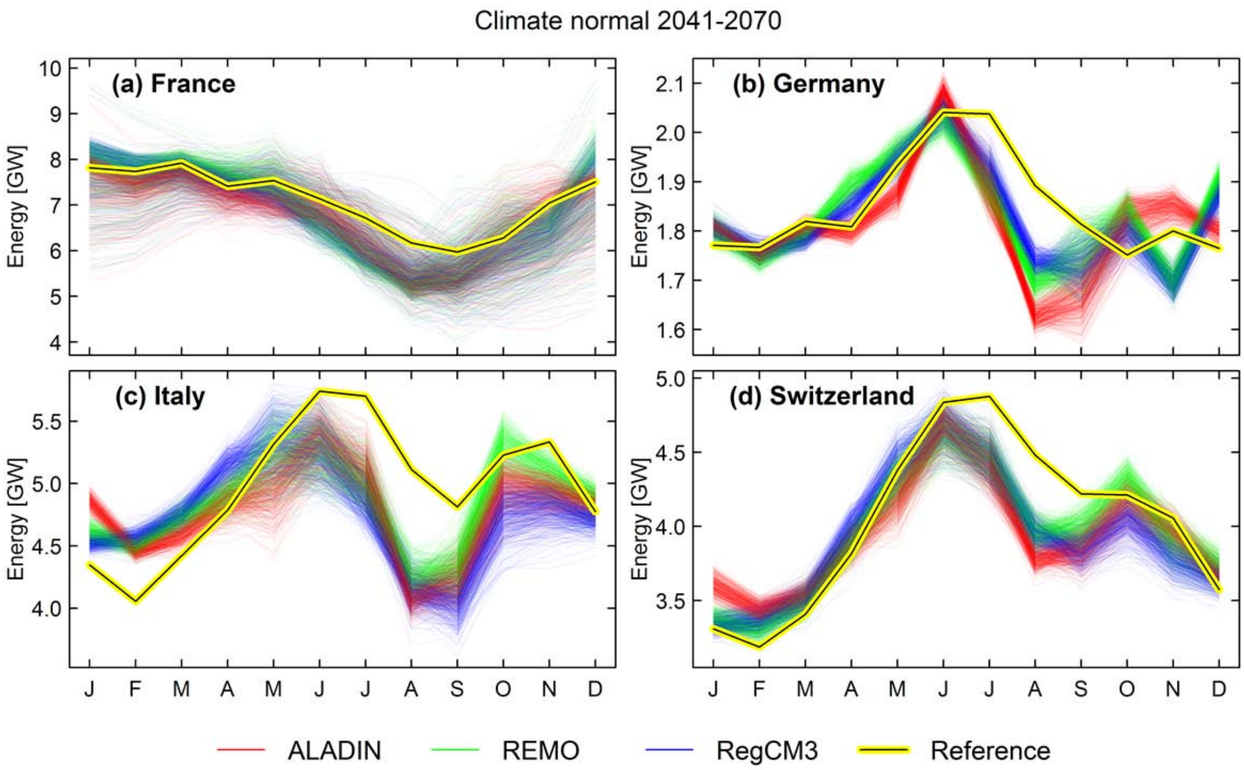

Figure A 5: Average energy generation potential per month in the climate normal 2041 to 2070.

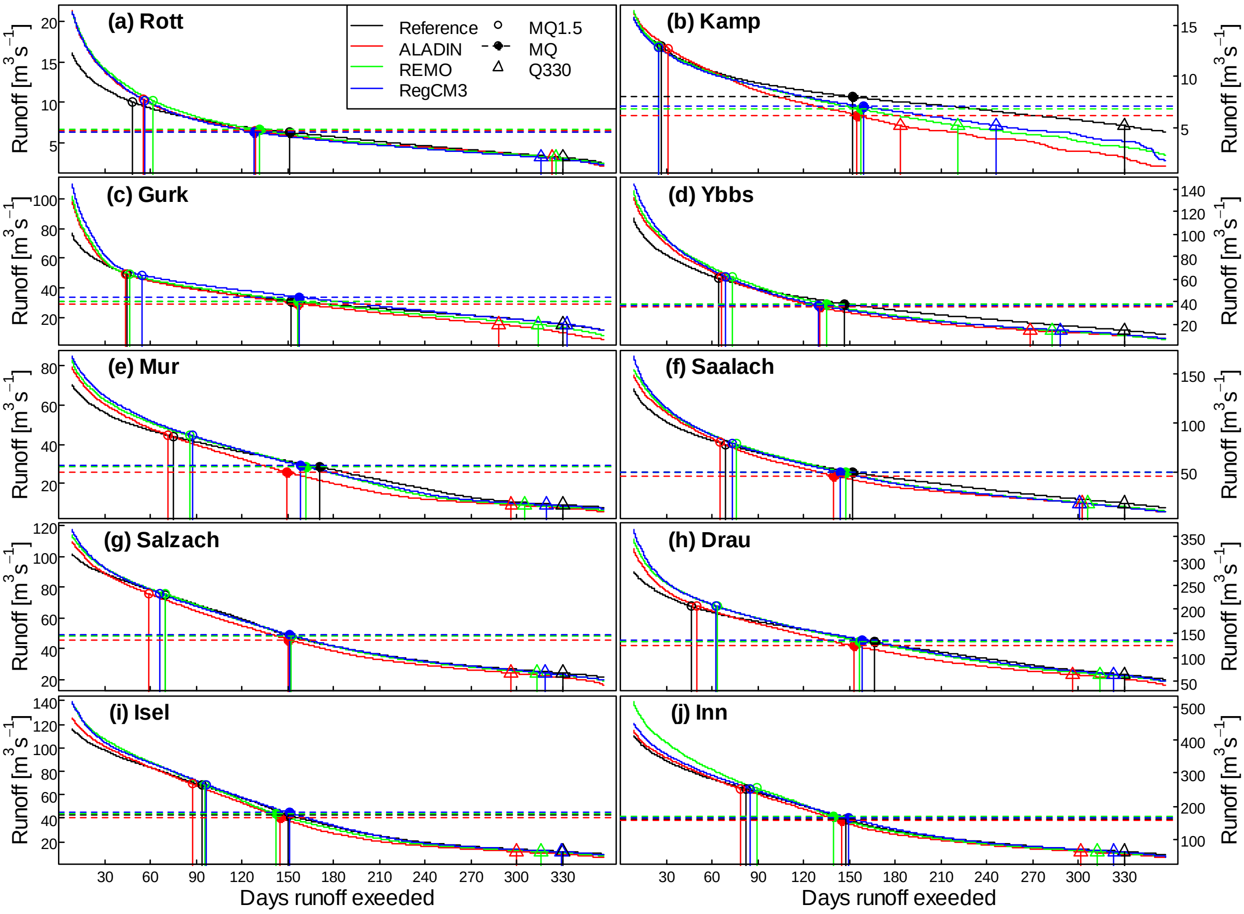

Figure A 6: Essential hydrological characteristics of the study basins during the standard normal 1951 to 1980 plotted along the flow duration curves. MQ1.5 refers to 1.5 times the MQ. MQ330 refers to days the runoff exceeds the value, that was Q330 during the reference period. Dashed lines highlight the discharge rates of MQ during the reference period (black) and during 1951 to 1980.

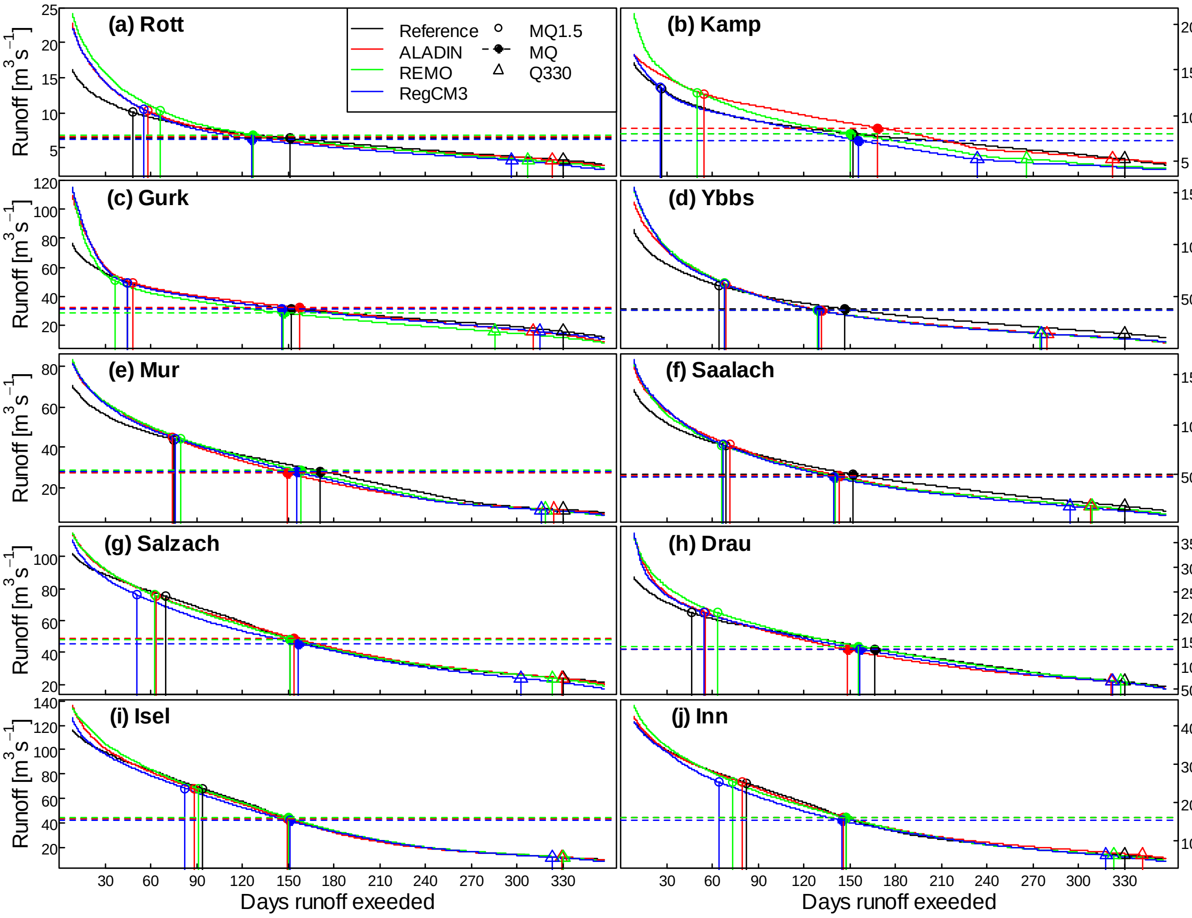

Figure A 7: Essential hydrological characteristics of the study basins during the standard normal 2011 to 2040 plotted along the flow duration curves. MQ1.5 refers to 1.5 times the MQ. MQ330 refers to days the runoff exceeds the value, that was Q330 during the reference period. Dashed lines highlight the discharge rates of MQ during the reference period (black) and during 2011 to 2040.

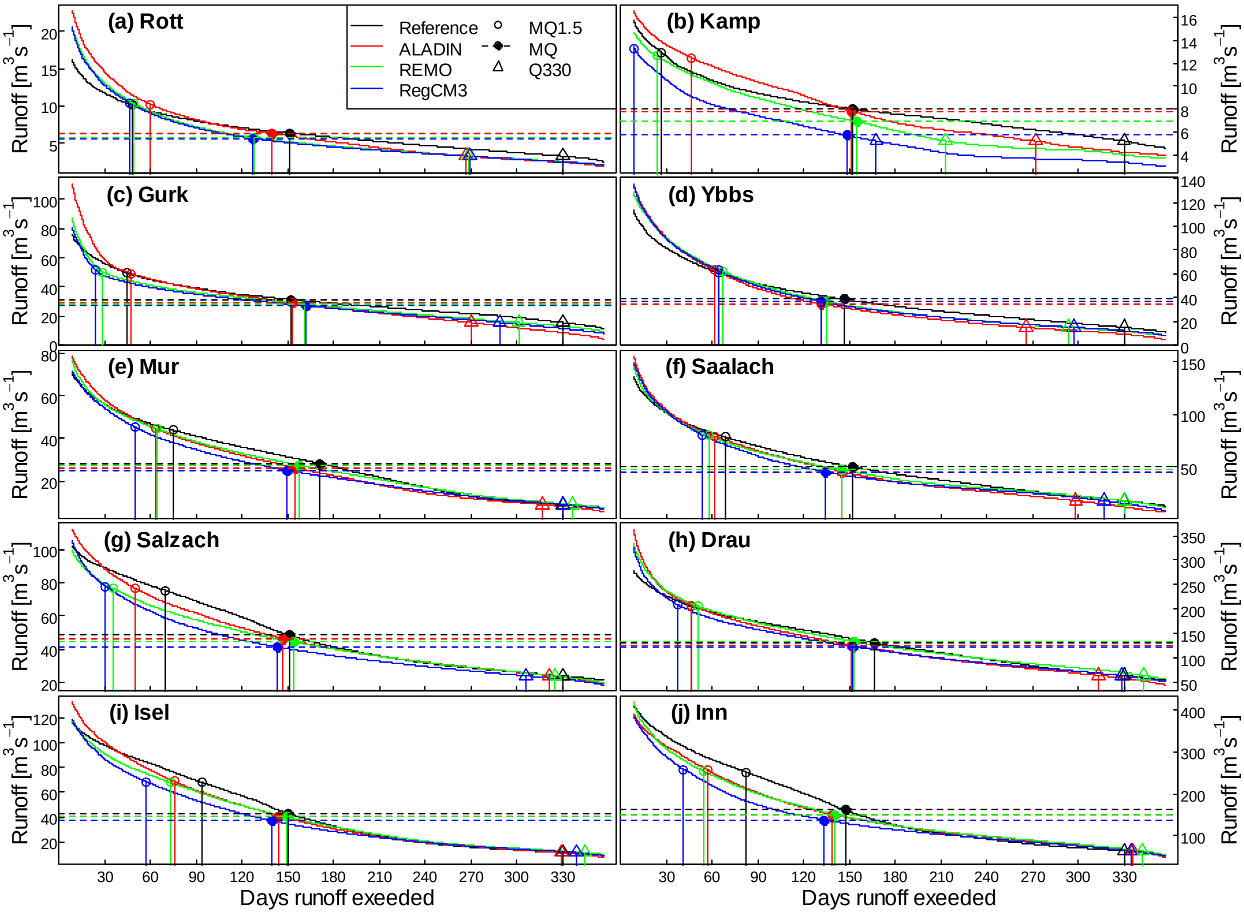

Figure A 8: Essential hydrological characteristics of the study basins during the standard normal 2041 to 2070 plotted along the flow duration curves. MQ1.5 refers to 1.5 times the MQ. MQ330 refers to days the runoff exceeds the value, that was Q330 during the reference period. Dashed lines highlight the discharge rates of MQ during the reference period (black) and during 2041 to 2070.

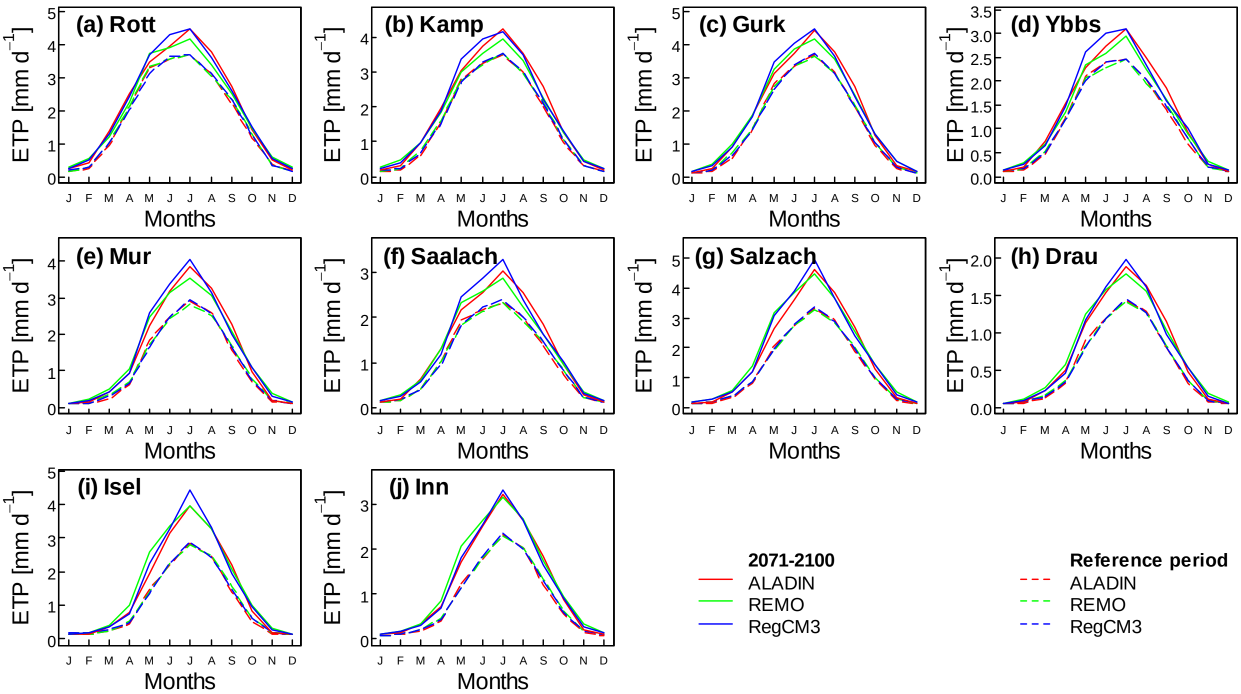

Figure A 9: Comparison of monthly potential evapotranspiration within the reference period and the climate normal at the end of the 21st century. Changes occur mainly during the summer months and are greater the higher the maximum elevation of the catchment.

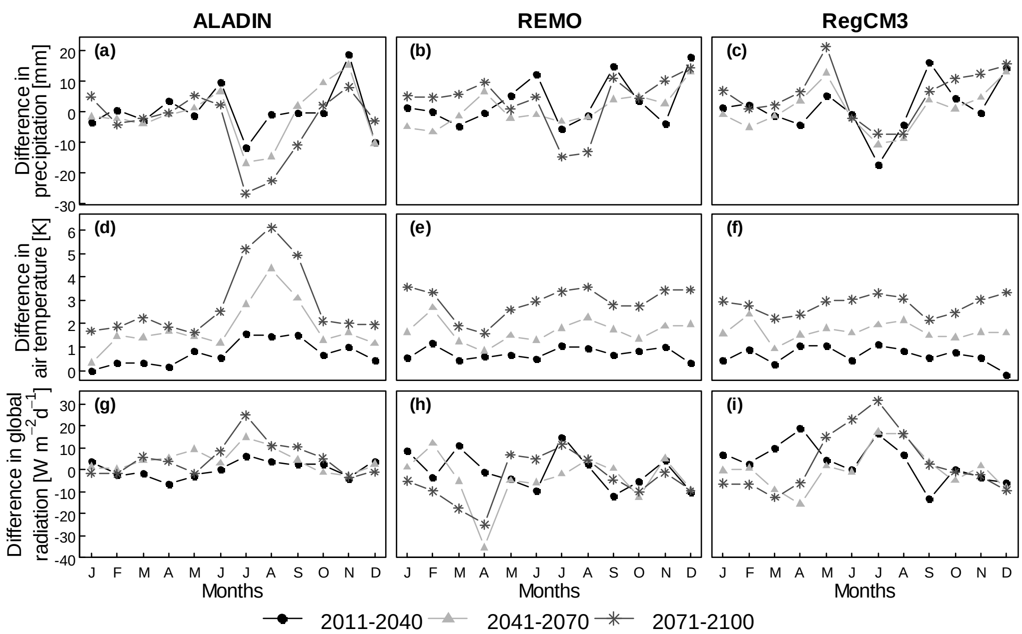

Figure A 10: Monthly changes in climatological data compared to the reference period for the catchment of river Rott.

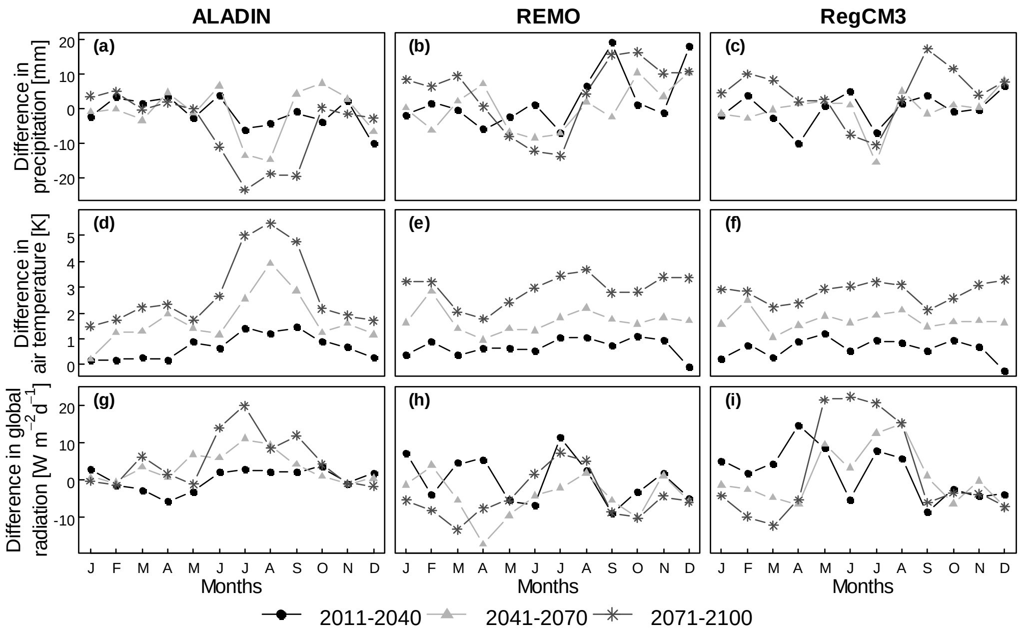

Figure A 11: Monthly changes in climatological data compared to the reference period for the catchment of river Kamp.

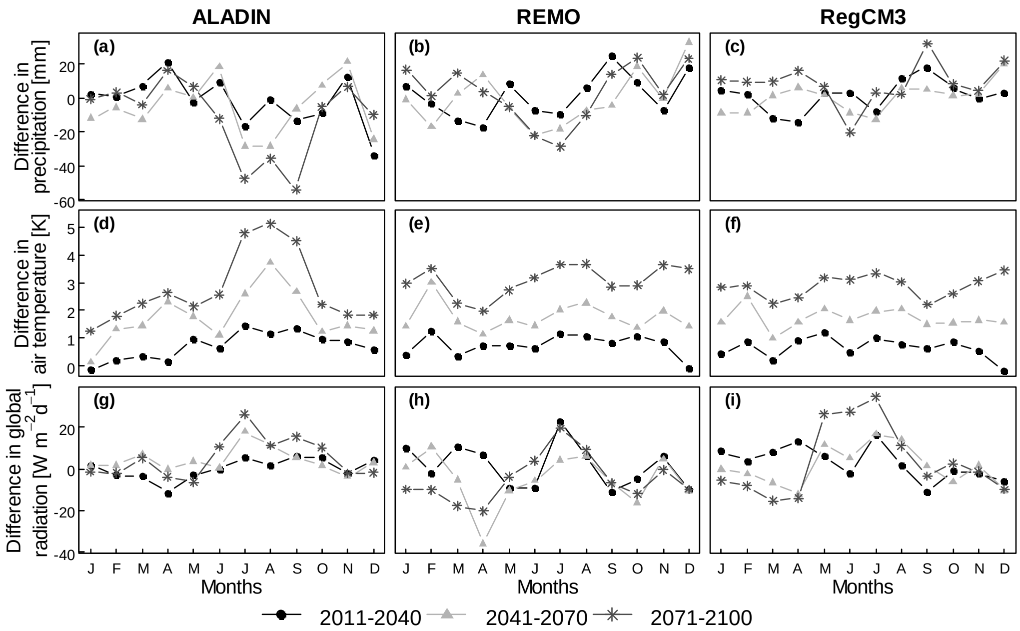

Figure A 12: Monthly changes in climatological data compared to the reference period for the catchment of river Ybbs.

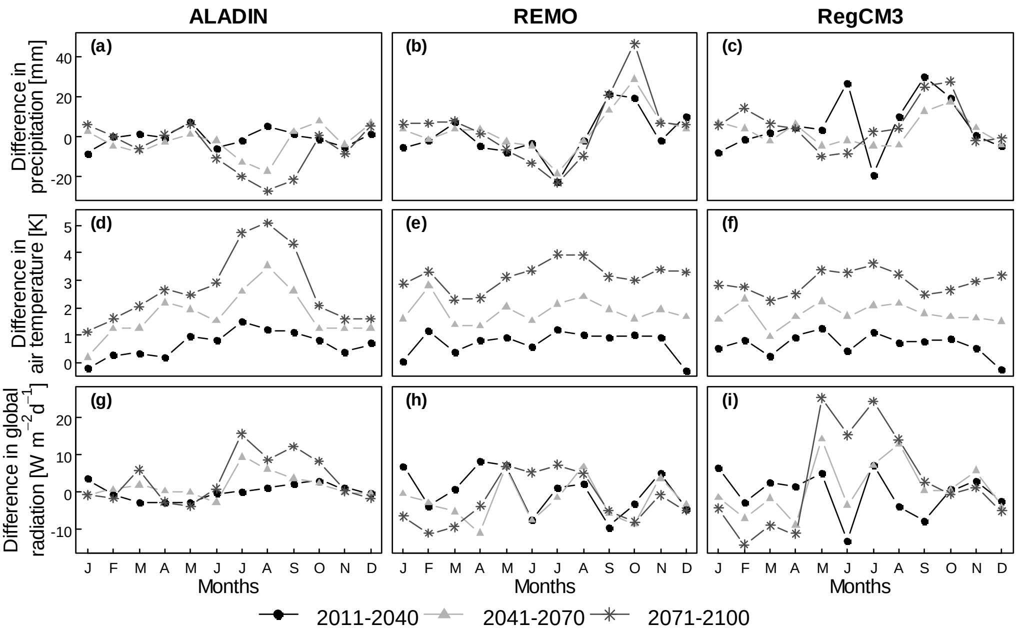

Figure A 13: Monthly changes in climatological data compared to the reference period for the catchment of river Gurk.

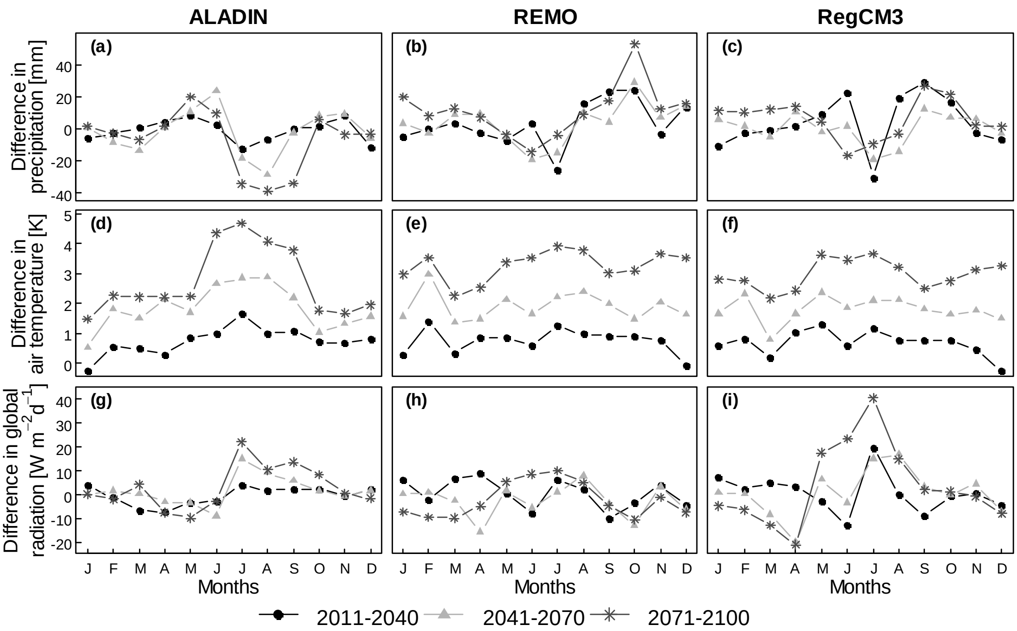

Figure A 14: Monthly changes in climatological data compared to the reference period for the catchment of river Mur.

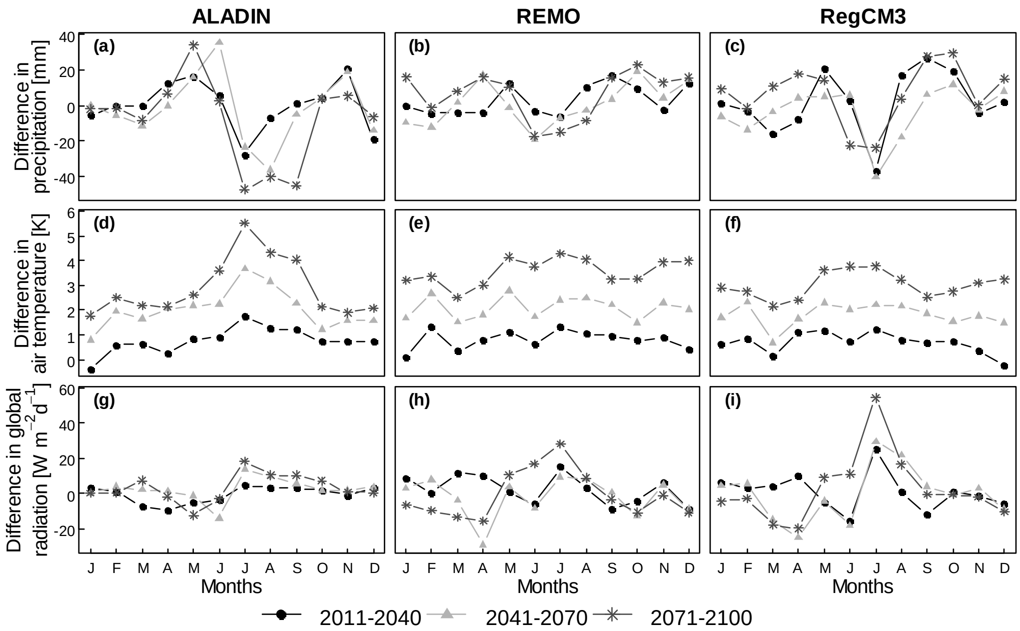

Figure A 15: Monthly changes in climatological data compared to the reference period for the catchment of river Salzach.

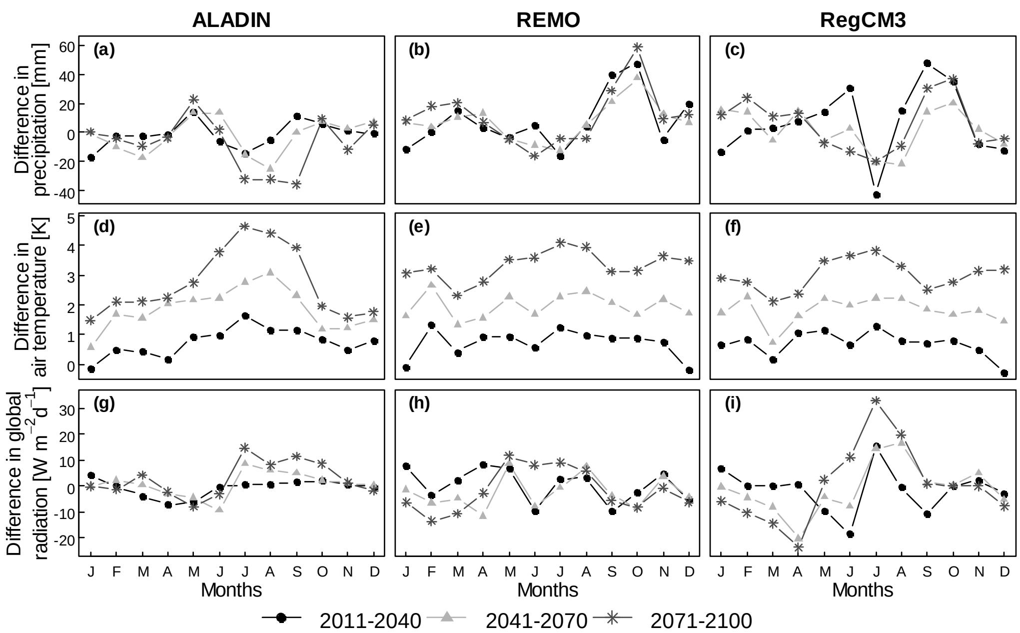

Figure A 16: Monthly changes in climatological data compared to the reference period for the catchment of river Drau.

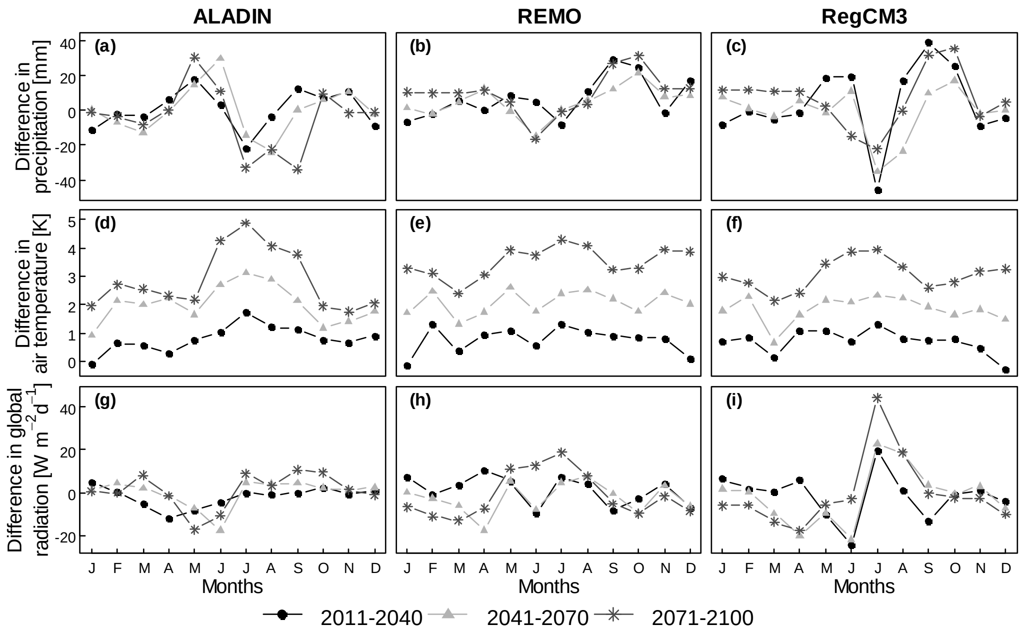

Figure A 17: Monthly changes in climatological data compared to the reference period for the catchment of river Isel.

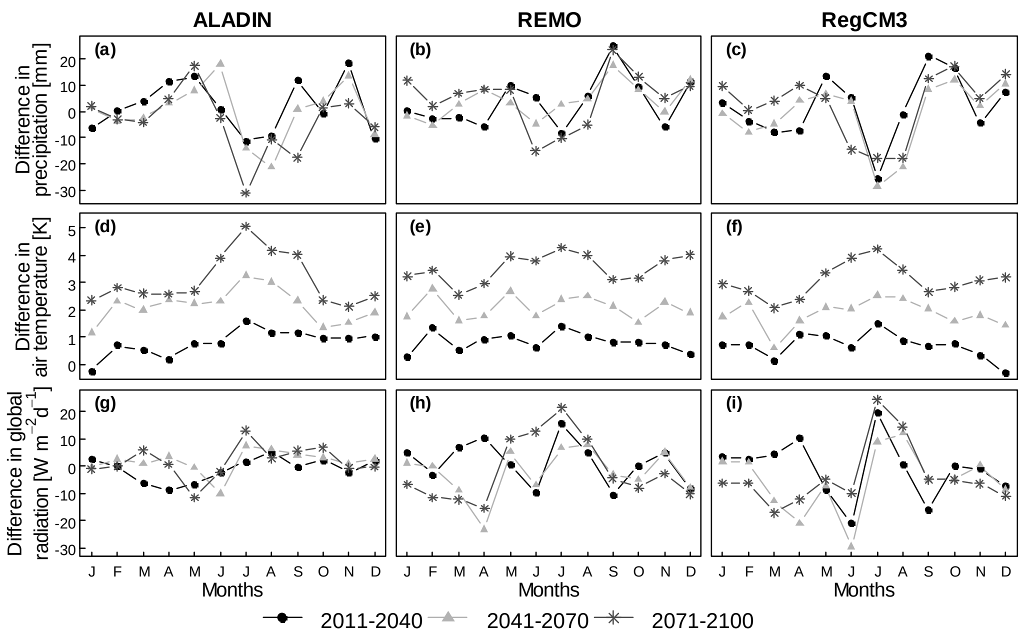

Figure A 18: Monthly changes in climatological data compared to the reference period for the catchment of river Inn.

10 Curriculum Vitae

Personal data

Name	Simon Frey
Date of birth	12.12.1982
Place of birth	Weingarten (Württemberg)
Country	Germany
Citizenship	German

Education

2002	Graduated from secondary school, Ravensburg, Germany
2003 – 2005	Study of Chemistry, University of Freiburg, Germany
2005 – 2010	Study of Hydrology, University of Freiburg, Germany. Minors: Soil sciences, Meteorology Title of thesis: Dating Techniques for Fast Components in Runoff using the cosmogenic radionuclides ^{7}Be and ^{22}Na. Supervised by Prof. Dr. Christoph Külls and Prof. Dr. Markus Weiler

Career Background

2011 - 2015	Research assistant at the Institute of Water Management, Hydrology and Hydraulic Engineering University of Natural Resources and Life Sciences, Vienna, Austria
2011 - 2014	Junior Scientist at AlpS GmbH, Innsbruck, Austria
Aug. 2010 - Feb. 2011	Research assistant at the Institute of Hydrology, Project: Strategic Environmental Assessment of the Central Namib 'Uranium Rush', University of Freiburg, Germany

Nov. 2008 - Jan. 2009	Work placement at the Büro für Angewandte Hydrologie, Berlin, Germany
Sep. 2008 - Oct. 2008	Work placement at the Leibniz-Institute of Freshwater Ecology and Inland Fisheries, Berlin, Germany

Publications

Frey, S. and Holzmann, H.: A conceptual, distributed snow redistribution model, Hydrol. Earth Syst. Sci. Discuss., 12(1), 609–637, doi:10.5194/hessd-12-609-2015, 2015.

Frey, S., Goler, R., Formayer, H. and Holzmann, H.: Die Auswirkungen möglicher Klimawandelszenarien auf das Erzeugungspotenzial von Wasserkraftwerken, Forum für Hydrol. und Wasserbewirtschaftung, 32.13, 145 – 152, 2013.

Frey, S., Külls, C. & Schlosser, C.: New Hydrological Age-Dating techniques using cosmogenic radionuclides Beryllium-7 and Sodium-22. Proceedings of the International Symposium on Isotopes in Hydrology, Marine Ecosystems, and Climate Change Studies Vol. 2: 361-368, ISSN: 0074-1884, 2013.

Presentations

Frey, S. & Külls, C.: Hydrological Age-Dating using cosmogenic radionuclides Be-7 and Na-22 in a meso-scale catchment in the Black Forest, Germany. Joint ICTP-IAEA Workshop on Evaluating Groundwater Pathways and Residence Times as part of Site Investigations and Post-Closure Safety Assessments for Geological Repositories. Trieste, Italy, 2013. Invited talk.

Frey, S., Goler, R., Formayer, H. & Holzmann H.: Die Auswirkung möglicher Klimawandelszenarien auf das Erzeugungspotenzial von Wasserkraftwerken. Tag der Hydrologie 2013, Bern, Switzerland, 2013.

Frey, S., Külls, C. & Schlosser, C.: New Hydrological Age-Dating techniques using cosmogenic radionuclides Beryllium-7 and Sodium-22. International Symposium on Isotopes in Hydrology, Marine Ecosystems, and Climate Change Studies, Monaco, 2011.

Posters

Frey, S. & Holzmann, H.: Berücksichtigung von Schneeverlagerungsprozessen bei der hydrologischen Modellierung alpiner Einzugsgebiete. Tri-Nationaler Workshop – Hydrologische Prozesse im Hochgebirge, Obergurgl, Austria, 2014.

Frey, S., Goler, R; Formayer, H. & Holzmann H.: Großskalige Wasserbilanzmodellierung zur Abschätzung des Wasserkraftpotentials europäischer Gebiete. 15. Österreichischer Klimatag, Innsbruck, Austria, 2014. Awarded with the second poster price.

Frey, S. & Holzmann, H.: Hydrological model uncertainties in climate change impact studies. European Geoscience Union General Assembly 2014, Vienna, Austria, 2014.

Frey, S. & Holzmann, H.: Dealing with snow accumulation in high mountains - A simple conceptual snow drift model. European Geoscience Union General Assembly 2013, Vienna, Austria, 2014.

Frey, S. & Holzmann, H.: Auswirkungen von möglichen Klimaveränderungen auf das Erzeugungspotential von Wasserkraftwerken in einem mesoskaligen Einzugsgebiet in den Hohen Tauern. Tag der Hydrologie 2012, Freiburg, Germany, 2012.

Frey, S. & Holzmann, H.: Snow cover modelling as an important tool in the rainfall runoff relationship. European Geoscience Union General Assembly 2012, Vienna, Austria, 2012.

Goler, R., Frey, S. Formayer, H. & Holzmann, H.: Einfluss möglicher Klimaszenarien auf das Erzeugungspotential von Wasserkraftwerken. 13. Österreichischer Klimatag, Vienna, Austria, 2012. Awarded with the poster prize for most innovative study topic.

Frey, S., Formayer, H. & Holzmann, H.: Auswirkungen von möglichen Klimaveränderungen auf das Erzeugungspotential von Wasserkraftwerken. 12. Österreichischer Klimatag, Vienna, Austria, 2011.

Vienna April 2015